Norwegian University of Life Sciences
Faculty of Chemistry, Biotechnology
and Food Science

Philosophiae Doctor (PhD)
Thesis 2022:38

Light-driven lytic polysaccharide monooxygenase (LPMO)-catalyzed solubilization of polysaccharides

Lysdrevet lytisk polysakkarid-monooksygenase (LPMO)-katalysert løseliggjøring av polysakkarider

Eirik Garpestad Kommedal

Light-driven lytic polysaccharide monooxygenase (LPMO)-catalyzed solubilization of polysaccharides

Lysdrevet lytisk polysakkaridmonooksygenase (LPMO)-katalysert løseliggjøring av polysakkarider

Philosophiae Doctor (PhD) Thesis

Eirik Garpestad Kommedal

Norwegian University of Life Sciences
Faculty of Chemistry, Biotechnology and Food Science

Ås (2022)

Thesis number 2022:38
ISSN 1894-6402
ISBN 978-82-575-1911-7

Table of contents

ACKNOWLEDGEMENTS ..... **I**

SUMMARY ..... **III**

SAMMENDRAG ..... **V**

LIST OF PAPERS ..... **VII**

1 INTRODUCTION **1**

1.1 SOURCES OF RENEWABLE BIOMASS 1

1.1.1 The plant cell wall *1*

1.1.2 Chitin-rich biomass *6*

1.2 MICROBIAL DEGRADATION OF RECALCITRANT POLYSACCHARIDES 9

1.2.1 Carbohydrate-active enzymes *9*

1.2.2 Degradation of recalcitrant biomass by secreted enzymes *13*

1.3 LYTIC POLYSACCHARIDE MONOOXYGENASES 15

1.3.1 History and classification *15*

1.3.2 LPMO structure *16*

1.3.3 The catalytic mechanism *19*

1.4 PHOTOBIOCATALYSIS 25

1.4.1 Light-driven LPMO reactions *28*

2 THESIS OUTLINE AND AIM OF THE RESEARCH **31**

3 MAIN RESULTS AND DISCUSSION **33**

3.1 PAPER I - CONTROLLED DEPOLYMERIZATION OF CELLULOSE BY LIGHT-DRIVEN LYTIC POLYSACCHARIDE OXYGENASES 33

3.2 PAPER II – VISIBLE LIGHT-EXPOSED LIGNIN FACILITATES CELLULOSE SOLUBILIZATION BY LYTIC POLYSACCHARIDE MONOOXYGENASES 39

3.3 PAPER III - NATURAL PHOTOREDOX CATALYSTS PROMOTE LIGHT-DRIVEN LYTIC POLYSACCHARIDE MONOOXYGENASE REACTIONS AND ENZYMATIC TURNOVER OF BIOMASS 44

4 CONCLUDING REMARKS AND FUTURE PERSPECTIVES **47**

5 REFERENCES **51**

6 PUBLICATIONS **71**

Acknowledgements

The work presented in this thesis was performed in the Protein Engineering and Proteomics (PEP) group at the Faculty of Chemistry, Biotechnology, and Food Science at the Norwegian University of Life Sciences from 2018 to 2022. The work was funded by the Norwegian Research Council through a project entitled ''Unravelling the secrets of oxidative biomass decomposition''.

I want to thank Vincent for giving me the opportunity to join the PEP group and dive deep into the world of redox enzymology and biomass decomposition. Thank you for creating an environment where I have had the trust and freedom to pursue my own curiosity. Your support and guidance have helped me develop as a person and scientist. I would also like to express my gratitude to my co-supervisor Gustav for showing me other aspects of LPMO research and for giving me the opportunity to learn new skills.

Throughout the last four years I have been part of a collaborative and supportive research environment and I'd like to thank everyone that I have interacted with for creating an inspiring work environment. Bastien and Zarah, thank you for introducing me to the LPMO world, fruitful discussions, and making me feel at home in PEP. To Anton and Heidi, who started their journey at the same time, thanks for all the conversations and discussions about science and life in general. Simen, thank you for helping me to understand lignin chemistry and your positive attitude. I have had the pleasure of supervising two master students, Camilla and Fredrikke, who have contributed to the work presented in this thesis. A special thanks to Lukas, Ole, Ivan, and Kelsi for the good times in and outside the lab. Lukas, I can't think of a better way to deal with a pandemic and lockdown during the second half of our PhDs than getting some fresh air on our road bikes.

A huge thanks to my family and friends who have been supportive and willing to listen to me talk about Nature's toolbox for deconstructing wood. I am forever grateful for the support of my wife, Karen Ane. You have experienced the ups and downs of my PhD alongside me and turned my head around when needed. A special thanks to my daughter, Eir, for making the last nine months of my PhD be equally much about your diapers, sleep, and development as about my own PhD work. Coming home to you and mom always cleared my head and seeing you smile made even the best day better.

Eirik Kommedal

Ås, April 2022

Summary

Lytic polysaccharide monooxygenases (LPMOs) are a recently discovered family of enzymes that catalyze oxidative cleavage of glycosidic bonds in insoluble polysaccharides at a liquid-solid interface. These enzymes are important for solubilization of crystalline polysaccharides, such as cellulose and chitin, which are key structural elements in plant cell walls and arthropod exoskeletons, respectively. Plant cell walls and insect exoskeletons are co-polymeric structures where cellulose and chitin are closely associated with photoredox-active phenolic compounds. Photodegradation of these phenolic compounds has been suggested to explain the observed enhancement of microbial decomposition of plant litter upon exposure to sunlight. The work presented in this thesis focused on studying the impact of light on LPMO activity with the aims of using photoredox catalysts for fine tuning of LPMO activity and obtaining a better understanding of the impact of light on turnover of biomass in Nature. The interplay between LPMOs, photoredox-active phenolic compounds present in natural LPMO substrates, and light led us to propose a possible enzymatic explanation for why light promotes microbial decomposition of biomass.

Paper I – Controlled depolymerization of cellulose by light-driven lytic polysaccharide oxygenases.

Paper I revisits light-driven LPMO reactions published prior to the discovery that LPMOs depend on hydrogen peroxide for catalysis, with the goal of determining the involvement of reactive oxygen species in these reactions. The results show that the catalytic activity of our model LPMO, AA10C from *Streptomyces coelicolor*, is dependent on H_2O_2 produced by light-exposed chlorophyllin or vanadium-doped titanium dioxide (V-TiO_2). For the chlorophyllin reaction system, we demonstrate that superoxide, $O_2^{\bullet-}$, is generated and suggest that this radical is the most likely reducing agent for the LPMO in this system. In the V-TiO_2 reaction system, $O_2^{\bullet-}$ does not appear to play a role and we suggest that the LPMO is reduced on the surface of the photoredox catalyst. Overall, this study highlights the importance of controlling the flux of reactive oxygen if one is to achieve stable enzymatic turnover of crystalline polysaccharides by LPMOs.

Paper II – Visible light-exposed lignin facilitates cellulose solubilization by lytic polysaccharide monooxygenases.

Paper II explores the use of lignin to fuel LPMO catalytic activity and how visible light impacts lignin-driven LPMO activity. The results show enhanced LPMO activity in lignin-driven reactions when these are exposed to visible light, and indicate that the ability of lignin to photocatalytically generate H_2O_2 determines LPMO efficiency. Consequently, using lignin as photoredox catalyst enables fine tuning of LPMO activity

by regulating production of H_2O_2. Direct interaction between a large lignin polymer and the copper active site of LPMOs is demonstrated, which shows that LPMOs can oxidize lignin like other lignin-active enzymes, such as ligninolytic peroxidases and laccases. NMR analysis of light-exposed lignin revealed light-induced oxidation of ring-conjugated unsaturated carbon double bonds resulting in an increased number of cinnamaldehyde end groups. Taken together, these results indicate that the observed boosting effect of light on microbial decomposition of plant litter may have an "enzymatic" explanation, as irradiation of lignin under aerobic conditions leads to the formation of a crucial co-substrate for LPMOs and redox enzymes involved in turning over biomass.

Paper III – Natural photoredox catalysts promote light-driven lytic polysaccharide monooxygenase reactions and enzymatic turnover of biomass.

Paper III builds on the idea from Paper II that redox active phenolic compounds naturally present in biomass enhance LPMO-activity when exposed to visible light. This paper demonstrates the ability of redox-active phenolic compounds in insect biomass, i.e., catecholamines, to photocatalytically reduce O_2 to H_2O_2 to fuel LPMO reactions. The results show that the LPMO activity is correlated with light-promoted *in situ* H_2O_2 generation and that the LPMO activity is inhibited by a competing H_2O_2-consuming enzyme. Importantly, LPMO-catalyzed solubilization of the chitin present in the insect biomass by a chitin-active LPMO was faster when the reaction was exposed to visible light. These results support the idea that the impact of light on biomass conversion in Nature relates to a boosting effect on the activity of biomass-converting redox enzymes, and that the light effect is not necessarily limited to increased availability of polysaccharides that results from photodegradation of phenolic compounds.

Sammendrag

Lytisk polysakkaridmonooksygenaser (LPMOer) er en nylig oppdaget enzymfamilie som katalyserer oksidativt brudd av glykosidbindinger i uløselige polysakkarider i grenseflaten mellom et fast stoff og en væske. Disse enzymene er essensielle for å løseliggjøre krystallinske polysakkarider, slik som cellulose og kitin, som spiller en strukturell nøkkelrolle i oppbyggingen av cellevegger hos planter og eksoskjeletter hos leddyr. Plantecellevegger og insekters eksoskjelett er kopolymere strukturer hvor cellulose og kitin finnes nært forbundet med fotoredoksaktive fenolforbindelser. Fotonedbrytning av disse fenolforbindelsene har blitt foreslått som en forklaring på hvorfor mikrobiell nedbrytning av plantemateriale forbedres når det eksponeres for sollys. Arbeidet i denne avhandling har fokusert på å studere hvordan lys påvirker LPMO-aktivitet med mål om å bruke fotoredokskatalysatorer til å kontrollere LPMO-aktivitet, og å oppnå en bedre forståelse av hvordan lys bidrar til nedbrytning av biomasse i naturen. Det observerte samspillet mellom LPMOer, fotoredoksaktive fenolforbindelser som finnes i naturlige LPMO-substrater, og lys førte til at vi foreslår en mulig enzymatisk forklaring på hvorfor lys fremmer mikrobiell nedbrytning av biomasse.

Artikkel I – Kontrollert depolymerisering av cellulose av lysdrevet lytisk polysakkaridmonooksygenaser.

Artikkel I gjennomgår lysdrevne LPMO-reaksjoner som ble publisert i forkant av oppdagelsen om at LPMOer bruker H_2O_2 for sin katalytiske aktivitet på nytt med mål om å bestemme om reaktive oksygenforbindelser er involvert for å fremme LPMO-aktivitet i disse systemene. Vi viser at aktiviteten til vår modell-LPMO, AA10C fra *Streptomyces coelicolor*, avhenger av H_2O_2 produsert av lys-eksponert klorofyllin eller vanadium-dopet titandioksid (V-TiO_2). For klorofyllin viser vi at superoksid, $O_2^{\bullet-}$, dannes og er den mest sannsynlige reduktanten for LPMOen i dette systemet. Med V-TiO_2 som fotoredokskatalysator finner vi ingen tegn på at det dannes $O_2^{\bullet-}$. Samlet sett viser denne studien hvor viktig det er å kontrollere strømmen av reaktive oksygenforbindelser for å oppnå stabil enzymkatalysert løseliggjøring av krystallinske polysakkarider og nødvendigheten av å bruke tidsserier fremfor et enkelt tidspunkt for å forstå de underliggende mekanismene som styrer den katalytiske aktiviteten til LPMOer i lysdrevne LPMO-reaksjoner.

Artikkel II – Synlig lys-eksponert lignin fasiliterer løseliggjøring av cellulose av lytisk polysakkaridmonooksygenaser.

Artikkel II utforsker bruken av lignin for å fremme LPMO-aktivitet og hvordan denne påvirkes av synlig lys. Resultatene viser økt LPMO-aktivitet i lignin-drevne reaksjoner

når disse blir eksponert for synlig lys og indikerer at ligninets evne til å fotokatalytisk danne H_2O_2 bestemmer LPMOens effektivitet. Konsekvensens av dette er at lignin kan brukes som en fotoredokskatalysator for å kontrollere LPMO-aktivitet ved å skreddersy H_2O_2-mengden som dannes. Direkte interaksjon mellom en ligninpolymer og kobberet i det aktive setet i LPMOer demonstreres og viser at LPMOer kan oksidere lignin tilsvarende andre ligninaktive-enzymer, som ligninaktive-peroksidaser og lakkaser. NMR-analyse av lyseksponert lignin avslørte at synlig lys forårsaker oksidasjon av karbon-karbon dobbeltbindinger som er konjugert med de aromatiske ringsystemene i ligninet og fører til en økning i antall kanelaldehydendegruppemotiver. Til sammen tyder disse resultatene på at forsterkereffekten av lys på mikrobiell nedbrytning av plantemateriale også kan ha en enzymatisk forklaring, ettersom lysbestråling av lignin under aerobe forhold fører til dannelse av kosubstrat for LPMOer og andre redoksenzymer som er involvert i nedbrytning av biomasse.

Artikkel III – Naturlig forekommende fotoredokskatalysatorer fremmer lysedrevne lytisk polysakkaridmonooksygenase-reaksjoner og enzymatisk nedbrytning av biomasse.

Artikkel III bygger på idéen fra Artikkel II om at naturlig forekommende redoksaktive fenolforbindelser i biomasse bidrar til økt LPMO-aktivitet når disse blir utsatt for synlig lys. Denne artikkelen demonstrerer evnen hos redoksaktive fenolforbindelser i insektsbiomasse til å fotokatalytisk redusere O_2 til H_2O_2 for å fremme LPMO-reaksjoner. Resultatene viser at LPMO-aktiviteten er korrelert med lys-fremmet *in situ* dannelse av H_2O_2 og at LPMO-aktiviteten hemmes av et konkurrende H_2O_2-avhengig enzym. Det er viktig å påpeke at LPMO-katalysert løseliggjøring av kitin fra insektsbiomasse med en kitinaktiv LPMO var raskere når reaksjonen ble eksponert for synlig lys. Disse resultatene støtter idéen om at lyset påvirker omdannelse av biomasse i naturen ved en forsterkereffekt på aktiviteten til redoksenzymene som omdanner biomasse, og at lyseffekter ikke nødvendigvis er begrenset til økt tilgang på polysakkaridene som følge av fotonedbrytning av fenolforbindelser.

List of papers

Paper I: Controlled depolymerization of cellulose by light-driven lytic polysaccharide oxygenases

Eirik G. Kommedal*, Bastien Bissaro*, Åsmund K. Røhr, Vincent G. H. Eijsink

Nat. Commun. **11**, 890 (2020)

Paper II: Visible light-exposed lignin facilitates cellulose solubilization by lytic polysaccharide monooxygenases

Eirik G. Kommedal, Camilla F. Angeltveit, Leesa J. Klau, Iván Ayuso-Fernández, Bjørnar Arstad, Simen G. Antonsen, Yngve Stenstrøm, Dag Ekeberg, Francisco Gírio, Florbela Carvalheiro, Svein J. Horn, Finn Lillelund Aachmann, Vincent G. H. Eijsink

Manuscript

Paper III: Natural photoredox catalysts promote light-driven lytic polysaccharide monooxygenase reactions and enzymatic turnover of biomass

Eirik G. Kommedal, Fredrikke Sæther, Thomas Hahn, Vincent G. H. Eijsink

Submitted manuscript

Co-authored publications not included in the thesis:

The lytic polysaccharide monooxygenase CbpD promotes *Pseudomonas aeruginosa* virulence in systemic infection

Fatemeh Askarian, Satoshi Uchiyama*, Helen Masson*, Henrik Vinther Sørensen, Ole Golten, Anne Cathrine Bunæs, Sophanit Mekasha, Åsmund K. Røhr, Eirik G. Kommedal, Judith Anita Ludviksen, Magnus Ø. Arntzen, Benjamin Schmidt, Raymond H. Zurich, Nina M. van Sorge, Vincent G. H. Eijsink, Ute Krengel, Tom Eirik Mollnes, Nathan E. Lewis, Victor Nizet, Gustav Vaaje-Kolstad

Nat. Commun. **12**, 1230 (2021)

* The authors contributed equally to this work.

1 Introduction

To achieve the much needed transition from fossil to renewable sources of energy and chemicals we need to make better use of biomass. Polysaccharides are abundant in biomass and their conversion, i.e., depolymerization, to simpler building blocks is a crucial step in biomass utilization. The two most abundant naturally occurring polysaccharides in nature are cellulose and chitin. Plants use cellulose, while fungi and arthropods use chitin for structural support and strengthening of cell walls and exoskeletons. The assembly of cellulose and chitin into crystalline fibers confers a high intrinsic resistance towards chemical and biological degradation. Furthermore, these polymers are invariably found embedded in complex co-polymeric structures, which makes their valorization in biorefinery applications even more difficult. However, Nature has not only developed the tools required to form these complex co-polymeric structures, Nature has also developed the tools to take them apart again and to make use of the stored energy. Acquiring a better understanding of how Nature degrades biomass and exploiting the new knowledge in biorefinery applications may contribute to a more renewable and sustainable future.

1.1 Sources of renewable biomass

1.1.1 The plant cell wall

The plant cell wall is the most abundant source of terrestrial biomass and serves a variety of functions. Cell walls provide structural integrity and mechanical strength as well as flexibility to allow cell expansion during growth, and they act as a barrier towards the environment and protect against pathogens (Somerville et al., 2004). Cellulose, hemicellulose, pectin, and lignin are the main building blocks of the plant cell wall and together these polymers form a complex co-polymeric matrix. The plant cell wall can be divided into three layers: the primary cell wall, the secondary cell wall, and the middle lamella (**Fig. 1**) (Rytioja et al., 2014). The primary cell wall is a flexible extracellular matrix that is deposited during cell growth and is composed of cellulose microfibrils that are non-covalently linked to hemicelluloses and pectin (Cosgrove, 2005). The secondary cell wall is deposited inside the primary cell wall once the cell has finished expanding, and the last step of secondary cell wall biosynthesis involves incorporation of lignin into the polysaccharide matrix (Meents et al., 2018). The middle lamella is pectin-rich and forms a boundary between two daughter cells during cell division. The middle lamella glues adjacent cells together and thus prevents cells from separating or sliding against each other (Zamil et al., 2017). The large majority of plant cell wall biomass comprises secondary cell walls. Plant cell wall biomass is often referred to as lignocellulosic biomass.

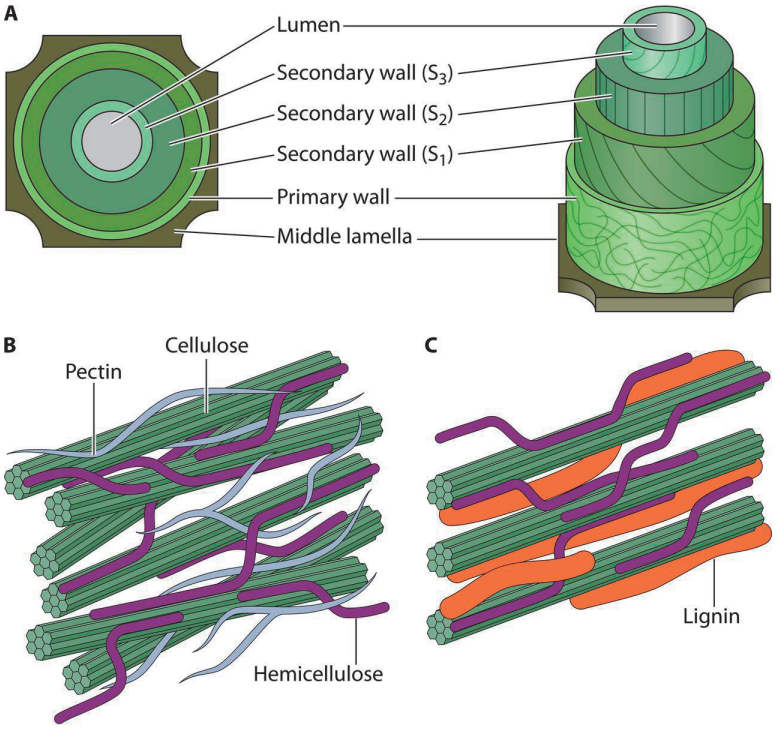

Fig. 1. Schematic illustration of plant cell wall structure. The plant cell wall consists of three main layers: the primary cell wall, the secondary cell wall, and the middle lamella as shown in **A**. The secondary cell wall is organized in three different stratums S1, S2, and S3 which differ in their orientation of cellulose microfibrils. In the S1 stratum the cellulose microfibrils cross over, in contrast to the S2 stratum where the cellulose microfibrils are oriented almost parallel to the axis of cell elongation, whilst in the S3 stratum the cellulose microfibrils display a flat helix structure (Timell, 1967). The interactions between the primary cell wall polysaccharides cellulose, hemicellulose, and pectin are shown in **B**. The interactions between polysaccharides and lignin in the secondary cell wall are shown in **C**. The figure was taken from Rytioja et al. (Rytioja et al., 2014).

Cellulose is the main polymer of the plant cell wall, representing 30-50 % of its dry matter content. The annual production of cellulose in Nature is estimated to amount to 10^{11} tons making cellulose the most abundant natural polysaccharide on Earth (Field et al., 1998). In cellulose, glucose molecules are linked together through β-(1,4)-glycosidic bonds. Two adjacent glucose units are rotated 180° relative to each other to form cellobiose, the repeating unit of cellulose (Cocinero et al., 2009). In plants, cellulose biosynthesis is performed by cellulose synthase complexes located at the plasma membrane. Individual cellulose synthases are assembled in trimeric cellulose synthase complexes which in turn form hexameric rosettes (Purushotham et al., 2020). Thus, 18 individual β-(1,4)-linked linear glucan chains are simultaneously generated in the same cellular location and these assemble to form cellulose microfibrils. The tight packing and crystalline nature of these microfibrils are caused by inter- and intramolecular hydrogen bonds and Van der Waals forces (Nishiyama et al., 2002, 2003; Notley et al.,

2004). Each glucose molecule, except for those at the reducing and non-reducing ends of the glucan chains, has two neighboring glucose units and it forms two hydrogen bonds with each of these (**Fig. 2A**). Cellulose is found in primary and secondary cell walls and generally displays higher crystallinity and a higher degree of polymerization in the latter (Meents et al., 2018).

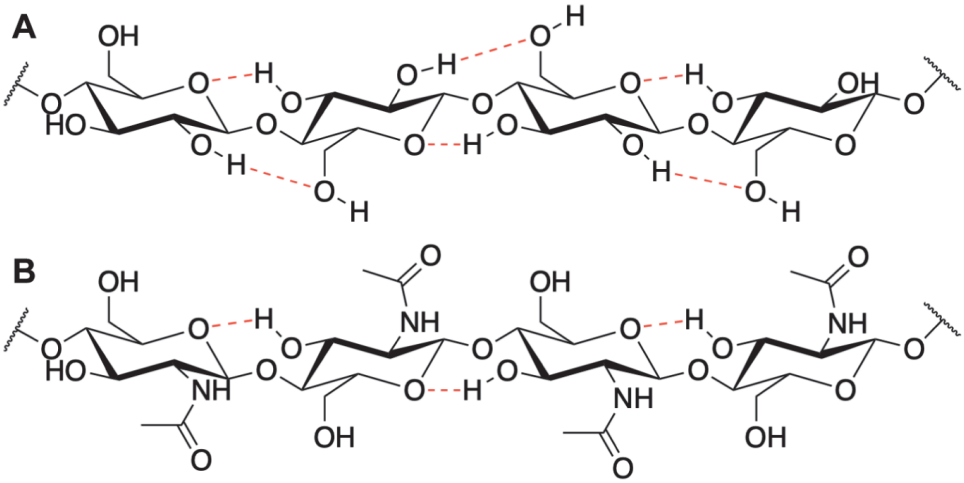

Fig. 2. Chemical structure of cellulose and chitin. The figure shows the chemical structure of cellulose (**A**) and chitin (**B**). The hydrogen bonding between neighboring glucose (**A**) and *N*-acetyl-D-glucosamine (**B**) units, in cellulose and chitin, respectively, is shown by dotted red lines.

Hemicelluloses make up 20-40% of lignocellulosic biomass and comprise a variety of linear and branched polysaccharides that are characterized by having β-(1,4)-linked backbones of glucose, mannose, or xylose, and by not being either cellulose or pectin (Scheller et al., 2010). Hemicelluloses include xyloglucans, xylans, mannans, glucomannans, and glucans with both β-(1,3) and β-(1,4) linkages. Of note, various hemicelluloses may contain modifications such as acetylations. Xylans are the dominant hemicelluloses in hardwood cell walls (Kirui et al., 2022), in contrast to softwood cell walls, which are characterized by high amounts of galactoglucomannans (Terrett et al., 2019). Xylans and galactoglucomannans bind to and coat the cellulose microfibrils in wood cell walls (Simmons et al., 2016; Terrett et al., 2019), and for xylan it has been shown that the degree and positioning of acetylations are important for cellulose binding (Grantham et al., 2017). Furthermore, xylans and mannans are important anchoring points for lignin in the secondary cell walls of plants (Kirui et al., 2022).

Lignin is the third major component of the plant secondary cell wall, constituting 20-30% of plant dry matter, and is believed to be crucial for plants to adapt from aquatic to terrestrial environments (Boerjan et al., 2003). Lignin provides structural rigidity

and mechanical strength to the plant stem and is important for water and solute transport as well as protecting plants against pathogens. Different plant taxa, cell types, and individual cell wall layers differ in the amount and composition of lignin, and lignin composition may also be influenced by the development stage and surrounding environment (Boerjan et al., 2003). Interestingly, lignin forms hydrophobic nanodomains that are physically separated from cellulose in grass cell walls (Kang et al., 2019). Lignin in grass cell walls primarily interacts with xylans via electrostatic interactions between methyl esters in the lignin and polar sugar groups (Kang et al., 2019). In wood cell walls on the other hand, lignin is colocalized with cellulose and preferentially binds to hydrophobic parts of cellulose by aligning the aromatic ring to the pyranose ring (Kirui et al., 2022; Vermaas et al., 2019). Due to its nature and its strong interactions with polysaccharides, lignin is a major contributor to the recalcitrance of lignocellulosic biomass towards microbial degradation.

Lignin is the most abundant naturally occurring aromatic polymer on Earth and is primarily made from three 4-hydroxyphenyl propanoid units, *p*-hydroxyphenyl (H), guaiacyl (G), and sinapyl (S) (**Fig. 3A**), but as many as 35 monomeric building blocks have been observed in natural lignins (Vanholme et al., 2019). Hardwood generally contains mostly G and S units, softwood contains mainly G units, and grasses generally contain G and S units, but with a higher H content than wood-derived biomass (Boerjan et al., 2003). Once the lignin precursors have been synthesized, they are transported from inside the cell and out to the cell wall, where they are polymerized (Meents et al., 2018). Lignin monomers depend on an activation step prior to lignin polymerization in which the monomers are oxidized (dehydrogenated) by laccases or peroxidases using either oxygen or hydrogen peroxide as co-substrate, respectively (**Fig. 3B**) (Tobimatsu et al., 2019). The resulting phenolic radicals are stabilized by delocalization of the unpaired radical electron in the aromatic ring system and coupling of these relatively stable radicals is favored in the β-position resulting in, almost exclusively, formation of β-O-4, β-β, and β-5 linkages (**Fig. 3B&C**) (Vanholme et al., 2010). This process will initially generate dimers, which again may be oxidized to engage in further oligomerization and polymerization reactions. Such stepwise coupling is considered the primary process for lignin polymer extension (Tobimatsu et al., 2019). Thus, lignin polymerization is described as a simple chemical reaction between two radicals that results in a highly complex and varied lignin polymer, where lignin monomers are linked together by various C-O and C-C bonds (Ralph et al., 2019).

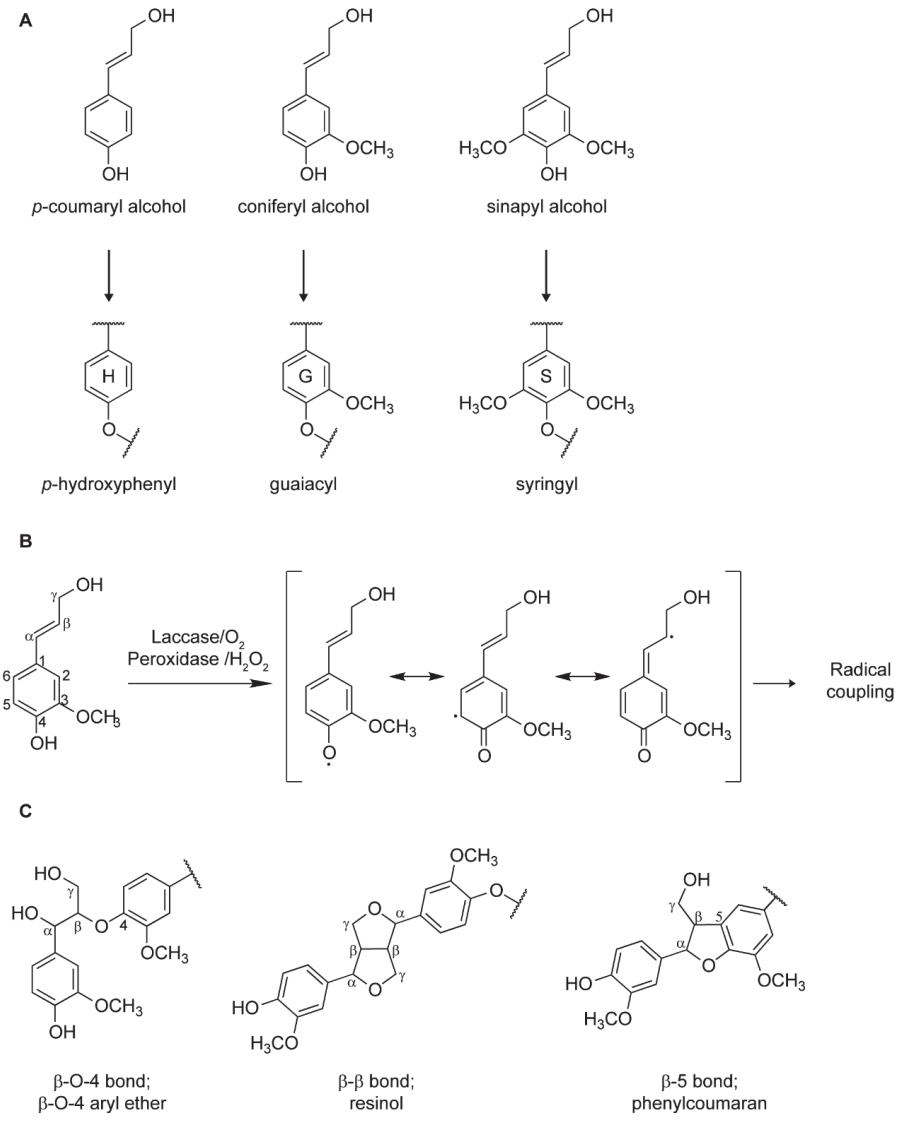

Fig. 3. Lignin monomer building blocks, their activation to radicals for lignin polymerization, and typical bonds found between lignin monomers in a lignin macromolecule. Lignin monomer precursors and their corresponding units after incorporation into lignin are shown in **A**. Radical formation of coniferyl alcohol by laccases or peroxidases and the corresponding resonance stabilized radical are shown in **B**. Note that the resonance forms shown in **B** only include the relevant locations for radical coupling for coniferyl alcohol, and that the number of methoxy-groups influences the number of positions available for coupling. Shown in **C** are commonly found bonds between lignin monomers.

1.1.2 Chitin-rich biomass

Chitin is the second most abundant polysaccharide in Nature with an estimated annual production of 10^{10}-10^{11} tons and is primarily found in arthropod exoskeletons and the cell walls of fungi and yeasts (Rinaudo, 2006). Two *N*-acetyl-D-glucosamine (GlcNAc) sugars linked by a β-(1,4) glycosidic bond and rotated 180° relative to each other make up the repeating unit of the chitin polymer, chitobiose (**Fig. 2B**). Single chitin chains pack together to form a crystalline and rather hydrophobic polysaccharide microfibril that is insoluble in water (Rinaudo, 2006). The chitin chains are held together by interchain molecular interactions that are dominated by hydrogen bonds from the C6-hydroxyl and the amine group on one chitin chain to the carbonyl group on the *N*-acetyl side chain on an adjacent chitin chain (Rinaudo, 2006). Chitin can exist as three different allomorphs, α, β, and γ, which differ in how the single chains are oriented towards each other (Zhu et al., 2016). In α-chitin the chains are antiparallel while in β-chitin the chains are parallel. In the third form, γ-chitin, both parallel and antiparallel arrangements of the individual chitin chains occur. α-chitin is the most abundant chitin form and is found in the cell walls of yeasts and fungi as well as in the exoskeletons of crustaceans and insects, while β-chitin is primarily found in diatoms and squid pens, possibly also in internal structures of insects (Zhu et al., 2016). Regardless of allomorph, organisms use chitin to provide mechanical strength and resilience to their cell walls and exoskeletons.

Similar to plant cell walls, chitin microfibrils do not appear in isolation but rather as part of co-polymeric structures that vary depending on the organism. Fungal cell walls are primarily composed of varying amounts of glucans, chitin, glycoproteins, and melanin, depending on the species and its morphological phase (Garcia-Rubio et al., 2020). The exoskeletons of crustaceans are made of proteins, minerals ($CaCO_3$), and chitin (Yan et al., 2015), whereas insect exoskeletons are composed of chitin, proteins, lipids, minerals, and catecholamines (Zhu et al., 2016).

The insect cuticle undergoes a sclerotization process, also known as quinone tanning, during which catecholamines are incorporated (Andersen, 2010). The two primary compounds incorporated into the insect cuticle during sclerotization are *N*-acetyldopamine (NADA) and *N*-β-alanyldopamine (NBAD) (**Fig. 4**) (Hopkins et al., 1982; Karlson et al., 1962). Sclerotization is an oxidative process where NADA and NBAD are oxidized by laccases or peroxidases using either oxygen or hydrogen peroxide as co-substrate, respectively, to *o*-quinones via formation of semiquinone radicals (Andersen, 2012). The resulting *o*-quinones can react directly with nucleophiles or be enzymatically isomerized to *p*-quinone methides which also can react with nucleophiles (**Fig. 4**) (Andersen, 2012). The *p*-quinone methide of NADA may be further isomerized to dehydro-NADA which reacts similarly to NADA (**Fig. 4**)

(Andersen, 2012). Nucleophiles present in the insect cuticle that can react with oxidized *o*-quinone or *p*-quinone methide forms of NADA and NBAD include water, imidazole nitrogens from histidine, amino groups found in lysine, β-alanine, or at the N-terminal of a protein, and possibly chitin (Christensen et al., 1991; Hopkins et al., 1999; Merritt et al., 1996; Schaefer et al., 1987). Of note, the semiquinone radical emerging during oxidation of NADA and NBAD by laccases or peroxidases may undergo similar radical coupling reactions as lignin monomers and generate dimeric or oligomeric catecholamines.

Insects are attractive for protein and lipid production for animal feed and human food. Insect larvae are not only rich in proteins and lipids, but insects can also help reduce organic waste, including food waste, by converting organic materials into insect biomass (Nguyen et al., 2015). Tons of insect biomass could possibly be generated in large scale insect farming facilities on a daily basis (Tomberlin et al., 2015). While terms like biorefining and bioresources have traditionally been linked to lignocellulosic biomass, the growing number of insect production facilities worldwide leads to increasing availability of insect by-products. Consequently, extraction and valorization of chitin from insect biomass is gaining interest and may become economically viable, providing an alternative to the traditional extraction of chitin from seafood waste streams such as crab and shrimp shells (Hahn et al., 2020).

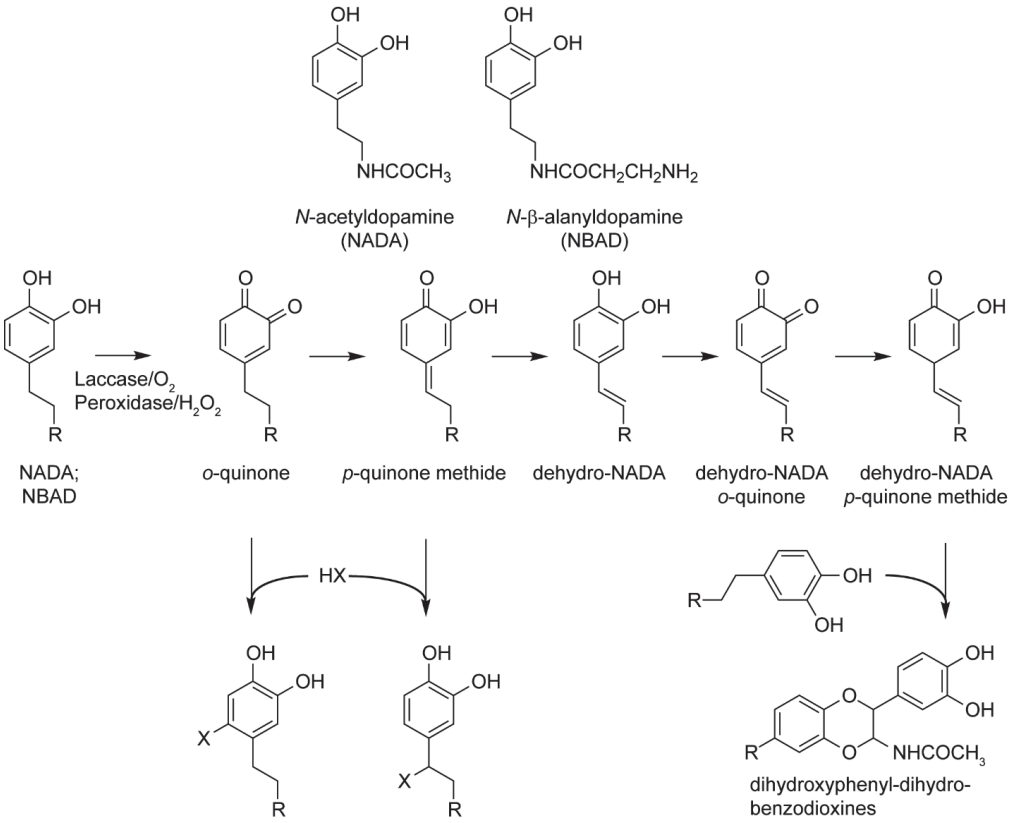

Fig. 4. Precursors, intermediates, and possible products formed during cuticular sclerotization. *N*-acetyldopamine (NADA) and *N*-β-alanyldopamine (NBAD) are thought to be the main precursors in sclerotization. They are enzymatically oxidized to *o*-quinones and further isomerized to *p*-quinone methides, both of which react with nucleophiles (HX; where X is the nucleophile). In addition, the *p*-quinone methide form of NADA can be converted to dehydro-NADA and undergo the same oxidation as NADA and NBAD. The *p*-quinone methide form of dehydro-NADA may react with catechols to form dihydroxyphenyl-dihydrobenzodioxines (Andersen, 2012). Of note, the oxidation of NADA and NBAD by laccases and peroxidases leads to formation of *o*-semiquinone radicals.

1.2 Microbial degradation of recalcitrant polysaccharides

The estimated annual production of both cellulose and chitin is on the order of $10^{10\text{-}11}$ tons and considering the similar molecular structures of these polymers it is no wonder that Nature has devised similar construction and deconstruction mechanisms for plant cell walls, fungal cell walls, and arthropod exoskeletons. The three main paradigms for deconstructing recalcitrant polysaccharides entail mechanisms based on cellulosomes, polysaccharide utilization loci (PUL), and secretion of free enzymes. Cellulosomes are multienzyme complexes that are employed by anaerobic bacteria and fungi to decompose lignocellulosic biomass, either while moving freely in the extracellular environment or while being attached to the cell surface (Artzi et al., 2017; Haitjema et al., 2017). The term polysaccharide utilization locus refers to a cluster of strictly regulated genes that encode the enzymes and proteins needed to decompose complex carbohydrates (Grondin et al., 2017). Specialized PULs have been described for many substrates, including cellulose (Naas et al., 2014), hemicelluloses (e.g. Larsbrink *et al.*, 2014), and chitin (Larsbrink et al., 2016). Bacteria and fungi can also secrete a plethora of free enzymes to convert recalcitrant biomass to simple sugars, which are taken up by the cell and metabolized (see 1.2.2). The diverse strategies developed by Nature to regain energy from biomass serve as inspiration for developing better ways to make use of biomass for production of fuels and chemicals.

1.2.1 Carbohydrate-active enzymes

Carbohydrate-active enzymes (CAZymes) are enzymes that are involved in the synthesis, modification, or degradation of carbohydrates and glycoconjugates, and they are classified in the Carbohydrate-Active Enzyme (CAZy) database, based on sequence similarity (Cantarel et al., 2009). The CAZy database categorizes enzymes based on their amino acid sequences and provides information on the observed substrate specificities and determined three-dimensional structures for each enzyme family. Until recently, the CAZy classification comprised glycoside hydrolases (GHs), glycosyltransferases (GTs), carbohydrate esterases (CEs), polysaccharide lyases (PLs), and carbohydrate-binding modules (CBMs). Although CBMs bind to polysaccharides without forming or breaking chemical bonds and as such are not directly involved in synthesis, modification or degradation of carbohydrates or glycoconjugates, they are still included in the CAZy database as they modulate the functionality of the carbohydrate-active enzymes (Cantarel et al., 2009). The discovery that proteins originally classified as CBM33s and GH61s were redox-active enzymes, now called lytic polysaccharide monooxygenases or LPMOs (see section 1.3), led to the establishment of a new enzyme class called auxiliary activities (AAs), comprising LPMOs, lignin-modifying enzymes, and other redox enzymes involved in biomass turnover (Levasseur et al., 2013).

The GH class comprises more than 170 enzyme families that hydrolyze the glycosidic bond between two carbohydrate moieties or between a carbohydrate moiety and a non-carbohydrate moiety. GHs involved in depolymerization of polysaccharides are characterized as exo- or endo-active, meaning that they cleave the polysaccharide from the chain end, i.e., the reducing end or the non-reducing end, or act on the interior of the polysaccharide chain, respectively (Horn et al., 2012). GTs catalyze the formation of a glycosidic bond between an acceptor molecule and an activated sugar molecule with a phosphate leaving group (Lairson et al., 2008). CEs employ a hydrolytic mechanism to deacetylate O- and N-substituted polysaccharides (Biely, 2012), one example being chitin deacetylases, which convert *N*-acetylglucosamine units in chitin to glucosamine. Unlike the hydrolytic GH enzymes mentioned above, PLs perform depolymerization of polysaccharides containing uronic acids by β-elimination, generating an unsaturated sugar at the new non-reducing end and a regular new reducing end (Garron et al., 2010).

Auxiliary activity enzymes are believed to act together with the above-mentioned CAZymes to enhance the deconstruction of lignocellulosic biomass (**Fig. 5**). LPMOs use redox chemistry and an oxygen co-substrate (O_2 or H_2O_2) to cleave polysaccharides; these enzymes currently populate CAZy families AA9, AA10, AA11, AA13, AA14, AA15, AA16, and AA17 and are discussed in detail in section 1.3, below. Conversion of lignocellulose also requires lignin-modifying enzymes including laccases and lignin-active peroxidases classified as AA1s and AA2s, respectively. Laccases are multicopper enzymes that oxidize aromatic molecules using O_2 as electron acceptor and are important lignin modifying enzymes (Giardina et al., 2010). Laccases are able to directly oxidize a range of phenolic compounds and may also carry out oxidation of non-phenolic aromatic compounds using mediators (Munk et al., 2015). Lignin-active peroxidases are dependent on H_2O_2 as oxidant and include manganese peroxidases, lignin peroxidases, and versatile peroxidases. Common to all three peroxidases is the $2e^-$ oxidation of their heme prosthetic group to generate the catalytically active oxo-ferryl intermediate species with concomitant reduction of H_2O_2 to H_2O, followed by two successive one-electron abstractions from a substrate (Sáez-Jiménez et al., 2015). Manganese peroxidases oxidize lignin by generating an Mn^{3+} species that is stabilized by a chelator. The chelated Mn^{3+} abstracts an electron from a phenolic hydroxyl in the lignin. Lignin peroxidases generate a highly reactive solvent-exposed tryptophan radical capable of abstracting an electron from both phenolic and non-phenolic parts in the lignin (Sáez-Jiménez et al., 2015). Versatile peroxidases combine the structural and catalytic features of an Mn^{2+}-binding site from manganese peroxidases and a solvent-exposed tryptophan residue from lignin peroxidases enabling them to oxidize both the phenolic and non-phenolic parts of lignin (Ruiz-Dueñas et al., 1999).

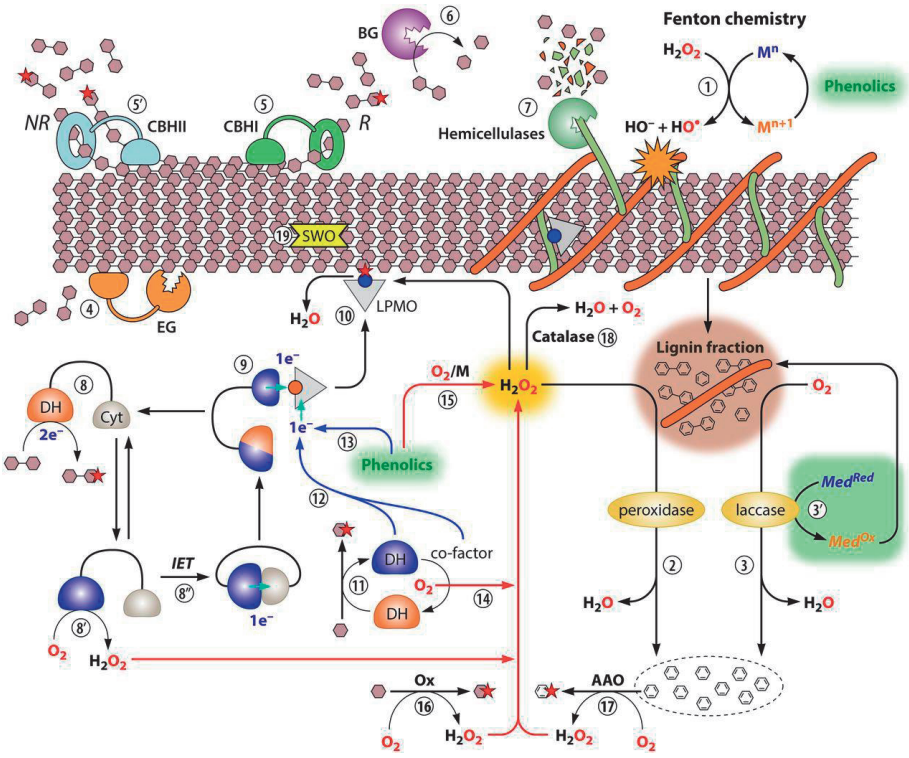

Fig. 5. An overview of the multitude of reactions taking place during biological deconstruction of lignocellulose. The figure and most of its legend were taken from Bissaro et al. (Bissaro et al., 2018b), who used this figure not only to illustrate complexity but also to show the potentially central role of H_2O_2 in biomass conversion (see section 1.3). The primary non-enzymatic component to lignocellulose deconstruction is Fenton chemistry (Step 1) which is based on generation of hydroxyl radicals. Peroxidases (step 2) and laccases (step 3) modify the lignin fraction. The main cellulases are endoglucanases (EGs) who act internally (step 4) and cellobiohydrolases, CBHI and CBHII, who act from the reducing (R) and non-reducing (NR) chain ends (steps 5 and 5') to release cellobiose. Cellobiose is further converted to glucose by β-glucosidases (BG) (step 6). The various cellulases also release minor amounts of cello-oligosaccharides oxidized at C1 or C4 by an LPMO, these oxidations are indicated by a red star. Hemicellulose and pectin are hydrolyzed by hemicellulases and pectinases, respectively (step 7). Cellobiose dehydrogenase (CDH) oxidizes cello-oligosaccharides (step 8) and the reducing equivalents obtained from dehydrogenation can be used to generate H_2O_2 (step 8') or transferred to the cytochrome (Cyt) domain (step 8''). A reduced Cyt can transfer an electron to an LPMO (step 9). The reduced LPMO oxidizes cellulose in the presence of O_2 and or H_2O_2 (step 10). Single domain dehydrogenases (DHs) and unbound, reduced cofactors can also activate the LPMO (steps 11 and 12). Phenolic compounds from lignin can also reduce the LPMO (step 13). Reduced phenolic compounds in presence of transition metals and single domain DHs can also generate H_2O_2 under aerobic conditions (steps 14 and 15, respectively). A variety of sugar active (Ox) and aryl alcohol (AAO) oxidases contribute to the production of H_2O_2 (Steps 16 and 17). Catalases ensure that excess H_2O_2 is removed by converting it to water and oxygen (Step 18). Expansins/swollenins (SWO) are believed to loosen the plant cell wall structure to make it more amorphous (step 19), but their mode of action remains unknown. Note that the stoichiometry for each reaction is not taken into account.

Other auxiliary enzymes involved in deconstruction of lignocellulosic biomass are the AA3, AA5, and AA7 oxidases in the glucose-methanol-choline oxidoreductase

superfamily, the copper radical oxidase (CRO) family, and the glucooligosaccharide oxidase family, respectively (Bissaro et al., 2018b). The glucose-methanol-choline oxidases are flavin-dependent enzymes that oxidize sugars and alcohols with corresponding reduction of O_2 to H_2O_2, while copper radical oxidases use copper as their redox cofactor to oxidize galactose, glyoxal, and primary alcohols with concomitant production of H_2O_2 from O_2 (Bissaro et al., 2018b; Levasseur et al., 2013). The flavin-dependent glucooligosaccharide oxidases are enzymes that catalyze the oxidation of the C1-hydroxyl group at the reducing end of a wide range of sugars using O_2 as an electron acceptor, resulting in H_2O_2 generation. The AA7 family recently experienced an expansion in terms of accepted substrates through a study that more than doubled the number of characterized family members (Haddad Momeni et al., 2021). Since these enzymes generate H_2O_2 their activity may affect the activity of other enzymes involved in biomass conversion such as lignin peroxidases and LPMOs (**Fig. 5**; section 1.3) (Bissaro et al., 2017, 2018b; Haddad Momeni et al., 2021; Kracher et al., 2020; Manavalan et al., 2021).

Class AA4 contains flavin-dependent vanillyl-alcohol oxidases, which are intracellular enzymes that metabolize lignin-derived aromatic alcohols and are, thus, important for a microorganism's ability to use lignocellulosic biomass as an energy source (Fraaije et al., 1997, 1998). Another class of intracellular enzymes involved in degrading aromatic compounds comprises the flavin-dependent 1,4-benzoquinone reductases in the AA6 family, which are involved in redox cycling of quinones (Levasseur et al., 2013). The AA8 family contains cytochrome domains involved in electron transport. Their ability to reduce ferric iron has led to speculations regarding a possible role in Fenton chemistry employed by brown-rot fungi to break down plant cell walls (Eastwood et al., 2011). Cellobiose dehydrogenase contains an AA3 domain and an AA8 domain, where the latter facilitates reoxidation of the AA3 domain by channeling electrons to an acceptor. One possible group of acceptors comprises the LPMOs, which are known to be reduced by cellobiose dehydrogenase (Kracher et al., 2016a) (**Fig. 5**). Indeed, physical interaction between the AA8 domain and LPMOs has been demonstrated (Courtade et al., 2016; Tan et al., 2015).

The pyrroloquinoline quinone (PQQ)-dependent pyranose dehydrogenase (PDH) from *Coprinopsis cinerea* (*Cc*PDH) forms the basis for the AA12 family (Matsumura et al., 2014). *Cc*PDH is secreted as a three domain protein composed of an N-terminal AA8 cytochrome domain and a C-terminal carbohydrate binding module with an AA12 PQQ-dependent dehydrogenase domain in between, and represents the only characterized member of this family (Matsumura et al., 2014). Like cellobiose dehydrogenase, pyranose dehydrogenase can fuel LPMO reactions (Várnai et al., 2018).

Reactive oxygen species can be generated by a number of enzymes during decomposition of lignocellulosic biomass and there is a need to minimize the potential for oxidative damage by these reactive oxygens. Catalases represent one way to limit the overall accumulation of H_2O_2 as these enzymes catalyze the disproportionation of H_2O_2 into O_2 and H_2O, and their activity is sometimes referred to as a "housekeeping activity" (Bissaro et al., 2018b). Catalases are highly effective at decomposing H_2O_2, but their affinity for H_2O_2 is in the mM range, i.e., orders of magnitude weaker compared to for instance peroxidases and LPMOs (Bissaro et al., 2018b). Superoxide dismutase (SOD) is another important enzyme, since it catalyzes the dismutation of $2O_2^{\bullet-}$ into O_2 and H_2O_2 (Fridovich, 1995). SOD removes one reactive oxygen species and produces another, meaning that its role is more complex than that of catalase. Adding to the complexity, Mn-dependent SODs from *Sphingobacterium sp*. T2 have been shown to catalyze aryl-C_α and C_α-C_β bond cleavage as well as O-demethylation in lignin, possibly due to SOD-generated hydroxyl radicals that react with lignin (Rashid et al., 2018).

1.2.2 Degradation of recalcitrant biomass by secreted enzymes

Deconstructing lignocellulosic biomass requires a multitude of enzymes to deal with the various components of the plant cell wall (**Fig. 5**). The crystalline nature of cellulose microfibrils makes them highly resistant to degradation, but bacteria and fungi have developed enzymatic cocktails capable of converting cellulose to glucose units. Secreted enzymes come as single catalytic domains or may contain additional domains such as a carbohydrate-binding module.

Endo-active cellulases cleave bonds in the amorphous regions of cellulose, while exo-active cellulases cleave off cellobiose from either the reducing or the non-reducing end of the cellulose chains. The resulting cellobiose is converted to two glucose units by β-glucosidases (Glass et al., 2013). For long it was believed that cellulose degradation was the result of the synergistic action by exo- and endo-active cellulases and a β-glucosidase (Payne et al., 2015). This concept changed upon the discovery of LPMOs and their ability to attack the crystalline surfaces of insoluble cellulose to provide novel chain ends for the cellulases to attack (Horn et al., 2012).

Quite some fundamental insight into how various enzymes contribute to degradation of compounds such as cellulose has come from studies of the enzymatic degradation of chitin (**Fig. 6**). Chitin forms microfibrils similar to cellulose, and a typical enzymatic machinery used for chitin degradation contains enzymes with properties similar to those of the cellulases discussed above. Detailed studies of chitin degradation by *Serratia marcescens* have demonstrated that this bacterium secretes three active chitinases (Sørlie et al., 2020; Suzuki et al., 1998; Tuveng et al., 2017; Vaaje-Kolstad et

al., 2013): ChiA and ChiB are exo-active enzymes acting from the reducing and non-reducing chain end, respectively, whereas ChiC is an endo-acting enzyme. In addition, *S. marcescens* produces a chitobiase, which serves the same role as β-glucosidases, and an LPMO, known as CBP21 or *Sm*AA10A (Vaaje-Kolstad *et al.*, 2013).

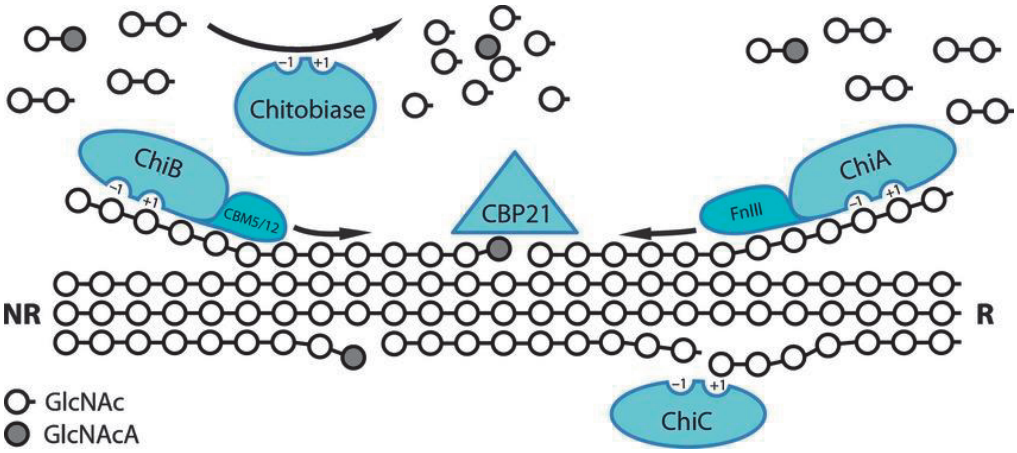

Fig 6. Chitin degradation by chitinolytic enzymes from *Serratia marcescens* as a model system to understand enzymatic degradation of recalcitrant polysaccharides. The chitin polymer is shown as tightly packed chains of GlcNAc (open circles). Two exo-active chitinases, ChiA and ChiB, depolymerize the chitin chain from the reducing and non-reducing chain end, respectively, while the endo-active chitinase, ChiC, acts on amorphous, i.e., non-crystalline, parts of the chitin polymer. The LPMO, CBP21 or *Sm*AA10A, oxidatively cleaves the glycosidic bonds on the chitin surface yielding aldonic acids (GlcNAcA; gray circles). The cuts in the chitin surface performed by *Sm*AA10A provide new chain ends for the chitinases. Chitobiose is converted to monomers by chitobiase. Note that ChiC has two additional domains, likely involved in substrate binding, which are not displayed. The figure was taken from Vaaje-Kolstad et al. (Vaaje-Kolstad et al., 2013).

1.3 Lytic polysaccharide monooxygenases

1.3.1 History and classification

In 1950, Reese et al postulated that biological solubilization of crystalline cellulose is a two-step process in which the first step, referred to as C_1, converts crystalline cellulose to a more accessible substrate from which soluble sugars are released in a second step, referred to as C_X (Reese et al., 1950). In 1974 it was shown that enzymatic cellulose solubilization was more efficient under aerobic conditions compared to anaerobic conditions, suggesting that a redox enzyme whose activity would remain unknown for more than three decades was important for enhanced cellulose solubilization (Eriksson et al., 1974). In 2005, biological solubilization of chitin by chitinases was shown to be boosted by a small protein named chitin-binding protein 21 (CBP21; now *Sm*AA10A) (Vaaje-Kolstad et al., 2005b, 2005a). The only known functional property of this protein until 2005 was binding of chitin (Suzuki et al., 1998). At the time, CBP21 was classified as a CBM33 and the 2005 publication considered the protein "non-catalytic", despite its now proven ability to boost chitinase activity (Vaaje-Kolstad et al., 2005a). Importantly, the authors of the 2005 paper concluded that CBP21 seemed to catalyze the "C_1" step in the C_1C_x process postulated by Reese et al. in 1950.

It would take another five years to discover that *Sm*AA10A (CBP21) was in fact an enzyme catalyzing oxidative cleavage of glycosidic bonds in crystalline chitin (Vaaje-Kolstad et al., 2010). One key observation leading to this discovery was that incubation of chitin with CBP21 and a reductant, in the presence of O_2, led to release of soluble oxidized chito-oligosaccharides into solution. Thus, it was concluded, that CBP21 carries out a monooxygenase reaction ($R\text{-}H + 2e^- + 2H^+ + O_2 \rightarrow R\text{-}OH + H_2O$) fueled by externally delivered electrons and using O_2 as the oxidant. A CBM33 from *Streptomyces coelicolor* (*Sc*AA10C) was shortly after demonstrated to oxidize cellulose (Forsberg et al., 2011). Structural similarities between CBM33s and GH61s had been reported in 2008 (Karkehabadi et al., 2008) and boosting effects of GH61s on cellulose solubilization by cellulases had also been reported (Harris et al., 2010; Merino et al., 2007). Accordingly, oxidative cleavage of cellulose by GH61 proteins was demonstrated in 2011 for GH61s from *Thermoascus aurantiacus* (*Ta*AA9A) (Quinlan et al., 2011), *Phanaerochete chrysosporium* (*Pc*AA9D) (Westereng et al., 2011), and *Neurospora crassa* (*Nc*AA9D, *Nc*AA9E, and *Nc*AA9M) (Phillips et al., 2011).

LPMOs are found in all domains of life and are important for biomass degrading organisms such as wood-rotting fungi and chitin-degrading bacteria. Initially, LPMOs were classified as carbohydrate binding modules (CBM33s) and glycoside hydrolases (GH61s) in the CAZy database but upon discovery of their catalytic activity, they were reclassified as auxiliary activities belonging to family AA9, for GH61s, and family AA10,

for CBM33s (Levasseur et al., 2013). Today, LPMOs are found in families AA9-11 and 13-17 with more than 10 000 entries in total, of which more than 80 were functionally characterized at the time of writing (April 2022). AA9s are of fungal origin and have activity on cellulose and various hemicelluloses, while AA10s are primarily of bacterial origin and active on chitin and/or cellulose. Families AA11 (Hemsworth et al., 2014) and AA13 (Vu et al., 2014) contain chitin- and starch-active fungal LPMOs, respectively. More recent additions to the LPMO families include AA14 LPMOs from white-rot and brown-rot basidiomycetes that are active on xylan coated cellulose fibrils (Couturier et al., 2018), AA15 LPMOs from insects that are active on chitin and cellulose (Sabbadin et al., 2018), AA16 LPMOs of fungal origin that are active on cellulose (Filiatrault-Chastel et al., 2019), and AA17 LPMOs, which are found in oomycetes where they oxidatively cleave pectin, thus contributing to the infectivity of these plant pathogens (Sabbadin et al., 2021). Since the discovery of LPMOs and their importance for biomass turnover, additional (potential) biological roles of these enzymes have emerged, related to bacterial pathogenicity (Askarian et al., 2021; Paspaliari et al., 2015), arthropod development (Sabbadin et al., 2018), plant infection (Sabbadin et al., 2021), fungal allorecognition (Gonçalves et al., 2019), fungal development (Rieder et al., 2021a), and bacterial cell wall remodeling (Zhong et al., 2022).

1.3.2 LPMO structure

LPMOs are characterized by a conserved β-strand core and a substrate binding surface with a solvent-exposed copper active (**Fig 7**). The core of the protein is made up of an immunoglobulin-like β-sandwich consisting of two β-sheets with seven to nine β-strands in total. The loops and helices connecting these β-strands provide structural variability (Tandrup et al., 2018). These connecting loops and helices help shape the substrate binding surface and as such contribute to substrate recognition, binding, and positioning. The substrate-binding surfaces of cellulose- and chitin-active LPMOs tend to be rather flat (**Fig. 7**) and thus seem perfectly tailored for interacting with crystalline polysaccharide surfaces.

LPMOs acting on the β-(1,4) glycosidic bonds in chitin and cellulose may oxidize C1 or C4, resulting in the formation of a lactone and a 4-keto sugar, respectively, which are in equilibrium with their hydrated forms, an aldonic acid and a gemdiol (**Fig. 8**). All known chitin-active LPMOs are strict C1-oxidizers while cellulose-active LPMOs perform oxidation on the C1 or the C4, or produce mixtures of C1- and C4-oxidized products. Fungi tend to produce many LPMOs and these may have varying properties. For example, *Neuorospora crassa*, *Myceliophthora thermophila*, and *Podospora anserina* all produce a variety of LPMOs including C1, C4, and C1/C4-oxidizing cellulose-active LPMOs (Frommhagen et al., 2018). To add to the complexity, a recent study reported generation of C4/C6 double oxidized cello-oligosaccharides by C1/C4 and C4-oxidizing

AA9s, whereas strict C1-oxidizing AA9s did not show this feature (Sun et al., 2022). It remains unclear whether C6 oxidation is productive, in the sense that it contributes to, or is a direct consequence of, chain cleavage. Although several LPMO structures have been published and the substrate specificities of even more LPMOs have been investigated, the structural determinants for LPMO substrate specificity and oxidative regioselectivity remain largely elusive (Danneels et al., 2019; Forsberg et al., 2018).

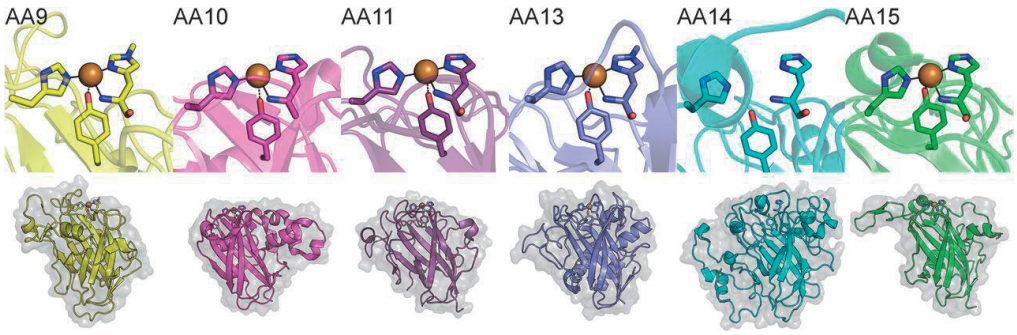

Fig. 7. Surface topology and active site configuration of LPMOs from various families. The figure shows the copper coordinating histidine brace and the buried axial tyrosine residue using a stick representation for LPMOs belonging to families AA9-11 and AA13-15. Note that for fungal LPMOs, the N-terminal histidine may carry a methylation as visible for the shown AA9 and AA13. For most AA10s, a phenylalanine residue replaces the tyrosine in the proximal axial position. The crystal structure of the AA14 shown in this figure was solved without copper, but EPR analysis has confirmed that this LPMO binds copper. The copper ion is represented by an orange sphere. PDB ID codes for the LPMOs represented in this figure are 5ACH (AA9), 5OPF (AA10), 4MAI (AA11), 4OPB (AA13), 5NO7 (AA14), and 5MSX (AA15). This figure was taken from Tandrup et al. (Tandrup et al., 2018).

Copper is key to LPMOs and the copper coordinating histidine brace is fully conserved in all known catalytically active LPMOs. The histidine brace consists of two histidines one of which is always the N-terminal histidine and copper is bound in an overall T-shaped configuration (**Fig. 7**) (Ciano et al., 2018; Quinlan et al., 2011). Copper binding is achieved through the NH_2-group and a nitrogen atom of the imidazole side chain of the N-terminal histidine and a nitrogen atom from the imidazole side chain of the second histidine (Ciano et al., 2018; Quinlan et al., 2011). Interestingly, Aachmann et al. showed that Cu(I) is more tightly bound than Cu(II) by an AA10 LPMO, which illustrates the potential of these enzymes to sequester and stabilize copper in its reduced, catalytically most active form (Aachmann et al., 2012).

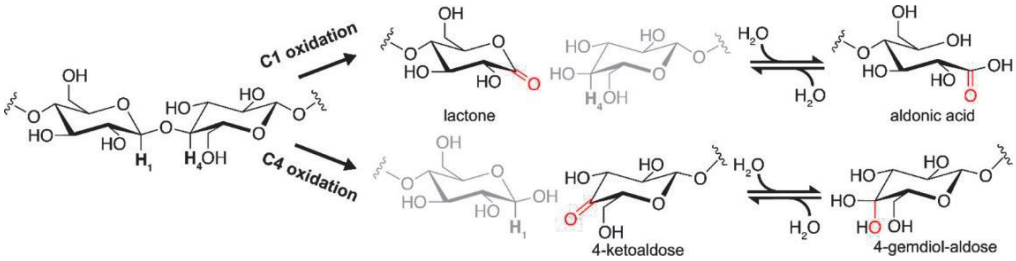

Fig. 8. LPMO-catalyzed oxidation of polysaccharides. The figure shows possible products generated upon LPMO-catalyzed oxidation of cellulose. The main oxidation products formed are a lactone or a 4-ketoaldose, which are in equilibrium with their hydrated aldonic acid and 4-gemdiol forms, respectively. This figure was taken from Chylenski et al. (Chylenski et al., 2019).

The histidine brace has also been observed in other proteins, such as particulate methane monooxygenase, pMMOs, (Koo et al., 2022), periplasmic copper binding proteins known as CopC (Udagedara et al., 2019), and fungal LPMO-like proteins referred to as X325 proteins. The latter proteins are not reduced by commonly used reductants such as ascorbate, nor do they cleave polysaccharides or produce H_2O_2 (a typical LPMO feature; see below) (Brander et al., 2020; Garcia-Santamarina et al., 2020; Labourel et al., 2020). In X325 proteins, the copper has an extra aspartate ligand which likely limits the redox activity of the bound copper (Garcia-Santamarina et al., 2020; Labourel et al., 2020).

The importance of the histidine brace for LPMO reactivity is well-established and represents the primary coordination sphere (**Fig. 7&9**). LPMOs show additional semi-conserved features close to the copper site in what may be referred to as the secondary coordination sphere (**Fig. 9**). The amino acids found in the secondary coordination sphere form a hydrogen bonding network around the histidine brace and mutagenesis studies have demonstrated the vital roles of several of these residues (Bissaro et al., 2020b; Harris et al., 2010; Loose et al., 2018; Span et al., 2017; Vaaje-Kolstad et al., 2005b). Key second sphere amino acid residues include a tyrosine or phenylalanine in a buried position axial to the copper (Phe219/Tyr171 in **Fig. 9**) and a glutamate or glutamine approximately 5 Å from the copper ion (Glu217/Gln169 in **Fig. 9**)(Chylenski et al., 2019; Span et al., 2017; Vaaje-Kolstad et al., 2017). The proximal axial coordination position of the copper is usually occupied by a tyrosine in fungal LPMOs while most AA10s contain a phenylalanine in this position (Hemsworth et al., 2013; Munzone et al., 2020; Vaaje-Kolstad et al., 2017). Opposite the phenylalanine or tyrosine, in the distal axial coordination position, AA10s have a conserved alanine (**Fig. 9A**), although variations occur, believed to limit the interaction with copper from the solvent and seemingly limiting copper reactivity to the one single accessible equatorial site (Munzone et al., 2020). In AA9s this distal axial position seems more accessible (Li et al., 2012). One conspicuous second sphere residue in AA9 LPMOs is a conserved third

histidine residue at about 5 Å from the copper (His160; **Fig. 9B**). Like the conserved Glu/Gln mentioned above, this conserved His may play a role in catalysis, e.g., by channeling protons and/or positioning reactive oxygen species. The catalytic mechanism of LPMOs is discussed below.

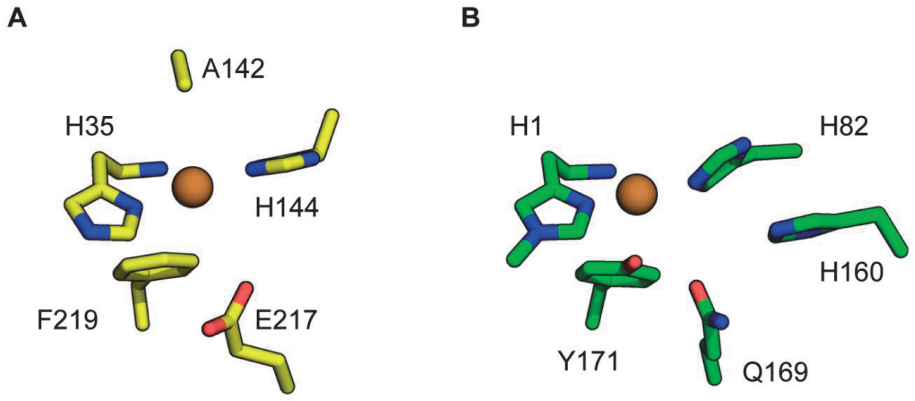

Fig. 9. Active site structural features of AA9s and AA10s. The figure shows the histidine brace and key secondary coordination sphere residues in AA9s and AA10s exemplified by the LPMO domains of *Sc*AA10C (PDB ID code 4OY7) (**A**) and *Nc*AA9M (PDB ID code 4EIS) (**B**). The copper ion is represented as a gold sphere. Note that *Nc*AA9M carries a methylation on the second nitrogen of the imidazole ring, a common post-translational modification in fungal AA9s.

1.3.3 The catalytic mechanism

In 2010, it was shown that the AA10A from *Serratia marcescens* in the presence of a reducing agent and molecular oxygen was able to oxidatively cleave glycosidic bonds in β-chitin, leading to the formation of aldonic acids (Vaaje-Kolstad et al., 2010). Experiments with radiolabeled $^{18}O_2$ in $H_2{}^{16}O$ and $^{16}O_2$ in $H_2{}^{18}O$ yielded aldonic acid products with a mass increase of +2 compared to reactions in $^{16}O/H_2{}^{16}O$ demonstrating that LPMOs use activated oxygen to oxidize chitin and that water is required to form the aldonic acid. Similar results were later shown for the cellulose-active AA9E from *Neurospora crassa* acting on amorphous cellulose (phosphoric acid-swollen cellulose, or PASC) (Beeson et al., 2012). Consequently, the LPMO reaction was described as a monooxygenase reaction, which implies that the enzyme requires two electrons, two protons, and molecular oxygen per catalytic cycle (**Fig. 10**).

The ability of LPMOs to activate O_2 leads to the generation of H_2O_2 in reactions lacking the substrate, i.e., reactions with only the LPMO and a reductant (Filandr et al., 2020; Kittl et al., 2012). The underlying mechanism for O_2-activation in the monooxygenase

reaction was investigated and it was suggested that the LPMO in its Cu(I)-state initially reduces O_2 to Cu(II)-superoxide, Cu(II)-$O_2^{\bullet-}$, and that further steps of electron and proton delivery lead to the formation of a copper-oxyl species, Cu(II)-$O^{\bullet}$ (**Fig. 10**) (Chylenski et al., 2019; S. Kim et al., 2014; Kjaergaard et al., 2014; B. Wang et al., 2019). This Cu-oxyl species is responsible for abstracting an H-atom from either the C_1 or C_4-position of the sugar to generate a Cu(II)-OH and the corresponding sugar radical onto which the OH rebounds to hydroxylate the sugar (Chylenski et al., 2019; S. Kim et al., 2014). This hydroxylation destabilizes the glycosidic bond and leads to spontaneous bond cleavage (Phillips et al., 2011). While computational work supports the occurrence of a productive monooxygenase reaction (Kjaergaard et al., 2014; B. Wang et al., 2019), experimental studies have shown that this reaction is slow (Bissaro et al., 2018b). Key questions related to how electrons and protons are delivered to the copper site of a substrate-bound LPMO in a timely manner remain elusive (Bissaro et al., 2018b).

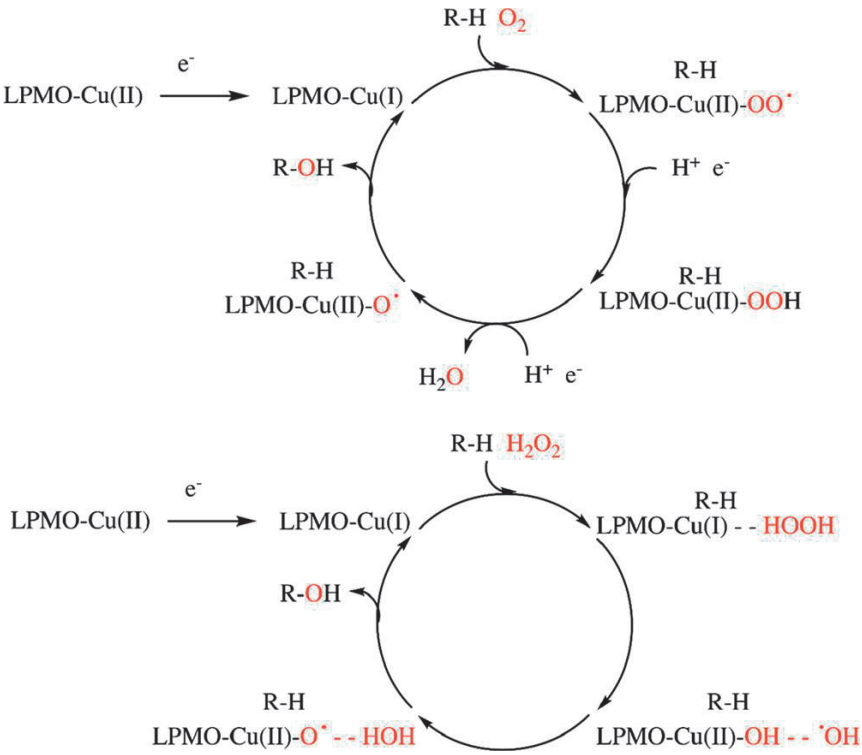

Fig. 10. LPMO reaction mechanism schemes. The figure shows the originally proposed monooxygenase reaction (upper) and the more recently proposed peroxygenase reaction (lower). Both reactions involve hydrogen atom abstraction from the substrate by the LPMO. Note that the upper reaction requires continuous and timely delivery of electrons and protons to the reaction center, whereas the lower reaction does not. The figure was taken from Chylenski et al. (Chylenski et al., 2019).

An elegant possible catalytic scenario explaining how LPMOs obtain the required reducing power and additional protons came when it was demonstrated that LPMOs can carry out peroxygenase reactions, which means that they use H_2O_2 rather than O_2 as co-substrate (**Fig. 10**) (Bissaro et al., 2017). Using competition experiments with $^{16}O_2$ and $H_2{}^{18}O_2$, Bissaro et al. showed that H_2O_2 is the preferred co-substrate. A subsequent study by Kuusk et al. on chitin degradation showed that the peroxygenase reaction is orders of magnitude faster than the monooxygenase reaction (Kuusk et al., 2018). The fact that H_2O_2 is the kinetically relevant co-substrate has since been confirmed in several studies carried out in different laboratories (Hangasky et al., 2018; Hedison et al., 2021; Jones et al., 2020; Kont et al., 2020; Kuusk et al., 2018, 2021; Rieder et al., 2021a, 2021b; Stepnov et al., 2021). Several reaction mechanisms were suggested along with the initial demonstration of peroxygenase activity, including mechanisms leading to the generation of a Cu-oxyl intermediate (Bissaro et al., 2017).

The discovery of the peroxygenase activity of LPMOs sparked a new round of modelling efforts to elucidate the reaction mechanism (**Fig. 10**). The first computational investigation of LPMO catalysis with H_2O_2 in presence of a polysaccharide substrate showed homolytic cleavage of H_2O_2 by the LPMO-Cu(I) to form a hydroxyl radical and a Cu(II)-OH. The hydroxyl radical does not abstract an H-atom from the substrate but rather abstracts an H-atom from the copper hydroxyl, resulting in the formation of water and a Cu(II)-O$^{\bullet}$ species that abstracts the hydrogen atom from the polysaccharide substrate (B. Wang et al., 2018). Wang and colleagues pointed out that both LPMO side chains and the bound substrate help in stabilizing and confining the hydroxyl radical, thus ensuring that the reaction is productive and avoiding oxidative damage to the active site (B. Wang et al., 2018). The results of this computational study are in perfect alignment with what was shown and suggested by Bissaro and co-workers in 2017, when they first described the peroxygenase activity of LPMOs. The same reactive intermediates as suggested by Wang et al. were also reported by Hedegård and Ryde using the same LPMO-substrate model. These authors analyzed both possible reaction scenarios, monooxygenase and peroxygenase, and showed that the reactive oxygen intermediate state is the same for both reactions, and that H-atom abstraction from the substrate by Cu-oxyl and from the Cu-hydroxyl are thermodynamically favorable (Hedegård et al., 2018). Using a more experimental approach, Jones and colleagues confirmed homolytic cleavage of H_2O_2 in productive LPMO reactions (Jones et al., 2020).

Based on a combination of experimental and computational work, Bissaro et al. presented a molecular mechanism for the chitinolytic peroxygenase reaction spanning from initial reduction of the copper site to substrate dissociation after catalysis (**Fig. 11**) (Bissaro et al., 2020b). This study showed that the two main barriers the enzyme must overcome to oxidize its substrate are cleaving H_2O_2 and abstraction of an H-atom from the substrate (see steps 4 and 6 in **Fig. 11**) (Bissaro et al., 2020b). Furthermore,

the results showed that the highly conserved second sphere residue Glu60 plays a crucial role in the ternary complex formed between the LPMO, the substrate, and H_2O_2. Bissaro et al. showed that hydrogen bonding interactions involving Glu60 help positioning and distorting bound H_2O_2 and thus facilitate homolytic cleavage. Glu60 also seems to help positioning the formed hydroxyl radical such that the Cu(II)-O$^{\bullet}$ reactive species is generated, while non-productive reactions are avoided. Figure 11 further shows how the Cu(II)-O$^{\bullet}$ species abstracts an H-atom from the sugar, after which the hydroxyl rebounds to the sugar, resulting in hydroxylation. Importantly, after the LPMO has made one cut in the substrate it is returned to the reduced Cu(I)-state and is ready to perform another catalytic cycle. This implies that the peroxygenase reaction requires priming, rather than stoichiometric amounts of reductant. Indeed, several studies have shown that a reduced LPMO presented with a polysaccharide substrate and H_2O_2 can perform multiple cuts before it needs to be re-reduced (Hedison et al., 2021; Kuusk et al., 2019; Müller et al., 2018; Rieder et al., 2021b).

The highly conserved Glu60 has been referred to as a "gatekeeping" residue that confines the active site in the enzyme-substrate complex and limits access of small molecules to the active site cavity of a substrate-bound LPMO (Bissaro et al., 2018a, 2020b). This residue is a glutamine for all LPMOs, except for cellulose- and chitin-active C1-oxidizing AA10s, and chitin-active AA11s, where it is a glutamate (Vaaje-Kolstad et al., 2017). Prior to assigning a function to this residue, several studies had indicated its essential role in catalysis as mutating this glutamate/glutamine residue led to a marked decrease in activity for both AA9s and AA10s (Harris et al., 2010; Loose et al., 2018; Span et al., 2017; Vaaje-Kolstad et al., 2005b). The first glimpse of the role of this glutamate/glutamine residue came from a model of *Sm*AA10A bound to crystalline chitin, which revealed the existence of a solvent-filled narrow tunnel connecting the copper site to the bulk solvent (Bissaro et al., 2018a). This tunnel would allow the passage of small molecules such as water, molecular oxygen, superoxide, and hydrogen peroxide, while larger molecules such as ascorbic acid (AscA) and phenolic compounds, which are commonly used as reducing agents for LPMOs, would be to too large to pass (Bissaro et al., 2018a). This potential gate keeping function comes in addition to the role played by Glu60 in positioning and controlling the H_2O_2 molecule and the hydroxyl radical, as discussed above. Indeed, Bissaro and coworkers showed that mutation of Glu60 not only leads to less activity but also to more oxidative damage to the LPMO, which is compatible with the hydroxyl radical being less controlled and more prone to engaging in damaging off pathway reactions (Bissaro et al., 2020b).

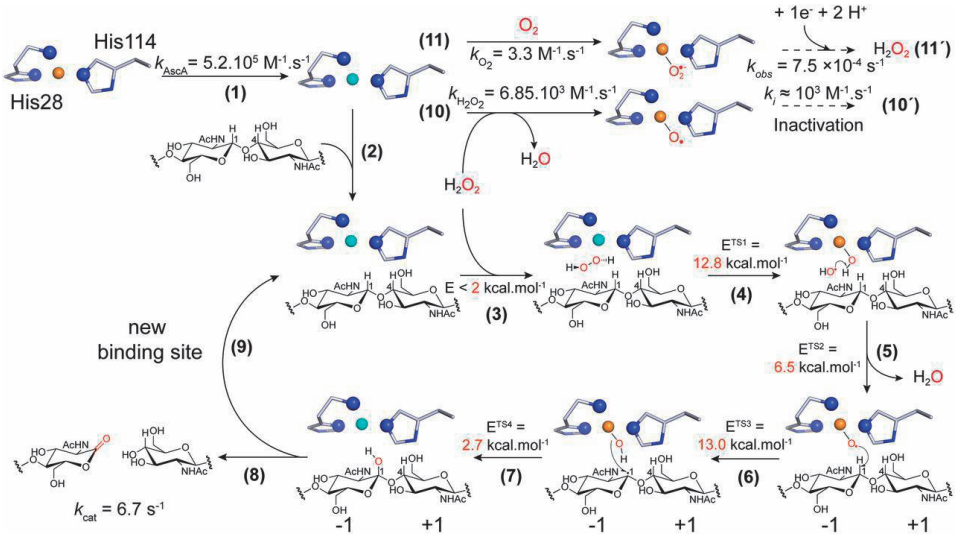

Fig. 11. Proposed LPMO peroxygenase reaction mechanism. The figure shows a proposed peroxygenase reaction mechanism starting with reduction of the copper center (step 1), binding of the polysaccharide substrate (step 2) and H_2O_2 entering the reaction cavity (step 3) and moving towards hydroxylation of the glycosidic bond and the enzyme dissociating from the substrate (steps 4-9). The LPMO-Cu(II) resting state is indicated by a gold-colored copper ion whereas the copper ion is colored cyan in the LPMO-Cu(I) active state. Step 4 represents the first of the two main energy barriers the enzyme must overcome during catalysis and involves homolytic cleavage of H_2O_2 to yield a Cu(II)-OH and a hydroxyl radical. The hydroxyl radical reacts with Cu(II)-OH to generate a Cu(II)-O$^\bullet$ species and a water molecule (step 5). The Cu(II)-O$^\bullet$ species abstracts a hydrogen atom from the substrate generating a sugar radical (step 6), which is the second energy barrier the enzyme must overcome during catalysis. The copper bound hydroxyl rebounds to hydroxylate the sugar leaving the LPMO in its active Cu(I)-state (step 7). The hydroxylation of the sugar leads to an elimination reaction inducing cleavage of the glycosidic bond and the LPMO-Cu(I) dissociates from the substrate (step 8). It is still unknown if the enzyme dissociates from its substrate before or after glycosidic bond cleavage. The LPMO-Cu(I) can bind to a new binding site and enter a new catalytic cycle (step 9). In absence of substrate, the LPMO-Cu(I) may react with H_2O_2 (step 10) which ultimately leads to oxidative damage and inactivation (Step 10'), or it may react with O_2 (step 11) in a reaction that leads to H_2O_2 production (Step 11'). The rates reported for step 1, 10, and 11 were determined experimentally in (Bissaro et al., 2020b), while the rates pertaining to step 10' and 11' were reported in (Kuusk et al., 2018) and (Bissaro et al., 2018b), respectively. The energies associated with steps 3-7 were determined by computational studies. The figure was taken from Bissaro et al. (Bissaro et al., 2020b).

Next to a glutamine (analogous to Glu60 in AA10s), AA9 LPMOs contain a conserved second sphere histidine residue (**Fig. 9**). The role of this glutamine and histidine and the interplay between these two residues, for example in controlling access to the active site and positioning and confining the various oxygen species, is of great interest, as is a comparison of the "Glu-arrangement" in AA10s with the "Gln-His-arrangement" in AA9s. Mutational studies have shown that both the Gln and the His are important for AA9 activity (Span et al., 2017), whereas structural studies suggest that the His may interact with the oxygen substrate (O'Dell et al., 2017).

While there now is overwhelming evidence that LPMOs are peroxygenases rather than monooxygenases, the issue remains debated in the field. One question is whether the monooxygenase reaction takes place at all. A remarkable feature of LPMOs and their solvent-exposed copper site is the ability to interact with a variety of electron donors. Reductants able to promote LPMO activity range from superoxide radicals (Bissaro et al., 2017, 2020a) via small molecular weight compounds such as AscA, gallic acid, and cysteine (Frommhagen et al., 2016; Kracher et al., 2016b; Rieder et al., 2021b; Stepnov et al., 2021, 2022a), to lignin (Paper II of this thesis; Hu et al., 2014; Muraleedharan et al., 2018; Rodríguez-Zúñiga et al., 2015; Westereng et al., 2015). The type of reductant strongly influences LPMO catalytic rates (Frommhagen et al., 2016, 2017; Kracher et al., 2016b; Rieder et al., 2021b; Stepnov et al., 2021, 2022a), despite the fact that the one-electron reduction of a resting LPMO is a very fast process (Kracher et al., 2016b). The influence of reductant of LPMO catalysis could relate to delivery of the second electron (in a monooxygenase scenario) or to the system's (i.e., reductant and LPMO together) ability to generate H_2O_2, as suggested more recently. Recent work by Stepnov et al. shows a clear correlation between LPMO activity and the system's ability to generate H_2O_2 *in situ* under apparent monooxygenase reaction conditions, indicating that the apparent monooxygenase reactions are in fact peroxygenase reactions limited by the system's ability to generate H_2O_2 (Stepnov et al., 2021, 2022b, 2022a).

1.4 Photobiocatalysis

Nature has developed exquisite photobiocatalytic reaction systems that enable photosynthetic organisms to harvest solar energy and use photons to carry out a highly demanding water splitting reaction. Photosynthesis provides Nature with an unlimited supply of reducing equivalents (i.e., electrons) to generate chemical energy in the form of NADPH and ATP, with molecular oxygen, O_2, as a by-product (**Fig. 12**). The chemical energy derived from sunlight is further used to convert CO_2 into glucose. The concomitant generation of O_2 has resulted in an oxygen rich atmosphere and has had dramatic consequences for the development of life on Earth, as the efficiency of cellular metabolism is increased by approximately 20-fold for aerobic respiration compared to anaerobic respiration (Barber, 2016).

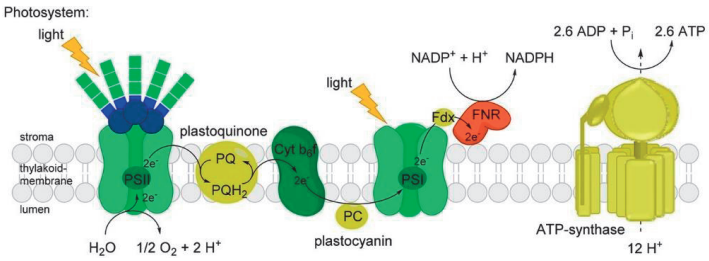

Figure 12. Photosystem I and II. The figure shows how photosystem II (PS II) and I (PS I) act together in photosynthesis whereby PS II oxidizes water when irradiated and the photoexcited electrons are relayed via redox cofactors to PS I where the electrons are transferred via ferredoxin (Fdx) to ferredoxin-NAD^+ reductase (FNR) and used to generate NADPH. The proton gradient generated as a result of this electron transfer process is a driving force for ATP synthesis by ATP synthase. This figure was adapted from Schmermund et al. (Schmermund et al., 2019).

Photosynthesis is carried out by two enzyme systems, photosystem (PS) I and II, that reside in the thylakoid membranes of photosynthetic organisms. PS I and PS II both harbor a pair of chlorophyll *a* molecules in their reaction centers that convert light energy into electrochemical energy. PS II absorbs visible light to generate a charge separation in the reaction center by exciting an electron thus leaving a hole. The resulting hole is a powerful oxidizing agent capable of driving the oxidation of $2H_2O$ to O_2, which generates $4e^-$ and $4H^+$. Excited electrons from chlorophyll *a* are channeled from PS II via pheophytins to plastoquinone (PQ). Reduction of plastoquinone (PQ) results in formation of plastoquinol (PQ^{2-}), which is protonated (PQH_2) by protons from the stroma. The liberation of protons in the lumen following water oxidation combined with plastoquinol binding protons from the stroma creates a proton gradient across the thylakoid membrane that drives ATP synthesis by ATP synthase. The electrons and protons bound by reduced plastoquinone are further relayed to cytochrome b_6f. Cytochrome b_6f releases the protons to the lumen while at the same time transferring the electrons to PS I via plastocyanin (Chitnis, 2001). Similar to PS II, upon light

exposure PS I absorbs a photon to generate a charge separation in the reaction center. The hole vacated by the excited electron in PS I is filled by an electron delivered from plastocyanin. The excited electron is relayed via redox centers in a redox chain ending at reduction of ferredoxin. Reduced ferredoxin is a powerful reductant that is involved in various metabolic reactions including NADPH production (Chitnis, 2001; Schmermund et al., 2019). After billions of years of evolution, Nature has left us with a single blueprint for photosynthetic water splitting, which continues to inspire development of photocatalysts today.

Photobiocatalysis aims to couple biocatalysis and photocatalysis to expand the reaction spectrum of enzymes or make use of light as a reactant in biocatalytic reactions (Bonfield et al., 2020; Lee et al., 2018; Romero et al., 2016; Schmermund et al., 2019). Such an approach requires a photoredox catalyst that absorbs light from the UV and/or visible part of the spectrum in such a manner that the absorbed photon promotes an electron from its ground state to a higher energy level excited state (Lee et al., 2018; Romero et al., 2016). In keeping with the terminology proposed by Romero and Nicewicz, the term photoredox catalyst describes a catalyst with the ability to participate in redox reactions in the excited state whereas a photosensitizer transfers energy (Romero et al., 2016). In their excited state, photoredox catalysts act as strong reducing or oxidizing agents. Photoinduced excitation of an electron generates a hole that is usually filled at the expense of a sacrificial electron donor (e.g., AscA, triethanolamine, ethylenediaminetetraacetic acid, or H_2O). The photoexcited electron can be transferred directly or indirectly, via mediators, to the redox center of oxidoreductases, or used to photochemically regenerate (reduce) an enzyme's co-factor (Lee et al., 2018; Schmermund et al., 2019). Most often a photoredox catalyst serves as a source of excited electrons promoting a subsequent biocatalytic step (**Fig. 13**) as indicated by numerous studies that report fueling the activity of reducing-equivalent-dependent redox enzymes with irradiated photoredox catalysts (Mifsud et al., 2014; van Schie et al., 2019b; Willot et al., 2019; W. Zhang et al., 2018). Of note, it has been shown that irradiating a nicotinamide-dependent ketoreductase, enzymes that reduce ketones to enantiomerically pure alcohols, with blue light enables the ketoreductase to convert racemic halolactones via an intermediate radical to chiral lactones, a reaction that does not occur in absence of light (Emmanuel et al., 2016). This shows that photobiocatalysis not only facilitates the harvesting of sunlight to generate reducing equivalents but can also enable new enzyme reactivities.

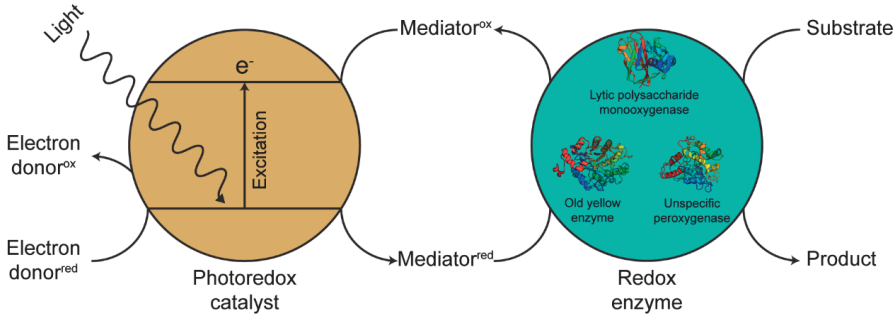

Figure 13. Photocatalytic generation of redox equivalents for oxidoreductases. The figure shows how a photoredox catalyst promotes an electron to a higher energy level upon absorbing a photon (hν), which makes the photoredox catalyst a strong reductant. An oxidized mediator accepts the electron from the photoredox catalyst and becomes reduced. The reduced mediator transfers the reducing equivalent to a redox enzyme which can then catalyze a redox reaction. Promotion and transfer of an electron from the photoredox catalyst to the mediator leaves a hole that is filled by an electron donor, often referred to as sacrificial electron donor. The structures of three different redox enzymes for which enzymatic activity has been demonstrated using a photoredox catalyst are shown as examples. These include the flavin-dependent old yellow enzyme from *Thermus scotoductus* (PDB ID: 3HGJ), the copper-dependent lytic polysaccharide AA10A from *Serratia marcescens* (PDB ID: 2BEM), and the heme-dependent unspecific peroxygenase from *Agrocybe aegerita* (PDB ID: 2YOR).

Direct electron transfer of an excited electron from the photoredox catalyst to the redox center of an enzyme represents an attractive scenario as the intermediate steps required in indirect transfer, involving mediator and/or cofactor (re-)generation, would no longer be required, which would make the catalytic process simpler and more cost-effective (Lee et al., 2018). Poor electron transfer kinetics, indirectly to mediators or directly to the enzyme, the possible generation of highly reactive ''off-pathway'' intermediates, and bleaching of the photoredox catalyst all limit the efficiency of photochemical activation of enzymes (Schmermund et al., 2019). The most common off-pathway intermediates would be reactive oxygen species, such as superoxide and hydrogen peroxide, and radicals resulting from oxidation of the sacrificial electron donor. As long as the photocatalytic generation of reducing equivalents relies on organic molecules as sacrificial electron donors, instead of water, the cost of this donor and of handling unwanted by-products formed upon oxidation of this donor need to be taken into account. The issues mentioned above can be mitigated by tuning the photoredox catalyst to use water as sacrificial electron donor, or enhance electron transfer to the enzyme, or by evolving the enzymes to more readily accept electrons from the photoredox catalyst, e.g. by engineering affinity for the catalyst in or near the enzyme's redox center (Schmermund et al., 2019).

Light-dependent regeneration of flavin and nicotinamide cofactors has been demonstrated for several enzymes (J. Kim et al., 2019; Lee et al., 2013; Mifsud et al., 2014; van Schie et al., 2019a), but common to all is their sensitivity to reactive oxygen

species, which are easily produced by photoredox catalysts under aerobic conditions, as O_2 readily accepts photoexcited electrons. As a consequence of the latter, enzymes that can utilize the products generated by oxygen reduction, i.e., superoxide radicals or hydrogen peroxide, represent interesting candidates for photobiocatalytic applications. One example of such enzymes are the unspecific peroxygenases (UPOs), which represent a promising alternative to the well-known cytochrome P450 monooxygenases for oxyfunctionalization reactions, such as hydroxylation of ethylbenzene to phenylethanol (Hofrichter et al., 2014; Y. Wang et al., 2017). UPOs harbor a heme prosthetic group and use H_2O_2 as oxidant. In the presence of high levels of H_2O_2 the heme group can suffer oxidative damage and, therefore, several methods for controlled *in situ* generation of H_2O_2 from O_2 have been explored, including the use of photoredox catalysts (van Schie et al., 2019b; Willot et al., 2019; W. Zhang et al., 2018). It has been shown that, compared to an initial addition or serial additions of diluted H_2O_2 solutions, *in situ* photochemical generation of H_2O_2 allows improved fine-tuning of H_2O_2 levels, thus enhancing enzyme operational stability and product yields. The LPMOs, which are monocopper enzymes (section 1.3), are another example.

1.4.1 Light-driven LPMO reactions

The first two studies that demonstrated light-driven LPMO activity were reported in 2016, when LPMOs were considered monooxygenases, and showed that two completely different photoredox catalysts were able to fuel LPMOs from families AA9 and AA10. In the first study, a combination of AscA or organosolv lignin as reductant (i.e., sacrificial electron donors) and chlorophyllin as photoredox catalyst was shown to increase the activity of the AA9E from *Thielavia terrestris* on amorphous cellulose by a 100-fold compared to reactions under standard monooxygenase conditions (Cannella et al., 2016). This landmark study showed that LPMOs could act much faster than previously assumed. The authors hypothesized that the two orders of magnitude increase in activity was due to photoexcited electrons originating from chlorophyllin that would be more efficient in driving the LPMO reaction compared to the non-excited electrons from regular reductants, while AscA was thought to regenerate chlorophyllin (Cannella et al., 2016). Later in 2016, this explanation for the spectacular increase in LPMO activity was questioned in a study that suggested that H_2O_2 generation by a combination of light-exposed chlorophyllin and reductant could be driving the reaction (Bissaro et al., 2016b). In a follow-up study it was shown that, under the reaction conditions used by Cannella et al., neither SOD nor catalase limited LPMO activity, which led the authors to conclude that reactive oxygen species were not the driving force for LPMO activity in this system, reinforcing the idea that photoexcited electrons were the most likely culprit for the high LPMO activity (Möllers et al., 2017).

In the second 2016 study showing light-driven LPMO activity, vanadium-doped titanium dioxide (V-TiO_2) was used as photocatalyst to (putatively) fuel the AA10C from *Streptomyces coelicolor* with reducing equivalents derived from splitting water and generating O_2 (Bissaro et al., 2016a). The reported catalytic activity was low compared to the activity for the chlorophyllin-driven reactions (Cannella et al., 2016), but did not require addition of extra reducing equivalents such as AscA. This study comprised the first demonstration of mediator-free electron transfer from a photocatalyst to the redox center of the enzyme (Bissaro et al., 2016a).

Paper I of this thesis (Bissaro et al., 2020a) presents an analysis of both these light-driven LPMO reactions, and sheds light on the underlying mechanisms. The work described in Paper I, which includes work described in (Bissaro et al., 2016b), leads to the conclusion that these light-driven reaction systems most likely work because the more efficient LPMO co-substrate, H_2O_2, is generated *in situ*, in a light-dependent manner. There is no doubt that these initial studies on light-driven LPMO catalysis helped pave the way for a better understanding of LPMO catalytic activity.

Building on the 2016 findings by Cannella et al., Blossom et al. investigated the effect of intermittent illumination of a chlorophyllin-mediated *Tt*AA9E reaction, using AscA as electron donor and various cellulosic substrates differing in their degree of crystallinity. This study showed that it was possible to reduce light exposure and achieve similar product levels with less energy input (Blossom et al., 2020), making the perspective of light-driven LPMO catalysis even more attractive. To gain further insight into this photocatalytic system, time course experiments were conducted using cellulose nanofibrils, which showed that LPMO activity was rapidly arrested with continuous irradiation, while the LPMO remained active for a longer time in reactions with reduced light-exposure (Blossom et al., 2020). The authors noted that this effect could be caused by (too) high levels of light-generated H_2O_2 that cause oxidative damage to the enzyme, but concluded that the most likely reason for cessation of product formation was reductant depletion by excess production of H_2O_2 (Blossom et al., 2020). Recent work by Stepnov et al. (Stepnov et al., 2022b) shows that both scenarios likely play a role. The usefulness of using a combination of light, chlorophyllin, and AscA to drive LPMO reactions has been shown in several subsequent studies describing the biochemical characterization of novel AA9s (Higasi et al., 2021; Sepulchro et al., 2021).

The spectrum of photoredox catalysts was extended to chlorophyll when it was shown that exposure to light of reaction mixtures with AscA and water-soluble chlorophyll-binding proteins promoted *Tt*AA9E activity on PASC and allowed controlled delivery of H_2O_2 to the LPMO (Dodge et al., 2020). The authors pointed out that *Tt*AA9E activity appeared primarily AscA-driven when AscA was added initially or when the same total

amount of AscA was added as two successive additions, at the start and halfway through the reaction. However, when they repeatedly added a dilute AscA solution they saw a beneficial effect of light exposure on LPMO activity. Interestingly, the authors proposed a reaction scheme in which light-exposed protein-bound chlorophyll acts as a photosensitizer, and not as a photoredox catalyst, that transfers energy to molecular oxygen leading to formation of singlet oxygen, $^1O_2$, which in turn reacts with AscA to form H_2O_2 which the LPMO can use to oxidize cellulose (Dodge et al., 2020).

Biocatalytic photoelectrochemical platforms provide another promising approach for harvesting solar energy for biocatalytic applications (Lee et al., 2018). Such reaction systems allow for separation of the anodic and the cathodic reactions, where water oxidation and transfer of reducing equivalents to the enzyme take place, respectively (Lee et al., 2018). The advantage of separating these reactions lies in the possibility of optimizing the conditions for each reaction separately. Successful demonstration of LPMO activity towards chitin using a photoelectrochemical cell was reported for the AA10A from *B*. *thuringiensis*, using a quinone (2,6-dimethyl-1,4-benzoquinone) as electron relay between the electrode and the enzyme at alkaline pH (H. Zhang et al., 2020). Although the authors suggested that the LPMO activates oxygen to solubilize the chitin after the LPMO is reduced by the reduced quinone mediator, i.e., hydroquinone, at alkaline pH it is more likely that autooxidation of the hydroquinone (Huynh et al., 2016; Song et al., 2010) was responsible for generating the H_2O_2 required for catalytic activity, as recently shown by Stepnov and co-workers for other reductants (Stepnov et al., 2021, 2022a).

It is noteworthy that the natural substrates of LPMOs contain aromatic compounds, such as lignin in plant cell walls (**Fig. 3**) and catecholamines in insect cuticles (**Fig. 4**), that are redox active and light sensitive. This raises questions as to if and how light may influence LPMO solubilization of cellulose and chitin in the presence of these aromatic compounds. These issues are explored in Paper II and Paper III of this thesis.

2 Thesis outline and aim of the research

When the work presented in this thesis was initiated, the breakthrough discovery that LPMOs catalyze a peroxygenase reaction had just been made (Bissaro et al., 2016b, 2017). Using a variety of experimental approaches, Bissaro et al. had shown that LPMOs are capable of using H_2O_2 as co-substrate, rather than O_2, to catalyze oxidative cleavage of glycosidic bonds (Bissaro et al., 2017). It was also shown that LPMOs suffer oxidative damage in their catalytic centers, ultimately leading to enzyme inactivation, if H_2O_2 is not delivered in a controlled manner (Bissaro et al., 2017). The work described in this thesis was based on the notion that photocatalytic reduction of O_2 to reactive oxygen species such as $O_2^{\bullet-}$ and H_2O_2, by a photoredox catalyst could enable controlled *in situ* production of reducing equivalents and the H_2O_2 co-substrate to fuel LPMO activity. The work described in Papers I, II, and III of this thesis was done to explore the possibility of using light to provide reducing equivalents and H_2O_2 in a controlled manner, with the ultimate aim of achieving a better understanding of LPMO catalysis and novel tools for exploiting these powerful copper catalysts.

Paper I deals with the mechanisms of how known, previously studied photobiocatalytic systems affect LPMO activity, whereas Paper II and III explore the potential roles of light-sensitive redox-active compounds that are naturally present in polysaccharide-rich biomass in light-driven LPMO catalysis. As outlined above, plants and insects have developed complex co-polymeric cell wall and cuticular structures, respectively, in which light-sensitive phenolic compounds play a key role. It is known that microbial conversion of plant litter is improved by exposure to sunlight (Austin et al., 2016; Berenstecher et al., 2020; Lin et al., 2018), an effect that so far has been attributed to an increased access to the carbohydrates at the expense of lignin degradation (Austin et al., 2016). Given that the phenolic compounds in plant cell walls and insect exoskeletons are chemically similar and possibly photoactive, and since LPMO action depends on reducing equivalents in the form of electrons or reduced O_2 (i.e., H_2O_2), the research described in Papers II and III was done to investigate if LPMOs enable light-driven biomass conversion by harvesting visible light using these phenolic compounds.

Prior to the discovery of LPMO catalyzed peroxygenase reactions, two papers had demonstrated light-driven LPMO activity, and both papers speculated on the underlying mechanisms (Bissaro et al., 2016a; Cannella et al., 2016). Thus, the objective of the work described in Paper I was to (re-)investigate the previously published light-driven LPMO reactions with focus on the role of reactive oxygen species. Paper I shows that reactive oxygen species are key to the impact of light-exposed chlorophyllin and V-TiO_2 on the catalytic activity of an AA10 LPMO and that light-driven LPMO activity can

be achieved in the absence of externally added reductants. We suggest that the LPMO is reduced by superoxide radicals or directly on the photoredox catalyst surface, for chlorophyllin and V-TiO_2, respectively, and show that these light-driven systems allow fine-tuning of LPMO activity by controlling the flux of reactive oxygen species, in particular H_2O_2.

Considering that sunlight promotes microbial conversion of lignocellulosic biomass (Austin et al., 2016; Berenstecher et al., 2020; Lin et al., 2018), that lignin is redox-active and light-sensitive, and that lignin can sustain LPMO activity on polysaccharide substrates (Muraleedharan et al., 2018; Westereng et al., 2015), we set out to assess the impact of light and lignin on LPMO activity in the study described in Paper II. The interplay between lignin and LPMOs was believed to involve an electron relay system where electrons are shuttled from high-molecular weight lignin to the LPMO copper site via low molecular weight lignin acting as an electron mediator (Muraleedharan et al., 2018; Westereng et al., 2015), whereas the possible impact of lignin on generation of H_2O_2 had not really been considered. The work described in Paper II was based on the hypotheses that the impact of lignin on LPMO activity could relate to *in situ* generation of H_2O_2 and that this process could be affected by light. Indeed, Paper II shows that LPMO activity is enhanced by exposing reaction mixtures to various lignin types and visible light. NMR was used to analyze light-induced structural changes in the lignin following light-exposure. Paper II also describes experiments with SOD and horseradish peroxidase (HRP) showing that light-exposed lignin reduces O_2 to H_2O_2 via formation of $O_2^{\bullet-}$, and that H_2O_2 formation drives the LPMO reaction. Finally, Paper II demonstrates the ability of LPMOs to oxidize polymeric lignin, albeit at lower rates compared to ligninolytic peroxidases.

Paper III builds on the results from Paper II and addresses the impact of light on conversion of insect biomass, which is a natural chitin-containing substrate rich in potentially light-sensitive catecholamines. The substrate used in this work consisted of pupal exuviae, which are the empty exoskeletons that are shed during maturation from the pupae stage to adult insects that emerge in large amounts during production of black soldier flies (*Hermetia illucens*). Paper III describes that light-exposed insect pupal exuviae drive LPMO activity by generating reducing equivalents and H_2O_2. First, Paper III describes the effects of light-exposed pupal exuviae on the activity of a cellulose-active model LPMO, including assessment of the impact of $O_2^{\bullet-}$-removing SOD and H_2O_2-removing HRP. Then, it is shown that solubilization of chitin in the pupal exuviae themselves, by a chitin-active LPMO, is promoted by exposure to visible light. The findings described in Papers II and III may provide an enzymatic explanation for the impact of light on biomass conversion in Nature.

3 Main results and discussion

3.1 Paper I - Controlled depolymerization of cellulose by light-driven lytic polysaccharide oxygenases

At the start of the work described in this thesis, it had just been shown that LPMOs carry out a peroxygenase reaction and use H_2O_2 rather than O_2 as co-substrate to oxidatively cleave glycosidic bonds in crystalline polysaccharides (Bissaro et al., 2017). The first reports of light-driven LPMO activity came prior to the discovery of LPMO peroxygenase activity and thus the authors of these reports did not seem to consider the possibility that H_2O_2, or other reactive oxygen species, governed LPMO activity in these reaction systems. This possible change in the catalytic mechanism of LPMOs led us to revisit previously published light-driven LPMO reactions and examine the underlying mechanisms, using the well-characterized cellulose-active AA10C from *Streptomyces coelicolor*, *Sc*AA10C, as model LPMO. *Sc*AA10C is a two-domain LPMO comprised of an N-terminal catalytic domain and a C-terminal family 2 CBM.

The first part of the study concerned the activity of *Sc*AA10C and H_2O_2 accumulation in reactions with Avicel, fueled by AscA in the dark, chlorophyllin (Chl) and light, and a combination of Chl, light, and AscA (Paper I: Figs. 2a-c). Here, it must be noted that the reaction with AscA in the dark displayed artificially high activity, likely due to the presence of free Cu(II) (Stepnov et al., 2021), as can be seen by comparing this reaction to a similar reaction reported by Bissaro et al. (2016), which shows one order of magnitude lower LPMO activity. Combining Chl/light/AscA resulted in much higher initial LPMO catalytic rates than the reaction with either AscA or Chl/light. This very high activity was accompanied by almost immediate inactivation of the LPMO. The reactions with AscA or Chl/light proceeded for longer time and, eventually, generated more oxidized products. Measurements of H_2O_2 accumulation in reactions lacking Avicel showed that the conditions giving lower, more steady LPMO activity generated much less H_2O_2 compared to the reaction with Chl/light/AscA. Interestingly, cessation of LPMO product formation in the various reactions with Avicel was accompanied by a spike in H_2O_2 levels, indicating that H_2O_2 was still produced but no longer consumed.

Directly comparing these results to the results obtained by Cannella et al. is difficult because i) the experimental conditions differ (e.g., light sources), (ii) the LPMOs differ (a CBM containing bacterial AA10 in this study and a CBM-free single domain fungal AA9 in Cannella et al.), and iii) Cannella et al. analyzed their results based on a single time point whereas the study of Paper I used progress curves to understand the reaction system. It is clear though that the seminal finding by Cannella et al. that LPMOs can be made to run very fast in reactions with AscA, chlorophyllin and light, is confirmed by

the results in Paper I. It is important to note that Paper I, in addition, provides the first demonstration of purely Chl/light-driven LPMO activity (i.e., in the absence of added reductant) that exceeds LPMO activity in reactions driven by reductant alone or reductant and Chl/light, and that the reductant was crucial for attaining the high catalytic activities described by Cannella et al. (see also Paper I, supplementary Figure 8). The work described in Paper I focused on Chl/light reactions without added reductant and demonstrated how LPMO activity is sustained by only Chl/light.

The supplementary material of Paper I contains data for other LPMOs, which were collected to demonstrate the general applicability of driving LPMO reactions with the Chl/light system (and no added reductant). The results show that the system indeed works for the other LPMOs, but reveal differences between these in terms of efficiency and reaction stability. The additional LPMOs tested are a chitin-active bacterial LPMO, for which the Chl/light system works better than 1 mM AscA, and a CBM-free single domain AA9, *Nc*AA9F. Similar to *Tt*AA9E used by Cannella et al., *Nc*AA9F is a C1-cellulose oxidizing AA9 without a CBM. Recent data show that these two enzymes are quite similar, also in the sense that both act on cellulose-bound xylan, a property possessed by only a subset of AA9 LPMOs (Tõlgo et al., 2022). Supplementary Figure 10b shows that for *Nc*AA9F, the reaction with Chl and light works, but is far less efficient and shows faster enzyme inactivation than the reaction with 1 mM AscA, as has also been observed for *Mt*AA9A (Sepulchro et al., 2021). Comparing the activity of *Nc*AA9F to *Sc*AA10C in reactions fueled by Chl/light reveals that *Sc*AA10C is near one order of magnitude more efficient in converting the *in situ* generated H_2O_2 into oxidized products (Paper I: Fig. 2a & Supplementary Fig. 10b). Since *Nc*AA9F is a single domain LPMO, while *Sc*AA10C harbors a CBM module, it is possible that *Nc*AA9F binds less strongly to cellulose and that the cellulose concentration was too low for *Nc*AA9F to productively turn over the H_2O_2 generated by Chl/light, resulting in rapid LPMO inactivation. For the reaction with 1 mM AscA, it is conceivable that H_2O_2 generation occurs in a more timely manner leading to more steady production of oxidized products and higher overall product formation, compared to the reaction driven by Chl/light. Another possibility that cannot be excluded is that AA9s are functionally distinct from AA10s, and that the two enzyme families have different activation and inactivation kinetics.

Reactions with SOD and catalase were performed to analyze the role of reactive oxygen species $O_2^{\bullet-}$ and H_2O_2 (Paper I: Figs. 2d-f). Addition of SOD led to faster generation of oxidized products from cellulose demonstrating that $O_2^{\bullet-}$ is formed, which has since been confirmed by others (Pan et al., 2020), and that its further reduction to H_2O_2 controls LPMO activity. Adding catalase to the reaction in the absence and presence of SOD resulted in prolonged *Sc*AA10C catalyzed cellulose solubilization by removing excess H_2O_2 and preventing LPMO inactivation. The observed boosting effect of SOD and

beneficial effect of catalase on LPMO activity is in contrast to the negligible impact of these two enzymes on LPMO activity reported by Möllers and colleagues (Möllers et al., 2017). We suspect that this discrepancy is due to the use of single time point measurements by Möllers et al. Interpretation of a single time point provides a snapshot of the reaction at a specific moment, whilst a progress curve captures how the reaction proceeds over time. For instance, the reaction with catalase does not show the beneficial effect of adding catalase until 6 h has passed (Paper I: Fig. 2d).

Supporting the idea that photogenerated H_2O_2 governs LPMO activity in these reactions, Fig. 3 in Paper I shows that both H_2O_2 generation and LPMO activity depend on the light intensity. These experiments revealed a discrepancy between H_2O_2 accumulation in reactions without LPMO (Chl/light/Avicel) and the (higher) amount of oxidized products in LPMO containing reactions. This difference most likely stems from the LPMO's ability to effectively utilize H_2O_2 for cellulose oxidation as LPMOs from different families acting on different substrates have all been shown to have a high affinity for H_2O_2 when in their reduced state (Kuusk et al., 2018, 2021; Rieder et al., 2021a). It is conceivable that in the reactions without the LPMO some H_2O_2 is lost due to secondary reactions with chlorophyllin and/or AscA. While not mentioned in Paper I, it is also possible that the H_2O_2 measurements suffered from signal suppression in the HRP assay which may occur if the assay contains multiple redox active compounds (Stepnov et al., 2021). Taken together the results depicted in Figs. 2 and 3 of Paper I strengthen the case for H_2O_2 as the kinetically relevant co-substrate for LPMOs and highlight the importance of fine-tuning delivery of H_2O_2.

LPMOs need to be reduced and can accept electrons from a wide range of electron donors. To identify the electron donor in the Chl/light reaction and to investigate the possibility of direct transfer of photoexcited electrons from Chl to the LPMO active site, attempts to measure LPMO reduction by fluorescence were made, without success. This led to devising a two-phased experimental setup in which the LPMO was pre-incubated with Chl/light as a first step before being mixed with substrate and H_2O_2 in the dark, all under anaerobic conditions. This led to very low LPMO activity compared to the control reaction with AscA and product levels did not depend on the pre-exposure to light (Paper I: Fig. 4). Thus, the LPMO was not reduced and direct transfer of photoexcited electrons from Chl to the LPMO seems unlikely (although some ambiguity exists, as discussed in Paper I). Thus, it seems likely that under standard, aerobic, conditions, the LPMO is reduced by $O_2^{\bullet-}$, given its favorable reduction potential and a previous study demonstrating that $O_2^{\bullet-}$ can fuel the activity of the same LPMO as used in Paper I (Bissaro et al., 2017). These results are in line with current knowledge regarding the (general) difficulty of directly transferring photoexcited electrons to the active site of oxidoreductases, compared to more facile indirect activation (Lee et al., 2018; Schmermund et al., 2019).

Chl (chlorophyllin) is a semi-synthetic derivative of chlorophyll in which the central magnesium ion of the porphyrin ring is substituted with a copper ion and the phytol tail is absent. One of the commonly found compounds in Chl is Chlorin e_6 and comparing the UV-Vis absorbance spectra, fluorescence properties, and electrochemical properties of Chl with chlorin e_6 before and after copper reconstitution revealed nearly identical spectroscopic features for Chl and Cu(II)-chlorin e_6 (Paper I: Supplementary Fig. 1) and highly similar electrochemical features (Paper I: Supplementary Fig. 2, Supplementary Table 1). These results indicate that Cu(II)-chlorin e_6 is the main component of Chl. Since the spectroscopic features of chlorin e_6 changed upon copper binding, we assessed if metalation also had an impact on H_2O_2 production and LPMO activity (Paper I: Fig. 5). Metalation of chlorin e_6 reduced the amount of H_2O_2 generated by nearly one and two orders of magnitude compared to Chl and non-metalated chlorin e_6, respectively (Paper I: Fig. 5a). When they were applied as photoredox catalysts in LPMO reactions, the reactions with non-metalated chlorin e_6 displayed a much faster initial rate accompanied by rapid LPMO inactivation, while Chl and Cu(II)-chlorin e_6 reactions proceeded at a similar pace for the first part of the reaction, despite the difference in H_2O_2 generation, before the reaction with Cu(II)-chlorin e_6 slowed down (Paper I: Fig. 5b). It is clear that metalation of these compounds is of major importance for their performance in light-driven LPMO catalysis.

A potential advantage of light-driven biocatalytic reactions is the ability to tailor the H_2O_2 production *in situ* and achieve high operational stability. AscA is a commonly used reductant in LPMO research, and, therefore, we set out to compare AscA-driven reactions with Chl/light-driven reactions. As previously noted, the LPMO activity in reactions with AscA reported in Fig. 2a and Fig. 6a (Paper I) was artificially high, most likely due to the presence of free copper that, as we realize today, promotes oxidation of ascorbic acid leading to generation of high levels of H_2O_2 (Stepnov et al., 2021). This effect of free copper varies between reductants and, as such, not every result obtained with AscA and a copper-contaminated LPMO may be generalizable. Addition of SOD to the AscA-driven LPMO reaction led to a somewhat higher initial rate and somewhat faster cessation of product formation compared to the reaction without SOD, indicating that superoxide was being formed (Paper I: Fig. 6a). The shift in the progress curve upon addition of SOD is typical for LPMO reactions with a surplus of H_2O_2; higher levels of H_2O_2 give faster initial rates and more rapid cessation of the reaction, likely due to enzyme inactivation. Similar to what was found for the Chl/light system, addition of catalase to the reaction with AscA slowed down LPMO activity but rescued the LPMO from early inactivation and thus led to high eventual product yields (Paper I: Fig. 6a). Like in the experiments depicted in Fig. 2, a spike in H_2O_2 levels was observed around the time when LPMO activity was arrested (Paper I: Fig. 6b). These experiments show that reactions with AscA, while sometimes working quite well, are not easy to control.

This may stem in part from the impact of free transition metals, as discussed below, and in recent work by Stepnov et al. (Stepnov et al., 2021, 2022b).

To gain further insight into AscA-driven LPMO reactions and the possible impact of free transition metals, H_2O_2 production, and LPMO activity in reactions with free copper and AscA were assessed. H_2O_2 production in reactions with 50 μM AscA was found to be strongly increased by free copper and this has later been confirmed by others, using up to 1 mM AscA (Shen et al., 2021; Stepnov et al., 2021). Fig. 7a in Paper I shows a clear trend of faster H_2O_2 production with increasing amounts of free copper (Paper I: Fig. 7a). Similarly, for the LPMO reaction, increasing the amount of free copper resulted in much faster initial generation of oxidized products. At the higher copper concentrations (1 μM and above) this high initial rate was accompanied by enzyme inactivation that was so fast that enzyme activity had already halted at the first measured time point. (Paper I: Fig. 7b).These results highlight the importance of taking care to avoid excess copper in LPMO preparations particularly when employing AscA as reductant.

The second report of light-driven LPMO activity concerned the use of V-TiO_2 as photoredox catalyst to provide *Sc*AA10C with the necessary reducing equivalents for catalytic activity without the need for a mediator (Bissaro et al., 2016a). Here, the authors showed that reactions with light-exposed V-TiO_2 containing LPMO and substrate resulted in production of low amounts of H_2O_2. This study was carried out prior to the discovery of the peroxygenase activity of LPMOs and the low levels of H_2O_2 accumulating in reactions containing LPMO and substrate, i.e., levels lower than expected, were explained by assuming that phosphate ions of the buffer modulate redox reactions at the surface of the photoredox catalyst to favor LPMO reduction over reduction of O_2 to H_2O_2 (Bissaro et al., 2016a). In hindsight, it is conceivable that H_2O_2 was actually produced in amounts that fueled the LPMO reaction and that the H_2O_2 levels remained low due to LPMO activity (Paper I: Figs. 2&6 and Paper II: Fig 1). Subsequent work with TiO_2-based photoredox catalysts has demonstrated that gold-coated (Au-)TiO_2 promotes the activity of an unspecific peroxygenase from *Agrocybe aegerita* because it catalyzes reduction of O_2 to generate H_2O_2 (W. Zhang et al., 2018).

To assess the potential formation of H_2O_2 upon irradiation of V-TiO_2, LPMO reactions were performed in the presence of increasing amounts of HRP, which led to increasingly inhibited LPMO reactions, demonstrating that photogenerated H_2O_2 sustained LPMO activity (Paper I: Fig. 8a). Reduction of O_2 to H_2O_2 can proceed through two pathways, either as a two-step single electron reduction process (i.e. $O_2 + e^- \rightarrow O_2^{\bullet-} + e^- + 2H^+ \rightarrow H_2O_2$) or as a one-step two electron reduction process (i.e. $O_2 + 2e^- + 2H^+ \rightarrow H_2O_2$), and the presence of a co-catalyst such as vanadium or gold on the TiO_2 surface favors the latter process (Burek et al., 2019).

In their original work, Bissaro and colleagues had demonstrated reduction of the LPMO in anaerobic settings which they attributed to a direct electron transfer from the photoredox catalyst to the active site of the LPMO (Bissaro et al., 2016a). Having demonstrated H_2O_2 formation by light-exposed V-TiO_2, we next investigated whether V-TiO_2 also generated $O_2^{\bullet-}$, which could possibly reduce the LPMO. To do so, increasing amounts of SOD were added to the LPMO reactions, which did not show any effect on LPMO activity (Paper I: Fig. 8b). It is possible that SOD effects were not observed because the upfront oxidation of water was the rate limiting step or because $O_2^{\bullet-}$ indeed is not formed, where the latter would imply that the LPMO is reduced at the V-TiO_2 surface. TiO_2 is known to occur in so-called anatase or rutile forms, referring to their crystal structures, which favor reduction of O_2 to H_2O_2 or $O_2^{\bullet-}$, respectively (Goto et al., 2004). The TiO_2 used to generate the V-TiO_2 used in this study was most likely a combination of mainly anatase and some rutile (Bissaro et al., 2016a; Jiang et al., 2018). If the V-TiO_2 was primarily in the anatase form and assuming that V-TiO_2 behaves similarly to TiO_2, then this may explain the absence of a SOD effect on LPMO activity (Paper I: Fig. 8b). It is interesting to note that LPMO reduction does not appear to be a limiting factor in the V-TiO_2-system since, in the original study, increasing the LPMO concentration linearly increased the product formation rate (Bissaro et al., 2016a).

Taken together, the results presented in Paper I show that light-driven LPMO activity using Chl or V-TiO_2 as photoredox catalyst depends on the ability of the photoredox catalysts to generate H_2O_2 and reducing equivalents. It would seem that catalysis in these systems is primarily limited by the rate of *in situ* H_2O_2 production, while enzyme stability depends on this rate not being too high. The main advantage of photoredox catalysts is tailored *in situ* H_2O_2 generation which allows for better operational stability of LPMOs and other H_2O_2-dependent redox enzymes.

3.2 Paper II – Visible light-exposed lignin facilitates cellulose solubilization by lytic polysaccharide monooxygenases

Microbial decomposition of plant biomass is enhanced by exposure to sunlight, an effect that has been attributed to light-driven changes in lignin structure that make the biomass polysaccharides more susceptible to degradation by carbohydrate-active enzymes (Austin et al., 2016; Berenstecher et al., 2020; Lin et al., 2018). Since lignin is light-sensitive and lignin has been shown to fuel LPMO activity in the dark, we investigated the possibility of using visible light-exposed lignin as photoredox catalyst to generate reducing equivalents and H_2O_2 needed for LPMO catalysis. The goal of the study described in Paper II was to investigate the impact of visible light on lignin containing LPMO reactions and to assess potential changes in the lignin structure following visible light irradiation.

To investigate the potential of ground and excited state lignin as reductant and source of H_2O_2 in LPMO reactions, we used commercially available Kraft lignin and the well-characterized C1-oxidizing cellulose active *Sc*AA10C as model LPMO. Kraft lignin is obtained from Kraft pulping processes where lignin and hemicellulose are separated from cellulose. The Kraft process results in a modified and condensed lignin structure that exhibits a reduced number of β-O-4 linkages with a corresponding increase in more recalcitrant C-C and C-O bonds, and in phenolic groups, compared to native lignin (Crestini et al., 2017; Lancefield et al., 2018). The first experiments were performed with various concentrations of LPMO (*Sc*AA10C: 0, 75, and 500 nM) and lignin (0.9 and 9 $g.L^{-1}$), with monitoring of LPMO product formation and *in situ* production of H_2O_2 over time. Reaction time courses revealed that light-exposed lignin produced H_2O_2 and promoted LPMO activity (Paper II: Fig 1). When H_2O_2 production exceeded the LPMO's ability to convert H_2O_2 into oxidized products, the LPMO was inactivated (Paper II: Fig. 1 and Supplementary Fig. 1). Control experiments in absence of lignin exposed to visible light showed no detectable LPMO activity (Paper II: Fig 2c) and reactions containing lignin in the dark showed very low LPMO activity (Paper II: Fig 2d). These findings indicated that LPMO activity was fueled by *in situ* H_2O_2 production that was promoted by light-exposure of lignin, and that care must be taken to avoid conditions that lead to LPMO inactivation.

While increased H_2O_2 generation correlated with increased LPMO activity (Paper II: Fig. 1), there was a discrepancy between the amount of H_2O_2 generated in reactions without LPMO compared to the levels of oxidized products detected in the reactions with LPMO. H_2O_2 accumulation was quantified using a modified version of the HRP/AmplexRed assay (Kittl et al., 2012). Since Kraft lignin serves as substrate for HRP (suppressing the signal obtained upon oxidation of AmplexRed), all H_2O_2 standard curves used to

determine H_2O_2 levels contained the same lignin concentration as the reactions being measured. Other factors, that could not be compensated for may also play a role. For example, lignin quenching the fluorescence signal of resorufin, the oxidation product of AmplexRed, in a lignin concentration-dependent manner. An alternative explanation for the discrepancy between observed levels of H_2O_2 and LPMO products may be based on the notion that the H_2O_2 levels measured in absence of LPMO are the net result of formation and degradation, both of which may be dependent on the light intensity (Burek et al., 2019) and on the presence redox-active moieties in the lignin itself (Kont et al., 2019). LPMOs in presence of substrate display a high affinity for H_2O_2 (K_m values in the low micromolar range; (Kuusk et al., 2018, 2021; Rieder et al., 2021a)) which enables efficient oxidation of cellulose. Thus, it is possible that, in reactions with the LPMO, abiotic turnover of H_2O_2 is inhibited because it is consumed efficiently by the LPMO. To probe if H_2O_2 is more rapidly consumed in a reaction containing the LPMO compared to a reaction without LPMO, 100 μM H_2O_2 was added to reactions in the dark containing lignin (0.9 g.L^{-1}), Avicel (10 g.L^{-1}), and LPMO (0 or 0.5 μM). The results showed that LPMO consumption of H_2O_2 outcompetes abiotic H_2O_2 decomposition (Paper II: Supplementary Fig. 2).

To gain a better understanding of the reaction system, the effects of LPMO concentration, substrate concentration, lignin concentration, and light intensity were investigated (Paper II: Fig. 2). 75 nM LPMO did not limit the reaction, but further reducing the LPMO concentration, to 50 and 25 nM, resulted in arrested product formation due to LPMO inactivation becoming noticeable (Paper II: Fig. 2a and Supplementary Fig. 1). The presence of cellulose particles in the reaction vessel reduces light transmittance (Blossom et al., 2020), and, as expected, higher Avicel concentrations resulted in lower LPMO activity (Paper II: Fig. 2b). Increasing the lignin concentration from 0.09 to 9 g.L^{-1} led to a near 50-fold increase in LPMO activity (Paper II: Fig. 2c). Interestingly, normalizing LPMO activity based on the photocatalyst concentration revealed that the reaction with 0.09 g.L^{-1} lignin performed slightly better than the reaction with 0.9 g.L^{-1}, and that these lignin concentrations gave approximately two-fold more product per g photocatalyst than the reaction with 9 g.L^{-1}(calculation based on Paper II: Fig. 2c). Performing reactions with increasing light intensity resulted in more than one order of magnitude increase in LPMO activity (Paper II: Fig. 2d). Taken together, the results of Figs. 1 and 2 show that the combination of lignin and light provides a tool for fueling and controlling LPMO activity through controlled delivery of H_2O_2 and adds to the notion that LPMO activity in these reactions is correlated with *in situ* production of H_2O_2.

To further analyze the impact of H_2O_2 on LPMO activity, competition experiments with HRP were performed. Adding HRP to visible light-irradiated LPMO reactions with lignin (0.9 g.L^{-1}) and Avicel (10 g.L^{-1}) resulted in almost complete inhibition, confirming that

LPMO activity is driven by H_2O_2 the production of which is promoted by light-exposed lignin (Paper II: Fig. 3a&b). While the work related to paper II was in progress, two studies demonstrated photocatalytic production of H_2O_2 by lignin, which may happen either as a two-step, single electron reduction of O_2 via $O_2^{\bullet-}$ to H_2O_2, or as a one-step, two-electron reduction of O_2 to H_2O_2 (J. Kim et al., 2022; Miglbauer et al., 2020). The suggestion by Miglbauer et al. that the most likely path to H_2O_2 is a two-step reduction of O_2 to H_2O_2 was confirmed experimentally by Kim et al., who also noted that one-step reduction to H_2O_2 can occur but is much less frequent. To probe for $O_2^{\bullet-}$ production by light-exposed lignin, LPMO reactions were performed with increasing amounts of SOD (Paper II: Fig 3c&d). These reactions showed that SOD clearly increased LPMO activity, demonstrating the formation of $O_2^{\bullet-}$ by light-exposed lignin and also showing that its further reduction to H_2O_2 limits LPMO activity.

Studies with the Chl/light system described in Paper I suggested that $O_2^{\bullet-}$ acts as LPMO reductant. Since the SOD experiments showed that $O_2^{\bullet-}$ is formed in the reactions with lignin and since it is well known that ground state lignin can act as a reducing agent for LPMOs (Kont et al., 2019; Muraleedharan et al., 2018; Westereng et al., 2015), there are two scenarios for reduction of the LPMO in the reaction set-ups of Paper II. To examine this matter, we took a closer look at the ability of the Kraft lignin to reduce LPMOs using stopped-flow kinetic measurements. To ascertain that LPMO reduction did not come from low molecular weight lignin, we measured LPMO activity and reduction using native and dialyzed Kraft lignin (Paper II: Fig. 4 and Supplementary Fig. 3 and 4). We observed minimal differences in LPMO activity using the two lignin preparations (Paper II: Fig 4a), and only a slightly lower rate of LPMO reduction with the dialyzed lignin compared to the native lignin (Paper II: Fig 4b). Put differently, the LPMO reduction rates mirror the ability of LPMOs to oxidize lignin, and the obtained lignin oxidation rates (in the range of 3×10^3 $M^{-1}.s^{-1}$) are only one order of magnitude lower than those observed for lignin oxidation by manganese peroxidase (Ayuso-Fernández et al., 2019) and between two and three orders of magnitude lower than the most efficient lignin peroxidases (Sánchez-Ruiz et al., 2021). Importantly, this is the first direct evidence that a lignin polymer can directly interact with the copper site of LPMOs.

Kraft lignin is a highly condensed water-soluble lignin and Paper II describes that its ability to photocatalytically reduce O_2 to H_2O_2 boosts LPMO catalyzed solubilization of cellulose. Various lignins, including a lignin model dimer, guaiacylglycerol-β-guaiacyl ether, were recently shown to generate H_2O_2 when exposed to visible light, and it has been suggested that oxidation of the C_α-OH moiety in β-O-4 linked lignin units (see Fig. 3 in the introduction) to C_α=O is involved and required for reducing O_2 to H_2O_2 (J. Kim et al., 2022). When we employed the same lignin model dimer, we were unable detect H_2O_2 generation and LPMO activity under similar conditions as those used by Kim et al. (data not shown).

To assess the impact of lignin type, and to facilitate subsequent studies of light-induced structural changes in the lignin, we assessed if water-insoluble organosolv lignin from spruce and birch could fuel LPMO catalysis when exposed to visible light. Organosolv lignin is obtained from organosolv pulping processes and results in a less modified lignin and a more homogeneous lignin preparation compared to Kraft lignin (Vishtal et al., 2011). Both organosolv lignins were found to boost LPMO activity when exposed to light, similarly to Kraft lignin (Paper II: Fig. 5).

NMR spectroscopy was applied to directly investigate if photocatalytic generation of H_2O_2 was associated with any structural changes in the lignin. For this, the different lignins were incubated in the dark or with visible light-exposure for 24 h in the absence of cellulose and LPMO. Following irradiation for 24 h, Kraft lignin exhibited a decrease in hydroxyl groups (Paper II: Supplementary Fig. 5). A possible explanation for this observation is that light-exposure of lignin leads to generation of phenoxyl radicals that radically couple with other parts of the lignin structure. For spruce and birch organosolv lignin, the irradiated lignins showed a decrease in olefinic signals (i.e., C=C bonds) with concomitant increase in aldehyde signals, such as cinnamaldehyde end groups, indicating that ring-conjugated olefins were oxidized by light (Paper II: Fig. 6 and Supplementary Figs. 6, 7, and 8) (Paulsson et al., 2012). Organosolv lignin from spruce contained β-1 stillbene structures and signals pertaining to these structures also decreased upon light-exposure (Paper II: Fig. 6b), indicating their light-induced oxidation (Paulsson et al., 2012; L. Zhang et al., 1994). Of note, while the impact of UV light on lignin structure has been studied quite extensively, the NMR data presented in Paper II comprise one of the first studies of the impact of visible light on lignin structure, which, as it turns out, may be considerable.

Treatment of lignin with LPMO in the dark did not yield detectable changes in the lignin structure, which is likely due in part to LPMO-catalyzed oxidation being much less extended than light-catalyzed oxidation. 1D proton spectra did reveal one structural change, namely increased shielding of hydroxyl groups (Paper II: Supplementary Fig. 9) which may be interpreted as the degree of hydrogen bonding of these hydroxyl groups. Most interestingly, oxidation by light led to deshielding of hydroxyl groups, showing that light and LPMOs oxidize lignin in different ways.

In the very recent study by Kim et al. showing light-driven H_2O_2 production by lignin, the authors detected H_2O_2 production in N_2-purged reactions, leading to the conclusion that excited state lignin can oxidize H_2O to H_2O_2 and O_2 (J. Kim et al., 2022). Incorporation of ^{18}O in in the product of UPO-catalyzed hydroxylation of ethylbenzene to phenylethanol performed in $H_2{}^{18}O$ confirmed lignin as a water oxidizing photocatalyst. This is an important finding since sacrificial electron donation by water

is ideal for photobiocatalytic reaction systems. Inspired by these findings, we investigated if water splitting by light-exposed lignin could promote LPMO activity under anaerobic conditions. Experiments were carried out under anaerobic conditions in $H_2{}^{18}O$. If excited lignin oxidized $H_2{}^{18}O$ to $H_2{}^{18}O_2$ and $^{18}O_2$, then the LPMO should generate aldonic acids (i.e., the hydrated products of LPMO catalysis) with an *m/z* shift of +4 compared to reactions in $H_2{}^{16}O$ and $^{16}O_2$, when analyzing products by MALDI-ToF-MS (Vaaje-Kolstad et al., 2010). However, only a control reaction with AscA and added $H_2{}^{18}O_2$ in $H_2{}^{18}O$ showed the expected +4 mass shift of the aldonic acids. As experimental setups and light sources differ, it is impossible to directly compare these results with the results obtained by Kim et al. In our hands, neither Kraft nor organosolv spruce lignin were able to oxidize water or promote anaerobic LPMO activity (Paper II).

3.3 Paper III - Natural photoredox catalysts promote light-driven lytic polysaccharide monooxygenase reactions and enzymatic turnover of biomass

Paper III builds on the idea that light impacts biomass conversion in Nature by promoting the activity of LPMOs and other biomass converting redox enzymes. Paper III examines the potential of redox-active compounds, most likely catecholamines, in insect biomass to harvest light energy to drive LPMO reactions and, thus, biomass conversion. For this purpose, we used milled pupal exuviae from *Hermetia illucens* (black solider fly). Pupal exuviae are the exoskeletons being shed during maturation from pupae to adult insect. This pupal exuviae contained 20% (w/w) chitin and 12.6% (w/w) phenolic compounds (Hahn et al., 2021). Washing the pupal exuviae removed soluble compounds absorbing in the 240 nm to 800 nm range (Paper III: Fig. S1) and reduced the total reducing capacity by 72% as measured by the Folin-Ciocalteu assay using gallic acid as a standard (Paper III: Fig. S2). To address light-driven LPMO activity with insect biomass we used the C1-oxidizing two-domain cellulose-active *Sc*AA10C as model LPMO (i.e., the same model LPMO as in the studies described in Papers I and II).

First, LPMO activity on Avicel was studied using washed and non-washed pupal exuviae with and without exposure to visible light (Paper III: Fig. 2). *Sc*AA10C catalyzed oxidation of Avicel was observed in all reactions containing pupal exuviae, and light-exposure resulted in a one – two orders of magnitude higher LPMO catalytic rate, compared to reactions in the dark (Paper III: Fig. 2). The reaction with non-washed pupal exuviae showed the highest initial activity but also a relatively rapid decrease in product formation, indicative of cessation of the LPMO reaction (Paper III: Fig. 2a). As shown in Papers I and II, such progress curves are typical for LPMO reactions containing more H_2O_2 than the LPMO can use in a productive manner, ultimately resulting in LPMO inactivation. Control reactions without pupal exuviae or replacing the LPMO by $CuSO_4$ showed no product formation, irrespective of light exposure (Paper III: Fig. 2 & Fig. S3), confirming the crucial role of the pupal exuviae in driving the reaction. Gallic acid is a commonly used reductant in LPMO research, and a reaction with gallic acid in the dark was included as a reference reaction. The reaction with irradiated washed pupal exuviae proceeded linearly for at least 6 h generating twice the amount of oxidized product compared to the reference reaction with gallic acid (Paper III: Fig. 2).

Based on the observed LPMO activity, ground state (i.e., not irradiated) pupal exuviae did not appear to generate H_2O_2 at levels relevant for LPMO catalysis. To test if LPMO activity was limited by system generated H_2O_2 in dark reactions containing washed pupal exuviae, we conducted an experiment where small amounts of H_2O_2 were added to drive the reaction (Paper III: Fig. S4). Addition of H_2O_2 did not boost LPMO activity in these reactions (Paper III: Fig. S4), in contrast to what has been observed for the same

LPMO in reactions containing small amounts of well-known LPMO reductants (Bissaro et al., 2017), leading us to conclude that access to both reducing equivalents (for LPMO priming reduction) and H_2O_2 limits LPMO activity in dark reactions. This is not surprising given that the reduction potential of a catecholamine model compound does not favor reduction our model LPMO (Xu et al., 1996).

Having obtained a successful proof-of-concept, a more detailed investigation on the effects of pupal exuviae concentration, light intensity, and substrate concentration on LPMO activity and the system's ability to produce H_2O_2 was carried out (Paper III: Fig. 3). Increasing the pupal exuviae concentration or light intensity both showed clear dose-response effects and led to higher LPMO activity (Paper III: Fig. 3A,C,D,F) and H_2O_2 accumulation (Paper III: Fig. 3B,C,E,F). As we observed in Paper II, higher substrate concentrations led to lower LPMO activity and lower levels of H_2O_2 (Paper III: Fig. 3G, H, I). As expected, the reaction without Avicel accumulated the most H_2O_2 (Paper III: Fig. 3H&I), clearly showing that light is attenuated by the insoluble substrate. All together, these results show that combining pupal exuviae and light enabled controlled LPMO-catalyzed depolymerization of cellulose by regulating the system's ability to generate H_2O_2.

Knowing that H_2O_2 accessibility limited LPMO activity in these reactions (Paper III: Fig. 3), we then addressed whether the amount of LPMO limited product formation in standard reactions with Avicel (10 $g.L^{-1}$), pupal exuviae (5 $g.L^{-1}$), and visible light irradiation (Paper III: Fig. 4A&B). When the LPMO was dosed at 100 nM, the reaction showed diminished product formation and activity was arrested early in the reaction, while dosing the LPMO from 250-2500 nM showed no discernable effect of LPMO concentration on product formation (Paper III: Fig. 4A&B). These findings further strengthen the notion that light-driven H_2O_2 generation determines LPMO activity in this system.

Additional proof that light-driven H_2O_2 production governed LPMO activity was obtained from competition experiments with HRP (Paper III: Fig. 4C&D). For these experiments, non-washed pupal exuviae was applied as the soluble phenolic compounds removed by washing provide substrates for HRP. LPMO activity was increasingly inhibited by increasing amounts of HRP to the extent that more than 95% of the LPMO activity was abolished when the HRP concentration (720 nM) slightly exceeded the LPMO concentration (500 nM) (Paper III: Fig. 4D). This result confirms that access to H_2O_2 determined LPMO activity under these conditions.

In Papers I and II, we addressed the role of superoxide in LPMO reactions containing chlorophyllin, V-TiO_2, and lignin as photoredox catalysts. In Paper I, we showed that $O_2^{\bullet-}$ was produced as SOD-catalyzed conversion of $O_2^{\bullet-}$ into H_2O_2 boosted LPMO activity. Furthermore, $O_2^{\bullet-}$ was concluded to be the most likely source of reducing equivalents for the LPMO. For V-TiO_2 however, formation of $O_2^{\bullet-}$ was not detected leading to the conclusion that $O_2^{\bullet-}$ was likely not produced in this system. As described in Paper II, the same SOD boosting effect of LPMO activity was observed using visible light-irradiated lignin. This latter finding corroborated recent findings showing that excited-state lignin-catalyzed reduction of O_2 to H_2O_2 proceeds via formation of $O_2^{\bullet-}$ (J. Kim et al., 2022). Paper III show that SOD had no impact on LPMO activity in reactions driven by irradiated pupal exuviae, leading to the conclusion that $O_2^{\bullet-}$ is not formed under these conditions (Paper III: Fig. 4E&F). Combining the observations that SOD does not influence light-driven LPMO activity with pupal exuviae and that LPMO activity in the dark reactions with exogenously supplied H_2O_2 was very low (because the LPMO is not reduced), raises the question as to the source of the reducing equivalents needed to generate the catalytically active LPMO-Cu(I) state. Considering that light-exposure of quinones and hydroquinones leads to formation of semiquinone radicals (Beck et al., 1982; Boule et al., 1992), it is conceivable that light-exposure of the catecholamines in the pupal exuviae leads to formation of semiquinone radicals that can reduce the LPMO.

Returning to the idea that light impacts biomass conversion in Nature by promoting the activity of LPMOs and other biomass converting redox enzymes, we then assessed whether light would affect degradation of the pupal exuviae themselves by a chitin-active LPMO, *Sm*AA10A, from the soil bacterium *Serratia marcescens*. Chitin solubilization reactions with *Sm*AA10A displayed the same light effects as the reactions with *Sc*AA10C on cellulose: exposure to visible light gave faster chitin solubilization and higher product yields (Paper III: Fig. 5). Altogether, there is no doubt that the impact of visible light on biomass conversion in Nature under aerobic conditions could, at least in part, be due to improved LPMO activity that is a result of increased H_2O_2 production catalyzed by redox-active compounds in plant (Paper II) or insect (Paper III) biomass. Increased H_2O_2 production will also fuel other H_2O_2-dependent redox enzymes, such as HRP used in control reactions, demonstrating that light effects on biomass conversion are not limited to LPMOs.

4 Concluding remarks and future perspectives

The work presented in this thesis unravels the underlying mechanisms of light-driven oxidative biomass decomposition by LPMOs. The various photoredox catalysts used in this work can provide LPMOs with the necessary reducing equivalents to generate the catalytically active LPMO-Cu(I) state, either when in their ground state, excited state, or via mediators (e.g., $O_2^{\bullet-}$). In their excited states, all the photoredox catalysts act as powerful reducing agents and catalyze reduction of O_2 to H_2O_2 (Papers I, II, III). The data presented in this thesis shows a systematic correlation between LPMO activity and the ability of the photoredox catalyst to generate H_2O_2 (Papers I, II, III). The fact that H_2O_2 is the kinetically relevant co-substrate limiting LPMO catalytic activity is further highlighted by multiple experiments showing inhibition of LPMO activity when an enzymatic H_2O_2 scavenger is present in the reactions. The experiments also show that H_2O_2 levels need to be controlled in order to avoid enzyme inactivation and that, under some circumstances, enzymes such as catalase and SOD may be beneficial for modifying these levels. In principle, the light-driven systems and the insights described above allow for fine-tuning of LPMO catalysis by controlling the flux of H_2O_2 *in situ*.

While light-driven LPMO reactions work nicely, the catalytic rates observed in all stable LPMO reactions described in Paper I-III are low. For example, the rates typically observed in these reactions are in the range of 0.01 – 0.1 s^{-1}, compared to reported rates for LPMO peroxygenase reactions ranging from 1 – 100 s^{-1} depending on the LPMO and the type of substrate (Hangasky et al., 2018; Kuusk et al., 2018, 2021; Rieder et al., 2021a, 2021b). Thus, in the reactions described above, we do not yet harness the full potential of LPMOs. On the other hand, the rates obtained in the studies described in Papers I-III are similar to the rates observed in reductant-driven LPMO reactions (Bissaro et al., 2018b) and even in successful industrial processes (Costa et al., 2020; Müller et al., 2018). For comparison, reported catalytic rates for cellobiohydrolases whose activity benefits from LPMO action, are in the order of 1 – 10 s^{-1} (Kurašin et al., 2011).

On a similar note, the rates observed in LPMO reactions fueled by light-exposed lignin are akin to recently reported rates for unspecific peroxygenase-catalyzed hydroxylation of various model substrates fueled by lignin-driven photocatalytic H_2O_2 generation (J. Kim et al., 2022). In this study, the authors compared lignin with other photoredox catalysts, including graphitic C_3N_4, gold-doped rutile TiO_2, and methylene blue, and concluded that lignin is the superior photoredox catalyst for fueling the activity of this unspecific peroxygenase. Another advantage of using lignin as photoredox catalyst is the possible ability of lignin to use water as sacrificial electron donor. While Kim et al.

did present data supporting water oxidation, the experiments described in Paper II do not support this scenario.

Abiotic factors influence biotic conversion of biomass in several ways, and studies have shown that light-exposure promotes biomass conversion (Austin et al., 2016, 2010, 2006; Berenstecher et al., 2020; Lin et al., 2018). The effect of light has been attributed to increased access of hydrolytic enzymes to polysaccharides contained in plant cell walls, that emerges as light exposure reduces barriers imposed by lignin (Austin et al., 2016). This thesis provides another, or even alternative, explanation based on the impact of light on the redox properties of aromatic compounds in the biomass. Paper II shows that lignin-driven LPMO activity is improved when reactions are exposed to visible light, due to photocatalytic production of reactive oxygen species. Paper III expands upon the findings described in Paper II by showing that light improves the activity of a chitin-active LPMO acting on a natural substrate that is rich in chitin and phenolic compounds. These results provide new avenues for understanding the effect of light-exposure on biomass conversion and constitute a possible molecular explanation for how light affects biomass turnover in Nature.

Nature has developed similar molecular building blocks for synthesizing plant cell walls and insect exoskeletons and similar enzyme systems to decompose these co-polymeric structures. All of this takes place either above or below ground, with various levels of sunlight and oxygen exposure. Given that above ground decomposition of biomass is faster than below ground and that the rigidifying structures of these recalcitrant materials are photoredox-active, it is interesting to speculate whether the interplay between light, photoredox-active structural components, and redox enzymes has influenced how these materials, and/or enzyme systems that degrade these materials, have evolved, and potentially co-evolved, over time.

In conclusion, the work described in this thesis strengthens the increasingly accepted notion that LPMOs are peroxygenases rather than monooxygenases and shows that photobiocatalytic reaction systems allow for controlled delivery of H_2O_2 to the LPMO. Photobiocatalytic reaction setups can be employed to gain further insight into operational stability and catalytic mechanism of LPMOs, as we did here. Eventually such insight will help in harnessing the full potential of LPMOs in industrial applications. Whether light-driven LPMO catalysis will find industrial applications depends on developments in bioprocess design and the nature of the LPMO application. Clearly, the use of light in industrial processing of lignocellulosic biomass at the required high (20 %) dry matter concentrations will be challenging due to limited light penetration. It is conceivable that novel applications of LPMOs emerge in the future, such as using these

enzymes to oxidize plastics or to catalyze specific oxidations of chemical compounds, that may benefit from light-driven control of catalysis.

Of particular interest is the finding that light-exposure of naturally occurring phenolic compounds, i.e., lignin from plant cell walls and catecholamines from insect exoskeletons, enhanced both the activity of HRP on soluble phenolic compounds and LPMO-driven solubilization of recalcitrant polysaccharides. Thus, next to insights that can potentially be exploited in biorefinery applications to contribute to a more renewable and sustainable future, the results presented above shed light on potentially important factors that influence microbial decomposition of biomass and the global carbon cycle.

5 References

Aachmann, F. L., Sørlie, M., Skjåk-Bræk, G., Eijsink, V. G. H., & Vaaje-Kolstad, G. (2012). NMR structure of a lytic polysaccharide monooxygenase provides insight into copper binding, protein dynamics, and substrate interactions. *Proceedings of the National Academy of Sciences of the United States of America*. https://doi.org/10.1073/pnas.1208822109

Andersen, S. O. (2010). Insect cuticular sclerotization: A review. *Insect Biochemistry and Molecular Biology*, *40*(3), 166–178. https://doi.org/https://doi.org/10.1016/j.ibmb.2009.10.007

Andersen, S. O. (2012). Cuticular sclerotization and tanning. In L. I. Gilbert (Ed.), *Insect Molecular Biology and Biochemistry* (pp. 167–192). Academic Press.

Artzi, L., Bayer, E. A., & Moraïs, S. (2017). Cellulosomes: bacterial nanomachines for dismantling plant polysaccharides. *Nature Reviews Microbiology*, *15*(2), 83–95. https://doi.org/10.1038/nrmicro.2016.164

Askarian, F., Uchiyama, S., Masson, H., Sørensen, H. V., Golten, O., Bunæs, A. C., Mekasha, S., Røhr, Å. K., Kommedal, E., Ludviksen, J. A., Arntzen, M. Ø., Schmidt, B., Zurich, R. H., van Sorge, N. M., Eijsink, V. G. H., Krengel, U., Mollnes, T. E., Lewis, N. E., Nizet, V., & Vaaje-Kolstad, G. (2021). The lytic polysaccharide monooxygenase CbpD promotes *Pseudomonas aeruginosa* virulence in systemic infection. *Nature Communications*, *12*(1), 1230. https://doi.org/10.1038/s41467-021-21473-0

Austin, A. T., & Ballaré, C. L. (2010). Dual role of lignin in plant litter decomposition in terrestrial ecosystems. *Proceedings of the National Academy of Sciences*, *107*(10), 4618–4622. https://doi.org/10.1073/pnas.0909396107

Austin, A. T., Méndez, M. S., & Ballaré, C. L. (2016). Photodegradation alleviates the lignin bottleneck for carbon turnover in terrestrial ecosystems. *Proceedings of the National Academy of Sciences*, *113*(16), 4392–4397. https://doi.org/10.1073/pnas.1516157113

Austin, A. T., & Vivanco, L. (2006). Plant litter decomposition in a semi-arid ecosystem controlled by photodegradation. *Nature*, *442*(7102), 555–558. https://doi.org/10.1038/nature05038

Ayuso-Fernández, I., Rencoret, J., Gutiérrez, A., Ruiz-Dueñas, F. J., & Martínez, A. T. (2019). Peroxidase evolution in white-rot fungi follows wood lignin evolution in plants. *Proceedings of the National Academy of Sciences*, *116*(36), 17900–17905. https://doi.org/10.1073/pnas.1905040116

Barber, J. (2016). Photosystem II: the water splitting enzyme of photosynthesis and the origin of oxygen in our atmosphere. *Quarterly Reviews of Biophysics*, *49*, e14. https://doi.org/10.1017/S0033583516000093

Beck, S. M., & Brus, L. E. (1982). Photooxidation of water by *p*-benzoquinone. *Journal of the American Chemical Society*, *104*(4), 1103–1104. https://doi.org/10.1021/ja00368a036

Beeson, W. T., Phillips, C. M., Cate, J. H. D., & Marletta, M. A. (2012). Oxidative cleavage

of cellulose by fungal copper-dependent polysaccharide monooxygenases. *Journal of the American Chemical Society*, *134*(2), 890–892. https://doi.org/10.1021/ja210657t

Berenstecher, P., Vivanco, L., Pérez, L. I., Ballaré, C. L., & Austin, A. T. (2020). Sunlight doubles aboveground carbon loss in a seasonally dry woodland in Patagonia. *Current Biology*, *30*(16), 3243-3251.e3. https://doi.org/https://doi.org/10.1016/j.cub.2020.06.005

Biely, P. (2012). Microbial carbohydrate esterases deacetylating plant polysaccharides. *Biotechnol. Adv.*, *30*(6), 1575–1588. https://doi.org/10.1016/j.biotechadv.2012.04.010

Bissaro, B., Forsberg, Z., Ni, Y., Hollmann, F., Vaaje-Kolstad, G., & Eijsink, V. G. H. (2016a). Fueling biomass-degrading oxidative enzymes by light-driven water oxidation. *Green Chemistry*, *18*(19), 5357–5366. https://doi.org/10.1039/C6GC01666A

Bissaro, B., Isaksen, I., Vaaje-Kolstad, G., Eijsink, V. G. H., & Røhr, Å. K. (2018a). How a lytic polysaccharide monooxygenase binds crystalline chitin. *Biochemistry*, *57*(12), 1893–1906. https://doi.org/10.1021/acs.biochem.8b00138

Bissaro, B., Kommedal, E., Røhr, Å. K., & Eijsink, V. G. H. (2020a). Controlled depolymerization of cellulose by light-driven lytic polysaccharide oxygenases. *Nature Communications*, *11*(1), 890. https://doi.org/10.1038/s41467-020-14744-9

Bissaro, B., Røhr, Å. K., Müller, G., Chylenski, P., Skaugen, M., Forsberg, Z., Horn, S. J., Vaaje-Kolstad, G., & Eijsink, V. G. H. (2017). Oxidative cleavage of polysaccharides by monocopper enzymes depends on H_2O_2. *Nature Chemical Biology*, *13*, 1123–1128. http://dx.doi.org/10.1038/nchembio.2470

Bissaro, B., Rohr, A. K., Skaugen, M., Forsberg, Z., Horn, S. J., Vaaje-Kolstad, G., & Eijsink, V. (2016b). Fenton-type chemistry by a copper enzyme: molecular mechanism of polysaccharide oxidative cleavage. *BioRxiv*. http://biorxiv.org/content/early/2016/12/27/097022.abstract

Bissaro, B., Streit, B., Isaksen, I., Eijsink, V. G. H., Beckham, G. T., DuBois, J. L., & Røhr, Å. K. (2020b). Molecular mechanism of the chitinolytic peroxygenase reaction. *Proceedings of the National Academy of Sciences*, *117*(3), 1504–1513. https://doi.org/10.1073/pnas.1904889117

Bissaro, B., Várnai, A., Røhr, Å. K., & Eijsink, V. G. H. (2018b). Oxidoreductases and Reactive Oxygen Species in Conversion of Lignocellulosic Biomass. *Microbiology and Molecular Biology Reviews*, *82*(4), e00029-18. https://doi.org/10.1128/MMBR.00029-18

Blossom, B. M., Russo, D. A., Singh, R. K., van Oort, B., Keller, M. B., Simonsen, T. I., Perzon, A., Gamon, L. F., Davies, M. J., Cannella, D., Croce, R., Jensen, P. E., Bjerrum, M. J., & Felby, C. (2020). Photobiocatalysis by a lytic polysaccharide monooxygenase using intermittent illumination. *ACS Sustainable Chemistry & Engineering*, *8*(25), 9301–9310. https://doi.org/10.1021/acssuschemeng.0c00702

Boerjan, W., Ralph, J., & Baucher, M. (2003). Lignin biosynthesis. *Annual Review of Plant Biology*, *54*(1), 519–546. https://doi.org/10.1146/annurev.arplant.54.031902.134938

Bonfield, H. E., Knauber, T., Lévesque, F., Moschetta, E. G., Susanne, F., & Edwards, L. J. (2020). Photons as a 21st century reagent. *Nature Communications*, *11*(1), 804. https://doi.org/10.1038/s41467-019-13988-4

Boule, P., Rossi, A., Pilichowski, J. F., & Grabner, G. (1992). Photoreactivity of hydroquinone in aqueous-solution. *New J. Chem.*, *16*, 1053–1062.

Brander, S., Horvath, I., Ipsen, J. Ø., Peciulyte, A., Olsson, L., Hernández-Rollán, C., Nørholm, M. H. H., Mossin, S., Leggio, L. Lo, Probst, C., Thiele, D. J., & Johansen, K. S. (2020). Biochemical evidence of both copper chelation and oxygenase activity at the histidine brace. *Scientific Reports*, *10*(1), 16369. https://doi.org/10.1038/s41598-020-73266-y

Burek, B. O., Bahnemann, D. W., & Bloh, J. Z. (2019). Modeling and optimization of the photocatalytic reduction of molecular oxygen to hydrogen peroxide over titanium dioxide. *ACS Catalysis*. https://doi.org/10.1021/acscatal.8b03638

Cannella, D., Möllers, K. B., Frigaard, N.-U., Jensen, P. E., Bjerrum, M. J., Johansen, K. S., & Felby, C. (2016). Light-driven oxidation of polysaccharides by photosynthetic pigments and a metalloenzyme. *Nature Communications*, *7*, 11134. http://dx.doi.org/10.1038/ncomms11134

Cantarel, B. L., Coutinho, P. M., Rancurel, C., Bernard, T., Lombard, V., & Henrissat, B. (2009). The Carbohydrate-Active EnZymes database (CAZy): an expert resource for Glycogenomics. *Nucleic Acids Res.*, *37*(suppl 1), D233–D238. https://doi.org/10.1093/nar/gkn663

Chitnis, P. R. (2001). Photosystem I: function and physiology. *Annual Review of Plant Physiology and Plant Molecular Biology*, *52*(1), 593–626. https://doi.org/10.1146/annurev.arplant.52.1.593

Christensen, A. M., Schaefer, J., Kramer, K. J., Morgan, T. D., & Hopkins, T. L. (1991). Detection of cross-links in insect cuticle by REDOR NMR spectroscopy. *Journal of the American Chemical Society*, *113*(18), 6799–6802. https://doi.org/10.1021/ja00018a013

Chylenski, P., Bissaro, B., Sørlie, M., Røhr, Å. K., Várnai, A., Horn, S. J., & Eijsink, V. G. H. (2019). Lytic polysaccharide monooxygenases in enzymatic processing of lignocellulosic biomass. *ACS Catalysis*, *9*(6), 4970–4991. https://doi.org/10.1021/acscatal.9b00246

Ciano, L., Davies, G. J., Tolman, W. B., & Walton, P. H. (2018). Bracing copper for the catalytic oxidation of C–H bonds. *Nature Catalysis*, *1*(8), 571–577. https://doi.org/10.1038/s41929-018-0110-9

Cocinero, E. J., Gamblin, D. P., Davis, B. G., & Simons, J. P. (2009). The building blocks of cellulose: the intrinsic conformational structures of cellobiose, its epimer, lactose, and their singly hydrated complexes. *Journal of the American Chemical Society*, *131*(31), 11117–11123. https://doi.org/10.1021/ja903322w

Cosgrove, D. J. (2005). Growth of the plant cell wall. *Nat. Rev. Mol. Cell Biol.*, *6*(11), 850–861. https://doi.org/10.1038/nrm1746

Costa, T. H. F., Kadic', A., Chylenski, P., Várnai, A., Bengtsson, O., Lidén, G., Eijsink, V. G. H., & Horn, S. J. (2020). Demonstration-scale enzymatic saccharification of sulfite-pulped spruce with addition of hydrogen peroxide for LPMO activation. *Biofuels, Bioproducts and Biorefining*, *14*(4), 734–745. https://doi.org/https://doi.org/10.1002/bbb.2103

Courtade, G., Wimmer, R., Røhr, Å. K., Preims, M., Felice, A. K. G., Dimarogona, M., Vaaje-Kolstad, G., Sørlie, M., Sandgren, M., Ludwig, R., Eijsink, V. G. H., & Lillelund Aachmann, F. (2016). Interactions of a fungal lytic polysaccharide monooxygenase with β-glucan substrates and cellobiose dehydrogenase. *Proceedings of the National Academy of Sciences*, *113*(21), 5922–5927. https://doi.org/10.1073/pnas.1602566113

Couturier, M., Ladevèze, S., Sulzenbacher, G., Ciano, L., Fanuel, M., Moreau, C., Villares, A., Cathala, B., Chaspoul, F., Frandsen, K. E., Labourel, A., Herpoël-Gimbert, I., Grisel, S., Haon, M., Lenfant, N., Rogniaux, H., Ropartz, D., Davies, G. J., Rosso, M. N., … Berrin, J. G. (2018). Lytic xylan oxidases from wood-decay fungi unlock biomass degradation. *Nature Chemical Biology*, *14*(3), 306–310. https://doi.org/10.1038/nchembio.2558

Crestini, C., Lange, H., Sette, M., & Argyropoulos, D. S. (2017). On the structure of softwood kraft lignin. *Green Chemistry*, *19*(17), 4104–4121. https://doi.org/10.1039/C7GC01812F

Danneels, B., Tanghe, M., & Desmet, T. (2019). Structural features on the substrate-binding surface of fungal lytic polysaccharide monooxygenases determine their oxidative regioselectivity. *Biotechnology Journal*, *14*(3), 1800211. https://doi.org/https://doi.org/10.1002/biot.201800211

Dodge, N., Russo, D. A., Blossom, B. M., Singh, R. K., van Oort, B., Croce, R., Bjerrum, M. J., & Jensen, P. E. (2020). Water-soluble chlorophyll-binding proteins from *Brassica oleracea* allow for stable photobiocatalytic oxidation of cellulose by a lytic polysaccharide monooxygenase. *Biotechnology for Biofuels*, *13*(1), 192. https://doi.org/10.1186/s13068-020-01832-7

Eastwood, D. C., Floudas, D., Binder, M., Majcherczyk, A., Schneider, P., Aerts, A., Asiegbu, F. O., Baker, S. E., Barry, K., Bendiksby, M., Blumentritt, M., Coutinho, P. M., Cullen, D., De Vries, R. P., Gathman, A., Goodell, B., Henrissat, B., Ihrmark, K., Kauserud, H., … Watkinson, S. C. (2011). The plant cell wall-decomposing machinery underlies the functional diversity of forest fungi. *Science*, *333*(6043), 762–765. https://doi.org/10.1126/science.1205411

Emmanuel, M. A., Greenberg, N. R., Oblinsky, D. G., & Hyster, T. K. (2016). Accessing non-natural reactivity by irradiating nicotinamide-dependent enzymes with light. *Nature*, *540*(7633), 414–417. https://doi.org/10.1038/nature20569

Eriksson, K.-E., Pettersson, B., & Westermark, U. (1974). Oxidation: an important enzyme reaction in fungal degradation of cellulose. *FEBS Letters*, *49*(2), 282–285. https://doi.org/10.1016/0014-5793(74)80531-4

Field, C. B., Behrenfeld, M. J., Randerson, J. T., & Falkowski, P. (1998). Primary

production of the biosphere: integrating terrestrial and oceanic components. *Science*, *281*(5374), 237–240. https://doi.org/10.1126/science.281.5374.237

Filandr, F., Man, P., Halada, P., Chang, H., Ludwig, R., & Kracher, D. (2020). The H_2O_2-dependent activity of a fungal lytic polysaccharide monooxygenase investigated with a turbidimetric assay. *Biotechnology for Biofuels*, *13*(1), 37. https://doi.org/10.1186/s13068-020-01673-4

Filiatrault-Chastel, C., Navarro, D., Haon, M., Grisel, S., Herpoël-Gimbert, I., Chevret, D., Fanuel, M., Henrissat, B., Heiss-Blanquet, S., Margeot, A., & Berrin, J.-G. (2019). AA16, a new lytic polysaccharide monooxygenase family identified in fungal secretomes. *Biotechnology for Biofuels*, *12*(1), 55. https://doi.org/10.1186/s13068-019-1394-y

Forsberg, Z., Bissaro, B., Gullesen, J., Dalhus, B., Vaaje-Kolstad, G., & Eijsink, V. G. H. (2018). Structural determinants of bacterial lytic polysaccharide monooxygenase functionality. *Journal of Biological Chemistry*, *293*(4), 1397–1412. https://doi.org/10.1074/jbc.M117.817130

Forsberg, Z., Vaaje-Kolstad, G., Westereng, B., Bunæs, A. C., Stenstrøm, Y., MacKenzie, A., Sørlie, M., Horn, S. J., & Eijsink, V. G. H. (2011). Cleavage of cellulose by a CBM33 protein. *Protein Science : A Publication of the Protein Society*, *20*(9), 1479–1483. https://doi.org/10.1002/pro.689

Fraaije, M. W., Pikkemaat, M., & Van Berkel, W. J. H. (1997). Enigmatic gratuitous induction of the covalent flavoprotein vanillyl-alcohol oxidase in *Penicillium simplicissimum*. *Applied and Environmental Microbiology*, *63*(2), 435–439. http://www.ncbi.nlm.nih.gov/pubmed/16535508

Fraaije, M. W., Van Den Heuvel, R. H. H., Roelofs, J. C. A. A., & Van Berkel, W. J. H. (1998). Kinetic mechanism of vanillyl-alcohol oxidase with short-chain 4-alkylphenols. *European Journal of Biochemistry*, *253*(3), 712–719. https://doi.org/10.1046/j.1432-1327.1998.2530712.x

Fridovich, I. (1995). Superoxide radical and superoxide dismutases. *Annual Review of Biochemistry*, *64*(1), 97–112. https://doi.org/10.1146/annurev.bi.64.070195.000525

Frommhagen, M., Koetsier, M. J., Westphal, A. H., Visser, J., Hinz, S. W. A., Vincken, J.-P., van Berkel, W. J. H., Kabel, M. A., & Gruppen, H. (2016). Lytic polysaccharide monooxygenases from *Myceliophthora thermophila* C1 differ in substrate preference and reducing agent specificity. *Biotechnology for Biofuels*, *9*(186), 1–17. https://doi.org/10.1186/s13068-016-0594-y

Frommhagen, M., Mutte, S. K., Westphal, A. H., Koetsier, M. J., Hinz, S. W. A., Visser, J., Vincken, J.-P., Weijers, D., van Berkel, W. J. H., Gruppen, H., & Kabel, M. A. (2017). Boosting LPMO-driven lignocellulose degradation by polyphenol oxidase-activated lignin building blocks. *Biotechnology for Biofuels*, *10*(1), 121. https://doi.org/10.1186/s13068-017-0810-4

Frommhagen, M., Westphal, A. H., van Berkel, W. J. H., & Kabel, M. A. (2018). Distinct substrate specificities and electron-donating systems of fungal lytic polysaccharide monooxygenases. *Frontiers in Microbiology*, *9*, 1–22. https://doi.org/10.3389/fmicb.2018.01080

Garcia-Rubio, R., de Oliveira, H. C., Rivera, J., & Trevijano-Contador, N. (2020). The fungal cell wall: *Candida*, *Cryptococcus*, and *Aspergillus* species. In *Frontiers in Microbiology* (Vol. 10). https://www.frontiersin.org/article/10.3389/fmicb.2019.02993

Garcia-Santamarina, S., Probst, C., Festa, R. A., Ding, C., Smith, A. D., Conklin, S. E., Brander, S., Kinch, L. N., Grishin, N. V, Franz, K. J., Riggs-Gelasco, P., Lo Leggio, L., Johansen, K. S., & Thiele, D. J. (2020). A lytic polysaccharide monooxygenase-like protein functions in fungal copper import and meningitis. *Nature Chemical Biology*, *16*(3), 337–344. https://doi.org/10.1038/s41589-019-0437-9

Garron, M.-L., & Cygler, M. (2010). Structural and mechanistic classification of uronic acid-containing polysaccharide lyases. *Glycobiology*, *20*(12), 1547–1573. https://doi.org/10.1093/glycob/cwq122

Giardina, P., Faraco, V., Pezzella, C., Piscitelli, A., Vanhulle, S., & Sannia, G. (2010). Laccases: a never-ending story. *Cellular and Molecular Life Sciences*, *67*(3), 369–385. https://doi.org/10.1007/s00018-009-0169-1

Glass, N. L., Schmoll, M., Cate, J. H. D., & Coradetti, S. (2013). Plant cell wall deconstruction by ascomycete fungi. *Annual Review of Microbiology*, *67*, 477–498. https://doi.org/10.1146/annurev-micro-092611-150044

Gonçalves, A. P., Heller, J., Span, E. A., Rosenfield, G., Do, H. P., Palma-Guerrero, J., Requena, N., Marletta, M. A., & Glass, N. L. (2019). Allorecognition upon fungal cell-cell contact determines social cooperation and impacts the acquisition of multicellularity. *Current Biology*, *29*(18), 3006-3017.e3. https://doi.org/https://doi.org/10.1016/j.cub.2019.07.060

Goto, H., Hanada, Y., Ohno, T., & Matsumura, M. (2004). Quantitative analysis of superoxide ion and hydrogen peroxide produced from molecular oxygen on photoirradiated TiO_2 particles. *Journal of Catalysis*, *225*(1), 223–229. https://doi.org/https://doi.org/10.1016/j.jcat.2004.04.001

Grantham, N. J., Wurman-Rodrich, J., Terrett, O. M., Lyczakowski, J. J., Stott, K., Iuga, D., Simmons, T. J., Durand-Tardif, M., Brown, S. P., Dupree, R., Busse-Wicher, M., & Dupree, P. (2017). An even pattern of xylan substitution is critical for interaction with cellulose in plant cell walls. *Nature Plants*, *3*(11), 859–865. https://doi.org/10.1038/s41477-017-0030-8

Grondin, J. M., Tamura, K., Déjean, G., Abbott, W. D., & Brumer, H. (2017). Polysaccharide Utilization Loci: Fueling Microbial Communities. *Journal of Bacteriology*, *199*(15), e00860-16. https://doi.org/10.1128/JB.00860-16

Haddad Momeni, M., Fredslund, F., Bissaro, B., Raji, O., Vuong, T. V, Meier, S., Nielsen, T. S., Lombard, V., Guigliarelli, B., Biaso, F., Haon, M., Grisel, S., Henrissat, B., Welner, D. H., Master, E. R., Berrin, J.-G., & Abou Hachem, M. (2021). Discovery of fungal oligosaccharide-oxidising flavo-enzymes with previously unknown substrates, redox-activity profiles and interplay with LPMOs. *Nature Communications*, *12*(1), 2132. https://doi.org/10.1038/s41467-021-22372-0

Hahn, T., Tafi, E., Paul, A., Salvia, R., Falabella, P., & Zibek, S. (2020). Current state of chitin purification and chitosan production from insects. *Journal of Chemical Technology & Biotechnology*, *95*(11), 2775–2795.

https://doi.org/https://doi.org/10.1002/jctb.6533

Hahn, T., Tafi, E., von Seggern, N., Falabella, P., Salvia, R., Thomä, J., Febel, E., Fijalkowska, M., Schmitt, E., Stegbauer, L., & Zibek, S. (2021). Purification of chitin from pupal exuviae of the black soldier fly. *Waste and Biomass Valorization*. https://doi.org/10.1007/s12649-021-01645-1

Haitjema, C. H., Gilmore, S. P., Henske, J. K., Solomon, K. V, de Groot, R., Kuo, A., Mondo, S. J., Salamov, A. A., LaButti, K., Zhao, Z., Chiniquy, J., Barry, K., Brewer, H. M., Purvine, S. O., Wright, A. T., Hainaut, M., Boxma, B., van Alen, T., Hackstein, J. H. P., … O'Malley, M. A. (2017). A parts list for fungal cellulosomes revealed by comparative genomics. *Nature Microbiology*, *2*(8), 17087. https://doi.org/10.1038/nmicrobiol.2017.87

Hangasky, J. A., Iavarone, A. T., & Marletta, M. A. (2018). Reactivity of O_2 versus H_2O_2 with polysaccharide monooxygenases. *Proceedings of the National Academy of Sciences*, *115*(19), 4915–4920. https://doi.org/10.1073/pnas.1801153115

Harris, P. V., Welner, D., McFarland, K. C., Re, E., Navarro Poulsen, J. C., Brown, K., Salbo, R., Ding, H., Vlasenko, E., Merino, S., Xu, F., Cherry, J., Larsen, S., & Lo Leggio, L. (2010). Stimulation of lignocellulosic biomass hydrolysis by proteins of glycoside hydrolase family 61: Structure and function of a large, enigmatic family. *Biochemistry*, *49*(15), 3305–3316. https://doi.org/10.1021/bi100009p

Hedegård, E. D., & Ryde, U. (2018). Molecular mechanism of lytic polysaccharide monooxygenases. *Chemical Science*, *9*(15), 3866–3880. https://doi.org/10.1039/c8sc00426a

Hedison, T. M., Breslmayr, E., Shanmugam, M., Karnpakdee, K., Heyes, D. J., Green, A. P., Ludwig, R., Scrutton, N. S., & Kracher, D. (2021). Insights into the H_2O_2-driven catalytic mechanism of fungal lytic polysaccharide monooxygenases. *The FEBS Journal*, *288*(13), 4115–4128. https://doi.org/https://doi.org/10.1111/febs.15704

Hemsworth, G. R., Henrissat, B., Davies, G. J., & Walton, P. H. (2014). Discovery and characterization of a new family of lytic polysaccharide monooxygenases. *Nature Chemical Biology*, *10*(2), 122–126. https://doi.org/10.1038/nchembio.1417

Hemsworth, G. R., Taylor, E., Kim, R. Q., Gregory, R. C., Lewis, S. J., Turkenburg, J. P., Parkin, A., Davies, G. J., & Walton, P. H. (2013). The copper active site of CBM33 polysaccharide oxygenases. *Journal of the American Chemical Society*. https://doi.org/10.1021/ja402106e

Higasi, P. M. R., Velasco, J. A., Pellegrini, V. O. A., de Araújo, E. A., França, B. A., Keller, M. B., Labate, C. A., Blossom, B. M., Segato, F., & Polikarpov, I. (2021). Light-stimulated *T. thermophilus* two-domain LPMO9H: Low-resolution SAXS model and synergy with cellulases. *Carbohydrate Polymers*, *260*, 117814. https://doi.org/https://doi.org/10.1016/j.carbpol.2021.117814

Hofrichter, M., & Ullrich, R. (2014). Oxidations catalyzed by fungal peroxygenases. *Current Opinion in Chemical Biology*, *19*, 116–125. https://doi.org/10.1016/j.cbpa.2014.01.015

Hopkins, T. L., Morgan, T. D., Aso, Y., & Kramer, K. J. (1982). *N*-β-alanyldopamine:

major role in insect cuticle tanning. *Science*, *217*(4557), 364–366. https://doi.org/10.1126/science.217.4557.364

Hopkins, T. L., Starkey, S. R., Xu, R., Merritt, M. E., Schaefer, J., & Kramer, K. J. (1999). Catechols involved in sclerotization of cuticle and egg pods of the grasshopper, *Melanoplus sanguinipes*, and their interactions with cuticular proteins. *Archives of Insect Biochemistry and Physiology*, *40*(3), 119–128.

Horn, S. J., Vaaje-Kolstad, G., Westereng, B., & Eijsink, V. G. H. (2012). Novel enzymes for the degradation of cellulose. *Biotechnology for Biofuels*, *5*(1), 45. https://doi.org/10.1186/1754-6834-5-45

Hu, J., Arantes, V., Pribowo, A., Gourlay, K., & Saddler, J. N. (2014). Substrate factors that influence the synergistic interaction of AA9 and cellulases during the enzymatic hydrolysis of biomass. *Energy & Environmental Science*, *7*(7), 2308. https://doi.org/10.1039/c4ee00891j

Huynh, M. T., Anson, C. W., Cavell, A. C., Stahl, S. S., & Hammes-Schiffer, S. (2016). Quinone $1e^-$ and $2e^-/2H^+$ reduction potentials: identification and analysis of deviations from systematic scaling relationships. *Journal of the American Chemical Society*, *138*(49), 15903–15910. https://doi.org/10.1021/jacs.6b05797

Jiang, X., Manawan, M., Feng, T., Qian, R., Zhao, T., Zhou, G., Kong, F., Wang, Q., Dai, S., & Pan, J. H. (2018). Anatase and rutile in evonik aeroxide P25: heterojunctioned or individual nanoparticles? *Catalysis Today*, *300*, 12–17. https://doi.org/https://doi.org/10.1016/j.cattod.2017.06.010

Jones, S. M., Transue, W. J., Meier, K. K., Kelemen, B., & Solomon, E. I. (2020). Kinetic analysis of amino acid radicals formed in H_2O_2-driven Cu^I LPMO reoxidation implicates dominant homolytic reactivity. *Proceedings of the National Academy of Sciences*, *117*(22), 11916–11922. https://doi.org/10.1073/pnas.1922499117

Kang, X., Kirui, A., Dickwella Widanage, M. C., Mentink-Vigier, F., Cosgrove, D. J., & Wang, T. (2019). Lignin-polysaccharide interactions in plant secondary cell walls revealed by solid-state NMR. *Nature Communications*, *10*(1), 347. https://doi.org/10.1038/s41467-018-08252-0

Karkehabadi, S., Hansson, H., Kim, S., Piens, K., Mitchinson, C., & Sandgren, M. (2008). The first structure of a glycoside hydrolase family 61 member, Cel61B from *Hypocrea jecorina*, at 1.6 A resolution. *Journal of Molecular Biology*, *383*(1), 144–154. https://doi.org/10.1016/j.jmb.2008.08.016

Karlson, P., & Sekeris, C. E. (1962). *N*-acetyl-dopamine as sclerotizing agent of the insect cuticle. *Nature*, *195*(4837), 183–184. https://doi.org/10.1038/195183a0

Kim, J., Lee, S. L., Tieves, F., Paul, C. E., Hollmann, F., & Park, C. B. (2019). Nicotinamide adenine dinucleotide as a photocatalyst. *Science Advances*, *5*(7), eaax0501. https://doi.org/10.1126/sciadv.aax0501

Kim, J., Nguyen, T. V. T., Kim, Y. H., Hollmann, F., & Park, C. B. (2022). Lignin as a multifunctional photocatalyst for solar-powered biocatalytic oxyfunctionalization of C–H bonds. *Nature Synthesis*, *1*(3), 217–226. https://doi.org/10.1038/s44160-022-00035-2

Kim, S., Ståhlberg, J., Sandgren, M., Paton, R. S., & Beckham, G. T. (2014). Quantum mechanical calculations suggest that lytic polysaccharide monooxygenases use a copper-oxyl, oxygen-rebound mechanism. *Proceedings of the National Academy of Sciences of the United States of America*, *111*(1), 149–154. https://doi.org/10.1073/pnas.1316609111

Kirui, A., Zhao, W., Deligey, F., Yang, H., Kang, X., Mentink-Vigier, F., & Wang, T. (2022). Carbohydrate-aromatic interface and molecular architecture of lignocellulose. *Nature Communications*, *13*(1), 538. https://doi.org/10.1038/s41467-022-28165-3

Kittl, R., Kracher, D., Burgstaller, D., Haltrich, D., & Ludwig, R. (2012). Production of four *Neurospora crassa* lytic polysaccharide monooxygenases in *Pichia pastoris* monitored by a fluorimetric assay. *Biotechnology for Biofuels*, *5*(1), 79. https://doi.org/10.1186/1754-6834-5-79

Kjaergaard, C. H., Qayyum, M. F., Wong, S. D., Xu, F., Hemsworth, G. R., Walton, D. J., Young, N. A., Davies, G. J., Walton, P. H., Johansen, K. S., Hodgson, K. O., Hedman, B., & Solomon, E. I. (2014). Spectroscopic and computational insight into the activation of O_2 by the mononuclear Cu center in polysaccharide monooxygenases. *Proceedings of the National Academy of Sciences of the United States of America*, *111*(24), 8797–8802. https://doi.org/10.1073/pnas.1408115111

Kont, R., Bissaro, B., Eijsink, V. G. H., & Väljamäe, P. (2020). Kinetic insights into the peroxygenase activity of cellulose-active lytic polysaccharide monooxygenases (LPMOs). *Nature Communications*, *11*(1), 5786. https://doi.org/10.1038/s41467-020-19561-8

Kont, R., Pihlajaniemi, V., Borisova, A. S., Aro, N., Marjamaa, K., Loogen, J., Büchs, J., Eijsink, V. G. H., Kruus, K., & Väljamäe, P. (2019). The liquid fraction from hydrothermal pretreatment of wheat straw provides lytic polysaccharide monooxygenases with both electrons and H_2O_2 co-substrate. *Biotechnology for Biofuels*, *12*(1), 235. https://doi.org/10.1186/s13068-019-1578-5

Koo, C. W., Tucci, F. J., He, Y., & Rosenzweig, A. C. (2022). Recovery of particulate methane monooxygenase structure and activity in a lipid bilayer. *Science*, *375*(6586), 1287–1291. https://doi.org/10.1126/science.abm3282

Kracher, D., Forsberg, Z., Bissaro, B., Gangl, S., Preims, M., Sygmund, C., Eijsink, V. G. H., & Ludwig, R. (2020). Polysaccharide oxidation by lytic polysaccharide monooxygenase is enhanced by engineered cellobiose dehydrogenase. *The FEBS Journal*, *287*(5), 897–908. https://doi.org/https://doi.org/10.1111/febs.15067

Kracher, D., & Ludwig, R. (2016a). Cellobiose dehydrogenase: an essential enzyme for lignocellulose degradation in nature – a review / cellobiosedehydrogenase: ein essentielles enzym für den lignozelluloseabbau in der natur – eine übersicht. *Die Bodenkultur: Journal of Land Management, Food and Environment*, *67*(3), 145–163. https://doi.org/doi:10.1515/boku-2016-0013

Kracher, D., Scheiblbrandner, S., Felice, A. K. G., Breslmayr, E., Preims, M., Haltrich, D., Eijsink, V. G. H., & Ludwig, R. (2016b). Extracellular electron transfer systems fuel cellulose oxidative degradation. *Science*, *352*(6289), 1098–1101.

https://doi.org/10.1126/science.aaf3165

Kurašin, M., & Väljamäe, P. (2011). Processivity of cellobiohydrolases is limited by the substrate. *Journal of Biological Chemistry*, *286*(1), 169–177. https://doi.org/https://doi.org/10.1074/jbc.M110.161059

Kuusk, S., Bissaro, B., Kuusk, P., Forsberg, Z., Eijsink, V. G. H., Sørlie, M., & Väljamäe, P. (2018). Kinetics of H_2O_2-driven degradation of chitin by a bacterial lytic polysaccharide monooxygenase. *Journal of Biological Chemistry*, *293*, 523–531. https://doi.org/10.1074/jbc.M117.817593

Kuusk, S., Kont, R., Kuusk, P., Heering, A., Sørlie, M., Bissaro, B., Eijsink, V. G. H., & Väljamäe, P. (2019). Kinetic insights into the role of the reductant in H_2O_2-driven degradation of chitin by a bacterial lytic polysaccharide monooxygenase. *Journal of Biological Chemistry* , *294*(5), 1516–1528. https://doi.org/10.1074/jbc.RA118.006196

Kuusk, S., & Väljamäe, P. (2021). Kinetics of H_2O_2-driven catalysis by a lytic polysaccharide monooxygenase from the fungus Trichoderma reesei. *Journal of Biological Chemistry*, *297*(5), 101256. https://doi.org/https://doi.org/10.1016/j.jbc.2021.101256

Labourel, A., Frandsen, K. E. H., Zhang, F., Brouilly, N., Grisel, S., Haon, M., Ciano, L., Ropartz, D., Fanuel, M., Martin, F., Navarro, D., Rosso, M.-N., Tandrup, T., Bissaro, B., Johansen, K. S., Zerva, A., Walton, P. H., Henrissat, B., Leggio, L. Lo, & Berrin, J.-G. (2020). A fungal family of lytic polysaccharide monooxygenase-like copper proteins. *Nature Chemical Biology*, *16*(3), 345–350. https://doi.org/10.1038/s41589-019-0438-8

Lairson, L. L., Henrissat, B., Davies, G. J., & Withers, S. G. (2008). Glycosyltransferases: structures, functions, and mechanisms. *Annu. Rev. Biochem.*, *77*, 521–555. https://doi.org/10.1146/annurev.biochem.76.061005.092322

Lancefield, C. S., Wienk, H. L. J., Boelens, R., Weckhuysen, B. M., & Bruijnincx, P. C. A. (2018). Identification of a diagnostic structural motif reveals a new reaction intermediate and condensation pathway in kraft lignin formation. *Chemical Science*, *9*(30), 6348–6360. https://doi.org/10.1039/C8SC02000K

Larsbrink, J., Rogers, T. E., Hemsworth, G. R., McKee, L. S., Tauzin, A. S., Spadiut, O., Klinter, S., Pudlo, N. A., Urs, K., Koropatkin, N. M., Creagh, A. L., Haynes, C. A., Kelly, A. G., Cederholm, S. N., Davies, G. J., Martens, E. C., & Brumer, H. (2014). A discrete genetic locus confers xyloglucan metabolism in select human gut Bacteroidetes. *Nature*, *506*(7489), 498–502. https://doi.org/10.1038/nature12907

Larsbrink, J., Zhu, Y., Kharade, S. S., Kwiatkowski, K. J., Eijsink, V. G. H., Koropatkin, N. M., McBride, M. J., & Pope, P. B. (2016). A polysaccharide utilization locus from *Flavobacterium johnsoniae* enables conversion of recalcitrant chitin. *Biotechnology for Biofuels*, *9*(1), 260. https://doi.org/10.1186/s13068-016-0674-z

Lee, S. H., Choi, D. S., Kuk, S. K., & Park, C. B. (2018). Photobiocatalysis: activating redox enzymes by direct or indirect transfer of photoinduced electrons. *Angewandte Chemie International Edition*, *57*(27), 7958–7985. https://doi.org/https://doi.org/10.1002/anie.201710070

Lee, S. H., Kwon, Y.-C., Kim, D.-M., & Park, C. B. (2013). Cytochrome P450-catalyzed O-dealkylation coupled with photochemical NADPH regeneration. *Biotechnology and Bioengineering*, *110*(2), 383–390. https://doi.org/https://doi.org/10.1002/bit.24729

Levasseur, A., Drula, E., Lombard, V., Coutinho, P. M., & Henrissat, B. (2013). Expansion of the enzymatic repertoire of the CAZy database to integrate auxiliary redox enzymes. *Biotechnology for Biofuels*, *6*(1), 41. https://doi.org/10.1186/1754-6834-6-41

Li, X., Beeson, W. T., Phillips, C. M., Marletta, M. A., & Cate, J. H. D. (2012). Structural basis for substrate targeting and catalysis by fungal polysaccharide monooxygenases. *Structure*, *20*(6), 1051–1061. https://doi.org/10.1016/j.str.2012.04.002

Lin, Y., Karlen, S. D., Ralph, J., & King, J. Y. (2018). Short-term facilitation of microbial litter decomposition by ultraviolet radiation. *Science of The Total Environment*, *615*, 838–848. https://doi.org/https://doi.org/10.1016/j.scitotenv.2017.09.239

Loose, J. S. M., Arntzen, M. Ø., Bissaro, B., Ludwig, R., Eijsink, V. G. H., & Vaaje-Kolstad, G. (2018). Multipoint precision binding of substrate protects lytic polysaccharide monooxygenases from self-destructive off-pathway processes. *Biochemistry*, *57*(28), 4114–4124. https://doi.org/10.1021/acs.biochem.8b00484

Manavalan, T., Stepnov, A. A., Hegnar, O. A., & Eijsink, V. G. H. (2021). Sugar oxidoreductases and LPMOs – two sides of the same polysaccharide degradation story? *Carbohydrate Research*, *505*, 108350. https://doi.org/https://doi.org/10.1016/j.carres.2021.108350

Matsumura, H., Umezawa, K., Takeda, K., Sugimoto, N., Ishida, T., Samejima, M., Ohno, H., Yoshida, M., Igarashi, K., & Nakamura, N. (2014). Discovery of a eukaryotic pyrroloquinoline quinone-dependent oxidoreductase belonging to a new auxiliary activity family in the database of carbohydrate-active enzymes. *PLoS ONE*, *9*(8), e104851. https://doi.org/10.1371/journal.pone.0104851

Meents, M. J., Watanabe, Y., & Samuels, A. L. (2018). The cell biology of secondary cell wall biosynthesis. *Annals of Botany*, *121*(6), 1107–1125. https://doi.org/10.1093/aob/mcy005

Merino, S. T., & Cherry, J. (2007). *Progress and Challenges in Enzyme Development for Biomass Utilization BT - Biofuels* (L. Olsson (ed.); pp. 95–120). Springer Berlin Heidelberg. https://doi.org/10.1007/10_2007_066

Merritt, M. E., Christensen, A. M., Kramer, K. J., Hopkins, T. L., & Schaefer, J. (1996). Detection of intercatechol cross-links in insect cuticle by solid-state carbon-13 and nitrogen-15 NMR. *Journal of the American Chemical Society*, *118*(45), 11278–11282. https://doi.org/10.1021/ja961621o

Mifsud, M., Gargiulo, S., Iborra, S., Arends, I. W. C. E., Hollmann, F., & Corma, A. (2014). Photobiocatalytic chemistry of oxidoreductases using water as the electron donor. *Nature Communications*, *5*, 3145. https://doi.org/10.1038/ncomms4145

Miglbauer, E., Gryszel, M., & Głowacki, E. D. (2020). Photochemical evolution of hydrogen peroxide on lignins. *Green Chemistry*, *22*(3), 673–677.

https://doi.org/10.1039/C9GC04324A

Möllers, K. B., Mikkelsen, H., Simonsen, T. I., Cannella, D., Johansen, K. S., Bjerrum, M. J., & Felby, C. (2017). On the formation and role of reactive oxygen species in light-driven LPMO oxidation of phosphoric acid swollen cellulose. *Carbohydrate Research*, *448*, 182–186. https://doi.org/10.1016/j.carres.2017.03.013

Müller, G., Chylenski, P., Bissaro, B., Eijsink, V. G. H., & Horn, S. J. (2018). The impact of hydrogen peroxide supply on LPMO activity and overall saccharification efficiency of a commercial cellulase cocktail. *Biotechnology for Biofuels*, *11*(1). https://doi.org/10.1186/s13068-018-1199-4

Munk, L., Sitarz, A. K., Kalyani, D. C., Mikkelsen, J. D., & Meyer, A. S. (2015). Can laccases catalyze bond cleavage in lignin? *Biotechnology Advances*, *33*(1), 13–24. https://doi.org/https://doi.org/10.1016/j.biotechadv.2014.12.008

Munzone, A., El Kerdi, B., Fanuel, M., Rogniaux, H., Ropartz, D., Réglier, M., Royant, A., Simaan, A. J., & Decroos, C. (2020). Characterization of a bacterial copper-dependent lytic polysaccharide monooxygenase with an unusual second coordination sphere. *The FEBS Journal*, *287*(15), 3298–3314. https://doi.org/https://doi.org/10.1111/febs.15203

Muraleedharan, M. N., Zouraris, D., Karantonis, A., Topakas, E., Sandgren, M., Rova, U., Christakopoulos, P., & Karnaouri, A. (2018). Effect of lignin fractions isolated from different biomass sources on cellulose oxidation by fungal lytic polysaccharide monooxygenases. *Biotechnology for Biofuels*, *11*(1), 296. https://doi.org/10.1186/s13068-018-1294-6

Naas, A. E., MacKenzie, A. K., Mravec, J., Schückel, J., Willats, W. G. T., Eijsink, V. G. H., & Pope, P. B. (2014). Do rumen bacteroidetes utilize an alternative mechanism for cellulose degradation? *MBio*, *5*(4), e01401-14. https://doi.org/10.1128/mBio.01401-14

Nguyen, T. T. X., Tomberlin, J. K., & Vanlaerhoven, S. (2015). Ability of black soldier fly (diptera: stratiomyidae) larvae to recycle food waste. *Environmental Entomology*, *44*(2), 406–410. https://doi.org/10.1093/ee/nvv002

Nishiyama, Y., Langan, P., & Chanzy, H. (2002). Crystal structure and hydrogen-bonding system in cellulose Iβ from synchrotron x-ray and neutron fiber diffraction. *Journal of the American Chemical Society*, *124*(31), 9074–9082. https://doi.org/10.1021/ja0257319

Nishiyama, Y., Sugiyama, J., Chanzy, H., & Langan, P. (2003). Crystal structure and hydrogen bonding system in cellulose Iα from synchrotron x-ray and neutron fiber diffraction. *Journal of the American Chemical Society*, *125*(47), 14300–14306. https://doi.org/10.1021/ja037055w

Notley, S. M., Pettersson, B., & Wågberg, L. (2004). Direct measurement of attractive van der waals' forces between regenerated cellulose surfaces in an aqueous environment. *Journal of the American Chemical Society*, *126*(43), 13930–13931. https://doi.org/10.1021/ja045992d

O'Dell, W. B., Agarwal, P. K., & Meilleur, F. (2017). Oxygen activation at the active site of a fungal lytic polysaccharide monooxygenase. *Angewandte Chemie*, *129*(3),

785–788. https://doi.org/10.1002/ange.201610502

Pan, Y., Ma, H., Li, Z., Du, Y., Liu, Y., Yang, J., & Li, G. (2020). Selective conversion of lignin model veratryl alcohol by photosynthetic pigment via photo-generated reactive oxygen species. *Chemical Engineering Journal*, *393*, 124772. https://doi.org/https://doi.org/10.1016/j.cej.2020.124772

Paspaliari, D. K., Loose, J. S. M., Larsen, M. H., & Vaaje-Kolstad, G. (2015). *Listeria monocytogenes* has a functional chitinolytic system and an active lytic polysaccharide monooxygenase. *FEBS Journal*, *282*(5), 921–936. https://doi.org/10.1111/febs.13191

Paulsson, M., & Parkås, J. (2012). Light-induced yellowing of lignocellulosic pulps–mechanisms and preventive methods. *BioResources*, *7*(4), 5995–6040.

Payne, C. M., Knott, B. C., Mayes, H. B., Hansson, H., Himmel, M. E., Sandgren, M., Ståhlberg, J., & Beckham, G. T. (2015). Fungal cellulases. *Chemical Reviews* 115(3), 1308–1448. https://doi.org/10.1021/cr500351c

Phillips, C. M., Beeson, W. T., Cate, J. H., & Marletta, M. A. (2011). Cellobiose dehydrogenase and a copper-dependent polysaccharide monooxygenase potentiate cellulose degradation by *Neurospora crassa*. *ACS Chemical Biology*, *6*(12), 1399–1406. https://doi.org/10.1021/cb200351y

Purushotham, P., Ho, R., & Zimmer, J. (2020). Architecture of a catalytically active homotrimeric plant cellulose synthase complex. *Science*, *369*(6507), 1089–1094. https://doi.org/10.1126/science.abb2978

Quinlan, R. J., Sweeney, M. D., Lo Leggio, L., Otten, H., Poulsen, J.-C. N., Johansen, K. S., Krogh, K. B. R. M., Jørgensen, C. I., Tovborg, M., Anthonsen, A., Tryfona, T., Walter, C. P., Dupree, P., Xu, F., Davies, G. J., & Walton, P. H. (2011). Insights into the oxidative degradation of cellulose by a copper metalloenzyme that exploits biomass components. *Proceedings of the National Academy of Sciences of the United States of America*, *108*(37), 15079–15084. https://doi.org/10.1073/pnas.1105776108

Ralph, J., Lapierre, C., & Boerjan, W. (2019). Lignin structure and its engineering. *Current Opinion in Biotechnology*, *56*, 240–249. https://doi.org/https://doi.org/10.1016/j.copbio.2019.02.019

Rashid, G. M. M., Zhang, X., Wilkinson, R. C., Fülöp, V., Cottyn, B., Baumberger, S., & Bugg, T. D. H. (2018). *Sphingobacterium sp*. T2 manganese superoxide dismutase catalyzes the oxidative demethylation of polymeric lignin via generation of hydroxyl radical. *ACS Chemical Biology*, *13*(10), 2920–2929. https://doi.org/10.1021/acschembio.8b00557

Reese, E. T., Siu, R. G., & Levinson, H. S. (1950). The biological degradation of soluble cellulose derivatives and its relationship to the mechanism of cellulose hydrolysis. *Journal of Bacteriology*, *59*(4), 485–497. https://doi.org/10.1128/jb.59.4.485-497.1950

Rieder, L., Petrović, D., Väljamäe, P., Eijsink, V. G. H., & Sørlie, M. (2021a). Kinetic characterization of a putatively chitin-active lpmo reveals a preference for soluble substrates and absence of monooxygenase activity. *ACS Catalysis*, *11*(18), 11685–

11695. https://doi.org/10.1021/acscatal.1c03344

Rieder, L., Stepnov, A. A., Sørlie, M., & Eijsink, V. G. H. (2021b). Fast and specific peroxygenase reactions catalyzed by fungal mono-copper enzymes. *Biochemistry*, *60*(47), 3633–3643. https://doi.org/10.1021/acs.biochem.1c00407

Rinaudo, M. (2006). Chitin and chitosan: Properties and applications. *Progress in Polymer Science*, *31*(7), 603–632. https://doi.org/https://doi.org/10.1016/j.progpolymsci.2006.06.001

Rodríguez-Zúñiga, U. F., Cannella, D., Giordano, R. de C., Giordano, R. de L. C., Jørgensen, H., & Felby, C. (2015). Lignocellulose pretreatment technologies affect the level of enzymatic cellulose oxidation by LPMO. *Green Chem.*, *17*(5), 2896–2903. https://doi.org/10.1039/C4GC02179G

Romero, N. A., & Nicewicz, D. A. (2016). Organic photoredox catalysis. *Chemical Reviews*, *116*(17), 10075–10166. https://doi.org/10.1021/acs.chemrev.6b00057

Ruiz-Dueñas, F. J., Martínez, M. J., & Martínez, A. T. (1999). Molecular characterization of a novel peroxidase isolated from the ligninolytic fungus *Pleurotus eryngii*. *Molecular Microbiology*, *31*(1), 223–235. https://doi.org/https://doi.org/10.1046/j.1365-2958.1999.01164.x

Rytioja, J., Hildén, K., Yuzon, J., Hatakka, A., de Vries, R. P., & Mäkelä, M. R. (2014). Plant-polysaccharide-degrading enzymes from basidiomycetes. *Microbiology and Molecular Biology Reviews*, *78*(4), 614–649. https://doi.org/10.1128/MMBR.00035-14

Sabbadin, F., Hemsworth, G. R., Ciano, L., Henrissat, B., Dupree, P., Tryfona, T., Marques, R. D. S., Sweeney, S. T., Besser, K., Elias, L., Pesante, G., Li, Y., Dowle, A. A., Bates, R., Gomez, L. D., Simister, R., Davies, G. J., Walton, P. H., Bruce, N. C., & McQueen-Mason, S. J. (2018). An ancient family of lytic polysaccharide monooxygenases with roles in arthropod development and biomass digestion. *Nature Communications*, *9*(1). https://doi.org/10.1038/s41467-018-03142-x

Sabbadin, F., Urresti, S., Henrissat, B., Avrova, A. O., Welsh, L. R. J., Lindley, P. J., Csukai, M., Squires, J. N., Walton, P. H., Davies, G. J., Bruce, N. C., Whisson, S. C., & McQueen-Mason, S. J. (2021). Secreted pectin monooxygenases drive plant infection by pathogenic oomycetes. *Science*, *373*(6556), 774–779. https://doi.org/10.1126/science.abj1342

Sáez-Jiménez, V., Baratto, M. C., Pogni, R., Rencoret, J., Gutiérrez, A., Santos, J. I., Martínez, A. T., & Ruiz-Dueñas, F. J. (2015). Demonstration of lignin-to-peroxidase direct electron transfer: a transiet-state kinetics, directed mutagenesis, EPR, and NMR study. *Journal of Biological Chemistry*, *290*(38), 23201–23213. https://doi.org/10.1074/jbc.M115.665919

Sánchez-Ruiz, M. I., Ayuso-Fernández, I., Rencoret, J., González-Ramírez, A. M., Linde, D., Davó-Siguero, I., Romero, A., Gutiérrez, A., Martínez, A. T., & Ruiz-Dueñas, F. J. (2021). Agaricales mushroom lignin peroxidase: from structure–function to degradative capabilities. In *Antioxidants* (Vol. 10, Issue 9). https://doi.org/10.3390/antiox10091446

Schaefer, J., Kramer, K. J., Garbow, J. R., Jacob, G. S., Stejskal, E. O., Hopkins, T. L., &

Speirs, R. D. (1987). Aromatic cross-links in insect cuticle: detection by solid-state 13C and 15N NMR. *Science*, *235*(4793), 1200–1204. https://doi.org/10.1126/science.3823880

Scheller, H. V., & Ulvskov, P. (2010). Hemicelluloses. *Annual Review of Plant Biology*, *61*(1), 263–289. https://doi.org/10.1146/annurev-arplant-042809-112315

Schmermund, L., Jurkaš, V., Özgen, F. F., Barone, G. D., Büchsenschütz, H. C., Winkler, C. K., Schmidt, S., Kourist, R., & Kroutil, W. (2019). Photo-biocatalysis: biotransformations in the presence of light. *ACS Catalysis*, *9*(5), 4115–4144. https://doi.org/10.1021/acscatal.9b00656

Sepulchro, A. G. V, Pellegrini, V. O. A., Dias, L. D., Kadowaki, M. A. S., Cannella, D., & Polikarpov, I. (2021). Combining pieces: a thorough analysis of light activation boosting power and co-substrate preferences for the catalytic efficiency of lytic polysaccharide monooxygenase *Mt*LPMO9A. *Biofuel Research Journal*, *8*(3), 1454–1464. https://doi.org/10.18331/BRJ2021.8.3.5

Shen, J., Griffiths, P. T., Campbell, S. J., Utinger, B., Kalberer, M., & Paulson, S. E. (2021). Ascorbate oxidation by iron, copper and reactive oxygen species: review, model development, and derivation of key rate constants. *Scientific Reports*, *11*(1), 7417. https://doi.org/10.1038/s41598-021-86477-8

Simmons, T. J., Mortimer, J. C., Bernardinelli, O. D., Pöppler, A.-C., Brown, S. P., deAzevedo, E. R., Dupree, R., & Dupree, P. (2016). Folding of xylan onto cellulose fibrils in plant cell walls revealed by solid-state NMR. *Nature Communications*, *7*, 13902. https://doi.org/10.1038/ncomms13902

Somerville, C., Bauer, S., Brininstool, G., Facette, M., Hamann, T., Milne, J., Osborne, E., Paredez, A., Persson, S., Raab, T., Vorwerk, S., & Youngs, H. (2004). Toward a systems approach to understanding plant cell walls. *Science*, *306*(5705), 2206–2211. https://doi.org/10.1126/science.1102765

Song, Y., & Buettner, G. R. (2010). Thermodynamic and kinetic considerations for the reaction of semiquinone radicals to form superoxide and hydrogen peroxide. *Free Radical Biology & Medicine*, *49*(6), 919–962. https://doi.org/10.1016/j.freeradbiomed.2010.05.009

Sørlie, M., Horn, S. J., Vaaje-Kolstad, G., & Eijsink, V. G. H. (2020). Using chitosan to understand chitinases and the role of processivity in the degradation of recalcitrant polysaccharides. *Reactive and Functional Polymers*, *148*, 104488. https://doi.org/https://doi.org/10.1016/j.reactfunctpolym.2020.104488

Span, E. A., Suess, D. L. M., Deller, M. C., Britt, R. D., & Marletta, M. A. (2017). The role of the secondary coordination sphere in a fungal polysaccharide monooxygenase. *ACS Chemical Biology*, *12*(4), 1095–1103. https://doi.org/10.1021/acschembio.7b00016

Stepnov, A. A., Christensen, I. A., Forsberg, Z., Aachmann, F. L., Courtade, G., & Eijsink, V. G. H. (2022a). The impact of reductants on the catalytic efficiency of a lytic polysaccharide monooxygenase and the special role of dehydroascorbic acid. *FEBS Letters*, *596*(1), 53–70. https://doi.org/https://doi.org/10.1002/1873-3468.14246

Stepnov, A. A., Eijsink, V. G. H., & Forsberg, Z. (2022b). Enhanced *in situ* H_2O_2 production explains synergy between an LPMO with a cellulose-binding domain and a single-domain LPMO. *Scientific Reports*, *12*(1), 6129. https://doi.org/10.1038/s41598-022-10096-0

Stepnov, A. A., Forsberg, Z., Sørlie, M., Nguyen, G.-S., Wentzel, A., Røhr, Å. K., & Eijsink, V. G. H. (2021). Unraveling the roles of the reductant and free copper ions in LPMO kinetics. *Biotechnology for Biofuels*, *14*(1), 28. https://doi.org/10.1186/s13068-021-01879-0

Sun, P., Laurent, C. V. F. P., Boerkamp, V. J. P., van Erven, G., Ludwig, R., van Berkel, W. J. H., & Kabel, M. A. (2022). Regioselective C4 and C6 double oxidation of cellulose by lytic polysaccharide monooxygenases. *ChemSusChem*, *15*(2), e202102203. https://doi.org/https://doi.org/10.1002/cssc.202102203

Suzuki, K., Suzuki, M., Taiyoji, M., Nikaidou, N., & Watanabe, T. (1998). Chitin Binding Protein (CBP21) in the culture supernatant of *Serratia marcescens* 2170. *Bioscience, Biotechnology, and Biochemistry*, *65*(1), 128–135. https://www.jstage.jst.go.jp/article/bbb/62/1/62_1_128/_article

Tan, T.-C., Kracher, D., Gandini, R., Sygmund, C., Kittl, R., Haltrich, D., Hällberg, B. M., Ludwig, R., & Divne, C. (2015). Structural basis for cellobiose dehydrogenase action during oxidative cellulose degradation. *Nature Communications*, *6*(May), 7542. https://doi.org/10.1038/ncomms8542

Tandrup, T., Frandsen, K. E. H., Johansen, K. S., Berrin, J.-G., & Lo Leggio, L. (2018). Recent insights into lytic polysaccharide monooxygenases (LPMOs). *Biochemical Society Transactions*, *46*(6), 1431–1447. https://doi.org/10.1042/BST20170549

Terrett, O. M., Lyczakowski, J. J., Yu, L., Iuga, D., Franks, W. T., Brown, S. P., Dupree, R., & Dupree, P. (2019). Molecular architecture of softwood revealed by solid-state NMR. *Nature Communications*, *10*(1), 4978. https://doi.org/10.1038/s41467-019-12979-9

Timell, T. E. (1967). Recent progress in the chemistry of wood hemicelluloses. *Wood Science and Technology*, *1*(1), 45–70. https://doi.org/10.1007/BF00592255

Tobimatsu, Y., & Schuetz, M. (2019). Lignin polymerization: how do plants manage the chemistry so well? *Current Opinion in Biotechnology*, *56*, 75–81. https://doi.org/https://doi.org/10.1016/j.copbio.2018.10.001

Tõlgo, M., Hegnar, O. A., Østby, H., Várnai, A., Vilaplana, F., Eijsink, V. G. H., & Olsson, L. (2022). Comparison of six lytic polysaccharide monooxygenases from *Thermothielavioides terrestris* shows that functional variation underlies the multiplicity of lpmo genes in filamentous fungi. *Applied and Environmental Microbiology*, *88*(6), e00096-22. https://doi.org/10.1128/aem.00096-22

Tomberlin, J. K., van Huis, A., Benbow, M. E., Jordan, H., Astuti, D. A., Azzollini, D., Banks, I., Bava, V., Borgemeister, C., Cammack, J. A., Chapkin, R. S., Čičková, H., Crippen, T. L., Day, A., Dicke, M., Drew, D. J. W., Emhart, C., Epstein, M., Finke, M., Zheng, L. (2015). Protecting the environment through insect farming as a means to produce protein for use as livestock, poultry, and aquaculture feed. *Journal of Insects as Food and Feed*, *1*(4), 307–309. https://doi.org/10.3920/JIFF2015.0098

Tuveng, T. R., Hagen, L. H., Mekasha, S., Frank, J., Arntzen, M. Ø., Vaaje-Kolstad, G., & Eijsink, V. G. H. (2017). Genomic, proteomic and biochemical analysis of the chitinolytic machinery of *Serratia marcescens* BJL200. *Biochimica et Biophysica Acta (BBA) - Proteins and Proteomics*, *1865*(4), 414–421. https://doi.org/https://doi.org/10.1016/j.bbapap.2017.01.007

Udagedara, S. R., Wijekoon, C. J. K., Xiao, Z., Wedd, A. G., & Maher, M. J. (2019). The crystal structure of the CopC protein from *Pseudomonas fluorescens* reveals amended classifications for the CopC protein family. *Journal of Inorganic Biochemistry*, *195*, 194–200. https://doi.org/https://doi.org/10.1016/j.jinorgbio.2019.03.007

Vaaje-Kolstad, G., Forsberg, Z., Loose, J. S., Bissaro, B., & Eijsink, V. G. (2017). Structural diversity of lytic polysaccharide monooxygenases. *Current Opinion in Structural Biology*, *44*, 67–76. https://doi.org/10.1016/j.sbi.2016.12.012

Vaaje-Kolstad, G., Horn, S. J., Sørlie, M., & Eijsink, V. G. H. (2013). The chitinolytic machinery of *Serratia marcescens* - a model system for enzymatic degradation of recalcitrant polysaccharides. *The FEBS Journal*. https://doi.org/10.1111/febs.12181

Vaaje-Kolstad, G., Horn, S. J., van Aalten, D. M. F., Synstad, B., & Eijsink, V. G. H. (2005a). The non-catalytic chitin-binding protein CBP21 from *Serratia marcescens* is essential for chitin degradation. *The Journal of Biological Chemistry*, *280*(31), 28492–28497. https://doi.org/10.1074/jbc.M504468200

Vaaje-Kolstad, G., Houston, D. R., Riemen, A. H. K., Eijsink, V. G. H., & van Aalten, D. M. F. (2005b). Crystal structure and binding properties of the *Serratia marcescens* chitin-binding protein CBP21. *The Journal of Biological Chemistry*, *280*(12), 11313–11319. https://doi.org/10.1074/jbc.M407175200

Vaaje-Kolstad, G., Westereng, B., Horn, S. J., Liu, Z., Zhai, H., Sørlie, M., & Eijsink, V. G. H. (2010). An oxidative enzyme boosting the enzymatic conversion of recalcitrant polysaccharides. *Science (New York, N.Y.)*, *330*(6001), 219–222. https://doi.org/10.1126/science.1192231

van Schie, M. M. C. H., Paul, C. E., Arends, I. W. C. E., & Hollmann, F. (2019a). Photoenzymatic epoxidation of styrenes. *Chemical Communications*, *55*(12), 1790–1792. https://doi.org/10.1039/C8CC08149B

van Schie, M. M. C. H., Zhang, W., Tieves, F., Choi, D. S., Park, C. B., Burek, B. O., Bloh, J. Z., Arends, I. W. C. E., Paul, C. E., Alcalde, M., & Hollmann, F. (2019b). Cascading g-C_3N_4 and peroxygenases for selective oxyfunctionalization reactions. *ACS Catalysis*, *9*(8), 7409–7417. https://doi.org/10.1021/acscatal.9b01341

Vanholme, R., De Meester, B., Ralph, J., & Boerjan, W. (2019). Lignin biosynthesis and its integration into metabolism. *Current Opinion in Biotechnology*, *56*, 230–239. https://doi.org/https://doi.org/10.1016/j.copbio.2019.02.018

Vanholme, R., Demedts, B., Morreel, K., Ralph, J., & Boerjan, W. (2010). Lignin Biosynthesis and Structure. *Plant Physiology*, *153*(3), 895–905. https://doi.org/10.1104/pp.110.155119

Várnai, A., Umezawa, K., Yoshida, M., & Eijsink, V. G. H. (2018). The pyrroloquinoline-

quinone-dependent pyranose dehydrogenase from *Coprinopsis cinerea* drives lytic polysaccharide monooxygenase Action. *Applied and Environmental Microbiology*, *84*(11), e00156-18. https://doi.org/10.1128/AEM.00156-18

Vermaas, J. V, Crowley, M. F., & Beckham, G. T. (2019). A quantitative molecular atlas for interactions between lignin and cellulose. *ACS Sustainable Chemistry & Engineering*, *7*(24), 19570–19583. https://doi.org/10.1021/acssuschemeng.9b04648

Vishtal, A. G., & Kraslawski, A. (2011). Challenges in industrial applications of technical lignins. *BioResources*, *6*(3), 3547–3568.

Vu, V. V, Beeson, W. T., Span, E. A., Farquhar, E. R., & Marletta, M. A. (2014). A family of starch-active polysaccharide monooxygenases. *Proceedings of the National Academy of Sciences of the United States of America*, *111*(38), 13822–13827. https://doi.org/10.1073/pnas.1408090111

Wang, B., Johnston, E. M., Li, P., Shaik, S., Davies, G. J., Walton, P. H., & Rovira, C. (2018). QM/MM studies into the H_2O_2-dependent activity of lytic polysaccharide monooxygenases: evidence for the formation of a caged hydroxyl radical intermediate. *ACS Catalysis*, *8*(2), 1346–1351. https://doi.org/10.1021/acscatal.7b03888

Wang, B., Walton, P. H., & Rovira, C. (2019). Molecular mechanisms of oxygen activation and hydrogen peroxide formation in lytic polysaccharide monooxygenases. *ACS Catalysis*. https://doi.org/10.1021/acscatal.9b00778

Wang, Y., Lan, D., Durrani, R., & Hollmann, F. (2017). Peroxygenases en route to becoming dream catalysts. What are the opportunities and challenges? *Current Opinion in Chemical Biology*, *37*, 1–9. https://doi.org/https://doi.org/10.1016/j.cbpa.2016.10.007

Westereng, B., Cannella, D., Wittrup Agger, J., Jørgensen, H., Larsen Andersen, M., Eijsink, V. G. H., & Felby, C. (2015). Enzymatic cellulose oxidation is linked to lignin by long-range electron transfer. *Scientific Reports*, *5*(November), 18561. https://doi.org/10.1038/srep18561

Westereng, B., Ishida, T., Vaaje-Kolstad, G., Wu, M., Eijsink, V. G. H., Igarashi, K., Samejima, M., Ståhlberg, J., Horn, S. J., & Sandgren, M. (2011). The putative endoglucanase *Pc*GH61D from *Phanerochaete chrysosporium* is a metal-dependent oxidative enzyme that cleaves cellulose. *PloS One*, *6*(11), e27807. https://doi.org/10.1371/journal.pone.0027807

Willot, S. J.-P., Fernández-Fueyo, E., Tieves, F., Pesic, M., Alcalde, M., Arends, I. W. C. E., Park, C. B., & Hollmann, F. (2019). Expanding the spectrum of light-driven peroxygenase reactions. *ACS Catalysis*, *9*(2), 890–894. https://doi.org/10.1021/acscatal.8b03752

Xu, R., Huang, X., Morgan, T. D., Prakash, O., Kramer, K. J., & Hawley, M. D. (1996). Characterization of products from the reactions of *N*-acetyldopamine quinone with *N*-acetylhistidine. *Archives of Biochemistry and Biophysics*, *329*(1), 56–64. https://doi.org/https://doi.org/10.1006/abbi.1996.0191

Yan, N., & Chen, X. (2015). Sustainability: Don't waste seafood waste. *Nature*,

524(7564), 155–157. https://doi.org/10.1038/524155a

Zamil, M. S., & Geitmann, A. (2017). The middle lamella—more than a glue. *Physical Biology*, *14*(1), 15004. https://doi.org/10.1088/1478-3975/aa5ba5

Zhang, H., Zhao, Y., Zhang, H., Zhou, H., Wang, H., Zong, X., Yin, H., & Li, C. (2020). Establishing inorganic-biological hybrid photoelectrochemical platform towards sustainable conversion of α-chitin. *Applied Catalysis B: Environmental*, *265*, 118558. https://doi.org/https://doi.org/10.1016/j.apcatb.2019.118558

Zhang, L., & Gellerstedt, G. (1994). Reactive structures in wood and high-yield pulps. IV. Daylight-induced oxidation of stilbene structures in the solid state. *Acta Chemica Scandinavica*, *48*(6), 490–497.

Zhang, W., Fernández-Fueyo, E., Ni, Y., van Schie, M., Gacs, J., Renirie, R., Wever, R., Mutti, F. G., Rother, D., Alcalde, M., & Hollmann, F. (2018). Selective aerobic oxidation reactions using a combination of photocatalytic water oxidation and enzymatic oxyfunctionalizations. *Nature Catalysis*, *1*(1), 55–62. https://doi.org/10.1038/s41929-017-0001-5

Zhong, X., Zhang, L., van Wezel, G. P., Vijgenboom, E., & Claessen, D. (2022). Role for a lytic polysaccharide monooxygenase in cell wall remodeling in *Streptomyces coelicolor*. *MBio*, e00456-22. https://doi.org/10.1128/mbio.00456-22

Zhu, K. Y., Merzendorfer, H., Zhang, W., Zhang, J., & Muthukrishnan, S. (2016). Biosynthesis, turnover, and functions of chitin in insects. *Annual Review of Entomology*, *61*(1), 177–196. https://doi.org/10.1146/annurev-ento-010715-023933

6 Publications

Controlled depolymerization of cellulose by light-driven lytic polysaccharide oxygenases

Kommedal EG*, Bisarro B*, Røhr ÅK, Eijsink VGH

Paper I

nature COMMUNICATIONS

ARTICLE

https://doi.org/10.1038/s41467-020-14744-9 OPEN

Controlled depolymerization of cellulose by light-driven lytic polysaccharide oxygenases

Bastien Bissaro[1,2,3], Eirik Kommedal[1,3], Åsmund K. Røhr[1] & Vincent G.H. Eijsink[1✉]

Lytic polysaccharide (mono)oxygenases (LPMOs) perform oxidative cleavage of polysaccharides, and are key enzymes in biomass processing and the global carbon cycle. It has been shown that LPMO reactions may be driven by light, using photosynthetic pigments or photocatalysts, but the mechanism behind this highly attractive catalytic route remains unknown. Here, prompted by the discovery that LPMOs catalyze a peroxygenase reaction more efficiently than a monooxygenase reaction, we revisit these light-driven systems, using an LPMO from *Streptomyces coelicolor* (*Sc*AA10C) as model cellulolytic enzyme. By using coupled enzymatic assays, we show that H_2O_2 is produced and necessary for efficient light-driven activity of *Sc*AA10C. Importantly, this activity is achieved without addition of reducing agents and proportional to the light intensity. Overall, the results highlight the importance of controlling fluxes of reactive oxygen species in LPMO reactions and demonstrate the feasibility of light-driven, tunable enzymatic peroxygenation to degrade recalcitrant polysaccharides.

[1] Faculty of Chemistry, Biotechnology and Food Science, Norwegian University of Life Sciences (NMBU), 1432 Ås Oslo, Norway. [2] INRAE, Aix Marseille University, UMR1163 Biodiversité et Biotechnologie Fongiques, 13009 Marseille, France. [3] These authors contributed equally: Bastien Bissaro, Eirik Kommedal. ✉email: vincent.eijsink@nmbu.no

Environmental threats and future shortage in fossil-based energy and chemicals call for the development of sustainable processes for converting renewable sources into carbon and energy. Plant biomass represents an abundant source of renewable material, mainly in the form of polysaccharides in plant cell walls. However, the co-polymeric and recalcitrant nature of these cell walls constitutes a major hurdle in the extraction and valorization of the carbohydrate building blocks. Chitin represents another abundant, but recalcitrant source of renewable material, found in e.g. the shells of insects and crustaceans. Facing the structural intricacies of these biomaterials, plant-degrading and chitin-degrading microorganisms have developed complex arsenals of chemical and enzymatic tools for their deconstruction. Among the enzymatic tools are enzymes today known as lytic polysaccharide monooxygenases (LPMOs), which play a major role in biomass conversion by oxidative cleavage and, thus, structural disruption of biopolymers such as chitin[1,2], cellulose[3–5], as well as co-polymeric structures made of cellulose and hemicelluloses[6–8]. This disruptive action boosts the depolymerizing action of glycoside hydrolases[1,2,5]. LPMOs, classified today in families 9–11 and 13–16 of the auxiliary activities (AA) in the Carbohydrate Active enZymes database[9], are ubiquitous enzymes with key roles in biological conversion of biomass by fungi and bacteria, but also with suggested roles in microbial pathogenicity[10–12]. LPMOs contribute to the efficiency of modern commercial cellulase cocktails used at industrial scale[13,14].

The use of light as a cheap energy source represents a key pillar of the emerging bioeconomy. Although the field of photocatalysis has been explored for decades, the field of photobiocatalysis, i.e., catalysis at the cross roads between photocatalysis and enzymology has been emerging more recently[15]. Harnessing the energy carried by visible light to drive biochemical processes, including enzymatic reactions, under eco-friendly conditions, constitutes a potentially valuable addition to currently available biotechnological tools. LPMO action requires energy in the form of reducing equivalents, and, in 2016, two studies were published that address the possibility of driving LPMO-catalyzed biomass conversion by light (Fig. 1)[16,17]. Cannella et al. showed that upon photo-excitation of pigments (e.g., chlorophyllin, *Chl*), and, notably, in the presence of a reductant, the activity of AA9E from *Thielavia terrestris* (*Tt*AA9E) on amorphous cellulose (PASC) could be boosted by up to two orders of magnitude[16]. In the same year, Bissaro et al. showed that a photocatalyst (vanadium-doped titanium dioxide, V-TiO_2), catalyzing the thermodynamically challenging oxidation of water upon exposure to visible light, could generate the necessary reducing equivalents for oxidation of crystalline cellulose (Avicel) by AA10C from *Streptomyces coelicolor* (*Sc*AA10C)[17]. Both studies discussed possible mechanistic scenarios behind the observed effects, but the underlying mechanisms of both systems remain to be clarified.

Recently, there have been major developments in our understanding of the LPMO mechanism. LPMOs are mono-copper enzymes that catalyze the hydroxylation of the C1 and/or the C4 carbon in scissile glycosidic bonds[4,18] (Fig. 1). Since the seminal study by Vaaje-Kolstad et al.[2], LPMOs have been considered as monooxygenases, requiring the delivery of O_2, two electrons and two protons for each catalytic cycle ($R\text{–}H + O_2 + 2e^- + 2\,H^+ \rightarrow R\text{–}OH + H_2O$) via different putative reaction pathways[19,20]. In laboratory conditions, LPMO reactions are typically fueled by dissolved oxygen and added external reductants, such as ascorbic acid (AscA)[2]. Subsequently to the publication of the photobiocatalytic studies mentioned above[16,17], we showed for one AA9-type and two AA10-type LPMOs that these enzymes, when supplied with both O_2 and H_2O_2, preferentially use H_2O_2 as co-substrate. This observation led us to suggest that the previously described need for O_2 may reflect the fact that O_2 is a precursor of H_2O_2 in standard aerobic conditions typically used in LPMO reactions[21,22]. The reaction with H_2O_2 is best described as that of a peroxygenase ($R\text{–}H + H_2O_2 \rightarrow R\text{–}OH + H_2O$), where the oxygen atom, the two protons and the reducing equivalents are supplied simultaneously in the form of H_2O_2 to an activated LPMO (i.e., the reduced LPMO-Cu(I) state). Subsequently, several experimental studies have confirmed the efficiency of H_2O_2-driven LPMO reactions for different LPMO/substrate systems[23–29]. Furthermore, modeling studies have demonstrated the feasibility of the peroxygenase reaction[23,30–33].

Clearly, this recent paradigm change calls for a re-investigation of light-driven cellulose oxidation by LPMOs, in particular the potential underlying role of reactive oxygen species (ROS). Here, we use coupled enzymatic assays to probe the roles of superoxide ($O_2^{\bullet-}$) and H_2O_2 in the oxidation of Avicel by *Sc*AA10C fueled by visible light-exposed Chl or V-TiO_2 (Fig. 1). We reveal the chemistry underlying light-driven LPMO action and show that light alone can drive LPMO catalysis. These results suggest avenues towards sustainable exploitation of mono-copper catalysts.

Results

Properties of chlorophyllin. Chlorophyllin (Chl), a water-soluble derivative of chlorophyll, is composed of a porphyrin ring metallated with copper (Fig. 1; see Methods section). We verified that the used commercial Chl has the expected absorbance and fluorescence properties, in part by comparison with copper-deficient chlorin e_6 and Cu(II)-reconstituted chlorin e_6 (Supplementary Fig. 1). The UV–Vis absorbance spectrum of Chl was nearly identical to that of Cu(II)-reconstituted chlorin e_6, suggesting that the latter metallated species is the main constituent of the Chl powder (Supplementary Fig. 1a). Likewise, reconstituted Cu(II)-chlorin e_6 and Chl showed equivalent fluorescence spectra (Supplementary Fig. 1b), with (expected) sharp excitation ($\lambda^{max} = 343$ nm) and emission peaks ($\lambda^{max} = 685$ nm), corroborating the fact that the photoactive species present in the Chl powder is Cu(II)-chlorin e_6.

It has been shown that photo-excited chlorophyll has a very low reduction potential ($E_0 = -0.55$ V vs. SHE[34]) and that saponified chlorophyll can catalyze the single electron reduction of O_2 into $O_2^{\bullet-}$[35], which requires a strong reductant ($E_0 = -0.33$ V vs. SHE[36]). However, no similar data exist for Chl, which displays a molecular structure similar to saponified chlorophyll but binds copper instead of magnesium.

To assess the redox properties of non photo-excited Chl species, we performed square-wave voltammetry experiments (Supplementary Table 1 and Supplementary Fig. 2) and found that the reduction potentials, E_p, of Chl, chlorin e_6 and metallated chlorin e_6 were all in the range of 0.6–0.7 V vs. SHE, in accordance with the reduction potentials for Chl and non-metallated chlorin e_6 reported by Novak and Komorsky-Lovric[37]. The measured reduction potentials of non photo-excited Chl species indicate that the LPMO in this study, *Sc*AA10C-Cu(II) ($E_0 \sim 0.236 \pm 0.007$ V vs. SHE[38]), cannot be reduced by these Chl species in absence of light.

Fueling LPMO reactions with light-activated chlorophyllin. We first repeated experiments initially described by Cannella et al.[16], i.e., combining AscA and Chl/light, using *Sc*AA10C and a lightning system we previously successfully used for the V-TiO_2 system[17]. Indeed, use of the Chl/light-AscA system gave very high initial catalytic rates, notably accompanied by almost immediate enzyme inactivation (Fig. 2a; orange curve, see the 25% curve in Supplementary Fig. 3a, c for more details concerning the initial phase of the reaction). In accordance with the work by Cannella

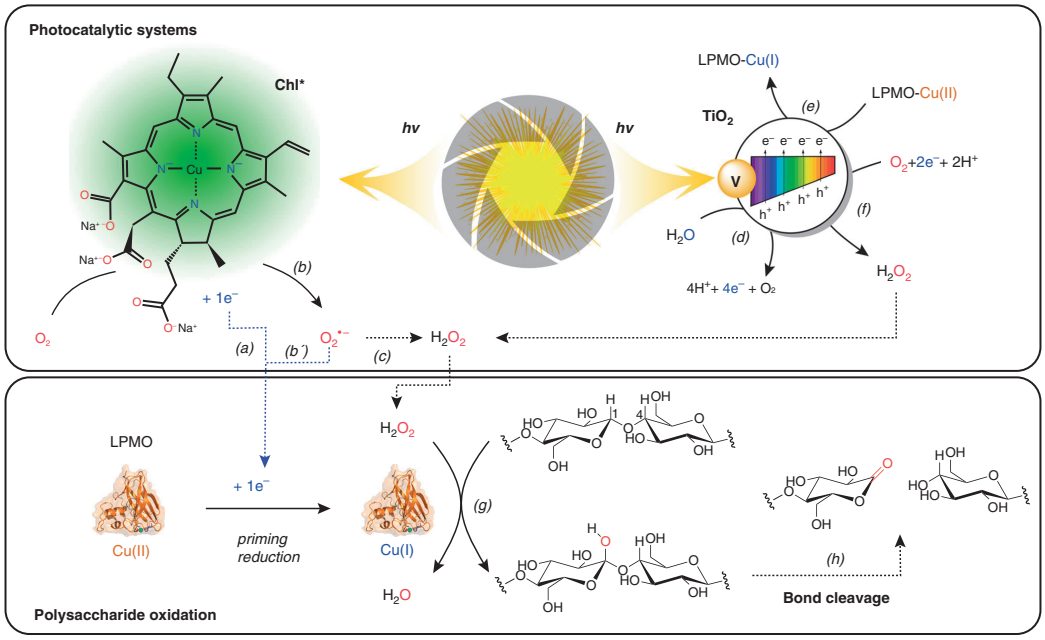

Fig. 1 Light-driven LPMO-catalyzed oxidation of cellulose. For the Chl-based system, Cannella et al.[16] proposed that photo-excited electrons activate the LPMO (*a*) and that reductants such as AscA or lignin could serve as electron donor to regenerate Chl (not shown). Here, we provide evidence for an alternative reduction pathway, where $O_2^{\bullet-}$, produced via single electron reduction of O_2 by photo-excited Chl (Chl*) (*b*), acts as reductant (*b'*). Disproportionation of $O_2^{\bullet-}$ to H_2O_2 (*c*) can occur spontaneously or be accelerated by enzymatic action (e.g., superoxide dismutase, SOD) or by chemical reactions, such as reduction by AscA. In the V-TiO_2 based system, reducing equivalents (in the form of excited electrons) are derived from V-TiO_2-mediated and light-promoted oxidation of water (*d*). Several reduction reactions can occur at the surface of V-TiO_2, including reduction of LPMO-Cu(II) to LPMO-Cu(I) (*e*[17]), reduction of O_2 to H_2O_2 (*f*[49,66]) or reduction of H_2O_2 to H_2O (not shown[67]). The lower panel shows that the LPMO reduced by either of the two systems uses the generated H_2O_2 for cellulose oxidation (*g*). Hydroxylation of the glycosidic bond carbon leads to spontaneous bond cleavage (*h*[30,68]). Of note, these schemes focus on H_2O_2-driven LPMO catalysis, whereas O_2-driven LPMO catalysis is not considered. See the main text for further details. The pigment shown in the top panel is the trisodium copper chlorin e_6, the main component of chlorophyllin (*Chl*).

et al.[16], the initial rates obtained with Chl/light-AscA were much higher than the rates obtained in a standard reaction with only AscA (Fig. 2a, blue curve). Yet, the standard reaction with only AscA produced more oxidized products compared to the reaction with Chl/light-AscA, because the LPMO stayed active for a much longer time (Fig. 2a). Interestingly, at the light intensities used here, which are considerably higher than those used by Cannella et al., the Chl/light system could also fuel the LPMO reaction in the absence of AscA, yielding relatively stable progress curves spanning several hours (Fig. 2a; black curve). Most importantly, this result shows that LPMO catalysis can take place with visible light as the only energy source (i.e., in the absence of added reducing power). Control experiments, including experiments in which the enzyme was replaced by various concentrations of Cu (II)SO_4 (0–1000 µM), did not yield LPMO products (Supplementary Fig. 4).

Figure 2c shows that the Chl/light-AscA system alone (i.e., in absence of an LPMO) rapidly produces large amounts of H_2O_2 and Fig. 2b shows that H_2O_2 accumulates early in the LPMO reaction, at a time point where the LPMO is no longer active (as shown by the progress curve in Fig. 2a). Without added AscA, the system produces much lower amounts of H_2O_2, at a more regular pace (Fig. 2c), and H_2O_2 does not accumulate in the LPMO reactions (Fig. 2b), likely because it is consumed by the LPMO, which stays active over a long-time period (Fig. 2a). The reaction with only AscA provides a less clear picture, but it is clear that H_2O_2 is produced under these conditions (Fig. 2c), and it is worthwhile noting the small peak in the apparent level of accumulated H_2O_2 at 240 min in the LPMO reaction (Fig. 2b), i.e., just after the LPMO has become inactive (Fig. 2a). All in all, the data shown in Fig. 2a–c are compatible with the notion that LPMO activity is correlated with the availability of H_2O_2 and, that too high levels of H_2O_2 in LPMO reactions lead to enzyme inactivation and subsequent H_2O_2 accumulation. Control experiments in which fresh reaction components (Avicel, AscA and/or LPMO) were added to a reaction with AscA+Chl/light after 60 min of incubation (i.e., long after product formation had ceased, Fig. 2a) showed that only addition of fresh LPMO led to the reinitiation of product formation, confirming the impact of enzyme inactivation (Supplementary Fig. 5).

We then assessed whether the ability of the Chl/light system to drive LPMO reactions could be linked to the expected production of $O_2^{\bullet-}$ by this system[35]. Superoxide dismutase (SOD) enzymatically converts $O_2^{\bullet-}$ to H_2O_2 (Supplementary Fig. 6) and screening of a range of SOD concentrations showed that low amounts of SOD (100 nM) increased the LPMO initial rate and that higher amounts of SOD (up to 1 µM) led to almost immediate inactivation of the LPMO (Fig. 2d; more data in Supplementary Fig. 7). Accordingly, we observed that addition of 100 nM SOD led to increased H_2O_2 production (Fig. 2f) while yielding relatively low H_2O_2 accumulation in the complete system (Fig. 2e). On the other hand, addition of 1 µM SOD led to higher

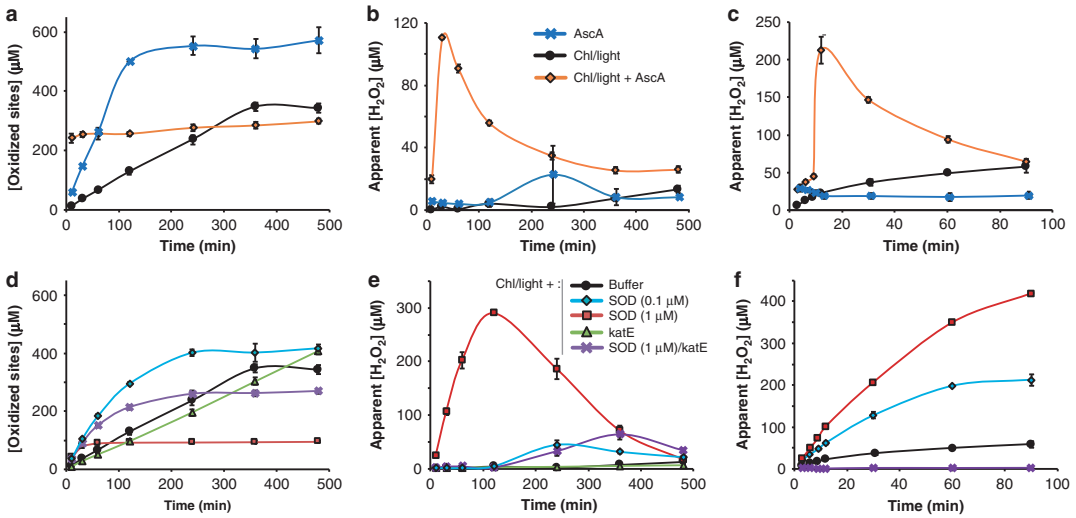

Fig. 2 Probing the role of reactive oxygen species in the light/Chl/LPMO system. The graphs show time-courses for the release of aldonic acid products (**a**, **d**) and apparent H_2O_2 levels (**b**, **e**) in LPMO (*Sc*AA10C, 0.5 μM) reactions with substrate (Avicel, 10 g L^{-1}), as well as apparent H_2O_2 levels in equivalent reactions lacking the LPMO (**c**, **f**). The top (**a**–**c**) panels show results for reactions fueled by Chl (500 μM) exposed to visible light ($I = 25\%$ I_{max}, approx. 42 W cm^{-2}) in the absence or presence of AscA (1 mM), or fueled by 1 mM AscA alone, in the dark. **d**–**f** Effect of SOD (0.1 or 1 μM) and catalase, katE (10 μg mL^{-1}), on the reaction fueled by Chl/light. The legend code displayed in **b** applies also to **a**, **c**; likewise the legend code in **e** applies also to **d**, **f**. All reactions were carried out in sodium phosphate buffer (50 mM, pH 7.0) at 40 °C, under magnetic stirring. Before product quantification, solubilized cello-oligosaccharides were hydrolyzed by *Tf*Cel5A, to convert the LPMO products to a mixture of only two oxidized products with a degree of polymerization of 2 and 3 [GlcGlc1A, $(Glc)_2Glc1A$], the amounts of which were summed up to yield the concentration of oxidized sites. It must be noted that the LPMO and the redox-active compounds in each of the reactions can engage in multiple side reactions, such as oxidation of AscA by H_2O_2 or generation of H_2O_2 by the LPMO, which explains why H_2O_2 levels are not stable and referred to as apparent. Error bars show ± s.d. ($n = 3$, independent experiments). Source data are provided as a Source Data file.

H_2O_2 levels (Fig. 2f) and accumulation of high levels of H_2O_2 in the reaction with the (rapidly inactivated) LPMO and substrate (Fig. 2e). These results indicate that the Chl/light system produces large amounts of $O_2^{\bullet-}$ and that the degree of conversion $O_2^{\bullet-}$ to H_2O_2, e.g., by SOD (Fig. 2d–f), determines both the catalytic rate and the stability of the LPMO.

Addition of catalase (katE), a H_2O_2 consuming enzyme (Supplementary Fig. 6), to the reaction containing a (too) high amount of SOD (1 μM) had a clear beneficial effect, leading to higher LPMO activity over a longer period (Fig. 2d) and little accumulation of H_2O_2 (Fig. 2f). Addition of catalase to the Chl/light system gave a stable LPMO reaction, with only a slight reduction in rate, no visible enzyme inactivation within the 12-h measuring period (Fig. 2d), and almost no accumulation of H_2O_2 (Fig. 2e). In light of the idea that H_2O_2 drives LPMO action, it may seem surprising that, while catalase expectedly abolished accumulation of H_2O_2 (Fig. 2f), it hardly affected, or even had a seemingly positive effect on, LPMO activity. There are, however, straightforward explanations for this paradox. Firstly, the beneficial effect of catalase on the reaction with 1 μM SOD is due to catalase removing the surplus of H_2O_2 that otherwise would lead to LPMO inactivation. Secondly, kinetic data[25,39] show that a reduced LPMO in the presence of substrate will easily compete with catalase for available H_2O_2; it is thus plausible that, while catalase consumes produced H_2O_2 in the absence of the LPMO (Fig. 2f), H_2O_2 will primarily be consumed by the LPMO in reactions containing both enzymes and an LPMO substrate (Fig. 2d).

If the ability of the Chl/light system to drive LPMO reactions indeed is due to the production of $O_2^{\bullet-}$, which is subsequently converted to H_2O_2, the huge effect of adding AscA (Fig. 2a–c) suggests that AscA catalyzes the otherwise spontaneous conversion of $O_2^{\bullet-}$ to H_2O_2, as has indeed been shown (see ref. [40]; Supplementary Fig. 6). Accordingly, the initial rate of LPMO catalysis and the degree of enzyme inactivation could be modulated by varying the amount of AscA (Supplementary Fig. 8).

Likewise, there was a clear correlation between the light intensity, which determines the rate of $O_2^{\bullet-}$ generation, and LPMO activity for both the Chl/light (Fig. 3 and Supplementary Fig. 3) and the Chl/light-AscA system (Supplementary Fig. 3). Figure 3 shows that the decrease in LPMO activity upon decreasing the light intensity applied to the Chl/light system (Fig. 3b) correlates with decreased production of H_2O_2 (measured in absence of the LPMO) (Fig. 3a). Importantly, in the absence of LPMO activity, H_2O_2 generated by Chl/light system will be further reduced, which implies that the measured apparent levels of H_2O_2 are likely an underestimation of the true levels of produced H_2O_2. On the other hand, when the LPMO and substrate are present, one could expect that the high affinity of the LPMO for H_2O_2 results in efficient integration of H_2O_2[25] in oxidized reaction products. Accordingly, while Fig. 3a shows an apparent retardation in the rate of H_2O_2 production in the absence of the LPMO, Fig. 3b shows a linear increase in LPMO products over time.

Taken together, the data presented above are compatible with a scenario in which the ability of the Chl/light and Chl/light-AscA systems to drive LPMO reactions is due to the light-driven generation of $O_2^{\bullet-}$, which is converted to H_2O_2. As shown by Fig. 2 and Supplementary Figs. 3, 7, 8 and discussed above, and in

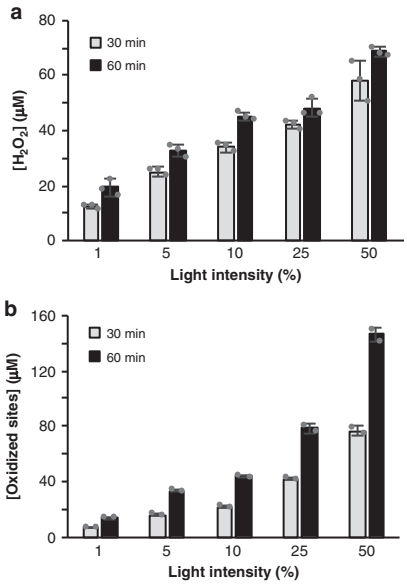

Fig. 3 The effect of light intensity on H_2O_2 production and LPMO activity in the Chl-system. The graphs show, for different light intensities (100% = approx. 168 W cm^{-2}), **a** the apparent quantity of H_2O_2 generated in reactions with Chl (500 μM)/light and Avicel and **b** the amount of soluble aldonic acid products released in identical reactions that also contained *Sc*AA10C (0.5 μM). See Supplementary Fig. 3b–d for complete time courses of *Sc*AA10C-catalyzed oxidation of Avicel. Note that direct quantitative comparison of the levels of produced H_2O_2 and oxidized products is not possible because only soluble LPMO products were quantified, and, more importantly, measured H_2O_2 levels reflect the net result of H_2O_2 production and H_2O_2-consuming side reactions, as discussed in the main text. All reactions were carried out in sodium phosphate buffer (50 mM, pH 7.0) at 40 °C, under magnetic stirring and contained 10 g L^{-1} Avicel. Before product quantification, solubilized cello-oligosaccharides were hydrolyzed by *Tf*Cel5A, to convert the LPMO products to a mixture of only two oxidized products with a degree of polymerization of 2 and 3 [GlcGlc1A, $(Glc)_2Glc1A$], the amounts of which were summed up to yield the concentration of oxidized sites. Error bars show ± s.d. ($n = 3$ for **a** and $n = 2$ for **b**, independent experiments). Source data are provided as a Source Data file.

agreement with several studies published since the discovery of the role of H_2O_2 in LPMO catalysis[22,25–29,41], H_2O_2 clearly is a double-edged sword: it can drive the LPMO reaction with high efficiency, but is also a potentially harmful entity if its levels are not controlled. Of note, while potentially harmful effects of H_2O_2 on enzymes due to non-specific oxidation reactions are well known, the deleterious effect of H_2O_2 on LPMOs is specific in the sense that the reaction of substrate-free, reduced LPMOs with H_2O_2 leads to oxidative damage in the catalytic center[22,42].

The dualistic impact of H_2O_2 could also explain why our present conclusions differ from those of Möllers and colleagues[43], who concluded that reactive oxygen species (ROS) are not part of light-driven LPMO catalysis. On the one hand, these authors observed that exposure of Chl/AscA to light leads to consumption of O_2. In accordance with our present results, this effect was attributed to the conversion of O_2 into $O_2^{\bullet-}$ and H_2O_2, as shown by increases in O_2 levels upon addition of SOD and catalase, respectively. On the other hand, Möllers et al. found that addition of catalase or SOD did not affect measured LPMO product levels, leading to the conclusion that the generated ROS do not affect LPMO catalysis. The absence of an effect of catalase on apparent LPMO activity is not surprising in light of kinetic considerations (see above). The absence of an effect of SOD could be due to the fact that Möllers et al. did not monitor LPMO activity over time and thus may have overlooked effects of LPMO inactivation. Perhaps, the authors encountered a situation similar to the one presented in Supplementary Fig. 9, where SOD effects are not visible because the LPMO becomes fully inactivated prior to the first sampling point. In our hands, SOD clearly has an effect on light-driven LPMO performance, as shown by Fig. 2d–f. Of course, one cannot exclude that *Tt*AA9E, the family AA9 LPMO used by Möllers et al., employs a different mechanism compared to *Sc*AA10C, in terms of both activation and inactivation.

LPMO reduction by light-activated chlorophyllin. Hydrogen peroxide-driven LPMO activity requires a priming reduction of the LPMO from the Cu(II) to the Cu(I) state[22,39]. The correlations between H_2O_2 availability and LPMO activity described above suggest that this priming reduction is not rate-limiting. This is supported by stopped-flow kinetics showing fast (4.2×10^5 M^{-1} s^{-1}) and full reduction of an AA10 LPMO when using as little as 5 μM AscA[23]. The situation may be different when using the Chl/light system, without added AscA. We have previously shown that superoxide, which is produced by the light-exposed Chl (Fig. 2), can serve as reductant[22]. Another option would be the direct reduction of the LPMO by photo-excited Chl, as suggested by Cannella et al.[16]. To probe this latter hypothesis, we initially attempted to monitor LPMO reduction by light-exposed Chl in anaerobic conditions using fluorescence[17], but we did not manage to establish conditions that allowed informative fluorescence measurements. In an alternative experiment, carried out under anaerobic conditions we first exposed the LPMO to Chl/light and then added substrate and H_2O_2, while switching off the light. Figure 4 shows that this approach led to only very low LPMO activity, compared to a control reaction with AscA, and that this activity was independent of the application of light. Thus, it would seem that light-induced reduction of the LPMO does not occur in anaerobic conditions, which supports the idea that, under aerobic conditions, the LPMO is mainly reduced by (oxygen-derived) superoxide and not by direct electron transfer from Chl to the LPMO.

Of note, however, this issue remains ambiguous. Given the expected low reduction potential of photo-excited chlorophyllin, efficient reduction of the LPMO may occur. Thus, it is possible that in the two-phase experiment of Fig. 4, the LPMO gets reduced but is re-oxidized before being transferred to the substrate/H_2O_2 mixture. Indeed, measurement of reduction potentials of the ground state Chl (>0.6 V vs. SHE; see above), present in the first phase of the experiment, indicate that it can act as an oxidant of LPMO-Cu(I), which would regenerate LPMO-Cu(II). In a real (i.e., one-phase) experiment, LPMO-Cu (I) would have several possible fates: (i) re-oxidation in solution by either ground state Chl, by O_2 or by H_2O_2, or, (ii) binding to the substrate and formation of a productive complex with the co-substrate, leading to substrate hydroxylation and cleavage. The distribution between these different pathways will depend on kinetics of the different reactions. Available kinetic studies predict that, in the presence of a suitable substrate, the productive substrate hydroxylation pathway will be favored[23,25].

Metalation of Chl affects H_2O_2 production and LPMO activity. The UV–Vis and fluorescence analyses of chlorin e_6 (Supplementary Fig. 1) showed that the photochemical properties of the

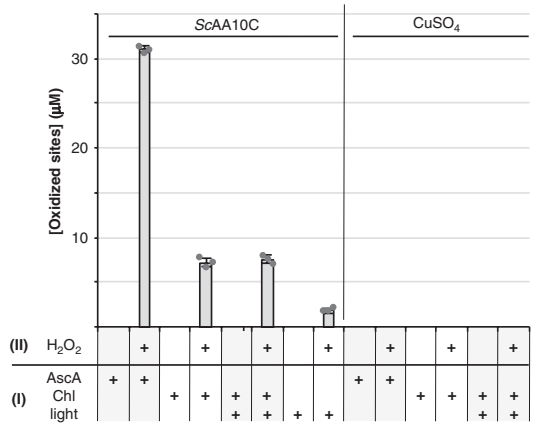

Fig. 4 Anaerobic activation of *Sc*AA10C by Chl/Light. The experiment consisted of two phases, namely a pretreatment phase (I) followed by an activity test phase (II). Conditions were varied as indicated by the +signs below the graph, as further explained below. All phases were performed under anaerobic conditions, at 25 °C. During phase (I), *Sc*AA10C (50 μM; note the high concentration) or $CuSO_4$ (50 μM; to assess the occurrence of transition metal-catalyzed non-enzymatic reactions) were incubated with either AscA (100 μM, i.e., a two-fold molar surplus relative to the LPMO) as positive control or Chl (500 μM) in sodium phosphate buffer (50 mM, pH 7.0), in sealed Quartz cuvettes, exposed or not to light (visible light, 25% I_{max}, ca. 42 W cm^{-2}). After 10 min of incubation (phase I), the pre-treated sample (50% of final volume) was mixed with a suspension of Avicel (10 g L^{-1} final) in sodium phosphate buffer (50 mM, pH 7.0) and, then, H_2O_2 (200 μM final) was added when indicated ("+" sign, otherwise replaced by water). Phase (II) reaction mixtures were incubated for 30 min before being heat-treated (100 °C, with shaking at 800 rpm) and filtered. Before product quantification, solubilized cello-oligosaccharides were hydrolyzed by *Tf*Cel5A, to convert the LPMO products to a mixture of only two oxidized products with a degree of polymerization of 2 and 3 [GlcGlc1A, $(Glc)_2Glc1A$], the amounts of which were summed up to yield the concentration of oxidized sites Error bars show ± s.d. ($n = 3$, independent experiments). Source data are provided as a Source Data file.

porphyrin ring are modulated by copper-binding[44]. Measurements of H_2O_2 production rates by light-exposed chlorin e_6 revealed a drastic effect of copper binding on apparent H_2O_2 production (Fig. 5a). Compared to light-exposed Chl, light-exposed Cu(II)-depleted chlorin e_6 produced much more H_2O_2, whereas Cu(II)-reconstituted chlorin e_6 produced much less H_2O_2. The fact that Cu(II) reconstituted-chlorin e_6 yields less H_2O_2 than the commercial preparation of Chl suggest that the latter likely is not fully saturated with copper. Our results clearly show that metalation of the pigment is an important parameter to take into account for future studies. Testing of these three compounds in LPMO reactions showed product formation patterns akin to what we describe above, where Cu(II)-depleted chlorin e_6 leads to very high LPMO activity and fast inactivation of the LPMO, while Chl and Cu(II)-chlorin e_6 give lower LPMO reaction rates and less inactivation (Fig. 5b). As discussed above, direct comparison of LPMO activity and the apparent ability of the corresponding LPMO-deficient system to generate (and accumulate) H_2O_2 is complicated by the many possible side reactions. For instance, Fig. 5b shows that reactions containing Chl or Cu(II)-chlorin e_6 yield equivalent LPMO activity (within the first 2 h) whereas the former system shows higher H_2O_2 accumulation in the absence of the LPMO (Fig. 5a). Still, Fig. 5 also points at a link between H_2O_2 generation and LPMO activity.

The AscA-driven reaction is complex and uncontrolled. For comparative purposes, and to further highlight the potential of the light-driven reactions described here, we also performed reactions with only AscA, a well-known and commonly used reductant to drive LPMO reactions[2,14,31]. The reactions yielded less clear-cut results (Fig. 6a–c) compared to the studies with Chl/light (Fig. 2), which is likely due to the many possible redox reactions involving AscA, superoxide and H_2O_2 (see Supplementary Fig. 6). However, the same overall trend stood out: both higher LPMO activity and faster apparent enzyme inactivation were correlated with higher H_2O_2 levels. As above, addition of a small amount of SOD gave a higher initial rate and faster inactivation. The addition of catalase yielded stable LPMO product formation over time (Fig. 6a), likely because catalase lowers the steady-state H_2O_2 concentration. By keeping apparent H_2O_2 levels low, the LPMO becomes less active, but is also less prone to inactivation.

On a side note, Fig. 6a illustrates the risk of assessing LPMO activity by measuring single time points. Assessment of the effect of catalase in the experiment shown in Fig. 6a at e.g., 120 min vs. e.g., 480 min would lead to opposite conclusions as to the effect of catalase on LPMO catalysis.

Figure 6c shows another complexity of reactions with added reductant, in that production of H_2O_2 occurred when mixing 1 mM AscA with only the substrate, Avicel (Fig. 6c). Similar amounts of H_2O_2 were measured when Avicel was replaced by *Sc*AA10C-Cu(II), where the latter is known to produce H_2O_2 when incubated with reductant and O_2 in the absence of substrate[45]. These results indicate that in these AscA-driven reactions, the substrate contributes to the generation of H_2O_2, possibly because of the pro-oxidant properties of AscA that become apparent in the presence of free metals (see ref. [46] and below) that may be present in Avicel.

Digging further into these complexities, we then tested the effect of the addition of free transition metals on the LPMO-independent production rate of H_2O_2 by AscA and on LPMO-catalyzed degradation of Avicel. Figure 7a shows that the rate of H_2O_2 production in AscA solutions increased drastically upon addition of $CuSO_4$. Due to technical limitations of the assay, only 50 μM AscA was present in the reactions displayed in Fig. 7a; at commonly used higher AscA concentrations (mM range), H_2O_2 production rates will be much higher. Figure 7b shows that the effect of $CuSO_4$ on H_2O_2 production rates is reflected in LPMO activity, with similar trends as those seen in e.g., the progress curves of Fig. 2: increased amounts of $CuSO_4$ led to higher initial catalytic rates (e.g., 0.13 μM min^{-1} vs. at least 19 μM min^{-1} in reactions with no added $CuSO_4$, vs. 1 μM $CuSO_4$, respectively) and to faster inactivation. At the higher $CuSO_4$ concentrations, the enzyme was already inactivated at the first measuring point. A contribution of free transition metals to H_2O_2 production in standard (i.e., O_2- and reductant-driven) LPMO reactions is an important parameter to consider since these metals may be present in significant amounts that vary between substrates and enzyme preparations. Such variations will inevitably lead to variations in observed LPMO activities.

Overall, it is clear that steady LPMO reactions require strict control of the delivery of reducing equivalents and H_2O_2, and of redox side reactions. Such control is likely not achieved in typical AscA-driven and O_2-driven reactions reported in the literature. On the other hand, such control may be achieved by the photobiocatalytic systems described here or by using enzymatic

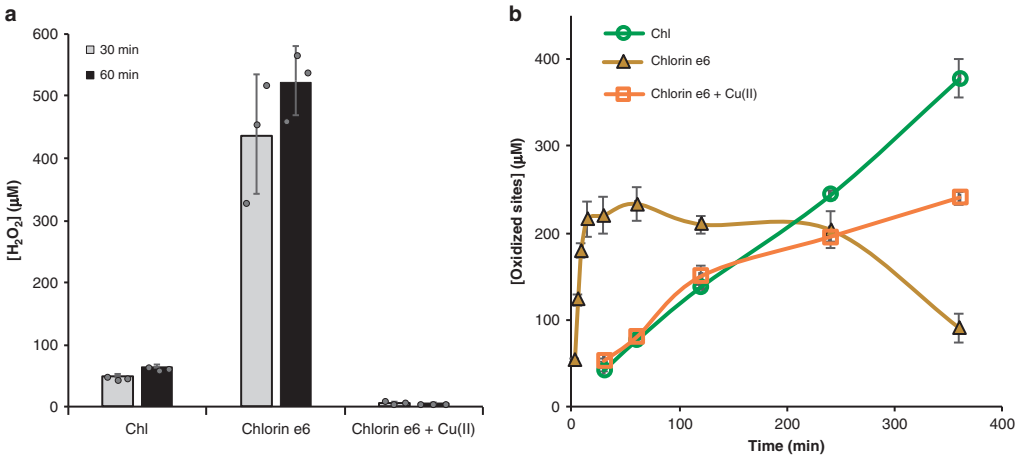

Fig. 5 Effect of copper on H_2O_2 generation by light-exposed Chl and chlorin e_6 and on light-driven LPMO activity. a H_2O_2 production by 500 μM of light-exposed Chl, chlorin e_6 or chlorin e_6 supplemented with 0.9 molar equivalents of Cu(II). **b** Time-course release of soluble aldonic acid products released from Avicel by *Sc*AA10C (1 μM) when fueled by light-exposed Chl, chlorin e_6 or chlorin e_6 complemented with 0.9 eq. Cu(II). All reactions were carried out with 500 μM pigment and exposed to visible light ($I = 25\%\ I_{max}$, approx. 42 W cm^{-2}), in sodium phosphate buffer (50 mM, pH 7.0) at 40 °C, under magnetic stirring. Before product quantification, solubilized cello-oligosaccharides were hydrolyzed by *Tf*Cel5A, to convert the LPMO products to a mixture of only two oxidized products with a degree of polymerization of 2 and 3 [GlcGlc1A, $(Glc)_2Glc1A$], the amounts of which were summed up to yield the concentration of oxidized sites. Error bars show ± s.d. ($n = 3$, independent experiments). Source data are provided as a Source Data file.

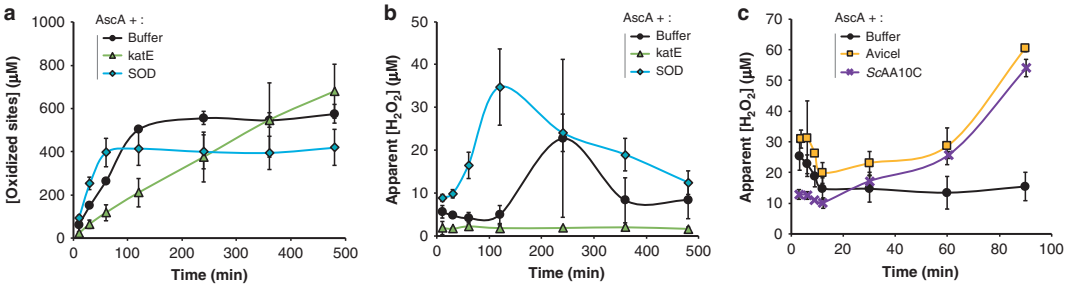

Fig. 6 Characterization of AscA-driven cellulose oxidation by *Sc*AA10C. The graphs show time-courses for the release of aldonic acid products (**a**) and apparent H_2O_2 levels (**b**) upon incubating Avicel (10 g L^{-1}) with *Sc*AA10C (0.5 μM) in presence of AscA (1 mM), in the dark. Reaction conditions varied in terms of the presence of SOD (0.1 μM) and katE (10 μg mL^{-1}). The legend code is indicated in each panel. **c** Apparent H_2O_2 levels during incubation of AscA (1 mM) with either *Sc*AA10C (0.5 μM) or Avicel (10 g L^{-1}) or with no addition (buffer). All reactions were carried out in sodium phosphate buffer (50 mM, pH 7.0) at 40 °C, under magnetic stirring. Before product quantification, solubilized cello-oligosaccharides were hydrolyzed by *Tf*Cel5A, to convert the LPMO products to a mixture of only two oxidized products with a degree of polymerization of 2 and 3 [GlcGlc1A, $(Glc)_2Glc1A$], the amounts of which were summed up to yield the concentration of oxidized sites. Error bars show ± s.d. ($n = 3$, independent experiments). Source data are provided as a Source Data file.

donors of both electrons and H_2O_2 such as cellobiose dehydrogenase[47,48]. These latter set-ups allow the in situ and gradual production of both reducing equivalents and H_2O_2, offering thereby much greater control over the reaction.

V-TiO_2-promoted photobiocatalytic oxidation of cellulose. Turning our attention to the previously described photobiocatalytic system using V-TiO_2 as photocatalyst and *Sc*AA10C as model enzyme[17] (Fig. 1), we then investigated whether also this system could be based on the generation of ROS to fuel a peroxygenase mechanism, rather than on the generation of electrons to fuel a monooxygenase mechanism. Irradiation of V-TiO_2 with visible light can lead to a variety of reactions, including production of H_2O_2 (Fig. 1; see ref. [49]), but the V-TiO_2/light system was originally thought to work by providing the LPMO with electrons analogous to reductants such as AscA.

The possible involvement of ROS was investigated by analyzing whether the addition of a peroxidase to the system would influence V-TiO_2/light-driven LPMO-catalyzed oxidation of cellulose (Fig. 8). In accordance with previous observations for standard LPMO reactions with the use of AscA or cellobiose dehydrogenase as source of reducing equivalents[22], V-TiO_2/light driven activity of *Sc*AA10C was increasingly inhibited when increasing the quantity of peroxidase (Fig. 8a). This result indicates that H_2O_2 is indeed generated in this photobiocatalytic system and sustains LPMO catalysis.

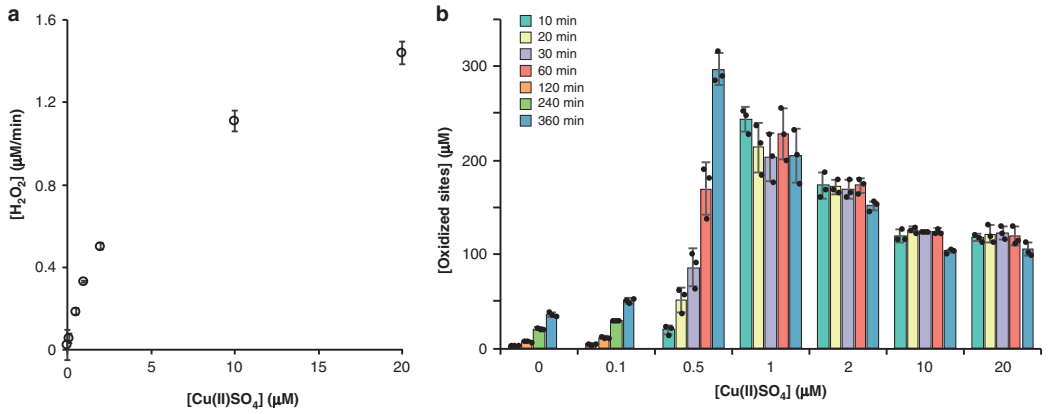

Fig. 7 Effect of free copper on non-enzymatic H_2O_2 production and *Sc*AA10C activity. a The graph shows the rate of H_2O_2 production in reactions containing AscA (50 μM) and varying amounts of Cu(II)SO_4 (0–20 μM), in sodium phosphate buffer (50 mM, pH 7.0), at 25 °C. **b** The graph shows the time course release of soluble oxidized products from Avicel (10 g L^{-1}) by *Sc*AA10C (1 μM) in presence of AscA (1 mM) and varying amounts of Cu(II)SO_4 (0–20 μM), in sodium phosphate buffer (50 mM, pH 6.0) and incubated in a thermomixer (1000 rpm, 40 °C). Note that soluble oxidized products were not detectable before 60 min incubation for reactions containing 0 μM and 0.1 μM of added free copper; therefore, the sampling was adapted (60, 120, 240, and 360 min). Before product quantification, solubilized cello-oligosaccharides were hydrolyzed by *Tf*Cel5A, to convert the LPMO products to a mixture of only two oxidized products with a degree of polymerization of 2 and 3 [GlcGlc1A, $(Glc)_2Glc1A$], the amounts of which were summed up to yield the concentration of oxidized sites. Error bars show ± s.d. ($n = 3$, independent experiments). Source data are provided as a Source Data file.

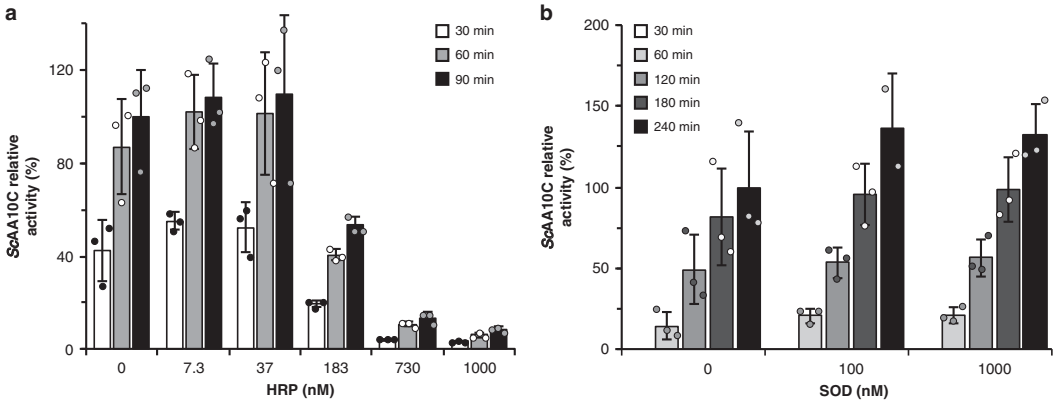

Fig. 8 Probing the underlying role of reactive oxygen species in the light/V-TiO_2/LPMO system. The graphs show time-courses for the release of aldonic acid products from Avicel (10 g L^{-1}) by *Sc*AA10C (1 μM) in the presence of varying amounts of **a** horseradish peroxidase (HRP) and **b** superoxide dismutase (SOD). All reactions were carried out in sodium phosphate buffer (50 mM, pH 7.0) at 40 °C, under magnetic stirring and were fueled by a suspension of V-TiO_2 (10 g L^{-1}) exposed to visible light ($I = 25\%$ I_{max}, approx. 42 W cm^{-2}). Activities are expressed relatively (in %) to the quantity of products measured at the last time point of the reference reaction (i.e., without HRP or SOD). Before product quantification, solubilized cello-oligosaccharides were hydrolyzed by *Tf*Cel5A, to convert the LPMO products to a mixture of only two oxidized products with a degree of polymerization of 2 and 3 [GlcGlc1A, $(Glc)_2Glc1A$], the amounts of which were summed up to yield the concentration of oxidized sites. Error bars show ± s.d. ($n = 3$, independent experiments). Control reactions in the dark without addition of HRP and SOD did not yield products. Note that the original work on the light/V-TiO_2 system[17] includes control reactions similar to those shown in Supplementary Fig. 4, which confirm that product formation depends on the enzyme and is not due to enzyme-independent reactions. Source data are provided as a Source Data file.

In our initial study, we observed low apparent H_2O_2 levels in reactions with LPMO[17]. With hindsight, we can conclude that H_2O_2 generated in these reactions was consumed by *Sc*AA10C. Given the importance of H_2O_2 in *Sc*AA10C catalysis and the occurrence of competing H_2O_2-consuming side-reactions at the V-TiO_2 surface (e.g., photodecomposition[50]), it is not certain that this photocatalyst is ideal for promoting LPMO activity. The photoreactivity of metal-doped TiO_2 depends on the nature and abundance of the metal used for doping[51] and it is possible that other TiO_2-based catalysts could be more suitable for light-driven LPMO catalysis. On this note, a 2018 study showed that a gold-coated TiO_2 photocatalyst can fuel the (H_2O_2-consuming) unspecific peroxygenase from *Agrocybe aegerita* to hydroxylate aliphatic and aromatic compounds[52]. The use of alternative

tailor-made photocatalysts designed for efficient H_2O_2 generation[53,54] to drive LPMO reactions probably represents an interesting avenue of investigation.

Experiments with SOD added to the reaction (Fig. 8b) indicated that free superoxide likely is not generated in the V-TiO_2/light/LPMO system, suggesting that the LPMO is reduced by reducing equivalents generated at the V-TiO_2 surface. Accordingly, we have previously shown that light-exposed V-TiO_2 reduces *Sc*AA10C under anaerobic conditions[17]. Of note, however, the rate-limiting step in this photobiocatalytic system likely resides in the thermodynamically challenging oxidation of water ($E_0^{ox} = -1.23$ V vs. SHE for H_2O/O_2)[17,55]. Thus, if an $O_2^{\bullet-}$ intermediate was formed, its accelerated conversion to H_2O_2 by SOD, may not be reflected in an increased LPMO rate, since none of the downstream reactions (relative to water oxidation) are rate-limiting. It is therefore difficult to conclude whether or not $O_2^{\bullet-}$ is produced, although the two-electron reduction of O_2 to H_2O_2 is thermodynamically much more likely than the single electron reduction to $O_2^{\bullet-}$ (Supplementary Fig. 6).

Light-driven activity of other LPMOs. Earlier work has shown that the V-TiO_2/light system can drive multiple LPMOs, belonging to different families and acting on different substrates. The functionality of this system was demonstrated for a bacterial, C1-oxidizing, chitin-active AA10 LPMO (*Sm*AA10A)[2], a fungal, C1-oxidizing, cellulose-active AA9 LPMO (*Pc*AA9D)[56] and a bacterial, C1/C4 oxidizing, cellulose-active AA10 LPMO (*Sc*AA10B)[38] (Fig. S3 in Bissaro et al.[17]).

To demonstrate the general applicability of the Chl/light system, we analyzed activity of *Sm*AA10A on chitin as well as the cellulose-oxidizing activity of a C1-oxidizing AA9 LPMO from the fungus *Neurospora crassa* (*Nc*AA9F or NCU03328)[57]. Supplementary Fig. 10 shows that both enzymes can be fueled by the Chl/light system, leading to chitin and cellulose oxidation, respectively. Of note, while showing the general applicability of the Chl/light system, these additional analyses showed that different LPMOs respond differently: while *Sm*AA10 performed better with Chl/light compared to AscA, *Nc*AA9F performed relatively poorly when driven by Chl/light and was rapidly inactivated. Differences in the way LPMOs respond to reductants and H_2O_2 are commonly observed[8,22,58] and deserve further attention in future research.

The data presented in this study pinpoint several complications related to interpreting the outcome of LPMO reactions and provide insight into light-driven LPMO catalysis. One technical challenge concerns the measuring of actual H_2O_2 production rates by a given system in which H_2O_2 is the final product (i.e., not immediately used by an enzyme such as an LPMO). Our study also shows the intricacy of interpreting the effects of accessory enzymes such as catalase and SOD and demonstrates the absolute need for analyzing progress curves, rather than relying on single time point measurements of product formation. SOD accelerates the conversion of $O_2^{\bullet-}$ into H_2O_2, which increases the LPMO initial rate but also leads to more rapid inactivation of the LPMO. On the other hand, catalase, by converting H_2O_2 into O_2 and H_2O, prevents accumulation of excess H_2O_2 and thus reduces LPMO inactivation. It is worth noting the linear progress curve that is obtained when using catalase in the light-driven reactions displayed in Fig. 2d. All in all, the present data clearly show that LPMOs use H_2O_2 and that controlling H_2O_2 levels is key to optimizing LPMO catalysis.

The set of experiments presented here demonstrates that when exposed to light, Chl can reduce O_2 to $O_2^{\bullet-}$ leading to H_2O_2 production, via either spontaneous disproportionation or chemical reduction (e.g., by AscA). H_2O_2 production can be regulated by light intensity but also by metalation of the porphyrin ring, which tunes the photochemical properties of the pigment. Although photo-excitation of the pigment is clearly needed to fuel LPMO activity, we were not able to discriminate whether reduction of the LPMO occurs via direct electron transfer from photo-excited Chl or via superoxide. Importantly, studies of a completely different system for light-driven driven LPMO catalysis, based on using V-TiO_2 particles, showed that also in this case light-driven oxidation of cellulose by the LPMO entails a peroxygenation reaction. Of note, the earlier study on driving LPMO reactions with the V-TiO_2/light system[17] showed that LPMO activity can be controlled by switching the light on or off and that the system also works when using regular sunlight.

Most importantly, our data show that these LPMO-catalyzed peroxygenation reactions can be fueled by light only and that other sources of energy, such as reducing equivalents used in standard LPMO reactions and in earlier work on light-driven LPMO catalysis, are not required. The use of light allows tunable in situ generation of H_2O_2 which then fuels polysaccharide oxidation at rates that are higher than those reported when LPMOs were still believed to act as monooxygenases only. Considering the large current interest in copper catalysts (e.g., Snyder et al.[59]), we expect that the present findings will have implications beyond processing of biomass.

Methods

Materials. Chemicals and enzymes were purchased from Sigma-Aldrich unless indicated otherwise. The crystalline cellulose used was Avicel® PH-101 (~50 µM particles). The superoxide dismutase (SOD, recombinantly expressed in *E. coli*) was stored (100 µM, eq. 1.63 mg mL^{-1}) in sodium phosphate buffer (100 mM, pH 7.5) at 4 °C. The peroxidase from horseradish (HRP, type II) was stored (0.5 mg mL^{-1}, eq. 100 U mL^{-1}) in sodium phosphate buffer (50 mM, pH 6.0) at 4 °C. The catalase katE from *Streptomyces sirex* (recombinantly expressed in *E. coli*) was produced in-house and stored (1.8 mg mL^{-1}) in Tris-HCl buffer (50 mM, pH 8.0) at −20 °C. Ascorbic acid (100 mM) and Amplex red (10 mM) stock solutions were prepared in water and DMSO respectively, aliquoted, stored at −20 °C, and thawed in the dark for 10 min just before use. The V-TiO_2 powder was kindly provided by Dr. Frank Hollmann (Delft University, Netherlands) and prepared according to a previously described protocol[60]. According to literature, the Chl purchased from Sigma consists of about 72% Cu(II)-chlorin e_6 and 10% Cu(II)-isochlorin e_4[37]. Chlorin e_6 was purchased from Frontier Scientific (Logan, Utah, USA). Copper-reconstituted chlorin e_6 was prepared by incubating chlorin e_6 with 0.9 molar equivalent of $CuSO_4$ for 30 min at 4 °C in deionized Milli-Q water.

Production and purification of recombinant LPMOs. The recombinant AA10 LPMO from *Streptomyces coelicolor* (*Sc*AA10C) was produced and purified according to previously described protocols[1,38]. Note that *Sc*AA10C refers to the wild-type full-length enzyme, which comprises an AA10 domain connected via a linker to a CBM2 domain (UniProt Q9RJY2). *Sc*AA10C was prepared and stored in sodium phosphate (50 mM, pH 6.0), copper-saturated with Cu(II)SO_4 and desalted (PD MidiTrap G-25, GE Healthcare) before use[10]. LPMOs from *Serratia marcescens* (*Sm*AA10A) and *Neurospora crassa* (*Nc*AA9F or NCU03328) were produced and purified as previously described[1,57] and copper saturated in the same way as for *Sc*AA10C, except that the buffer was Bis-Tris pH 6.5 and pH 6.0, respectively.

Standard photobiocatalytic reaction conditions. The reactor was a cylindrical glass vial (1.1 mL) with conical bottom (Thermo Scientific) and the reaction volume was 500 µL. Typical reactions were carried out as follows: the enzyme (0.5 µM) and Avicel (10 g L^{-1}) were mixed in sodium phosphate buffer (50 mM final concentration after all additions; pH 7.0 or 6.0 for Chl and V-TiO_2 studies, respectively) followed by incubation at 40 °C under magnetic stirring during 20 min. Photobiocatalytic reactions contained either chlorophyllin or chlorin e_6 (500 µM, unless stated otherwise) or V-TiO_2 (5 mg mL^{-1}) as a light harvester. The reaction was initiated by adding ascorbic acid (to a final concentration of 1 mM, unless stated otherwise), and/or turning on the light ($I = 25\%$ I_{max}, eq. to 42 W cm^{-2}[,17], unless stated otherwise). At regular intervals, 55 µL samples were taken from the reaction mixtures and soluble fractions were immediately separated from the insoluble substrate by filtration using a 96-well filter plate (Millipore) operated with a vacuum manifold. When it was needed to also measure H_2O_2 in the reaction mixture, the 55 µL sample was mixed with 55 µL of NaOAc buffer (50 mM, pH 4.5) before filtration (see below). By separating soluble and insoluble fractions, LPMO activity is stopped, as the LPMO used in this study does not oxidize soluble cello-oligosaccharides. Filtered samples were frozen (−20 °C) prior to further analysis. Prior to product quantification, 30 µL of sample was mixed with

30 µL of a solution of endoglucanase Cel5A from *Thermobifida fusca* (*Tf*Cel5A, 2 µM in the premix) prepared in Bis-Tris buffer (25 mM, pH 6.0), followed by incubation overnight at 40 °C to convert the solubilized cello-oligosaccharides to a mixture of glucose, cellobiose and C1-oxidized products with a degree of polymerization of 2 and 3 [GlcGlc1A, (Glc)2Glc1A]. For chlorin e_6, the 50 µL reaction mixture was mixed with 50 µL 0.2 M CH_3COONa pH 4.0 prior to filtration to ensure chlorin e_6 precipitation on the filters. *Tf*Cel5A for treatment of samples containing chlorin e_6 was prepared in 0.2 M CH_3COONa pH 6.5 (to increase pH for efficient solubilization of cello-oligosaccharides) and added to the filtrate as described above.

Analysis of reaction products. For qualitative analysis, samples were analysed by MALDI-TOF MS, as previously described[2]. For quantitative analysis, cello-oligosaccharides (native and oxidized) were separated by high performance anion exchange chromatography (HPAEC) and monitored by pulsed amperometric detection (PAD) using a Dionex Bio-LC equipped with a CarboPac PA1 column as previously described[61]. Chromatograms were recorded and analyzed using Chromeleon 7.0 software. Oxidized dimers and trimers were quantified using GlcGlc1A and $(Glc)_2Glc1A$ standards obtained by incubating (40 °C, 1000 rpm) cellobiose (2 mM) or cellotriose (2 mM) with the cellobiose dehydrogenase from *Myriococcum thermophilum* (*Mt*CDH,[62] 2 µM, 3 successive additions every 24 h to obtain maximum conversion of 95%). Chito-oligosaccharides resulting from the action of *Sm*AA10A on β-chitin were analyzed using a Dionex Ultimate 3000 UHPLC system equipped with a Rezex RFQ-Fast acid H^+ (8%) 7.8 × 100 mm column as previously described[45]. The elution of chitooligosaccharides was monitored using a UV detector (194 nm). Prior to analysis of solubilized mixtures of chitooligosaccharides, these chitooligosaccharides were hydrolyzed with a chitobiase, *Sm*GH20, from *S. marcescens* (1 µM final concentration) yielding chitobionic acid as the only oxidized product[10].

H_2O_2 production measurements. The method is adapted from a previously reported protocol[57] with some modifications explained hereinafter. For each reaction (carried out as described above), 55 µL were sampled at regular intervals and mixed with 55 µL of NaOAc buffer (50 mM, pH 4.5) before filtration as described above. Notably, the decrease in pH obtained by the addition of NaOAc makes chlorophyllin insoluble, meaning that this compound (if present) was removed from the solution during the filtration step, leading to a transparent and stable filtrate usable for colorimetric analysis. Thirty microliter of each filtrate was saved for analysis of oxidized products analysis when applicable (cf above). For reactions with chlorin e_6 (metallated and non-metallated), a slightly different treatment was applied to remove the pigment: both chlorin e_6 compounds were diluted in a 1:1 ratio with sodium acetate (200 mM, pH 4.0).

To determine the H_2O_2 concentration (in all reactions devoid of pigment and for those containing Chl), 50 µL of the filtrate (or dilutions of it, if necessary) were mixed with 50 µL of a premix composed of HRP (10 U/mL) and Amplex Red (200 µM, 2% DMSO, in the premix) in sodium phosphate buffer (50 mM, pH 7.5). For chlorin e_6, 10 µL of the filtrated sample was combined with 90 µL premix of HRP and Amplex Red (10 U/mL and 200 µM final concentrations respectively), while for chlorin e_6-Cu(II) 50 µL filtrate was combined with 50 µL HRP and Amplex Red premix (10 U/mL and 200 µM final concentrations, respectively). The buffer used was sodium phosphate (250 mM, pH 7.0) to ensure proper buffering. The reaction mixture (100 µL) was incubated in a 96-well microtiter plate during 10 min before recording the absorbance at 540 nm. For each set of measurements, a blank and H_2O_2 standards were prepared alike the corresponding samples and subjected to the same buffer treatment. Also, an average background control was included to account for the absorbance coming from residual soluble chlorophyllin (small quantities were observed for time points beyond 4 h). To generate this background control, 18 µL portions of the filtrates from each sample of a triplicate chlorophyllin-containing reaction were pooled. 50 µL of this 54 µL pool (or a dilution equivalent to the one used for the reaction containing Amplex red) was mixed with 50 µL of a premix made of HRP (10 U/mL) and DMSO (2% in the premix) in sodium phosphate buffer (50 mM, pH 7.5) (i.e., the same premix as previously described but without Amplex red). The difference (if any) between this background control and the blank sample was used to correct for absorbance generated by residual chlorophyllin.

Verification of superoxide dismutase (SOD) activity. SOD activity was verified according to a published protocol[63]. In brief, a stock solution of pyrogallol (15 mM) was prepared in 10 mM HCl; the tube was wrapped in aluminum foil and kept on ice. Prior to each measurement, the background absorbance (A_{325} nm) of 50 mM Tris-HCl pH 8.0 was monitored and allowed to stabilize. For the reference reaction, pyrogallol was added to a final concentration of 200 µM and the A_{325} nm was measured every 10 s for 5 min. For the superoxide dismutase (SOD) reactions, SOD was quickly added after the pyrogallol to final concentrations of 10, 100, 500, and 1000 nM. The solution was pipetted up and down for mixing and the A_{325} nm was recorded every 10 s for 5 min with the same conditions as for the reference reaction i.e., 200 µM pyrogallol in 50 mM Tris-HCl pH 8.0.

Voltammetric measurements. Stock solutions of chlorophyllin and chlorin e_6 (5 mM) were prepared fresh each day in deionized Milli-Q water. These were protected from light in aluminum foil and kept on ice. Prior to voltammetric measurements, Chl or chlorin e_6 was diluted ten-fold (500 µM) in potassium phosphate buffer (100 mM, pH 7.0) supplemented with KCl as supporting electrolyte (100 mM). The voltammetric measurements were carried out using an MCS-200 potentiostat (BioLogic, France) and EC-lab software (BioLogic, France). The voltammograms were recorded using a three-electrode system (eDAQ, Australia) with a glassy-carbon electrode (GCE) of 1.0 mm diameter as the working electrode, an Ag/AgCl (3.4 M KCl) electrode as a reference electrode, and a platinum covered titanium wire as a counter electrode. The glassy-carbon electrode was cleaned before each measurement. It was rinsed with deionized Milli-Q water prior to polishing using a 0.05 µm Alumina polishing slurry (eDAQ, Australia) on a wet polishing cloth. Then, the electrode was rinsed with deionized Milli-Q water before and after a 30 s sonication step. The solutions were degassed by nitrogen sparging before the electrochemical measurements, and a nitrogen blanket over the solution was maintained during the experiments. All experiments were performed at room temperature in the dark. To obtain the square-wave voltammograms, we used the same parameters as described in ref. [37]. The pulse height (amplitude) was 50 mV, the step height (potential increment) was 2 mV and the pulse width (frequency) was 0.4 ms (1250 Hz), which corresponds to a scan rate of 2500 mV s^{-1}. The Ag/AgCl reference electrode was calibrated each day by cyclic voltammetry using potassium ferricyanide $[K_3Fe(CN)_6]$ (1 mM) in potassium phosphate buffer (100 mM pH 7.0) supplemented with KCl as supporting electrolyte (100 mM). All the potentials reported were adjusted to refer to the standard hydrogen electrode (SHE) using the conversion factor $E_{Ag/AgCl}$ vs. SHE = 222.49 mV for our reference electrode[64]. Of note, some previously determined potentials used in this paper were reported relative to the NHE; the difference between the two is that the SHE is appr. 6 mV lower than the NHE[65].

Fluorescence measurements. Fluorescence signals were recorded using a Cary Eclipse Fluorescence spectrophotometer (Agilent Technologies) using a 2 mL quartz cuvette (Hellma Analytics, 101-QS). Data acquisition was performed at room temperature with a PMT detector voltage of 600 V. Excitation and emission spectra were acquired at respective maximum emitting and exciting wavelengths, determined iteratively and shown in Supplementary Fig. 1.

Reporting summary. Further information on research design is available in the Nature Research Reporting Summary linked to this article.

Data availability

Data supporting the findings of this work are available within the paper and its Supplementary Information files and from the corresponding author upon reasonable request. A reporting summary for this Article is available as a Supplementary Information file. The source data underlying Figs. 2, 3, 4, 5, 6, 7, 8 as well as Supplementary Figs. 3, 5, 7, 8, 9, 10, 11, and Supplementary Table 1 are available as a Source Data file.

Received: 8 August 2019; Accepted: 28 January 2020;
Published online: 14 February 2020

References

1. Vaaje-Kolstad, G., Horn, S. J., van Aalten, D. M. F., Synstad, B. & Eijsink, V. G. H. The non-catalytic chitin-binding protein CBP21 from Serratia marcescens is essential for chitin degradation. *J. Biol. Chem.* **280**, 28492–28497 (2005).
2. Vaaje-Kolstad, G. et al. An oxidative enzyme boosting the enzymatic conversion of recalcitrant polysaccharides. *Science* **330**, 219–222 (2010).
3. Forsberg, Z. et al. Cleavage of cellulose by a CBM33 protein. *Protein Sci.* **20**, 1479–1483 (2011).
4. Quinlan, R. J. et al. Insights into the oxidative degradation of cellulose by a copper metalloenzyme that exploits biomass components. *Proc. Natl Acad. Sci. USA* **108**, 15079–15084 (2011).
5. Harris, P. V. et al. Stimulation of lignocellulosic biomass hydrolysis by proteins of glycoside hydrolase family 61: structure and function of a large, enigmatic family. *Biochemistry* **49**, 3305–3316 (2010).
6. Frommhagen, M. et al. Discovery of the combined oxidative cleavage of plant xylan and cellulose by a new fungal polysaccharide monooxygenase. *Biotechnol. Biofuels* **8**, 101 (2015).
7. Couturier, M. et al. Lytic xylan oxidases from wood-decay fungi unlock biomass degradation. *Nat. Chem. Biol.* **14**, 306–310 (2018).
8. Petrović, D. M. et al. Comparison of three seemingly similar lytic polysaccharide monooxygenases from Neurospora crassa suggests different roles in plant biomass degradation. *J. Biol. Chem.* **294**, 15068–15081 (2019).

9. Levasseur, A., Drula, E., Lombard, V., Coutinho, P. M. & Henrissat, B. Expansion of the enzymatic repertoire of the CAZy database to integrate auxiliary redox enzymes. *Biotechnol. Biofuels* **6**, 41 (2013).
10. Loose, J. S. M., Forsberg, Z., Fraaije, M. W., Eijsink, V. G. H. & Vaaje-Kolstad, G. A rapid quantitative activity assay shows that the Vibrio cholerae colonization factor GbpA is an active lytic polysaccharide monooxygenase. *FEBS Lett.* **588**, 3435–3440 (2014).
11. Agostoni, M., Hangasky, J. A. & Marletta, M. A. Physiological and molecular understanding of bacterial polysaccharide monooxygenases. *Microbiol. Mol. Biol. Rev.* **81**, e00015–e00017 (2017).
12. Chiu, E. et al. Structural basis for the enhancement of virulence by viral spindles and their in vivo crystallization. *Proc. Natl Acad. Sci.* **112**, 3973–3978 (2015).
13. Johansen, K. S. Lytic polysaccharide monooxygenases: the microbial power tool for lignocellulose degradation. *Trends Plant Sci.* **21**, 926–936 (2016).
14. Bissaro, B., Varnai, A., Røhr, Å. K. & Eijsink, V. G. H. Oxidoreductases and reactive oxygen species in lignocellulose biomass conversion. *Microbiol. Mol. Biol. Rev.* **4**, e00029 (2018).
15. Maciá-Agulló, J. A., Corma, A. & Garcia, H. Photobiocatalysis: the power of combining photocatalysis and enzymes. *Chemistry* **21**, 10940–10959 (2015).
16. Cannella, D. et al. Light-driven oxidation of polysaccharides by photosynthetic pigments and a metalloenzyme. *Nat. Commun.* **7**, 11134 (2016).
17. Bissaro, B. et al. Fueling biomass-degrading oxidative enzymes by light-driven water oxidation. *Green. Chem.* **18**, 5357–5366 (2016).
18. Phillips, C. M., Beeson, W. T., Cate, J. H. & Marletta, M. A. Cellobiose dehydrogenase and a copper-dependent polysaccharide monooxygenase potentiate cellulose degradation by Neurospora crassa. *ACS Chem. Biol.* **6**, 1399–1406 (2011).
19. Beeson, W. T., Vu, V. V., Span, E. A., Phillips, C. M. & Marletta, M. A. Cellulose degradation by polysaccharide monooxygenases. *Annu. Rev. Biochem.* **84**, 923–946 (2015).
20. Walton, P. H. & Davies, G. J. On the catalytic mechanisms of lytic polysaccharide monooxygenases. *Curr. Opin. Chem. Biol.* **31**, 1–13 (2016).
21. Bissaro, B.et al. Fenton-type chemistry by a copper enzyme: molecular mechanism of polysaccharide oxidative cleavage. bioRxiv https://doi.org/10.1101/097022 (2016).
22. Bissaro, B. et al. Oxidative cleavage of polysaccharides by monocopper enzymes depends on H_2O_2. *Nat. Chem. Biol.* **13**, 1123–1128 (2017).
23. Bissaro, B. et al. Molecular mechanism of the chitinolytic peroxygenase reaction. *Proc. Natl Acad. Sci.* **117**, 1504–1513 (2020).
24. Wang, D., Li, J., Wong, A. C. Y., Aachmann, F. L. & Hsieh, Y. S. Y. A colorimetric assay to rapidly determine the activities of lytic polysaccharide monooxygenases. *Biotechnol. Biofuels* **11**, 215 (2018).
25. Kuusk, S. et al. Kinetics of H_2O_2-driven degradation of chitin by a bacterial lytic polysaccharide monooxygenase. *J. Biol. Chem.* **293**, 523–531 (2018).
26. Breslmayr, E. et al. A fast and sensitive activity assay for lytic polysaccharide monooxygenase. *Biotechnol. Biofuels* **11**, 79 (2018).
27. Hangasky, J. A., Iavarone, A. T. & Marletta, M. A. Reactivity of O_2 versus H_2O_2 with polysaccharide monooxygenases. *Proc. Natl Acad. Sci.* **115**, 4915–4920 (2018).
28. Petrović, D. M. et al. Methylation of the N-terminal histidine protects a lytic polysaccharide monooxygenase from auto-oxidative inactivation. *Protein Sci.* **27**, 1636–1650 (2018).
29. Müller, G., Chylenski, P., Bissaro, B., Eijsink, V. G. H. & Horn, S. J. The impact of hydrogen peroxide supply on LPMO activity and overall saccharification efficiency of a commercial cellulase cocktail. *Biotechnol. Biofuels* **11**, 209 (2018).
30. Wang, B. et al. QM/MM studies into the H_2O_2-dependent activity of lytic polysaccharide monooxygenases: evidence for the formation of a caged hydroxyl radical intermediate. *ACS Catal.* **8**, 1346–1351 (2018).
31. Wang, B., Walton, P. H. & Rovira, C. Molecular mechanisms of oxygen activation and hydrogen peroxide formation in lytic polysaccharide monooxygenases. *ACS Catal.* **9**, 4958–4969 (2019).
32. Hedegård, E. D. & Ryde, U. Molecular mechanism of lytic polysaccharide monooxygenases. *Chem. Sci.* **9**, 3866–3880 (2018).
33. Chylenski, P. et al. Lytic polysaccharide monooxygenases in enzymatic processing of lignocellulosic biomass. *ACS Catal.* **9**, 4970–4991 (2019).
34. Seely, R. The energetics of electron transfer of chlorophyll and other compounds. *Photochem. Photobiol.* **27**, 639–654 (1978).
35. Jahnke, L. S. & Frenkel, A. W. Evidence for the photochemical production of superoxide mediated by saponified chlorophyll. *Biochem. Biophys. Res. Commun.* **66**, 144–150 (1975).
36. Wood, P. M. The potential diagram for oxygen at pH 7. *Biochem. J.* **253**, 287–289 (1988).
37. Novak, I. & Komorsky-Lovrić, Š. Square-wave voltammetry of sodium copper chlorophyllin on glassy-carbon and paraffin-impregnated graphite electrode. *Electroanalysis* **24**, 1957–1965 (2012).
38. Forsberg, Z. et al. Structural and functional characterization of a conserved pair of bacterial cellulose-oxidizing lytic polysaccharide monooxygenases. *Proc. Natl Acad. Sci. USA* **111**, 8446–8451 (2014).
39. Kuusk, S. et al. Kinetic insights into the role of the reductant in H_2O_2-driven degradation of chitin by a bacterial lytic polysaccharide monooxygenase. *J. Biol. Chem.* **294**, 1516–1528 (2019).
40. Nishikimi, M. Oxidation of ascorbic acid with superoxide anion generated by the xanthine-xanthine oxidase system. *Biochem. Biophys. Res. Commun.* **63**, 463–468 (1975).
41. Forsberg, Z. et al. Structural determinants of bacterial lytic polysaccharide monooxygenase functionality. *J. Biol. Chem.* **293**, 1397–1412 (2018).
42. Loose, J. S. M. et al. Multi-point precision binding of substrate protects LPMOs from self-destructive off-pathway processes. *Biochemistry* **57**, 4114–4124 (2018).
43. Möllers, K. B. et al. On the formation and role of reactive oxygen species in light-driven LPMO oxidation of phosphoric acid swollen cellulose. *Carbohydr. Res.* **448**, 182–186 (2017).
44. Gouterman, M. in *The Porphyrins, Volume III: Physical Chemistry* (ed. Dolphin, D.) 1–165 (Academic Press, 1978).
45. Mutahir, Z. et al. Characterization and synergistic action of a tetra-modular lytic polysaccharide monooxygenase from Bacillus cereus. *FEBS Lett.* **592**, 2562–2571 (2018).
46. Buettner, G. R. & Jurkiewicz, Ba Catalytic metals, ascorbate and free radicals: combinations to avoid. *Radiat. Res.* **145**, 532–541 (1996).
47. Loose, J. S. M. et al. Activation of bacterial lytic polysaccharide monooxygenases with cellobiose dehydrogenase. *Protein Sci.* **25**, 2175–2186 (2016).
48. Bennati-Granier, C. et al. Substrate specificity and regioselectivity of fungal AA9 lytic polysaccharide monooxygenases secreted by Podospora anserina. *Biotechnol. Biofuels* **8**, 90 (2015).
49. Sheng, H., Ji, H., Ma, W., Chen, C. & Zhao, J. Direct four-electron reduction of O_2 to H_2O on TiO_2 surfaces by pendant proton relay. *Angew. Chem. Int. Ed.* **52**, 9686–9690 (2013).
50. Li, X., Chen, C. & Zhao, J. Mechanism of photodecomposition of H_2O_2 on TiO_2 surfaces under visible light irradiation. *Langmuir* **17**, 4118–4122 (2001).
51. Choi, W., Termin, A. & Hoffmann, M. R. The role of metal ion dopants in quantum-sized TiO_2: correlation between photoreactivity and charge carrier recombination dynamics. *J. Phys. Chem.* **98**, 13669–13679 (1994).
52. Zhang, W. et al. Selective aerobic oxidation reactions using a combination of photocatalytic water oxidation and enzymatic oxyfunctionalizations. *Nat. Catal.* **1**, 55–62 (2018).
53. Etacheri, V., Di Valentin, C., Schneider, J., Bahnemann, D. & Pillai, S. C. Visible-light activation of TiO_2 photocatalysts: advances in theory and experiments. *J. Photochem. Photobiol. C* **25**, 1–29 (2015).
54. Fukuzumi, S., Lee, Y. M. & Nam, W. Solar-driven production of hydrogen peroxide from water and dioxygen. *Chem. Eur. J.* **24**, 5016–5031 (2018).
55. Kumar, S. G. & Devi, L. G. Review on modified TiO_2 photocatalysis under UV/visible light: selected results and related mechanisms on interfacial charge carrier transfer dynamics. *J. Phys. Chem. A* **115**, 13211–13241 (2011).
56. Westereng, B. et al. The putative endoglucanase PcGH61D from Phanerochaete chrysosporium is a metal-dependent oxidative enzyme that cleaves cellulose. *PLoS ONE* **6**, e27807 (2011).
57. Kittl, R., Kracher, D., Burgstaller, D., Haltrich, D. & Ludwig, R. Production of four Neurospora crassa lytic polysaccharide monooxygenases in Pichia pastoris monitored by a fluorimetric assay. *Biotechnol. Biofuels* **5**, 79 (2012).
58. Várnai, A., Umezawa, K., Yoshida, M. & Eijsink, V. G. H. The pyrroloquinoline-quinone dependent pyranose dehydrogenase from Coprinopsis cinerea (CcPDH) drives lytic polysaccharide monooxygenase (LPMO) action. *Appl. Environ. Microbiol.* **24**, e00156–18 (2018).
59. Snyder, B. E. R., Bols, M. L., Schoonheydt, R. A., Sels, B. F. & Solomon, E. I. Iron and copper active sites in zeolites and their correlation to metalloenzymes. *Chem. Rev.* **118**, 2718–2768 (2018).
60. Choi, S. H. et al. The influence of non-stoichiometric species of V/TiO_2 catalysts on selective catalytic reduction at low temperature. *J. Mol. Catal. A Chem.* **304**, 166–173 (2009).
61. Westereng, B. et al. Efficient separation of oxidized cello-oligosaccharides generated by cellulose degrading lytic polysaccharide monooxygenases. *J. Chromatogr. A* **1271**, 144–152 (2013).
62. Zamocky, M. et al. Cloning, sequence analysis and heterologous expression in Pichia pastoris of a gene encoding a thermostable cellobiose dehydrogenase from Myriococcum thermophilum. *Protein Expr. Purif.* **59**, 258–265 (2008).
63. Li, X. Improved pyrogallol autoxidation method: a reliable and cheap superoxide-scavenging assay suitable for all antioxidants. *J. Agric. Food Chem.* **60**, 6418–6424 (2012).
64. Spitzer, P. et al. in *Handbook of Reference Electrodes*. (eds. Inzelt, G. et al.) 77–143 (Springer, Berlin, Heidelberg, 2013).
65. Ramette, R. W. Outmoded terminology: the normal hydrogen electrode. *J. Chem. Educ.* **64**, 885 (1987).

66. Diesen, V. & Jonsson, M. Formation of H_2O_2 in TiO_2 photocatalysis of oxygenated and deoxygenated aqueous systems: a probe for photocatalytically produced hydroxyl radicals. *J. Phys. Chem. C* **118**, 10083–10087 (2014).
67. Fujishima, A., Rao, T. N. & Tryk, D. A. Titanium dioxide photocatalysis. *J. Photochem. Photobiol. C* **1**, 1–21 (2000).
68. Beeson, W. T., Phillips, C. M., Cate, J. H. D. & Marletta, M. A. Oxidative cleavage of cellulose by fungal copper-dependent polysaccharide monooxygenases. *J. Am. Chem. Soc.* **134**, 890–892 (2012).

Acknowledgements

We thank F. Hollmann for providing vanadium coated TiO_2 and Zarah Forsberg and Gustav Vaaje-Kolstad for helpful discussions. We thank Jennifer Loose, Lukas Rieder and John-Kristian Jameson at NMBU, Ås for providing katE, *Sm*AA10A, and *Nc*AA9F respectively. This work was supported by the Research Council of Norway through grants 262853 & 240967. This work was also supported by the EU in the framework of the Marie-Curie FP7 COFUND People Program, through the award of an AgreenSkills fellowship (grant n° 267196), and by the French Institut National de la Recherche Agronomique (INRA).

Author contributions

B.B. and V.G.H.E. conceived the study. B.B. and E.K. performed experiments. B.B., E.K., A.K.R., and V.G.H.E. interpreted data. B.B. and V.G.H.E wrote the initial draft. All authors contributed in writing the current version of the manuscript.

Competing interests

The authors declare no competing interests.

Additional information

Supplementary information is available for this paper at https://doi.org/10.1038/s41467-020-14744-9.

Correspondence and requests for materials should be addressed to V.G.H.E.

Peer review information *Nature Communications* thanks Yves Hsieh and the other, anonymous, reviewer(s) for their contribution to the peer review of this work.

Reprints and permission information is available at http://www.nature.com/reprints

Publisher's note Springer Nature remains neutral with regard to jurisdictional claims in published maps and institutional affiliations.

SUPPLEMENTARY INFORMATION FOR

Controlled Depolymerization of Cellulose by Light-Driven Lytic Polysaccharide Oxygenases

Bastien Bissaro[1,2,†], Eirik Kommedal[1,†], Åsmund K. Røhr[1] and Vincent G.H. Eijsink[1*]

[1]Faculty of Chemistry, Biotechnology and Food Science, Norwegian University of Life Sciences (NMBU), N-1432 Ås, Norway

[2]INRAE, Aix Marseille University, UMR1163 Biodiversité et Biotechnologie Fongiques, 13009, Marseille, France

[†] These authors contributed equally
* corresponding author: vincent.eijsink@nmbu.no

This file includes:

Supplementary Figures
Supplementary Tables
Supplementary References

Supplementary Figures

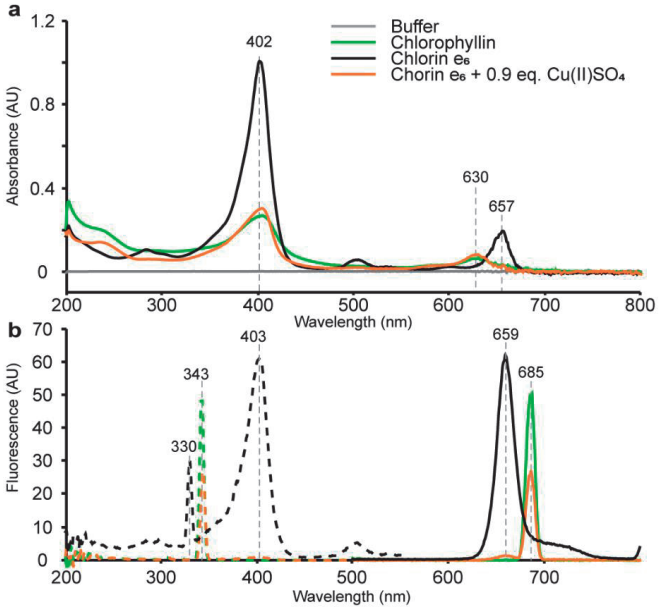

Supplementary Figure 1. Absorbance and fluorescence spectral characterization of chlorophyllin and chlorin e_6. (a) Absorbance spectra of chlorophyllin (12.5 µM; green line), copper-free chlorin e_6 (12.5 µM; black line) and chlorin e_6 complemented with 0.9 eq. of $Cu(II)SO_4$ (12.5 µM; orange line). The Soret (λ^{max} = 402 nm) and Q_y (λ^{max} = 630 nm) bands are characteristic of porphyrin rings; depletion of copper gave an expected[1] red shift of the Q_y band for chlorin e_6 (λ^{max} = 657 nm). **(b)** Emission (solid lines) and excitation (dotted lines) fluorescence spectra of chlorophyllin (5 µM; Ex343/Em685, green lines), chlorin e_6 (125 nM; Ex403/Em659, black lines) and chlorin e_6 complemented with 0.9 eq. of $Cu(II)SO_4$ (5 µM; Ex343/Em685, orange lines). The spectra show that copper binding quenches the fluorescence signal and induces a shift in the optimal excitation and emission wavelengths, which is consistent with changes in electronic properties. All solutions were prepared in potassium phosphate buffer (100 mM, pH 7.0) with 100 mM KCl and flushed with N_2.

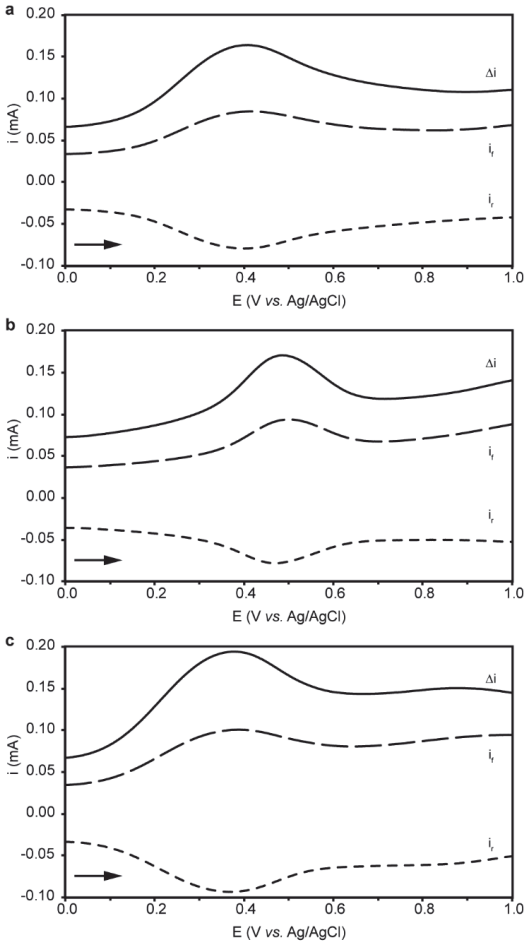

Supplementary Figure 2. Square-wave voltammograms for chlorophyllin compounds. The panels show the square-wave voltammograms obtained for **(a)** Chl (500 μM), **(b)** chlorin e_6 (500 μM), and **(c)** chlorin e_6-Cu(II) (500 μM). All chlorophyllin compounds were prepared in potassium phosphate buffer (100 mM, pH 7.0) with KCl (100 mM) as supporting electrolyte in anaerobic conditions and protected from light using aluminum foil. The amplitude was 50 mV, the potential increment 2 mV and the frequency 1250 Hz. All potentials were recorded *versus* an Ag/AgCl reference electrode and were adjusted to refer to the standard hydrogen electrode (SHE) using $E_{Ag/AgCl\ vs.\ SHE} = 222.49\ mV$[2].

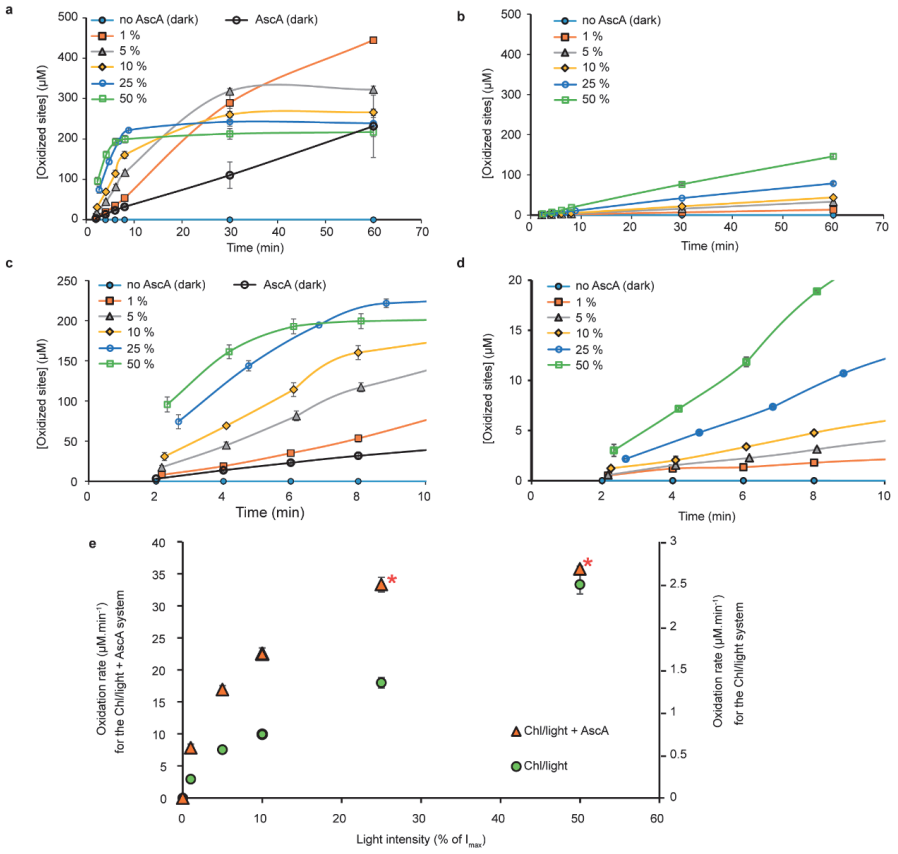

Supplementary Figure 3. The effect of light intensity on *Sc*AA10C-catalyzed cellulose oxidation fueled by Chl/light. *Sc*AA10C reactions in **(a)** the presence of AscA (1 mM) and **(b)** the absence of AscA. Panels **(c)** and **(d)** show enlargements of parts of panels **(a)** and **(b)**, respectively. Panels **(a)** and **(c)** also show data for a reaction with only AscA (1 mM). Panel **(e)** shows the approximate initial oxidation rates (expressed as µM of oxidized sites/min) as a function of light intensity for both systems. Note the different Y-axes; the system with AscA is much faster. For reactions carried out in the presence of AscA and with a light intensity of I = 25 or 50 % of I_{max} the reaction was so fast that the rate (derived from the 2 first time points) is probably underestimated (red stars). Reactions were carried out with 0.5 µM *Sc*AA10C in sodium phosphate buffer (50 mM, pH 7.0) at 40 °C, under magnetic stirring and exposed to visible light (I = 0-50% I_{max}, approx. 0-84 W.cm^{-2}). Before product quantification, solubilized cello-oligosaccharides were hydrolyzed by *Tf*Cel5A, to convert the LPMO products to a mixture of only two oxidized products with a degree of polymerization of 2 and 3 [GlcGlc1A, $(Glc)_2$Glc1A], the amounts of which were summed up to yield the concentration of oxidized sites. Error bars show ± s.d. (n = 2, independent experiments). Source data are provided as a Source Data file.

Of note, the light intensities used in our study are higher than those used by Cannella and colleagues[10]. This Figure (and corresponding Figure 3 in the main text) show that it is possible to use lower light intensities, but the reactions then proceed slower.

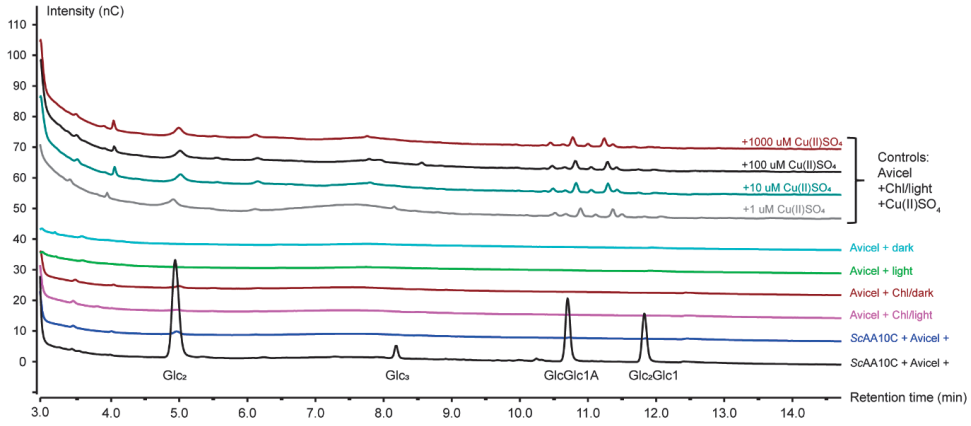

Supplementary Figure 4. Control reactions to check for the occurrence of copper-catalyzed Fenton-type chemistry. The picture shows chromatographic product profiles obtained in various control reactions. In the upper four reactions, the enzyme, *Sc*AA10C, was replaced by different concentrations of Cu(II)SO_4 (0 – 1000 µM) whereas the positive control reaction at the bottom, contained 1 µM of *Sc*AA10C. Product profiles obtained in additional control reactions (no light, no enzyme or copper, no chlorophyllin) are also shown. Reactions were carried out in sodium phosphate buffer (50 mM, pH 7.0) at 40 °C, under magnetic stirring with Avicel (10 $g.L^{-1}$) and Chl (500 µM) and exposed to visible light (I = 25 % I_{max}, approx. 42 $W.cm^{-2}$), as indicated. Before chromatographic analysis, the samples were treated with a cellulase, *Tf*Cel5A, to convert soluble products to a mixture of only two oxidized products with a degree of polymerization of 2 and 3 [GlcGlc1A, $(Glc)_2Glc1A$]. The figure shows a superimposition of the resulting chromatograms. Minor amounts of non-specific products can be observed in the $CuSO_4$ controls, which are not observed in the LPMO-containing reactions, which only show the expected oxidized oligosaccharides. Two independent replicates of the experiment were carried out.

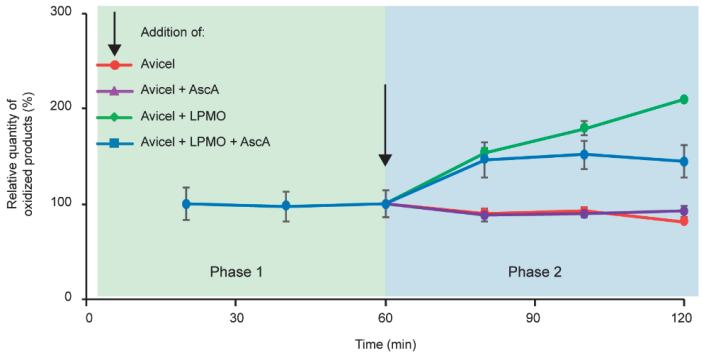

Supplementary Figure 5. Control reactions to check for inactivation of the LPMO during incubation with Chl/light and AscA. The figure shows time courses for the release of oxidized products from Avicel by *Sc*AA10C. Samples were withdrawn every 20 min and filtered to stop the reactions. In phase 1 (0-60 min), *Sc*AA10C (0.5 µM) was incubated with Avicel (5 $g.L^{-1}$) in presence of AscA (1 mM) and Chl (500 µM)/light. In phase 2 (60 – 120 min), subsequently to the 60 min sampling, the reactions were supplemented (black arrow) with fresh reaction components (given concentrations are final concentrations of the added material after mixing), as follows: Avicel (5 $g.L^{-1}$) (red circles); Avicel (5 $g.L^{-1}$) and AscA (1 mM) (purple triangles); Avicel (5 $g.L^{-1}$) and *Sc*AA10C (0.5 µM) (green diamonds); Avicel (5 $g.L^{-1}$), AscA (1 mM) and *Sc*AA10C (0.5 µM) (blue squares). To achieve this, the phase 1 mixtures (380 µL) were diluted with solutions containing Avicel (100 $g.L^{-1}$), AscA (100 mM) and/or *Sc*AA10C (25 µM) to obtain the concentrations given above. Reactions were carried out in sodium phosphate buffer (50 mM, pH 7.0) at 40 °C, under magnetic stirring and exposed to visible light (I = 25 % I_{max}, approx. 42 $W.cm^{-2}$). Before product quantitation, solubilized cello-oligosaccharides were hydrolyzed with *Tf*Cel5A, to convert the LPMO products to a mixture of only two oxidized products with a degree of polymerization of 2 and 3 [GlcGlc1A, $(Glc)_2Glc1A$], the amounts of which were analyzed by HPLC and summed up to yield the concentration of oxidized sites. The quantities of oxidized products are expressed as percentage of the quantity of products measured at 60 min. The dilution factor due to the addition of fresh reaction components in phase 2 was taken into account. Error bars show ± s.d. (n = 2, independent experiments). Source data are provided as a Source Data file.

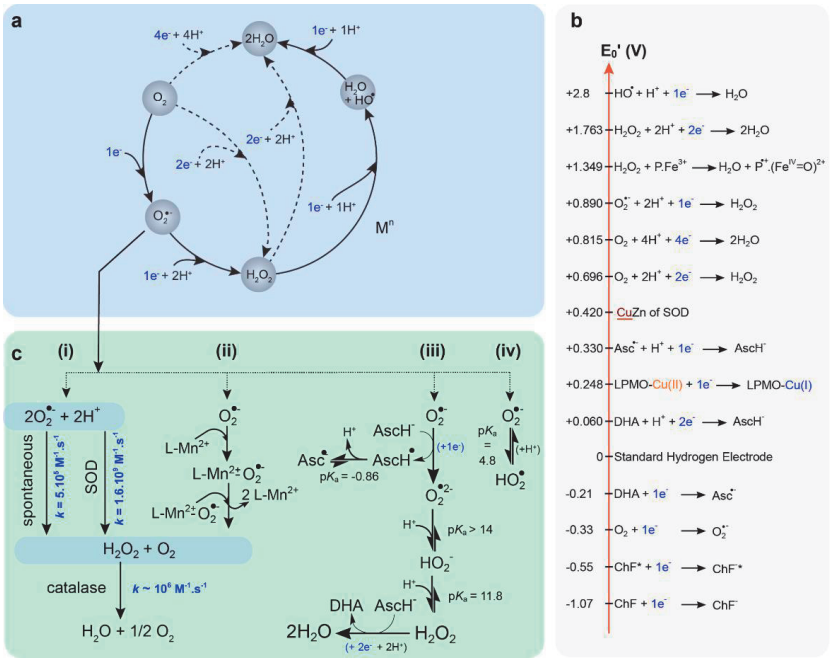

Supplementary Figure 6. Generation and fate of ROS. Panel **(a)** (blue frame) shows the reduction cycle for O_2 and derived ROS. Panel **(b)** (grey frame) shows potentials for reduction reactions potentially occurring in the systems under study. Single electron redox potentials of different ascorbic acid species at pH 7.0 were obtained from Figure 8 of Iyanagi et al.[3]. Reduction potential values (at pH 7.0, *vs* SHE) for O_2 and ROS couples were retrieved from Wood et al.[4] and those for the oxidized state (ChF) and the photoexcited triplet state (ChF*) of chlorophyll *a* from Seely et al.[5]. Panel **(c)** shows different pathways for the conversion of $O_2^{\bullet-}$ to other ROS. $O_2^{\bullet-}$ can be disproportionated to H_2O_2 spontaneously or enzymatically (by SOD) (**pathway i**) but also by manganese-binding complexes (e.g. L=phosphate[6]) (**pathway ii**). $O_2^{\bullet-}$ can also be further reduced (e.g. by AscA) to a peroxide ion ($O_2^{\bullet 2-}$), which is in fast equilibrium with H_2O_2 in non-alkaline conditions (**pathway iii**). In agreement with redox potentials (panel **b**), it has been shown in the literature that the reduction of $O_2^{\bullet-}$ to H_2O_2 can be accelerated by AscA[7,8], as also observed here (**Figure 3c**). In acidic conditions, $O_2^{\bullet-}$ can be protonated (pK_a = 4.8) yielding a hydroperoxyl radical (**pathway iv**). H_2O_2 can be further reduced to H_2O by reductants (e.g. by AscA) or enzymes (e.g. by catalase), as indicated in the Figure. Rate constants reported in panel **(c)** were retrieved from Augusto et al.[9]. DHA, dehydroascorbic acid; M^n, reduced free metal.

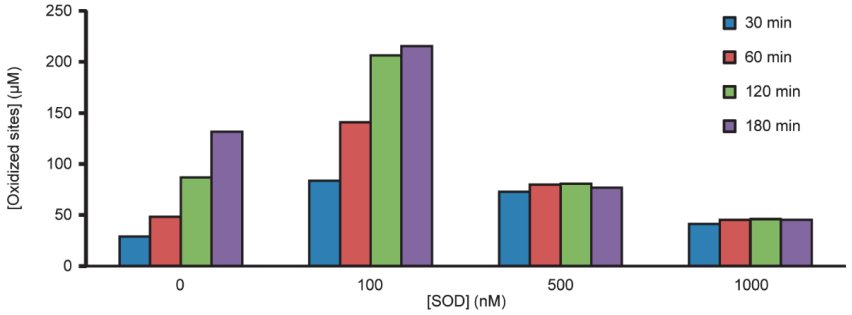

Supplementary Figure 7. The impact of SOD on *Sc*AA10C-catalyzed oxidation of Avicel fueled by the Chl/light system. The figure shows time courses for the release of aldonic acid products from Avicel (10 $g.L^{-1}$) by *Sc*AA10C (0.5 µM) fueled by Chl (500 µM)/light, in reaction mixtures supplemented with different concentrations of SOD (0-1000 nM) and with no AscA. Reactions were carried out in sodium phosphate buffer (50 mM, pH 7.0) at 40 °C, under magnetic stirring and exposed to visible light (I = 25% I_{max}, approx. 42 $W.cm^{-2}$). Before product quantification, solubilized cello-oligosaccharides were hydrolyzed by *Tf*Cel5A, to convert the LPMO products to a mixture of only two oxidized products with a degree of polymerization of 2 and 3 [GlcGlc1A, $(Glc)_2Glc1A$], the amounts of which were summed up to yield the concentration of oxidized sites. This figure shows the trade-off between SOD-catalyzed increased generation of H_2O_2 in the reaction mixtures, leading to higher LPMO catalytic rates, and enzyme inactivation. 100 nM SOD gives a higher initial LPMO rate, higher yields after 180 min but also signs of faster inactivation, i.e. slowing down of product formation in the later phase of the reaction (compared to the reaction without SOD). At higher SOD concentrations (i.e. higher levels of generated H_2O_2), the LPMO is inactivated very rapidly, so fast in fact that the product yield after 30 min does not reach the level reached at 100 nM SOD. This screening experiment was carried out once (n =1). Source data are provided as a Source Data file.

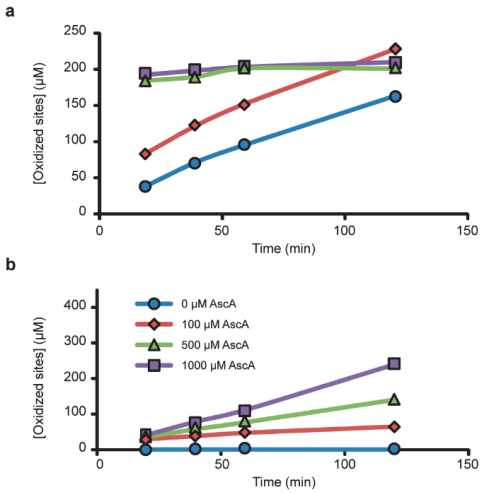

Supplementary Figure 8. The impact of the ratio between Chl and AscA on LPMO activity and stability. The figures show time courses for the release of oxidized products from Avicel (10 $g.L^{-1}$) by *Sc*AA10C (0.5 µM) in combination with different doses (0-1000 µM) of AscA **(a)** with (500 µM) and **(b)** without Chl. Reactions were carried out in sodium phosphate buffer (50 mM, pH 7.0) at 40 °C, under magnetic stirring and exposed to visible light (I = 25% I_{max}, approx. 42 $W.cm^{-2}$). Before product quantification, solubilized cello-oligosaccharides were hydrolyzed by *Tf*Cel5A, to convert the LPMO products to a mixture of only two oxidized products with a degree of polymerization of 2 and 3 [GlcGlc1A, $(Glc)_2Glc1A$], the amounts of which were summed up to yield the concentration of oxidized sites. This figure shows that, as expected, AscA alone can drive the LPMO action in a concentration-dependent manner. The Chl/light system works without AscA, but becomes very effective in the presence of higher AscA concentrations. However, these latter conditions lead to rapid inactivation of the LPMO. This screening experiment was carried out once (n =1). Source data are provided as a Source Data file.

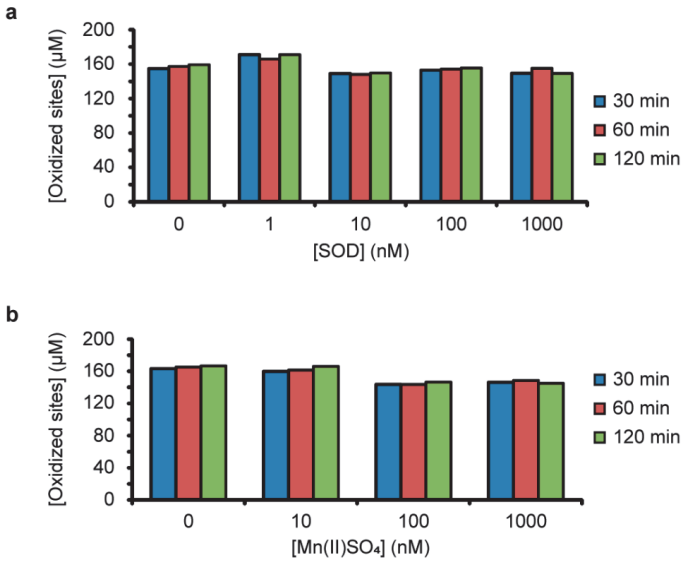

Supplementary Figure 9. The impact of SOD or Mn(II)SO_4 on the rate of light-induced LPMO-catalyzed cellulose degradation. The graphs show time courses for the release of aldonic acid products from Avicel (10 $g.L^{-1}$) by *Sc*AA10C (0.5 µM) fueled by the Chl (500 µM)/light + AscA (1 mM) system and supplemented with different doses of **(a)** SOD (0-1000 µM) or **(b)** Mn(II)SO_4, which remove superoxide enzymatically and chemically, respectively (carbonate or phosphate manganese complexes are described as SOD equivalents, see pathway (ii) in **Supplementary Figure 6**). Reactions (300 µL total volume) were carried out in sodium phosphate buffer (50 mM, pH 7.0) at 40 °C, under magnetic stirring and exposed to visible light (I = 25% I_{max}, approx. 42 $W.cm^{-2}$). Before product quantification, solubilized cello-oligosaccharides were hydrolyzed by *Tf*Cel5A, to convert the LPMO products to a mixture of only two oxidized products with a degree of polymerization of 2 and 3 [GlcGlc1A, $(Glc)_2Glc1A$], the amounts of which were summed up to yield the concentration of oxidized sites. The results show that at the first time point, the LPMO is inactivated and that addition of superoxide-removing agents does not change this. This screening experiment was carried out once (n =1). Source data are provided as a Source Data file.

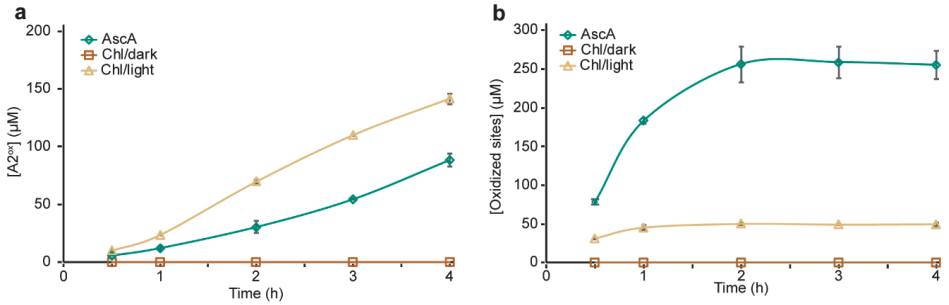

Supplementary Figure 10. Chl/light driven activity of other LPMOs. The figures show time courses for the release of oxidized products from **(a)** β-chitin (10 g.L^{-1}) by *Sm*AA10A (0.5 µM) and **(b)** Avicel (10 g.L^{-1}) by *Nc*AA9F (0.5 µM) in presence of AscA (1 mM), Chl (500 µM)/dark or Chl (500 µM)/light. The color code is provided in the figure. Reactions were carried out in sodium phosphate buffer (50 mM, pH 7.0) at 40 °C, under magnetic stirring and exposed to visible light (I = 25 % I_{max}, approx. 42 W.cm^{-2}). Before product quantitation, solubilized chito-oligosaccharides were hydrolyzed using a chitobiase, *Sm*GH20, to convert soluble LPMO products to chitobionic acid ($A2^{ox}$) and N-acetylglucosamine, after which the former was quantified by HPLC analysis. Solubilized cello-oligosaccharides were hydrolyzed using a cellulase, *Tf*Cel5A, to convert the LPMO products to a mixture of only two oxidized products with a degree of polymerization of 2 and 3 [GlcGlc1A, $(Glc)_2Glc1A$], the amounts of which were analyzed by HPLC summed up to yield the concentration of oxidized sites. Error bars show ± s.d. (n = 2, independent experiments). Source data are provided as a Source Data file.

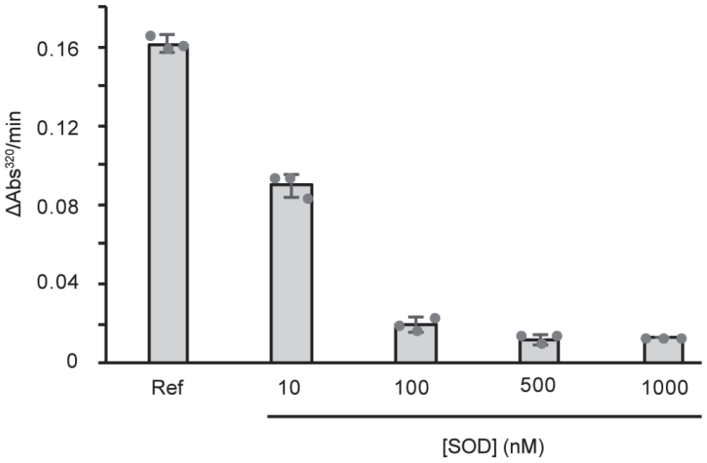

Supplementary Figure 11. Inhibition of pyrogallol auto-oxidation by SOD to verify SOD activity. The figure shows the rate of formation of purpurogallin, measured as the change in absorbance at 320 nm derived from a 5-min linear time-course. Purpurogallin is generated by auto-oxidation of pyrogallol and its formation is dependent on the availability of superoxide generated during the first step of the auto-oxidation process[11]. The reference reaction ("Ref") consists of pyrogallol (200 μM) in Tris-HCl buffer (50 mM, pH 8.0) and shows maximum auto-oxidation of pyrogallol and, thus, maximum formation of purpurogallin. Addition of different amounts of SOD (0-1000 nM) inhibits the formation of purpurogallin in a dose-dependent manner, which demonstrates that the SOD is active. All reactions were carried out at 25 °C. The reactions were initiated by the addition of pyrogallol and the absorbance was measured every 10 s for 5 min. The stock solution of pyrogallol was prepared in 10 mM HCl to prevent auto-oxidation. Error bars show ± s.d. (n = 3, independent experiments). Source data are provided as a Source Data file.

Supplementary Tables

Supplementary Table 1. Square-wave voltammetric peak potentials of chlorophyllin compounds[a].

Chl species	E_p (V vs. SHE)
Chlorophyllin	0.634 ± 0.004 V
Chlorin e_6	0.709 ± 0.003 V
Chlorin e_6-Cu(II)	0.601 ± 0.019 V

[a] Chl (500 μM), chlorin e_6 (500 μM), and chlorin e_6-Cu(II) (500 μM) were prepared in potassium phosphate buffer (100 mM, pH 7.0) with KCl (100 mM) as supporting electrolyte in anaerobic conditions and protected from light using aluminum foil. The amplitude was 50 mV, the potential increment 2 mV and the frequency 1250 Hz. All potentials were recorded *versus* an Ag/AgCl reference electrode and were adjusted to refer to the standard hydrogen electrode (SHE) using $E_{Ag/AgCl\ vs.\ SHE}$ = 222.49 mV[2]. The errors correspond to the standard deviation of three independent experiments. Source data are provided as a Source Data file.

Supplementary References

1. Gouterman, M. in *The Porphyrins, Volume III: Physical Chemistry* (ed. Dolphin, D.) (Academic Press, San Diego, 1978).
2. Spitzer, P. *et al.* in *Handbook of Reference Electrodes* (ed. Inzelt G., Lewenstam A., Scholz F.) (Springer-Verlag Berlin and Heidelberg GmbH & Co. KG, Berlin, 2013).
3. Iyanagi, T., Yamazaki, I. & Anan, K. F. One-electron oxidation-reduction properties of ascorbic acid. *Biochim. Biophys. Acta* **806**, 255–261 (1985).
4. Wood, P. M. The potential diagram for oxygen at pH 7. *Biochem. J.* **253**, 287–289 (1988).
5. Seely, R. The energetics of electron transfer of chlorophyll and other compounds. *Photochem. Photobiol.* **27**, 639–654 (1978).
6. Barnese, K., Gralla, E. B., Valentine, J. S. & Cabelli, D. E. Biologically relevant mechanism for catalytic superoxide removal by simple manganese compounds. *Proc. Natl. Acad. Sci. U. S. A.* **109**, 6892–6897 (2012).
7. Scarpa, M., Stevanatos, R., Vigiinos, P. & Rig, A. Superoxide ion as active intermediate in the autoxidation of ascorbate by molecular oxygen. *J. Biol. Chem.* **258**, 6695–6697 (1983).
8. Nishikimi, M. Oxidation of ascorbic acid with superoxide anion generated by the xanthine-xanthine oxidase system. *Biochem. Biophys. Res. Commun.* **63**, 463–468 (1975).
9. Augusto, O. & Miyamoto, S. in *Principles of free radical biomedicine* (ed. Pantopoulos, K., Schipper, H.) (Nova Science, New York, 2011).
10. Cannella, D. *et al.* Light-driven oxidation of polysaccharides by photosynthetic pigments and a metalloenzyme. *Nat. Comm.* **7**, (2016).
11. Li, X. Improved pyrogallol autoxidation method: a reliable and cheap superoxide-scavenging assay suitable for all antioxidants. *J. Agric. Food Chem.* **60**, 6418–6424 (2012).

Visible light-exposed lignin facilitates cellulose solubilization by lytic polysaccharide monooxygenases

Kommedal EG, Angeltveit CF, Klau LJ, Ayuso-Fernández I, Arstad B, Antonsen SG, Stenstrøm Y, Ekeberg D, Gírio F, Carvalheiro F, Horn SJ, Aachmann FL, Eijsink VGH

Paper II

Visible light-exposed lignin facilitates cellulose solubilization by lytic polysaccharide monooxygenases

Eirik G. Kommedal[1], Camilla F. Angeltveit[1], Leesa J. Klau[2], Iván Ayuso-Fernández[1], Bjørnar Arstad[3], Simen G. Antonsen[1], Yngve Stenstrøm[1], Dag Ekeberg[1], Francisco Gírio[4], Florbela Carvalheiro[4], Svein J. Horn[1], Finn Lillelund Aachmann[2], Vincent G. H. Eijsink[1*]

[1] Faculty of Chemistry, Biotechnology and Food Science, Norwegian University of Life Sciences (NMBU), 1432 Ås, Norway

[2] Department of Biotechnology and Food Science, Norwegian University of Science and Technology (NTNU), 7491 Trondheim, Norway

[3] SINTEF Industry, Process Chemistry and Functional Materials, 0373 Oslo, Norway

[4] National Laboratory of Energy and Geology (LNEG), 1649-038 Lisboa, Portugal

[*] Corresponding author: vincent.eijsink@nmbu.no

GRAPHICAL ABSTRACT

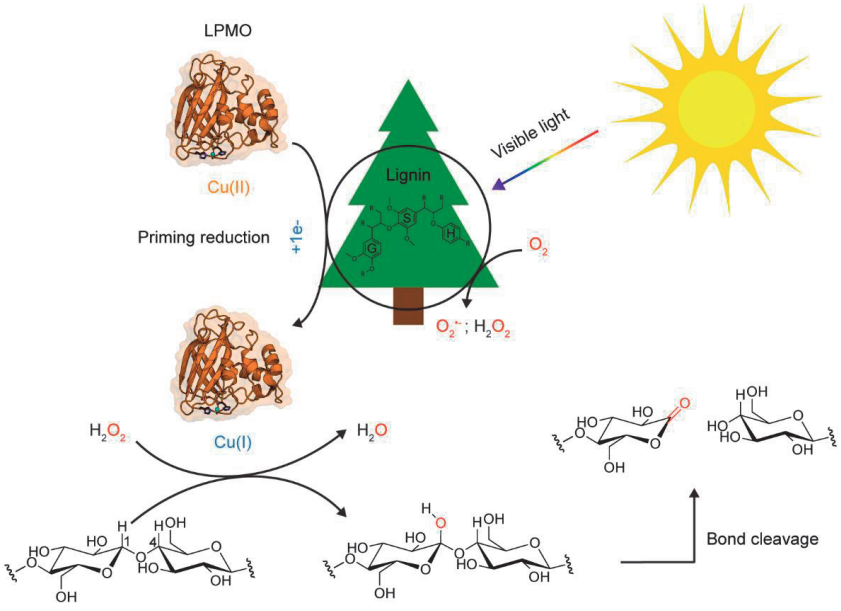

ABSTRACT

Lytic polysaccharide monooxygenases (LPMOs) catalyze oxidative cleavage of glycosidic bonds in crystalline polysaccharides such as cellulose and are crucial for the conversion of plant biomass in Nature and in industrial applications. Sunlight promotes microbial conversion of plant litter in Nature, and this effect has been attributed to photochemical degradation of lignin, a major redox-active component of secondary plant cell walls that limits enzyme access to the cell wall carbohydrates. Here, we show that exposure of lignin to visible light facilitates cellulose solubilization by LPMOs by promoting formation of H_2O_2 that fuels LPMO catalysis, which is accompanied by oxidation of ring-conjugated olefins. At the same time, the LPMO oxidizes phenolic hydroxyls in the polymeric lignin, leading to the priming reduction that is needed to bring the enzyme into its catalytically competent state. The discovery that light-driven abiotic reactions in Nature can fuel H_2O_2-dependent redox enzymes involved in biomass conversion may offer new opportunities for bioprocessing and, most importantly, provides an enzymatic explanation for the known effect of visible light on biomass conversion.

Keywords: Lytic polysaccharide monooxygenase, lignin, cellulose, photobiocatalysis, biomass conversion, redox enzymes

INTRODUCTION

In Nature, selective oxidation of non-activated C-H bonds in crystalline polysaccharides is crucial for efficient aerobic decomposing of plant biomass. Every year, 100 billion tons of CO_2 and H_2O are converted to cellulose by photosynthetic organisms (Field et al., 1998), making lignocellulosic plant biomass the most abundant natural material on Earth and a large reservoir of renewable carbon that can be transformed to chemicals and fuels. However, plant cell walls have evolved to become recalcitrant co-polymeric structures to provide mechanical strength and rigidity and to provide resistance against pathogen attack, and are, thus, hard to break down (Kirui et al., 2022). Plant cell wall-degrading microorganisms have solved this challenge by developing multi-component enzymatic tools that act synergistically to process this highly complex and recalcitrant biomass.

Lytic polysaccharide monooxygenases (LPMOs) are a relatively recently discovered group of oxidative enzymes that contribute to enzymatic conversion of biomass (Harris et al., 2010; Vaaje-Kolstad et al., 2005a, 2010). They are abundant in Nature and classified, based on their sequences, in the auxiliary activity (AA) families 9-11 and 13-17 of the Carbohydrate Active enZymes (CAZy) database (Levasseur et al., 2013). LPMOs are mono-copper enzymes (Phillips et al., 2011; Quinlan et al., 2011) that catalyze oxidative cleavage of glycosidic bonds in cellulose (Forsberg et al., 2011; Quinlan et al., 2011) and chitin (Vaaje-Kolstad et al., 2010). LPMOs were first considered monooxygenases as the activity was shown to depend on the presence of molecular oxygen, but recent studies have demonstrated that H_2O_2 is the kinetically relevant co-substrate making these enzymes peroxygenases rather than monooxygenases (Bissaro et al., 2017, 2020b; Hangasky et al., 2018; Hedison et al., 2021; Jones et al., 2020; Kuusk et al., 2018; Rieder et al., 2021; Stepnov et al., 2022). The oxidative action of LPMOs disrupts the crystalline polysaccharide surface (Eibinger et al., 2014; Song et al., 2018) thus promoting depolymerization by hydrolytic enzymes (Müller et al., 2018; Vaaje-Kolstad et al., 2010). It is generally accepted that LPMOs are the C1 factor hypothesized by Elwyn Reese and co-workers in 1950 (Reese et al., 1950) and that LPMOs explain why Eriksson et al. were able show, in 1974, that oxygen promotes biomass conversion by a fungal secretome (Eriksson et al., 1974).

LPMO catalysis was first thought to require delivery of two electrons, two protons and molecular oxygen per catalytic cycle in what would be a monooxygenase reaction ($R\text{-}H + 2e^- + 2H^+ + O_2 \rightarrow R\text{-}OH + H_2O$), whereas in the peroxygenase reaction, a reduced LPMO can catalyze multiple turnovers with H_2O_2 ($R\text{-}H + H_2O_2 \rightarrow R\text{-}OH + H_2O$) (Chylenski et al., 2019). A standard monooxygenase reaction set-up involves incubating the LPMO with substrate and a reductant under aerobic conditions and it has been shown that a wide variety of reducing compounds and reducing equivalent-delivering enzymes can drive LPMO reactions (Bissaro et al., 2020a; Chalak et al., 2019; Frommhagen et al., 2016, 2018; Hegnar et al., 2019; Kont et al., 2019; Kracher et al., 2016; Muraleedharan et al., 2018; Phillips et al., 2011; Westereng et al., 2015). It is currently being debated whether observed monooxygenase reactions are in fact peroxygenase reactions that are limited by the *in situ* generation of H_2O_2 by LPMO-catalyzed or abiotic oxidation of the reductant (e.g., Bissaro et al., 2018 (Bissaro et al., 2018)). Importantly, like many other redox enzymes, high levels of H_2O_2 combined with low levels of substrate will lead to autocatalytic oxidative damage in the catalytic center of the enzyme

(Bissaro et al., 2017; Kuusk et al., 2021; Müller et al., 2018). H_2O_2-driven LPMO catalysis is clearly a double-edged sword enabling high enzymatic activity at the possible cost of enzyme inactivation.

Light represents an abundant and cheap source of energy that can be harvested by a photoredox catalyst to tailor H_2O_2 levels to enzymatic reactions (Schmermund et al., 2019; van Schie et al., 2019). Light-driven LPMO reactions were first described in 2016. Cannella et al. showed that the activity of a fungal LPMO acting on amorphous cellulose (PASC) could be boosted dramatically by adding chlorophyllin, a photosynthetic pigment, and light, next to the reductant, ascorbic acid (AscA) (Cannella et al., 2016). Light-driven activity of a bacterial LPMO from *Streptomyces coelicolor* (*Sc*AA10C) on crystalline cellulose (Avicel) using irradiated vanadium-doped titanium dioxide (V-TiO_2) was demonstrated later the same year (Bissaro et al., 2016). Both studies discussed molecular mechanisms for the observed LPMO activity, but neither considered light-induced formation of H_2O_2 from O_2 as the primary driver for LPMO activity in these reactions, which, later, was shown to be the key driver of LPMO activity in these light-fueled reaction systems (Bissaro et al., 2020a).

The impact of light on biomass conversion is of great interest, with repercussions spanning from the global carbon cycle to industrial biorefining. Light has been demonstrated to facilitate microbial decomposition of plant litter by increasing the accessibility of cell wall polysaccharides to enzymatic conversion (Austin et al., 2016, 2010, 2006; Berenstecher et al., 2020; Lin et al., 2018). Since secondary plant cell walls, the natural substrates of LPMOs, are rich in lignin, and since lignin is photoactive and can promote formation of H_2O_2 (Kim et al., 2022; Miglbauer et al., 2020), we hypothesized that light-driven redox processes involving lignin and LPMO activity can help explaining the observed photofacilitation of biomass decomposition.

Here we report a detailed biochemical study of cellulose degradation by *Sc*AA10C, a well-studied model LPMO from the soil actinomycete *Streptomyces coelicolor*, using light-exposed lignin to fuel the LPMO reaction. We show that light-exposure of lignin has a large effect on LPMO activity and that this effect is driven by the ability of lignin to promote

generation of H_2O_2. We also show that the necessary priming reduction of the LPMO may be achieved through direct interactions with polymeric lignin and that LPMOs, thus, can oxidize lignin similar to what is observed for ligninolytic peroxidases and laccases. Using NMR spectroscopy, we demonstrate the impact of visible light on the lignin structure, revealing effects on olefinic structures. Next to providing deep insight into how lignin and light-exposed lignin affect LPMO activity, this study offers an alternative, enzyme-based explanation for the effect of light on biomass turnover in the biosphere.

RESULTS

Photocatalytic hydrogen peroxide generation by lignin fuels LPMO activity on cellulose

Previous studies have demonstrated lignin's ability to fuel the LPMO reaction and this was thought to reflect lignin's ability to deliver the electrons needed by the LPMO to carry out a monooxygenase reaction (Cannella et al., 2016; Hu et al., 2014; Muraleedharan et al., 2018; Westereng et al., 2015). (Cannella et al., 2016). To gain more insight into lignin's ability to fuel LPMO reactions and to assess the impact of light we used a well-studied cellulose-active C1-oxidizing LPMO from *Streptomyces coelicolor* (*Sc*AA10C, also known as CelS2) and Avicel (i.e., crystalline cellulose).

In the first set of experiments, we used commercially available kraft lignin to fuel solubilization of crystalline cellulose by *Sc*AA10C and we measured both LPMO product formation and the accumulation of H_2O_2 in reactions exposed to light (Figure 1). As expected, oxidized cello-oligosaccharides were not generated in reactions lacking the LPMO (Figure 1a). At the lower lignin concentration (0.9 $g.L^{-1}$), the reaction without LPMO showed accumulation of H_2O_2, whereas the reaction with 75 nM or 500 nM LPMO showed almost identical linear progress curves for LPMO product formation and no accumulation of H_2O_2. This suggests that, under these conditions, the LPMO reaction was limited by generation of H_2O_2. At the higher lignin concentration (9 $g.L^{-1}$), accumulation of H_2O_2 in the reaction without LPMO was much higher (Figure 1b). In the reaction with only 75 nM LPMO, product formation stopped within the first hour (Figure 1a) and H_2O_2 accumulated at a rate similar to the reaction without LPMO (Figure 1b), indicating that the LPMO had been inactivated due to an overload of H_2O_2 (Bissaro et al., 2020a; Blossom et al., 2020; Rieder et al., 2021). To

demonstrate enzyme inactivation, three separate reactions identical to the 9 $g.L^{-1}$ lignin, 75 nM LPMO reaction of Figure 1 were set up and after one hour, substrate, enzyme and substrate, or a reductant and substrate were added. Only the reaction to which fresh enzyme was added showed resumed LPMO activity (Supplementary Figure 1), confirming that, indeed, enzyme inactivation had occurred. On the other hand, 500 nM LPMO was sufficient to productively converted all H_2O_2 generated during the course of the 6 h reaction into oxidized cello-oligosaccharides and no H_2O_2 accumulation was observed in this reaction (Figure 1). Consequently, product formation in the reaction with 9 $g.L^{-1}$ lignin and 500 nM LPMO was much faster than in any of the other reactions.

While Figure 1 shows that there is a clear correlation between the amount of H_2O_2 generated in the reaction system and LPMO activity, there is a marked difference between the H_2O_2 levels generated in absence of LPMO (Figure 1b) and the amount of oxidized product formed in LPMO-containing reactions (Figure 1a). If the apparent H_2O_2 levels in Figure 1b equal the true levels and if one accepts the premise that access to H_2O_2 limits the LPMO reaction, H_2O_2 levels in the reaction without LPMO and LPMO product levels should be similar. One potential explanation resides in the HRP/Amplex Red assay used to determine H_2O_2 levels. Kraft lignin serves as substrate for HRP, which will suppress the Amplex Red signal. This effect was, however, compensated for since all H_2O_2 standard curves used to determine H_2O_2 accumulation with the HRP/Amplex Red assay contained the same lignin concentration as the reaction being analyzed. Another explanation lies in the abiotic consumption of H_2O_2. The levels of H_2O_2 measured in the absence of the LPMO are the net result of formation and degradation, both of which may be dependent on light, as has been shown for a different photocatalyst (Burek et al., 2019), and on the presence redox-active moieties in the lignin itself (Kont et al., 2019). Since LPMOs in presence of substrate have high affinity for H_2O_2 (K_m values in the low micromolar range; (Kuusk et al., 2018, 2021; Rieder et al., 2021) it is conceivable that the LPMO peroxygenase reaction outcompetes abiotic consumption of H_2O_2 through reactions with lignin, which would explain the discrepancy between apparent H_2O_2 measured and LPMO product levels. A control experiment indicated that, indeed, H_2O_2 consumption by the LPMO is faster than abiotic H_2O_2 consumption (Supplementary Figure 2).

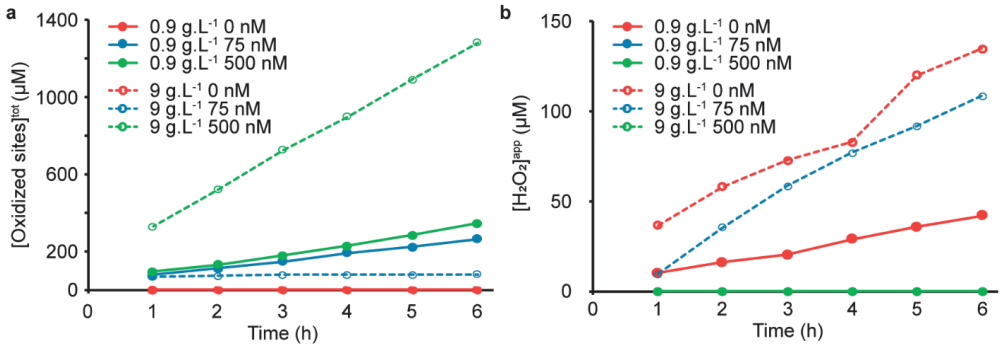

Figure 1. LPMO depolymerization of cellulose using Kraft lignin as photocatalyst. The graphs show time-courses for the production of oxidized LPMO products (**a**) and apparent H_2O_2 levels (**b**) in photobiocatalytic reactions containing LPMO (*Sc*AA10C; 0, 75, or 500 nM), substrate (Avicel, 10 g.L^{-1}) and photocatalyst (Kraft lignin; 0.9 or 9 g.L^{-1}). All reactions were carried out in sodium phosphate buffer (50 mM, pH 7.0) at 40°C under magnetic stirring and exposed to visible light (I=10% I_{max}, approx. 16.8 W.cm^{-2}). 50 µL aliquots were taken every hour and diluted with 50 µL water prior to boiling for oxidized product analysis or H_2O_2 quantification using the Amplex Red/HRP assay. The reactions were performed as duplicates and showed generally 10% or less variation between replicates except for the reaction with 0.9 g.L^{-1} and 500 nM *Sc*AA10C where the deviations were less than 22% between replicates. No oxidized products were detected in reactions lacking LPMO (**a**) and H_2O_2 only accumulated in reactions without LPMO regardless of lignin concentration except for the reaction with 9 g.L^{-1} lignin and 75 nM LPMO (**b**). Reactions in the dark showed much lower product levels, as shown in Figure 2.

To further understand the lignin/light/LPMO system, each reaction component in a standard reaction with *Sc*AA10C (0.5 µM), Avicel (10 g.L^{-1}), lignin (0.9 g.L^{-1}), and light (I=10% I_{max}, corresponding to approx. 16.8 W.cm^{-2}) was varied. Further reduction of the LPMO concentration to below 75 nM showed that the LPMO became limiting at lower concentrations (Figure 2a). At 50 nM LPMO, product formation appeared to level off between 3 and 6 h, and further reducing the LPMO concentration to 25 nM resulted in cessation of product formation after 90 min due to enzyme inactivation (Figure 2a).

Increasing the Avicel concentration led to a decrease in LPMO activity (Figure 2b). While this may seem counterintuitive, it has been shown that higher Avicel concentrations attenuate more photons (Blossom et al., 2020) which would reduce lignin-catalyzed H_2O_2 formation. As for the lignin concentration, a clear dose-response effect was already visible in the data of Figure 1 and Figure 2c shows that further lowering of the lignin concentration leads to less LPMO activity, confirming the dose-response relationship. Figure 2d shows a clear dose-response effect for the light and shows that the reaction with the standard amount of light used here (I=10% I_{max}) is one order of magnitude faster than a reaction in the dark.

No LPMO activity was detected in absence of lignin (Figure 2c). Taken together, the results displayed in Figures 1 and 2 demonstrate that lignin and light combined enable fine-tuning of LPMO reactions and that increased LPMO activity correlates with conditions that favor H_2O_2 production.

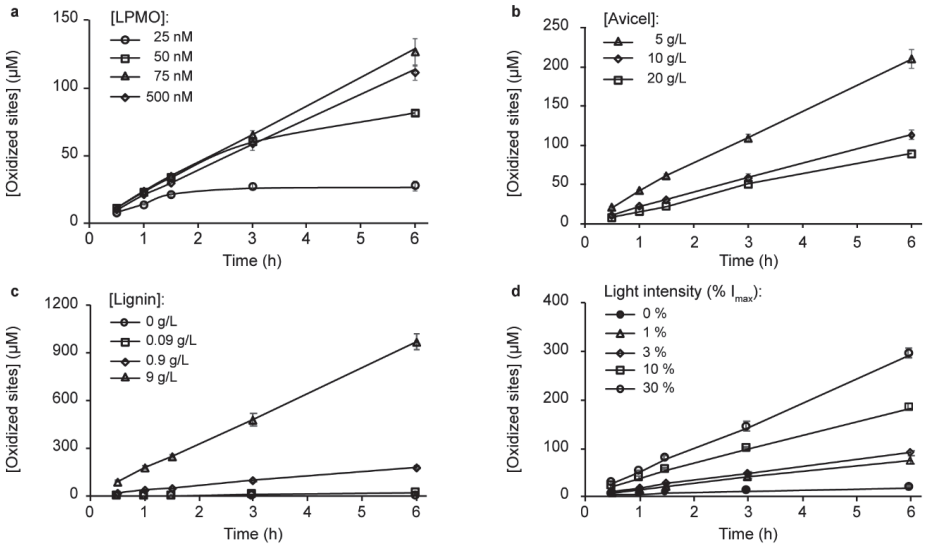

Figure 2. Influence of the LPMO, Avicel, and lignin concentrations and light intensity on LPMO catalyzed solubilization of cellulose. The graphs show time-courses for the release of aldonic acid products in reactions with varying (**a**) LPMO concentration, (**b**) Avicel concentration, (**c**) Kraft lignin concentration, and (**d**) light intensity. All reactions were carried out in sodium phosphate buffer (50 mM, pH 7.0) at 40°C under magnetic stirring with exposure to visible light (10% I_{max}, approx. 16.8 $W.cm^{-2}$ unless otherwise specified), and contained LPMO (*Sc*AA10C, 0.5 µM), Avicel (10 $g.L^{-1}$), and lignin (0.9 $g.L^{-1}$), unless otherwise specified. Before product quantification, solubilized cello-oligosaccharides were hydrolyzed by *Tf*Cel6A to convert LPMO products with varying degree of polymerization (DP) to a mixture of DP 2 and 3 [GlcGlc1A, (Glc)2Glc1A], the amounts of which were summed up to yield the concentration of oxidized sites. Error bars show ± s.d. (n = 3, independent experiments).

To demonstrate that light-driven H_2O_2 generation is fueling the LPMO reaction, competition experiments were performed with increasing amounts of horseradish peroxidase (HRP). No additional substrate for HRP was needed as the soluble lignin used in these reactions is a suitable substrate for this enzyme. The LPMO reaction was increasingly inhibited by increasing amounts of HRP (Figure 3a). Plotting the rate of LPMO catalytic activity against the HRP concentration showed more than 85% inhibition of LPMO activity with 193 nM HRP and almost complete inhibition, >97% inhibition, with 1930 nM HRP (Figure 3b). These

experiments clearly show that the LPMO reaction is fuelled by the H_2O_2 generated from light-irradiated lignin.

Two recent studies have demonstrated H_2O_2 generation by light-exposed lignin, which may be the result two single-electron reductions of O_2 leading to $O_2^{\bullet-}$ and then H_2O_2 or of a one-step, two-electron reduction of O_2 to H_2O_2 (Kim et al., 2022; Miglbauer et al., 2020). Of note, the superoxide radical can likely act as reductant for the LPMO (Bissaro et al., 2020a; Koppenol et al., 2010). To assess possible formation of superoxide we carried out reaction with superoxide dismutase (SOD), which converts superoxide to H_2O_2 and O_2. Adding increasing amounts of SOD (0 - 3000 nM) to an irradiated reaction with lignin (0.9 g.L^{-1}), Avicel (10 g.L^{-1}), and *Sc*AA10C (0.5 µM) led to a near four-fold increase in the LPMO rate (Figure 3c&d), showing that superoxide was indeed generated from light-exposed lignin and that access to H_2O_2 limits LPMO activity in these conditions.

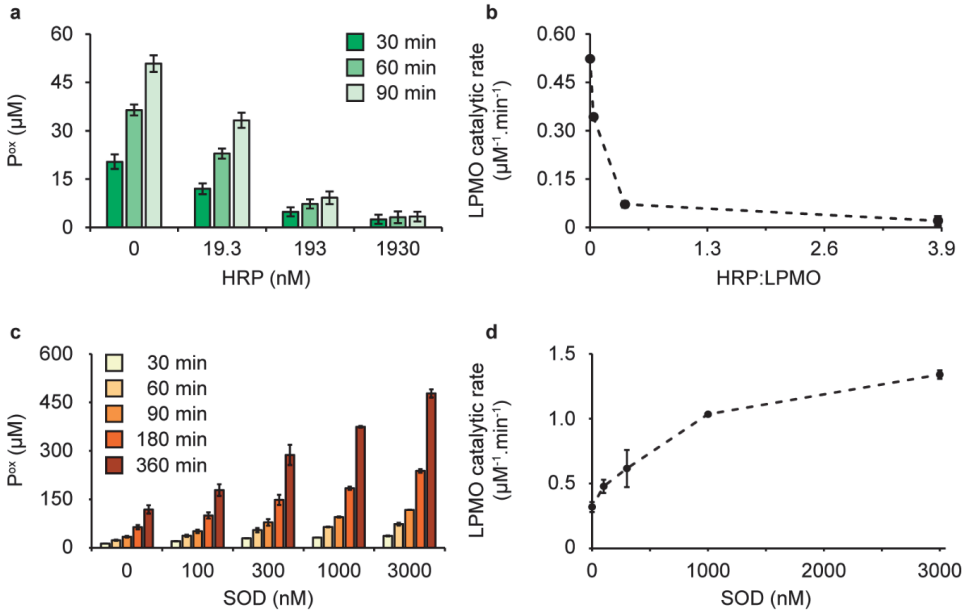

Figure 3. Probing the role of reactive oxygen species in the light/lignin/LPMO system. The graphs show time-courses for the formation of oxidized products (**a**,**c**) and the corresponding apparent catalytic rates (**b**, **d**) for reactions with Avicel (10 g.L^{-1}), *Sc*AA10C (0.5 µM), Kraft lignin (0.9 g.L^{-1}), and light-exposure in the presence of varying amounts of horseradish peroxidase (HRP) (**a**,**b**) and superoxide dismutase (SOD) (**c**,**d**). The rates shown in (**b**) were derived from linear regression analysis using all three time points in (**a**) with R^2>0.99 for all reactions with 0, 19.3, 193 nM HRP except for one replicate with 193 nM with R^2>0.93. For the reactions with 1930 nM HRP the product levels were very low and showed larger variability as these levels were close to

the detection limit of the analytical method. The rates in (**d**) were derived using linear regression analysis for all time points displayed in **(c)** and all reactions gave progress curves with R^2>0.99. All reactions were carried out in sodium phosphate buffer (50 mM, pH 7.0) at 40°C, under magnetic stirring and exposed to visible light (I=10% I_{max}, approx. 16.8 W.cm^{-2}). Before product quantification, solubilized cello-oligosaccharides were hydrolyzed with *Tf*Cel6A to convert LPMO products with varying degree of polymerization (DP) to a mixture of DP 2 and 3 [GlcGlc1A, (Glc)2Glc1A], the amounts of which were summed up to yield the concentration of oxidized sites. The experiments were performed as three (**a**) or two (**c**) independent replicates and error bars show ± s.d.

LPMO reduction by lignin

Superoxide and lignin have both been suggested as competent reducing agents for LPMOs (Bissaro et al., 2020a; Muraleedharan et al., 2018; Westereng et al., 2015). To create insight into the role of lignin in LPMO reduction, we assessed the ability of lignin to reduce the LPMO using stopped-flow kinetic measurements. We first attempted to do so with *Sc*AA10C, but for this LPMO the combination of a weak signal and signal quenching by lignin prevented the determination of rates from the kinetic traces (Supplementary Figure 3c). Changing from the cellulose-active *Sc*AA10C to the chitin-active *Sm*AA10A, with a stronger fluorescence signal, allowed proper determination of lignin oxidation rates (Figure 4b). Of note, a control experiment showed that, just as cellulose degradation by *Sc*AA10C, chitin degradation by *Sm*AA10A was boosted by light-exposed lignin (Supplementary Figure 4).

To rule out that LPMO reduction was caused by small phenolic or other low molecular weight compounds present in the commercial Kraft lignin preparation, we measured LPMO reduction both with native Kraft lignin and dialyzed Kraft lignin. Such a dialysis step is often performed when studying lignin peroxidases to remove traces of Mn^{2+} (Sáez-Jiménez et al., 2016). The effect of lignin dialysis was minimal, both for light-driven cellulose oxidation by *Sc*AA10C and for reduction of *Sm*AA10A (Figure 4 & Supplementary Figures 3a&b). Figure 4a shows that reactions with native and dialyzed Kraft-lignin generated similar levels of oxidized products during a 6 h reaction with light-exposure. For reactions in the dark, the dialyzed lignin resulted in lower LPMO activity compared to the already slow reaction with native Kraft lignin (Figure 4a). Figure 4b shows that anaerobic reduction of *Sm*AA10A, and, thus oxidation of lignin, happens with second order rate constants, k_{1app}^{lignin}, of $3.7 \cdot 10^3$ M.s^{-1} and $2.9 \cdot 10^3$ M.s^{-1}, for non-dialyzed and dialyzed Kraft lignin, respectively. It is worth noting that these results indicate that a high molecular weight lignin polymer can directly interact with the copper site of LPMOs.

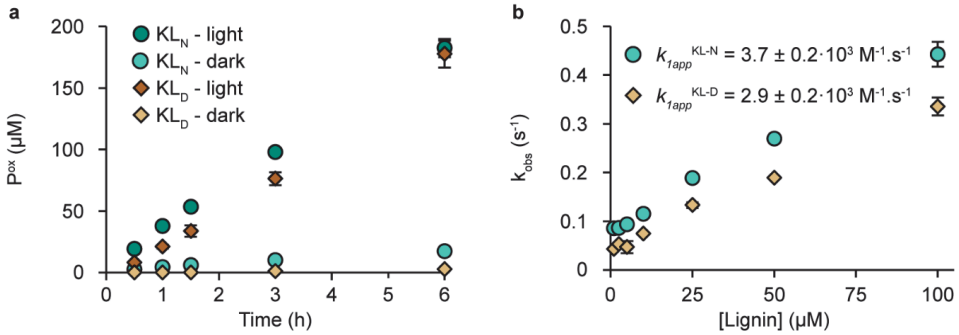

Figure 4. Lignin-driven *Sc*AA10C-catalyzed solubilization of cellulose and reduction kinetics for *Sm*AA10A. (**a**) The figure shows time courses for the formation of solubilized oxidized products by *Sc*AA10C (0.5 μM) in reactions with native (KL_N) or dialyzed (KL_D) Kraft lignin (0.9 $g.L^{-1}$) and Avicel (10 $g.L^{-1}$) in sodium phosphate buffer (50 mM, pH 7.0) at 40°C with magnetic stirring, in the dark or when irradiated by white light (I=10% I_{max}, approx. 16.8 $W.cm^{-2}$). Before product quantification, solubilized oxidized products were converted to a mixture of cellobionic and cellotrionic acid by incubation with *Tf*Cel6A at room temperature overnight. (**b**) The figure shows the observed pseudo-first-order constants, k_{obs}, for reduction of *Sm*AA10A-Cu(II) as a function the Kraft lignin concentration. Kraft lignin concentrations were calculated based on an average molecular mass (provided by the supplier) of 10 000 g/mol for both lignin preparations; since the average mass of the dialyzed lignin is expected to be somewhat higher, compared to the native lignin, the second order rate constant for the dialyzed lignin is underestimated. *Sm*AA10A-Cu(II) (10 μM) was anaerobically mixed with varying concentrations of native (KL_N) and dialyzed (KL_D) Kraft lignin, and the change in fluorescence was monitored as a function of time. The reactions were carried out in sodium phosphate buffer (50 mM, pH 7.0) at 25°C. Data were fit with single exponential functions to give observed rate constants (k_{obs}) at each substrate concentration. The apparent second order rate constant k_{1app}^{lignin} was determined from linear regression using the reported data points and displayed an R^2>0.99. Error bars in **a** and **b** show ± s.d. (n = 3, independent experiments). Note that the reaction with KL_N is the same as the reaction reported in Figure 2.

Studies with other lignin types

Kraft lignin is produced from kraft pulping of wood to separate cellulose from hemicellulose and lignin using sodium hydroxide and sodium sulfide. This process generates a modified and condensed lignin structure compared to native lignin with an increase in phenolic groups and recalcitrant C-C and C-O bonds, and a reduced number of less recalcitrant β-O-4 bonds (Crestini et al., 2017; Lancefield et al., 2018). To assess the impact of lignin type on light-enhanced LPMO activity, we performed experiments similar to those reported above in which the soluble Kraft lignin was replaced by insoluble organosolv lignin obtained from either spruce or birch. Figure 5 shows that light-exposure drastically enhanced the ability of insoluble organosolv lignin to fuel the LPMO reaction, similar to what was observed with Kraft lignin.

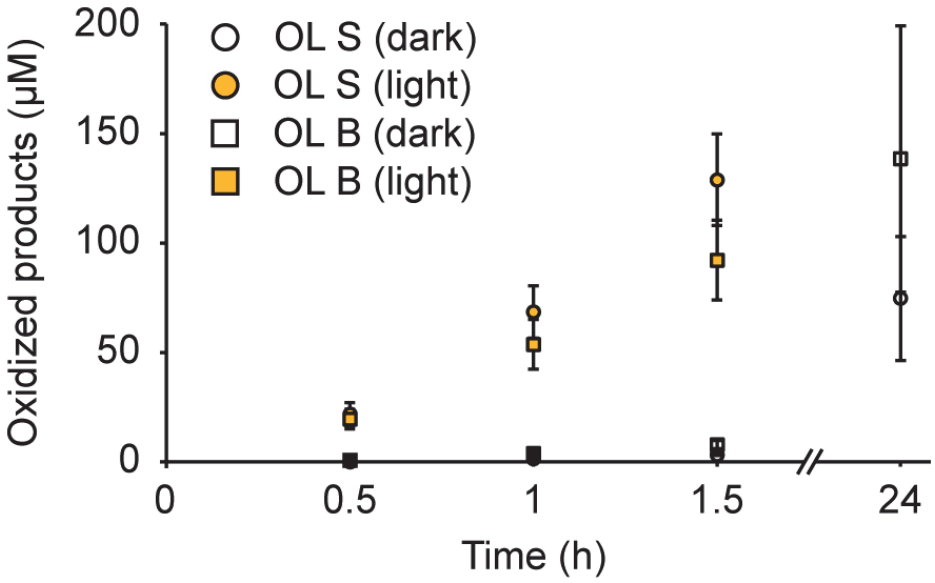

Figure 5. LPMO-catalyzed depolymerization of cellulose using organosolv lignin as photocatalyst. The graph shows time courses for the production of oxidized products in photobiocatalytic reactions containing *Sc*AA10C (500 nM), Avicel (10 $g.L^{-1}$), and organosolv lignin (OL) from spruce (S) or birch (B) (2.5 $g.L^{-1}$). All reactions were carried out in sodium phosphate buffer (50 mM, pH 6.0) at 40°C under magnetic stirring and exposed or not to visible light (I=10% I_{max}, approx. 16.8 $W.cm^{-2}$). The light-exposed reactions were incubated for 1.5 h while the dark reactions were incubated for 24 h. Before product quantification, solubilized cello-oligosaccharides were hydrolyzed with *Tf*Cel6A to convert soluble LPMO products, with varying degree of polymerization (DP), to a mixture of DP 2 and 3 [GlcGlc1A, (Glc)2Glc1A], the amounts of which were summed up to yield the concentration of oxidized sites. Error bars show ± s.d. (n = 3, independent experiments). OL was prepared as a stock suspension (25 $g.L^{-1}$) in water since DMSO and/or alcohols may act as radical scavengers and/or sacrificial electron donors, and thoroughly mixed prior to adding lignin to the reaction vials.

Light-induced structural changes of lignin

The boosting effect of light on lignin-driven LPMO-catalyzed oxidation of cellulose originates from the ability of lignin to photocatalytically reduce O_2 to $O_2^{\bullet-}$ and H_2O_2. Ring-conjugated double bonds, like those found in the cinnamyl alcohol building blocks, when they are in an end group position, β-1 stilbenes, and carbonyl moieties, including Cα-carbonyls, are known lignin structures that absorb light (Paulsson et al., 2012). Irradiating Cα-carbonyls in lignin with UV-light leads to excited state carbonyls which may abstract phenolic hydrogens to yield phenoxyl radicals, but visible light does not provide the energy needed to excite Cα-carbonyls (Neumann et al., 1989). Recently, it has been proposed that the Cα-OH moieties of β-O-4 bonds in lignin are involved in O_2 reduction to H_2O_2, resulting in the conversion of Cα-OH to Cα=O (Kim et al., 2022). Supporting this notion, Kim et al.

showed photocatalytic reduction of O_2 to H_2O_2 using a model lignin dimer, guaiacylglycerol-β-guaiacyl ether, which contains two guaiacyl units linked together via a β-O-4 bond and harbors a Cα-OH. The Cα-OH was shown to be photocatalytically oxidized to Cα=O with concomitant H_2O_2 formation, whereas the lignin monomers coniferyl alcohol and sinapyl alcohol were shown unable to photocatalytically reduce O_2 to H_2O_2 (Kim et al., 2022). However, when we employed the same lignin dimer in light-exposed LPMO reactions we did not observe H_2O_2 formation nor LPMO activity (data not shown). Thus, we searched for other modifications (oxidations) in the lignin that are promoted by light exposure.

NMR spectroscopy was used to investigate light-induced and LPMO-induced changes in the lignin structures directly. All lignins were incubated for 24 h with or without exposure to visible light (I=10% I_{max}, corresponding to approx. 16.8 $W.cm^{-2}$). For Kraft lignin, light-exposure resulted in a decrease in the signal corresponding to hydroxyl groups (Supplementary Figure 5), which could be due to generation of phenoxyl radicals (i.e., oxidation of phenolic hydroxyl groups) that radically couple with other parts of the lignin structure. More extensive analyses were done with the organosolv lignins. For organosolv lignin from both birch and spruce, the light treated sample showed an increase in cinnamaldehyde end groups (see Figure 6a&b for spruce and Supplementary Figure 6a&b for birch; more details in Supplementary Figures 7 & 8), a decrease in carbon-carbon double bonds (Supplementary Figures 7 & 8), and, in the case of spruce, a notable decrease in β-1 stilbene signals ($SB1_{\alpha}$, $SB1_2$, $SB1_6$ in Figure 6a&b). Overall, the spectra of light-exposed organosolv lignin showed a decrease in signals associated with olefins, accompanied by an increase in aldehyde signals (Supplementary Figures 7 & 8). The decrease in olefinic signals together with increase in aldehydes are consistent with light-induced oxidation of ring-conjugated olefins (Paulsson et al., 2012).

Given that *Sc*AA10C oxidizes lignin, and organosolv lignin sustained slow cellulose solubilization by *Sc*AA10C in the dark, we attempted to measure changes in the organosolv lignin structure following reactions in the dark with LPMO, in the absence or presence of Avicel. The lignin structure appeared to be unaffected by the LPMO regardless of the presence of Avicel (Figures 6c&d, supplementary Fig 6c&d). When Avicel was included the

373 presence of soluble C-1 oxidized cello-oligosaccharides (Figure 5d, supplementary Figs. 6d,
374 7 & 8) was clearly detectable, showing that the LPMO was active.

375

376 Protons of the hydroxyl groups in light-treated lignin occur at a higher chemical shift and so
377 are on average more deshielded compared to dark-incubated lignin. In contrast, addition of
378 the LPMO resulted in hydroxyl protons becoming more shielded, as shown by a lower
379 chemical shift (Supplementary Figure 9). The degree of shielding may be interpretated as the
380 degree of hydrogen bonding, as hydroxyl groups are strongly deshielded by hydrogen bonds
381 (Pretsch et al., 2009). These patterns were observed for both the spruce and the birch lignin
382 and suggest that light-driven oxidation and LPMO-catalyzed oxidation of lignin have
383 different chemical consequences. Oxidation of ring-conjugated olefins, promoted by light,
384 could lead to some depolymerization of the lignin (as also suggested by the increase in
385 cinnamaldehyde end groups), resulting in increased hydrogen bonding and deshielded
386 hydroxyl groups. On the other hand, LPMOs will oxidize hydroxyl groups (Kracher et al.,
387 2016), which could lead to radical formation and increased polymerization. Apart from the
388 shielding effect no effects of LPMO treatment on the lignin structure could be detected, which
389 is not surprising, given that a reduced LPMO can catalyze multiple peroxygenase reactions
390 and that, thus, oxidation of lignin by the LPMO may be much less frequent than the oxidations
391 that generate H_2O_2.

392

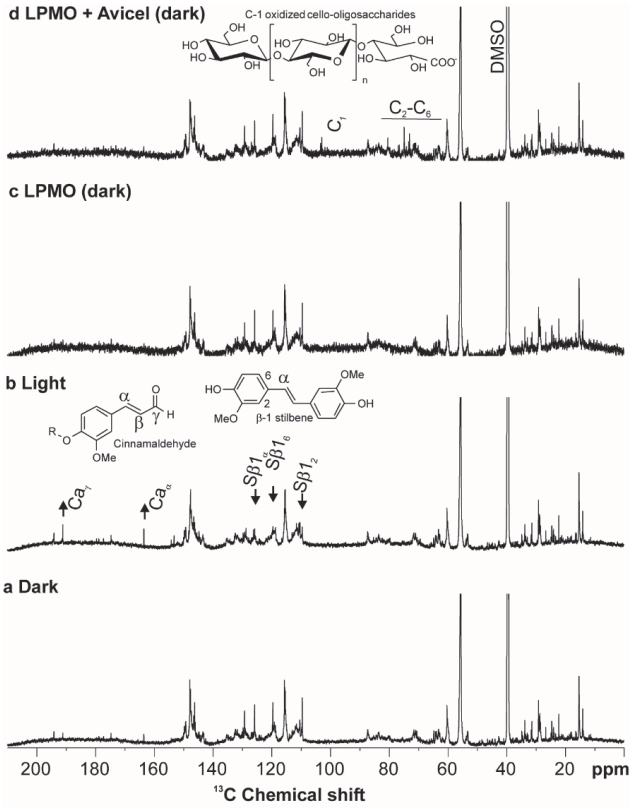

Figure 6. **Following the effect of light-induced and LPMO-induced changes in organosolv spruce lignin using 1D carbon NMR spectroscopy.** The panels show the spectra obtained for organosolv lignin from spruce (10 $g.L^{-1}$) incubated for 24 h in the dark (**a**), with light-exposure (I=10% I_{max}, corresponding to approx. 16.8 $W.cm^{-2}$) (**b**), in the dark with *Sc*AA10C (500 nM) (**c**), or in the dark with *Sc*AA10C (500 nM) and Avicel (10 $g.L^{-1}$) (**d**). All reactions were performed in sodium phosphate buffer (50 mM, pH 6.0) at 40°C with magnetic stirring. The NMR samples were prepared by dissolving 20-40 mg treated lignin in 480 µL DMSO-d_6 (99.96 atom % D) and the carbon spectrum was recorded at 25 °C on an 800 MHz instrument. Note that the reactions without LPMO contained approx. 40 mg lignin while the reactions with LPMO contained approx. 20 mg lignin. To account for the differences in lignin concentration the intensity of all spectra was adjusted to be equal for the signal at ~28 ppm. Identified chemical moieties are based on partial assignment using ^{13}C-HSQC and previous values reported in the literature. Signals from β-1 stilbene ($S\beta1_\alpha$, $S\beta1_2$ and $S\beta1_6$) (Lancefield et al., 2018), cinnamaldehyde (Ca_α and Ca_γ) (Lancefield et al., 2018; Ralph et al., 2009), and C-1 oxidized cello-oligosaccharides (C_1, C_2-C_6 where the number refers to ring carbon for the monosaccharide) (Westereng et al., 2013) are indicated. Changes in the abundance of selected chemical moieties are indicated with an up arrow for increase and a down arrow for decrease upon light treatment, and R indicates further coupling to the lignin polymer (b).

Probing for lignin-driven cellulose solubilization by ScAA10C under anaerobic conditions with light-exposure

It has been claimed, recently, that lignin may photocatalytically oxidize H_2O to H_2O_2 and O_2 (Kim et al., 2022), which would mean that irradiated lignin should be able to fuel the LPMO

reaction under anaerobic conditions. Therefore, anaerobic experiments with ScAA10C and Avicel in $H_2{}^{18}O$ were performed, using two different lignins (soluble Kraft lignin and insoluble organosolv lignin from spruce). *Sc*AA10C-catalyzed cellulose oxidation involves hydroxylation at the C1-position of the scissile glycosidic bond to form a lactone which is in equilibrium with its hydrated form, the aldonic acid. If lignin oxidizes $H_2{}^{18}O$ to $H_2{}^{18}O_2$ and $^{18}O_2$, the aldonic acid products formed by *Sc*AA10C should display an m/z shift of +4 when analyzed by MALDI-TOF MS compared to products generated in a reaction with regular $H_2{}^{16}O$. Reactions with AscA (1 mM), acting as reductant, with or without added $H_2{}^{18}O_2$ (0 or approx. 40 μM), in $H_2{}^{18}O$ and in the absence of lignin were performed as controls. The reaction containing only AscA should not lead to any product formation in true anaerobic conditions whilst the reaction containing AscA and $H_2{}^{18}O_2$ should provide a positive control for oxidized products with an m/z of +4.

Chromatographic analysis of reaction mixtures after 20 h of incubation under 'anaerobic' conditions, showed that all reactions, including the control reactions but except the reaction with added $H_2{}^{18}O_2$, had generated low levels of LPMO products. The product levels were similar in all these reactions, regardless of the reductant (AscA or lignin), indicating that O_2 was limiting. Product levels were higher in the reaction with added $H_2{}^{18}O_2$. MALDI-ToF MS analyses confirmed the formation of oxidized products and showed that only the reaction with added $H_2{}^{18}O_2$ had generated aldonic acid products with a m/z of +4 relative to products generated in standard reactions with only ^{16}O. Aldonic acid products observed in all other reactions showed a m/z shift of +2, as one would expect if the oxidant contains ^{16}O (creating a ^{16}O lactone) and the reaction is run in $H_2{}^{18}O$ (incorporating one heavy O upon hydrolysis of the lactone). Most likely traces of $^{16}O_2$ were present in the reactions, which also explains the low levels of product formed in the control reaction with AscA only. Thus, in the reaction set-ups used in the present study, neither Kraft lignin nor organosolv spruce lignin were able to catalyze water oxidation and promote anaerobic LPMO activity.

DISCUSSION

Biotic degradation of recalcitrant carbohydrates in plant litter is promoted by sunlight. This effect is believed to stem from photodegradation of lignin in secondary plant cell walls, which would increase the availability of cell wall carbohydrates for enzymatic degradation (Austin

et al., 2016, 2010, 2006; Berenstecher et al., 2020). LPMOs are key to aerobic solubilization of cellulose and other polysaccharides (Couturier et al., 2018; Hegnar et al., 2021) from plant cell walls and, in the present study, we show that the impact of light on biomass degradation may relate to the activity of these enzymes. We show that irradiation of lignin promotes lignin oxidation and formation of H_2O_2, which fuels the LPMO reaction. Notably, abiotic generation of H_2O_2 in the biomass may also promote the activity of other biomass-converting and H_2O_2-consuming enzymes, for example lignin peroxidases.

This study provides further evidence for H_2O_2-driven LPMO activity and adds to the notion that LPMOs are peroxygenases, and that the monooxygenase activity of these enzymes, if existing at all, is of minor importance, kinetically. We demonstrate that LPMO activity is improved in conditions generating higher H_2O_2 levels and is inhibited by HRP, supporting the notion that the LPMO reaction is H_2O_2-dependent. Since LPMOs are susceptible to autocatalytic inactivation (Bissaro et al., 2017; Kadić et al., 2021), as also demonstrated here, in Figure 1 and Supplementary Figure 1, regulating the amount of H_2O_2 available to the LPMO is important. The use of lignin and light not only offers a cheap an abundant source of reducing power for LPMO reactions, but could also be used to obtain better control and regulation, as previously shown for light-driven LPMO reactions with chlorophyllin (Blossom et al., 2020). It should be noted that the use of light to control LPMO activity in commercial bioreactors operating at high dry matter concentrations with for instance lignocellulose will be challenging as light is heavily attenuated in reaction slurries.

LPMO catalysis depends on reducing equivalents that are needed to bring the enzyme in its reduced, catalytically competent state. Since a once reduced LPMO can catalyze multiple peroxygenase reactions (Hedison et al., 2021; Kuusk et al., 2019; Müller et al., 2018) and since most LPMO reactions likely are limited by available H_2O_2, the amount of LPMO reduction needed to maintain optimal reaction speed is somewhat unclear but is certainly much lower than the need for in situ generation of H_2O_2. We show here that LPMOs can oxidize polymeric lignin directly to recruit electrons and do so at an appreciable rate. The rates determined in our stopped-flow experiments are one order of magnitude lower than those observed for lignin oxidation by manganese peroxidase (Ayuso-Fernández et al., 2019), between two and three orders of magnitude lower than the most efficient lignin peroxidases

(Sánchez-Ruiz et al., 2021), and two orders of magnitude lower than LPMO reduction by one of the most efficient small molecule reductants, AscA (Bissaro et al., 2020b). To the best of our knowledge, our data comprise the first evidence for the ability of an LPMO to directly interact with, and oxidize, a lignin polymer.

While photoyellowing and photobleaching of lignin are well-known phenomena (Paulsson et al., 2012), and studies on the impact of visible light on lignin model compounds and lignin combined with photoredox catalysts have been reported (Kärkäs et al., 2016; Magallanes et al., 2019), to our knowledge not much is known about the structural modifications that may occur when pure polymeric lignin is exposed to visible light (λ = 400 – 700 nm). Our NMR analysis reveals that visible light-exposure of lignin results in oxidation of ring-conjugated carbon-carbon double bonds with a concomitant increase in cinnamaldehyde groups (Figure 6, Supplementary figures 6, 7, 8, & 9). Following light-exposure the lignin hydroxyl groups experience an increase in hydrogen bonding, an effect that is opposite of what was found when the lignin was incubated in the presence of an LPMO, in the dark. This indicates that light-induced oxidation of lignin and LPMO-catalyzed lignin oxidation are distinct reactions

The present findings that LPMO and peroxidase reactions can be fueled by light-exposed lignin may have wide implications for how we understand biological processes related to biomass conversion in Nature. Lignin is abundant in plant biomass, which could make many processes involving biomass light sensitive. Interestingly, LPMO action was recently shown to be a major contributor to the infectivity of the potato pathogen *Phytophtora infestans* (Sabbadin et al., 2021) and one may wonder if infectivity is affected by light. On another note, our findings suggest that the impact of plowing on biomass conversion in agricultural soils not only relates to access to O_2 but also to access to light that promotes reduction of O_2 to H_2O_2. It would be of interest to investigate whether the interplay between light, redox-active structural components, and enzymes such as LPMOs has had an impact on the evolution of lignin-rich materials or the enzyme systems that degrade these. No matter these potential wider implications, the present study provides important insight into the complex roles of lignin and light in biomass conversion and the catalytic potential of LPMOs.

ACKNOWLEDGEMENTS

This work was financed by the Norwegian Research Council through grants 262853, 257622, 315385, 268002, 269408, and 268002, and by the European Commission through the ERC-SyG-2019 project CUBE with grant number 856446.

MATERIALS AND METHODS

Materials

The crystalline cellulose used in this study was Avicel PH-101 (50 µm particles; Sigma-Aldrich). A 10 mM stock solution of AmplexRed (Thermo Fisher Scientific) was prepared in DMSO, aliquoted, and stored at -20°C in the dark. Aliquots were thawed in the dark for 10 min before use and were used only once. Lignin stock solutions were prepared fresh in water each day in aluminum foil wrapped tubes and kept on ice. Kraft lignin, with an average molecular mass of 10 000 g/mol, was purchased from Sigma-Aldrich (Product number: 471003) and stored at room temperature in the dark. Dialyzed Kraft lignin was prepared by dialyzing approximately 25 mL of a saturated Kraft lignin solution against 5 L of ultrapure Milli-Q treated water overnight three times, using a Spectra/Por® membrane with a MWCO of 3500 Da, after which the material was freeze-dried (Supplementary Figure 10).

Organosolv lignins were obtained from spruce and birch. Debarked knife-milled wood (<2 mm) was used as feedstocks for organosolv treatments conducted in a 600 mL stirred high-pressure reactor (Parr, USA) using 50 wt % aqueous ethanol as solvent and a biomass content in the reactor of 10 wt %. The wood suspensions were kept at 190 ºC for 90 min or 120 min, for birch or spruce, respectively. After the treatment, the slurries were separated using a hydraulic press (Sotel, Portugal) and the liquid phase was vacuum filtered (Whatman filter paper no.1). Lignin precipitation was performed by diluting the organosolv hydrolysates with water (1:4, w/w). Precipitation experiments were conducted at room temperature, with magnetic stirring for 2 h. After that, the suspension was centrifuged (Sigma, Germany) for 30 min at 12000 *g*. Supernatants were discarded and lignin was dried at 45ºC for at least 48 h.

Enzymes

The model enzyme, *Sc*AA10C (UniProt Q9RJY2) from *Streptomyces coelicolor*, was recombinantly produced and purified as previously described (Forsberg et al., 2011), copper-saturated (Loose et al., 2014) and desalted using a PD MidiTrap column (G-25, GE Healthcare; (Stepnov et al., 2021)) with buffer exchange to sodium phosphate (25 mM, pH 6.0). *Sm*AA10A (UniProt O83009) was produced and purified as previously described (Vaaje-Kolstad et al., 2005b), copper-saturated similarly to *Sc*AA10C, and stored in the same buffer. Mn-dependent superoxide dismutase (Mn-SOD) from *E. coli* (Sigma-Aldrich, S5639) was solubilized in Tris-HCl (10 mM, pH 8.0) and desalted (PD MidiTrap G-25, GE Healthcare) in the same buffer before use. Horseradish peroxidase (HRP, type II) (Sigma-Aldrich, P8250) was solubilized in ultrapure Milli-Q treated water and filtered (Filtropur S, 0.2 µm PES, Sarstedt). All enzymes were stored at 4°C.

Standard photobiocatalytic LPMO reactions

Standard photobiocatalytic reactions were carried out in a cylindrical glass vial (1.1 mL) with a conical bottom (Thermo Scientific) with 500 µL reaction volume, unless otherwise specified. The light source (Lightningcure L9588, Hamamatsu) was equipped with a filter with a spectral distribution of 400 – 700 nm (L9588-03, Hamamatsu) and placed 1 cm above the liquid surface. Standard reactions contained *Sc*AA10C (0.5 µM), Avicel (10 $g.L^{-1}$), and Kraft lignin (0.9 $g.L^{-1}$) in sodium phosphate buffer (50 mM; pH 7.0), unless otherwise specified. The reactions were incubated for 15 min in the dark at 40°C under magnetic stirring prior to adding lignin and starting the reactions by turning on the light (I=10% I_{max}, equivalent to 16.8 $W.cm^{-2}$). At regular intervals, 60 µL samples were removed from the reaction mixture and filtered using a 96-well filter plate (Millipore) and a vacuum manifold to stop the LPMO reaction. The filtered samples (35 µL) were stored at -20°C prior to product quantification. A stock solution of recombinant, purified Cel6A from *Themobifida fusca* (*Tf*Cel6A; (Calza et al., 1985)) was prepared in sodium phosphate buffer (50 mM; pH 6.0) and added to the filtrate to a final concentration of 2 µM, followed by incubation overnight at room temperature, to convert solubilized oxidized products to a mixture of C1-oxidized products with a degree of polymerization of 2 and 3 (GlcGlc1A and Glc_2Glc1A).

For measuring total oxidized products (i.e., both soluble and insoluble, as in Figure 1), 50 µL samples were removed from the reaction, diluted with 50 µL H_2O and boiled for 15 min at 100°C, cooled on ice, and stored at -20°C prior to HPAEC-PAD analysis of oxidized products as described below. To prepare the samples for HPAEC-PAD analysis, 150 µL *Tf*Cel6A (5 µM final concentration) was added to 100 µL reaction suspension and the reaction was incubated in a thermomixer at 37°C and 1200 rpm for 42 h to degrade all cellulosic material

Detection and quantification of oxidized and native products

Oxidized cello-oligosaccharides were analyzed by HPAEC-PAD performed with a Dionex ICS5000 system (Dionex, Sunnyvale, CA, USA) equipped with a CarboPac PA200 analytical column (3x250 mm) as previously described (Westereng et al., 2013). Chromatograms were recorded and analyzed using Chromeleon 7.0 software. Quantitative analysis of C1-oxidizing LPMO activity was based on quantification of cellobionic acid (GlcGlc1A) and cellotrionic acid (Glc_2Glc1A), which were obtained after treating reaction filtrates with *Tf*Cel6A, as described above. Standards of GlcGlc1A and Glc_2Glc1A were prepared by treating cellobiose and cellotriose with cellobiose dehydrogenase (Zámocký et al., 2008).

Oxidized chito-oligosaccharides were qualitatively analyzed using an Agilent 1290 HPLC system with a HILIC column using UV-detection, as described elsewhere (Mekasha et al., 2020; Nakagawa et al., 2015). Chito-oligosaccharides with a degree of polymerization from 2 to 6 were treated with a chito-oligosaccharide oxidase (Heuts et al., 2008) to generate the corresponding oxidized chito-oligosaccharides (Loose et al., 2014), which were used as standards.

H_2O_2 accumulation and consumption

This method was adapted from previously published methods (Bissaro et al., 2020a; Kittl et al., 2012) and modified as explained below. H_2O_2 accumulation in the light-exposed reactions containing lignin (0.9 or 9 $g.L^{-1}$), LPMO (0, 75 or 500 nM), and Avicel (10 $g.L^{-1}$) that are depicted in Figure 1 was measured as follows: At given time points, 50 µL sample was withdrawn from the reaction and mixed with 50 µL H_2O before filtering as described above for LPMO reactions. 50 µL filtrate was recovered and diluted with water, after which 100 µL

of diluted sample was mixed with 20 µL H_2O and 80 µL of a premix composed of HRP (0.4 µM) and AmplexRed (0.4 mM) in sodium phosphate buffer (0.4 M; pH 6.0). The H_2O_2 standard curve (0, 1, 2, 5, 10 µM) was prepared by mixing 80 µL of the same HRP/AmplexRed premix with 20 µL of an aqueous lignin solution to achieve approximately the same lignin concentration as for the reaction being measured, and lastly with 100 µL H_2O_2 solution (0, 2, 4, 10, 20 µM). All reaction mixtures were prepared in a non-transparent 96-well microtiter plate. The reaction mixtures were shaken for 30 s and incubated for 5 min at 30°C prior to measuring fluorescence every 10 s for 2 min using 530/590 nm excitation/emission wavelengths in a Varioskan Lux plate reader (ThermoFisher Scientific).

H_2O_2 consumption reactions were performed using the same conditions as the reactions for H_2O_2 production and were initiated by adding H_2O_2. Samples (50 µL) were withdrawn from the reaction at given time points (5, 10, 15, 40, 80, 120 min) and diluted with water prior to filtering the reaction mixture and measuring remaining H_2O_2, as described above.

Transient state kinetics of LPMO reduction by lignin

We used the differences in intrinsic fluorescence between the Cu(II) and Cu(I) states of *Sm*AA10A or *Sc*AA10C to measure the kinetics of LPMO reduction by Kraft lignin. Single-mixing experiments were carried out with a stopped-flow rapid spectrophotometer (SFM4000, BioLogic Science Instruments, Grenoble, France) coupled to a photomultiplier with an applied voltage of 600 V for detection. The excitation wavelength was set to 280 nm, and fluorescence was collected with a 340 nm bandpass filter. Single-mixing experiments were carried out by mixing LPMO-Cu(II) (5 µM final concentration after mixing, 50 mM sodium phosphate buffer, pH 7.0) with different concentrations of lignin (ranging from 1 to 100 µM final concentrations after mixing), in triplicates. All reagents were deoxygenated using a Schlenk line with N_2 flux and subsequently prepared in sealed syringes in an anaerobic chamber. The stopped-flow rapid spectrophotometer was flushed with a large excess of anaerobic buffer before coupling the sealed syringes and performing the experiments.

Kinetics data analysis

The fluorescence data monitored with the stopped-flow was fitted to a single exponential function ($y = a + b \cdot e^{-kobs \cdot t}$) using the BioKine32 V4.74.2 software (BioLogic Science Instruments, Grenoble, France) to obtain the first order rate constant (k_{1obs}) for each lignin concentration. Plots of k_{1obs} vs lignin concentration were fitted using linear least squares regression to obtain the apparent second order rate constant of the reduction step (k_{1app}^{lignin}) with SigmaPlot v14.0.

NMR analyses

Kraft lignin (15 $g.L^{-1}$) and organosolv lignin from birch or spruce (10 $g.L^{-1}$) were incubated for 24 h in sodium phosphate (50 mM, pH 7.0 and pH 6.0, respectively) at 40°C under magnetic stirring with or without exposure to visible light (I=10% I_{max}, equivalent to 16.8 $W.cm^{-2}$). For the incubations with organosolv lignin from birch or spruce, reactions were also performed in the presence of *Sc*AA10C (500 nM) alone or *Sc*AA10C(500 nM) in combination with Avicel (10 $g.L^{-1}$) to probe for putative LPMO-induced structural changes in the lignin. The reactions containing LPMO were performed as duplicates as opposed to the reactions treated with light or not in absence of LPMO, which were performed as four replicates. After 24 h, identical reactions were pooled and freeze-dried prior to NMR analyses.

The lyophilized organosolv lignin (20-40 mg) was dissolved in 480 µL of deuterated dimethyl sulfoxide (DMSO-d_6 99.96 atom % D Sigma-Aldrich, Norway) and transferred into a 5 mm LabScape Stream NMR tube (Bruker LabScape). For NMR analyses all homo- and heteronuclear experiments were recorded on a Bruker AV-IIIHD 800 MHz spectrometer (Bruker BioSpin AG, Fälladen, Switzerland) equipped with a 5 mm cryogenic CP-TCI z-gradient probe. The spectra were recorded, processed and analyzed using TopSpin 3.6pl7 and TopSpin 4.0.7 software (Bruker BioSpin AG, Fällanden, Switzerland).

For chemical shift assignment the following one- and two-dimensional NMR experiments were recorded at 25 °C for both the birch and spruce lignin sample series: 1D carbon with power-gated decoupling and 30° flip angle (spectral width 220 ppm, spectral resolution 64k points, number of scans 4096, interscan delay 4s) , 1D proton with 30° flip angle (spectral

width 14 ppm, spectral resolution 64k points, number of scans 16, interscan delay 1s), 2D {^{1}H-^{13}C} heteronuclear single quantum coherence (HSQC) with multiplicity editing (spectral width C 200 ppm/ H 14 ppm, spectral resolution H 2k/ C 256k points, number of scans 32, interscan delay 2s).

NMR spectroscopy investigations of Kraft lignin were performed with a Bruker Avance III 400 MHz spectrometer equipped with a BBFO Plus double resonance probe head at 25 °C. 1H 1D spectra were acquired using 8 single transients and a recycle delay of 10s. 2D {^{1}H-^{13}C} HSQC spectra were acquired of all the samples. The spectra were processed by proper signal phasing and baseline correction to reduce integration errors. A line broadening factor of 1.5 Hz was applied to enhance the signal-to-noise ratio. The spectra were processed using MestreNova software v 10.0.2.

Verification of superoxide dismutase (SOD) activity

SOD activity was assessed using a published assay protocol (Bissaro et al., 2020a; Li, 2012). In alkaline conditions, autooxidation of pyrogallol leads to formation of $O_2^{\bullet-}$ which converts pyrogallol to purpurogallin, which absorbs strongly at 325 nm (Li, 2012). A stock solution of pyrogallol (15 mM in 10 mM HCl) was prepared in an aluminum foil wrapped tube and stored on ice and stock solutions of SOD were prepared in Tris-HCl (10 mM, pH 8.0) and kept on ice. All reactions were performed in 50 mM Tris-HCl pH 8.0 and were initiated by addition of pyrogallol (to 0.2 mM) immediately followed by addition of SOD (to 0, 10, 100, 1000 nM) and the absorbance at 325 nm was measured every 10 s for 3 min in a Hitachi U-1900 spectrophotometer. The inhibitory effect of SOD on pyrogallol autooxidation is shown in Supplementary Figure 11.

REFERENCES

Austin, A. T., & Ballaré, C. L. (2010). Dual role of lignin in plant litter decomposition in terrestrial ecosystems. *Proceedings of the National Academy of Sciences*, *107*(10), 4618–4622. https://doi.org/10.1073/pnas.0909396107

Austin, A. T., Méndez, M. S., & Ballaré, C. L. (2016). Photodegradation alleviates the

694 lignin bottleneck for carbon turnover in terrestrial ecosystems. *Proceedings of the*
695 *National Academy of Sciences*, *113*(16), 4392–4397.
696 https://doi.org/10.1073/pnas.1516157113

697 Austin, A. T., & Vivanco, L. (2006). Plant litter decomposition in a semi-arid ecosystem
698 controlled by photodegradation. *Nature*, *442*(7102), 555–558.
699 https://doi.org/10.1038/nature05038

700 Ayuso-Fernández, I., Rencoret, J., Gutiérrez, A., Ruiz-Dueñas, F. J., & Martínez, A. T.
701 (2019). Peroxidase evolution in white-rot fungi follows wood lignin evolution in
702 plants. *Proceedings of the National Academy of Sciences*, *116*(36), 17900–17905.
703 https://doi.org/10.1073/pnas.1905040116

704 Berenstecher, P., Vivanco, L., Pérez, L. I., Ballaré, C. L., & Austin, A. T. (2020). Sunlight
705 doubles aboveground carbon loss in a seasonally dry woodland in Patagonia. *Current*
706 *Biology*, *30*(16), 3243-3251.e3.
707 https://doi.org/https://doi.org/10.1016/j.cub.2020.06.005

708 Bissaro, B., Forsberg, Z., Ni, Y., Hollmann, F., Vaaje-Kolstad, G., & Eijsink, V. G. H.
709 (2016). Fueling biomass-degrading oxidative enzymes by light-driven water oxidation.
710 *Green Chemistry*, *18*(19), 5357–5366. https://doi.org/10.1039/C6GC01666A

711 Bissaro, B., Kommedal, E., Røhr, Å. K., & Eijsink, V. G. H. (2020a). Controlled
712 depolymerization of cellulose by light-driven lytic polysaccharide oxygenases. *Nature*
713 *Communications*, *11*(1), 890. https://doi.org/10.1038/s41467-020-14744-9

714 Bissaro, B., Røhr, Å. K., Müller, G., Chylenski, P., Skaugen, M., Forsberg, Z., Horn, S. J.,
715 Vaaje-Kolstad, G., & Eijsink, V. G. H. (2017). Oxidative cleavage of polysaccharides
716 by monocopper enzymes depends on H_2O_2. *Nature Chemical Biology*, *13*, 1123–1128.
717 http://dx.doi.org/10.1038/nchembio.2470

718 Bissaro, B., Streit, B., Isaksen, I., Eijsink, V. G. H., Beckham, G. T., DuBois, J. L., & Røhr,
719 Å. K. (2020b). Molecular mechanism of the chitinolytic peroxygenase reaction.
720 *Proceedings of the National Academy of Sciences*, *117*(3), 1504–1513.
721 https://doi.org/10.1073/pnas.1904889117

722 Bissaro, B., Várnai, A., Røhr, Å. K., & Eijsink, V. G. H. (2018). Oxidoreductases and
723 reactive oxygen species in conversion of lignocellulosic Biomass. *Microbiology and*
724 *Molecular Biology Reviews*, *82*(4), e00029-18. https://doi.org/10.1128/MMBR.00029-

Blossom, B. M., Russo, D. A., Singh, R. K., van Oort, B., Keller, M. B., Simonsen, T. I., Perzon, A., Gamon, L. F., Davies, M. J., Cannella, D., Croce, R., Jensen, P. E., Bjerrum, M. J., & Felby, C. (2020). Photobiocatalysis by a lytic polysaccharide monooxygenase using intermittent illumination. *ACS Sustainable Chemistry & Engineering*, *8*(25), 9301–9310. https://doi.org/10.1021/acssuschemeng.0c00702

Burek, B. O., Bahnemann, D. W., & Bloh, J. Z. (2019). Modeling and optimization of the photocatalytic reduction of molecular oxygen to hydrogen peroxide over titanium dioxide. *ACS Catalysis*. https://doi.org/10.1021/acscatal.8b03638

Calza, R. E., Irwin, D. C., & Wilson, D. B. (1985). Purification and characterization of two β-1,4-endoglucanases from *Thermomonospora fusca*. *Biochemistry*, *24*(26), 7797–7804. https://doi.org/10.1021/bi00347a044

Cannella, D., Möllers, K. B., Frigaard, N.-U., Jensen, P. E., Bjerrum, M. J., Johansen, K. S., & Felby, C. (2016). Light-driven oxidation of polysaccharides by photosynthetic pigments and a metalloenzyme. *Nature Communications*, *7*, 11134. http://dx.doi.org/10.1038/ncomms11134

Chalak, A., Villares, A., Moreau, C., Haon, M., Grisel, S., d'Orlando, A., Herpoël-Gimbert, I., Labourel, A., Cathala, B., & Berrin, J.-G. (2019). Influence of the carbohydrate-binding module on the activity of a fungal AA9 lytic polysaccharide monooxygenase on cellulosic substrates. *Biotechnology for Biofuels*, *12*(1), 206. https://doi.org/10.1186/s13068-019-1548-y

Chylenski, P., Bissaro, B., Sørlie, M., Røhr, Å. K., Várnai, A., Horn, S. J., & Eijsink, V. G. H. (2019). Lytic polysaccharide monooxygenases in enzymatic processing of lignocellulosic biomass. *ACS Catalysis*, *9*(6), 4970–4991. https://doi.org/10.1021/acscatal.9b00246

Couturier, M., Ladevèze, S., Sulzenbacher, G., Ciano, L., Fanuel, M., Moreau, C., Villares, A., Cathala, B., Chaspoul, F., Frandsen, K. E., Labourel, A., Herpoël-Gimbert, I., Grisel, S., Haon, M., Lenfant, N., Rogniaux, H., Ropartz, D., Davies, G. J., Rosso, M. N., … Berrin, J. G. (2018). Lytic xylan oxidases from wood-decay fungi unlock biomass degradation. *Nature Chemical Biology*, *14*(3), 306–310. https://doi.org/10.1038/nchembio.2558

Crestini, C., Lange, H., Sette, M., & Argyropoulos, D. S. (2017). On the structure of softwood kraft lignin. *Green Chemistry*, *19*(17), 4104–4121. https://doi.org/10.1039/C7GC01812F

Eibinger, M., Ganner, T., Bubner, P., Rosker, S., Kracher, D., Haltrich, D., Ludwig, R., Plank, H., & Nidetzky, B. (2014). Cellulose surface degradation by a lytic polysaccharide monooxygenase and its effect on cellulase hydrolytic efficiency. *The Journal of Biological Chemistry*, 0–22. https://doi.org/10.1074/jbc.M114.602227

Eriksson, K.-E., Pettersson, B., & Westermark, U. (1974). Oxidation: An important enzyme reaction in fungal degradation of cellulose. *FEBS Letters*, *49*(2), 282–285. https://doi.org/10.1016/0014-5793(74)80531-4

Field, C. B., Behrenfeld, M. J., Randerson, J. T., & Falkowski, P. (1998). Primary production of the biosphere: integrating terrestrial and oceanic components. *Science*, *281*(5374), 237–240. https://doi.org/10.1126/science.281.5374.237

Forsberg, Z., Vaaje-Kolstad, G., Westereng, B., Bunæs, A. C., Stenstrøm, Y., MacKenzie, A., Sørlie, M., Horn, S. J., & Eijsink, V. G. H. (2011). Cleavage of cellulose by a CBM33 protein. *Protein Science : A Publication of the Protein Society*, *20*(9), 1479–1483. https://doi.org/10.1002/pro.689

Frommhagen, M., Koetsier, M. J., Westphal, A. H., Visser, J., Hinz, S. W. A., Vincken, J.-P., van Berkel, W. J. H., Kabel, M. A., & Gruppen, H. (2016). Lytic polysaccharide monooxygenases from *Myceliophthora thermophila* C1 differ in substrate preference and reducing agent specificity. *Biotechnology for Biofuels*, *9*(186), 1–17. https://doi.org/10.1186/s13068-016-0594-y

Frommhagen, M., Westphal, A. H., van Berkel, W. J. H., & Kabel, M. A. (2018). Distinct substrate specificities and electron-donating systems of fungal lytic polysaccharide monooxygenases. *Frontiers in Microbiology*, *9*(MAY), 1–22. https://doi.org/10.3389/fmicb.2018.01080

Hangasky, J. A., Iavarone, A. T., & Marletta, M. A. (2018). Reactivity of O_2 versus H_2O_2 with polysaccharide monooxygenases. *Proceedings of the National Academy of Sciences*, *115*(19), 4915–4920. https://doi.org/10.1073/pnas.1801153115

Harris, P. V., Welner, D., McFarland, K. C., Re, E., Navarro Poulsen, J. C., Brown, K., Salbo, R., Ding, H., Vlasenko, E., Merino, S., Xu, F., Cherry, J., Larsen, S., & Lo

Leggio, L. (2010). Stimulation of lignocellulosic biomass hydrolysis by proteins of glycoside hydrolase family 61: Structure and function of a large, enigmatic family. *Biochemistry*, *49*(15), 3305–3316. https://doi.org/10.1021/bi100009p

Hedison, T. M., Breslmayr, E., Shanmugam, M., Karnpakdee, K., Heyes, D. J., Green, A. P., Ludwig, R., Scrutton, N. S., & Kracher, D. (2021). Insights into the H_2O_2-driven catalytic mechanism of fungal lytic polysaccharide monooxygenases. *The FEBS Journal*, *288*(13), 4115–4128. https://doi.org/https://doi.org/10.1111/febs.15704

Hegnar, O. A., Østby, H., Petrović, D. M., Olsson, L., Várnai, A., & Eijsink, V. G. H. (2021). Quantifying oxidation of cellulose-associated glucuronoxylan by two lytic polysaccharide monooxygenases from *Neurospora crassa*. *Applied and Environmental Microbiology*, *87*(24), e01652-21. https://doi.org/10.1128/AEM.01652-21

Hegnar, O. A., Petrovic, D. M., Bissaro, B., Alfredsen, G., Várnai, A., Eijsink, V. G. H., & Master, E. R. (2019). pH-dependent relationship between catalytic activity and hydrogen peroxide production shown via characterization of a lytic polysaccharide monooxygenase from *Gloeophyllum trabeum*. *Applied and Environmental Microbiology*, *85*(5), e02612-18. https://doi.org/10.1128/AEM.02612-18

Heuts, D. P. H. M., Winter, R. T., Damsma, G. E., Janssen, D. B., & Fraaije, M. W. (2008). The role of double covalent flavin binding in chito-oligosaccharide oxidase from Fusarium graminearum. *Biochemical Journal*, *413*(1), 175–183. https://doi.org/10.1042/BJ20071591

Hu, J., Arantes, V., Pribowo, A., Gourlay, K., & Saddler, J. N. (2014). Substrate factors that influence the synergistic interaction of AA9 and cellulases during the enzymatic hydrolysis of biomass. *Energy & Environmental Science*, *7*(7), 2308. https://doi.org/10.1039/c4ee00891j

Jones, S. M., Transue, W. J., Meier, K. K., Kelemen, B., & Solomon, E. I. (2020). Kinetic analysis of amino acid radicals formed in H_2O_2-driven Cu^I LPMO reoxidation implicates dominant homolytic reactivity. *Proceedings of the National Academy of Sciences*, *117*(22), 11916–11922. https://doi.org/10.1073/pnas.1922499117

Kadić, A., Várnai, A., Eijsink, V. G. H., Horn, S. J., & Lidén, G. (2021). In situ measurements of oxidation–reduction potential and hydrogen peroxide concentration as tools for revealing LPMO inactivation during enzymatic saccharification of

cellulose. *Biotechnology for Biofuels*, *14*(1), 46. https://doi.org/10.1186/s13068-021-01894-1

Kärkäs, M. D., Matsuura, B. S., Monos, T. M., Magallanes, G., & Stephenson, C. R. J. (2016). Transition-metal catalyzed valorization of lignin: the key to a sustainable carbon-neutral future. *Organic & Biomolecular Chemistry*, *14*(6), 1853–1914. https://doi.org/10.1039/C5OB02212F

Kim, J., Nguyen, T. V. T., Kim, Y. H., Hollmann, F., & Park, C. B. (2022). Lignin as a multifunctional photocatalyst for solar-powered biocatalytic oxyfunctionalization of C–H bonds. *Nature Synthesis*, *1*(3), 217–226. https://doi.org/10.1038/s44160-022-00035-2

Kirui, A., Zhao, W., Deligey, F., Yang, H., Kang, X., Mentink-Vigier, F., & Wang, T. (2022). Carbohydrate-aromatic interface and molecular architecture of lignocellulose. *Nature Communications*, *13*(1), 538. https://doi.org/10.1038/s41467-022-28165-3

Kittl, R., Kracher, D., Burgstaller, D., Haltrich, D., & Ludwig, R. (2012). Production of four *Neurospora crassa* lytic polysaccharide monooxygenases in *Pichia pastoris* monitored by a fluorimetric assay. *Biotechnology for Biofuels*, *5*(1), 79. https://doi.org/10.1186/1754-6834-5-79

Kont, R., Pihlajaniemi, V., Borisova, A. S., Aro, N., Marjamaa, K., Loogen, J., Büchs, J., Eijsink, V. G. H., Kruus, K., & Väljamäe, P. (2019). The liquid fraction from hydrothermal pretreatment of wheat straw provides lytic polysaccharide monooxygenases with both electrons and H_2O_2 co-substrate. *Biotechnology for Biofuels*, *12*(1), 235. https://doi.org/10.1186/s13068-019-1578-5

Koppenol, W. H., Stanbury, D. M., & Bounds, P. L. (2010). Electrode potentials of partially reduced oxygen species, from dioxygen to water. *Free Radical Biology and Medicine*, *49*(3), 317–322. https://doi.org/https://doi.org/10.1016/j.freeradbiomed.2010.04.011

Kracher, D., Scheiblbrandner, S., Felice, A. K. G., Breslmayr, E., Preims, M., Haltrich, D., Eijsink, V. G. H., & Ludwig, R. (2016). Extracellular electron transfer systems fuel cellulose oxidative degradation. *Science*, *352*(6289), 1098–1101. https://doi.org/10.1126/science.aaf3165

Kuusk, S., Bissaro, B., Kuusk, P., Forsberg, Z., Eijsink, V. G. H., Sørlie, M., & Väljamäe, P. (2018). Kinetics of H_2O_2-driven degradation of chitin by a bacterial lytic

polysaccharide monooxygenase. *Journal of Biological Chemistry*, *293*, 523–531. https://doi.org/10.1074/jbc.M117.817593

Kuusk, S., Kont, R., Kuusk, P., Heering, A., Sørlie, M., Bissaro, B., Eijsink, V. G. H., & Väljamäe, P. (2019). Kinetic insights into the role of the reductant in H_2O_2-driven degradation of chitin by a bacterial lytic polysaccharide monooxygenase. *Journal of Biological Chemistry* , *294*(5), 1516–1528. https://doi.org/10.1074/jbc.RA118.006196

Kuusk, S., & Väljamäe, P. (2021). Kinetics of H_2O2-driven catalysis by a lytic polysaccharide monooxygenase from the fungus *Trichoderma reesei*. *Journal of Biological Chemistry*, *297*(5), 101256. https://doi.org/https://doi.org/10.1016/j.jbc.2021.101256

Lancefield, C. S., Wienk, H. L. J., Boelens, R., Weckhuysen, B. M., & Bruijnincx, P. C. A. (2018). Identification of a diagnostic structural motif reveals a new reaction intermediate and condensation pathway in kraft lignin formation. *Chemical Science*, *9*(30), 6348–6360. https://doi.org/10.1039/C8SC02000K

Levasseur, A., Drula, E., Lombard, V., Coutinho, P. M., & Henrissat, B. (2013). Expansion of the enzymatic repertoire of the CAZy database to integrate auxiliary redox enzymes. *Biotechnology for Biofuels*, *6*(1), 41. https://doi.org/10.1186/1754-6834-6-41

Li, X. (2012). Improved pyrogallol autoxidation method: a reliable and cheap superoxide-scavenging assay suitable for all antioxidants. *Journal of Agricultural and Food Chemistry*, *60*(25), 6418–6424. https://doi.org/10.1021/jf204970r

Lin, Y., Karlen, S. D., Ralph, J., & King, J. Y. (2018). Short-term facilitation of microbial litter decomposition by ultraviolet radiation. *Science of The Total Environment*, *615*, 838–848. https://doi.org/https://doi.org/10.1016/j.scitotenv.2017.09.239

Loose, J. S. M., Forsberg, Z., Fraaije, M. W., Eijsink, V. G. H., & Vaaje-Kolstad, G. (2014). A rapid quantitative activity assay shows that the *Vibrio cholerae* colonization factor GbpA is an active lytic polysaccharide monooxygenase. *FEBS Letters*, *588*(18), 3435–3440. https://doi.org/10.1016/j.febslet.2014.07.036

Magallanes, G., Kärkäs, M. D., Bosque, I., Lee, S., Maldonado, S., & Stephenson, C. R. J. (2019). Selective C–O bond cleavage of lignin systems and polymers enabled by sequential palladium-catalyzed aerobic oxidation and visible-light photoredox catalysis. *ACS Catalysis*, *9*(3), 2252–2260. https://doi.org/10.1021/acscatal.8b04172

Mekasha, S., Tuveng, T. R., Askarian, F., Choudhary, S., Schmidt-Dannert, C., Niebisch, A., Modregger, J., Vaaje-Kolstad, G., & Eijsink, V. G. H. (2020). A trimodular bacterial enzyme combining hydrolytic activity with oxidative glycosidic bond cleavage efficiently degrades chitin. *Journal of Biological Chemistry*, *295*(27), 9134–9146. https://doi.org/https://doi.org/10.1074/jbc.RA120.013040

Miglbauer, E., Gryszel, M., & Głowacki, E. D. (2020). Photochemical evolution of hydrogen peroxide on lignins. *Green Chemistry*, *22*(3), 673–677. https://doi.org/10.1039/C9GC04324A

Müller, G., Chylenski, P., Bissaro, B., Eijsink, V. G. H., & Horn, S. J. (2018). The impact of hydrogen peroxide supply on LPMO activity and overall saccharification efficiency of a commercial cellulase cocktail. *Biotechnology for Biofuels*, *11*(1). https://doi.org/10.1186/s13068-018-1199-4

Muraleedharan, M. N., Zouraris, D., Karantonis, A., Topakas, E., Sandgren, M., Rova, U., Christakopoulos, P., & Karnaouri, A. (2018). Effect of lignin fractions isolated from different biomass sources on cellulose oxidation by fungal lytic polysaccharide monooxygenases. *Biotechnology for Biofuels*, *11*(1), 296. https://doi.org/10.1186/s13068-018-1294-6

Nakagawa, Y. S., Kudo, M., Loose, J. S. M., Ishikawa, T., Totani, K., Eijsink, V. G. H., & Vaaje-Kolstad, G. (2015). A small lytic polysaccharide monooxygenase from *Streptomyces griseus* targeting α- and β-chitin. *The FEBS Journal*, *282*(6), 1065–1079. https://doi.org/10.1111/febs.13203

Neumann, M. G., & Machado, A. E. H. (1989). The role of oxygen in the photodegradation of lignin in solution. *Journal of Photochemistry and Photobiology B: Biology*, *3*(4), 473–481. https://doi.org/https://doi.org/10.1016/1011-1344(89)80073-9

Paulsson, M., & Parkås, J. (2012). Light-induced yellowing of lignocellulosic pulps–mechanisms and preventive methods. *BioResources*, *7*(4), 5995–6040.

Phillips, C. M., Beeson, W. T., Cate, J. H., & Marletta, M. A. (2011). Cellobiose dehydrogenase and a copper-dependent polysaccharide monooxygenase potentiate cellulose degradation by *Neurospora crassa*. *ACS Chemical Biology*, *6*(12), 1399–1406. https://doi.org/10.1021/cb200351y

Pretsch, E., Bühlmann, P., Affolter, C., Pretsch, E., Bhuhlmann, P., & Affolter, C. (2009).

Structure determination of organic compounds (Vol. 13). Springer.

Quinlan, R. J., Sweeney, M. D., Lo Leggio, L., Otten, H., Poulsen, J.-C. N., Johansen, K. S., Krogh, K. B. R. M., Jørgensen, C. I., Tovborg, M., Anthonsen, A., Tryfona, T., Walter, C. P., Dupree, P., Xu, F., Davies, G. J., & Walton, P. H. (2011). Insights into the oxidative degradation of cellulose by a copper metalloenzyme that exploits biomass components. *Proceedings of the National Academy of Sciences of the United States of America*, *108*(37), 15079–15084. https://doi.org/10.1073/pnas.1105776108

Ralph, S. A., Ralph, J., & Landucci, L. L. (2009). *NMR Database of Lignin and Cell Wall Model Compounds*.

Reese, E. T., Siu, R. G., & Levinson, H. S. (1950). The biological degradation of soluble cellulose derivatives and its relationship to the mechanism of cellulose hydrolysis. *Journal of Bacteriology*, *59*(4), 485–497. https://doi.org/10.1128/jb.59.4.485-497.1950

Rieder, L., Petrović, D., Väljamäe, P., Eijsink, V. G. H., & Sørlie, M. (2021). Kinetic characterization of a putatively chitin-active LPMO reveals a preference for soluble substrates and absence of monooxygenase activity. *ACS Catalysis*, *11*(18), 11685–11695. https://doi.org/10.1021/acscatal.1c03344

Sabbadin, F., Urresti, S., Henrissat, B., Avrova, A. O., Welsh, L. R. J., Lindley, P. J., Csukai, M., Squires, J. N., Walton, P. H., Davies, G. J., Bruce, N. C., Whisson, S. C., & McQueen-Mason, S. J. (2021). Secreted pectin monooxygenases drive plant infection by pathogenic oomycetes. *Science*, *373*(6556), 774–779. https://doi.org/10.1126/science.abj1342

Sáez-Jiménez, V., Rencoret, J., Rodríguez-Carvajal, M. A., Gutiérrez, A., Ruiz-Dueñas, F. J., & Martínez, A. T. (2016). Role of surface tryptophan for peroxidase oxidation of nonphenolic lignin. *Biotechnology for Biofuels*, *9*(1), 198. https://doi.org/10.1186/s13068-016-0615-x

Sánchez-Ruiz, M. I., Ayuso-Fernández, I., Rencoret, J., González-Ramírez, A. M., Linde, D., Davó-Siguero, I., Romero, A., Gutiérrez, A., Martínez, A. T., & Ruiz-Dueñas, F. J. (2021). Agaricales mushroom lignin peroxidase: from structure–function to degradative capabilities. In *Antioxidants* (Vol. 10, Issue 9). https://doi.org/10.3390/antiox10091446

Schmermund, L., Jurkaš, V., Özgen, F. F., Barone, G. D., Büchsenschütz, H. C., Winkler,

C. K., Schmidt, S., Kourist, R., & Kroutil, W. (2019). Photo-biocatalysis: biotransformations in the presence of light. *ACS Catalysis*, *9*(5), 4115–4144. https://doi.org/10.1021/acscatal.9b00656

Song, B., Li, B., Wang, X., Shen, W., Park, S., Collings, C., Feng, A., Smith, S. J., Walton, J. D., & Ding, S.-Y. (2018). Real-time imaging reveals that lytic polysaccharide monooxygenase promotes cellulase activity by increasing cellulose accessibility. *Biotechnology for Biofuels*, *11*(1), 41. https://doi.org/10.1186/s13068-018-1023-1

Stepnov, A. A., Christensen, I. A., Forsberg, Z., Aachmann, F. L., Courtade, G., & Eijsink, V. G. H. (2022). The impact of reductants on the catalytic efficiency of a lytic polysaccharide monooxygenase and the special role of dehydroascorbic acid. *FEBS Letters*, *596*(1), 53–70. https://doi.org/https://doi.org/10.1002/1873-3468.14246

Stepnov, A. A., Forsberg, Z., Sørlie, M., Nguyen, G.-S., Wentzel, A., Røhr, Å. K., & Eijsink, V. G. H. (2021). Unraveling the roles of the reductant and free copper ions in LPMO kinetics. *Biotechnology for Biofuels*, *14*(1), 28. https://doi.org/10.1186/s13068-021-01879-0

Vaaje-Kolstad, G., Horn, S. J., van Aalten, D. M. F., Synstad, B., & Eijsink, V. G. H. (2005a). The non-catalytic chitin-binding protein CBP21 from *Serratia marcescens* is essential for chitin degradation. *The Journal of Biological Chemistry*, *280*(31), 28492–28497. https://doi.org/10.1074/jbc.M504468200

Vaaje-Kolstad, G., Houston, D. R., Riemen, A. H. K., Eijsink, V. G. H., & van Aalten, D. M. F. (2005b). Crystal structure and binding properties of the *Serratia marcescens* chitin-binding protein CBP21. *The Journal of Biological Chemistry*, *280*(12), 11313–11319. https://doi.org/10.1074/jbc.M407175200

Vaaje-Kolstad, G., Westereng, B., Horn, S. J., Liu, Z., Zhai, H., Sørlie, M., & Eijsink, V. G. H. (2010). An oxidative enzyme boosting the enzymatic conversion of recalcitrant polysaccharides. *Science (New York, N.Y.)*, *330*(6001), 219–222. https://doi.org/10.1126/science.1192231

van Schie, M. M. C. H., Zhang, W., Tieves, F., Choi, D. S., Park, C. B., Burek, B. O., Bloh, J. Z., Arends, I. W. C. E., Paul, C. E., Alcalde, M., & Hollmann, F. (2019). Cascading g-C_3N_4 and peroxygenases for selective oxyfunctionalization reactions. *ACS Catalysis*, *9*(8), 7409–7417. https://doi.org/10.1021/acscatal.9b01341

973 Westereng, B., Cannella, D., Wittrup Agger, J., Jørgensen, H., Larsen Andersen, M.,
974 Eijsink, V. G. H., & Felby, C. (2015). Enzymatic cellulose oxidation is linked to lignin
975 by long-range electron transfer. *Scientific Reports*, *5*(November), 18561.
976 https://doi.org/10.1038/srep18561

977 Westereng, B., Wittrup Agger, J., Horn, S. J., Vaaje-Kolstad, G., Aachmann, F. L.,
978 Stenstrøm, Y., & Eijsink, V. G. H. (2013). Efficient separation of oxidized cello-
979 oligosaccharides generated by cellulose degrading lytic polysaccharide
980 monooxygenases. *Journal of Chromatography A*, *1271*(1), 144–152.
981 https://doi.org/http://dx.doi.org/10.1016/j.chroma.2012.11.048

982 Zámocký, M., Schümann, C., Sygmund, C., O'Callaghan, J., Dobson, A. D. W., Ludwig,
983 R., Haltrich, D., & Peterbauer, C. K. (2008). Cloning, sequence analysis and
984 heterologous expression in Pichia pastoris of a gene encoding a thermostable
985 cellobiose dehydrogenase from *Myriococcum thermophilum*. *Protein Expression and*
986 *Purification*, *59*(2), 258–265. https://doi.org/https://doi.org/10.1016/j.pep.2008.02.007

987

Supplementary information

Visible light-exposed lignin facilitates cellulose solubilization by lytic polysaccharide monooxygenases

Eirik G. Kommedal[1], Camilla F. Angeltveit[1], Leesa J. Klau[2], Iván Ayuso-Fernández[1], Bjørnar Arstad[3], Simen G. Antonsen[1], Yngve Stenstrøm[1], Dag Ekeberg[1], Francisco Gírio[4], Florbela Carvalheiro[4], Svein J. Horn[1], Finn Lillelund Aachmann[2], Vincent G. H. Eijsink[1*]

[1] Faculty of Chemistry, Biotechnology and Food Science, Norwegian University of Life Sciences (NMBU), 1432 Ås, Norway

[2] Department of Biotechnology and Food Science, Norwegian University of Science and Technology (NTNU), 7491 Trondheim, Norway

[3] SINTEF Industry, Process Chemistry and Functional Materials, 0373 Oslo, Norway

[4] National Laboratory of Energy and Geology (LNEG), 1649-038 Lisboa, Portugal

[*] Corresponding author: vincent.eijsink@nmbu.no

The supplementary information includes

Supplementary Figures 1 to 11

Supplementary references

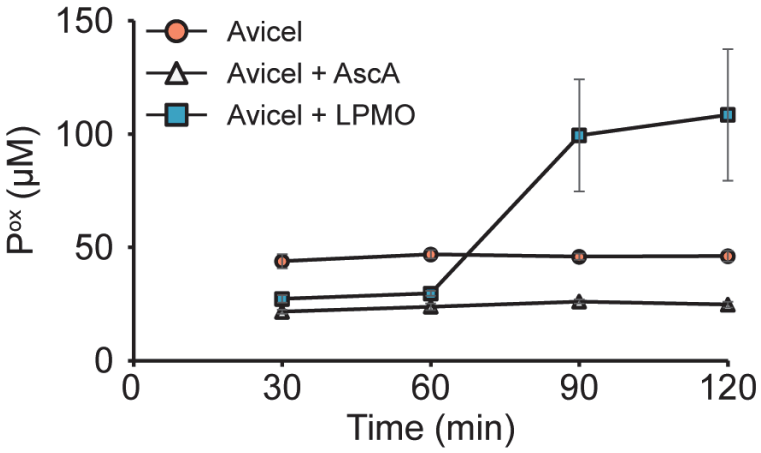

Supplementary Figure 1. Probing for LPMO inactivation. The graphs show time-courses for the release of aldonic acid products. All reactions were carried out with similar initial conditions: Avicel (10 $g.L^{-1}$), Kraft lignin (9 $g.L^{-1}$) and *Sc*AA10C (75 nM) in sodium phosphate buffer (50 mM, pH 7.0) at 40°C under magnetic stirring and exposed to visible light (I=10% I_{max}, approx. 16.8 $W.cm^{-2}$). After 60 min, Avicel (2.3 $g.L^{-1}$), Avicel (2.3 $g.L^{-1}$) and LPMO (100 nM), or Avicel (2.3 $g.L^{-1}$) and reductant (2.3 mM) were added to separate reactions, as indicated in the Figure. Upon sampling, reactions were stopped by filtration, separating the LPMO from its substrate. Before product quantification, solubilized cello-oligosaccharides were hydrolyzed with *Tf*Cel6A to convert LPMO products, with varying degree of polymerization (DP), to a mixture of DP 2 and 3 [GlcGlc1A, (Glc)2Glc1A], the amounts of which were summed up to yield the concentration of solubilized oxidized sites. Error bars show ± s.d. (n = 3, independent experiments).

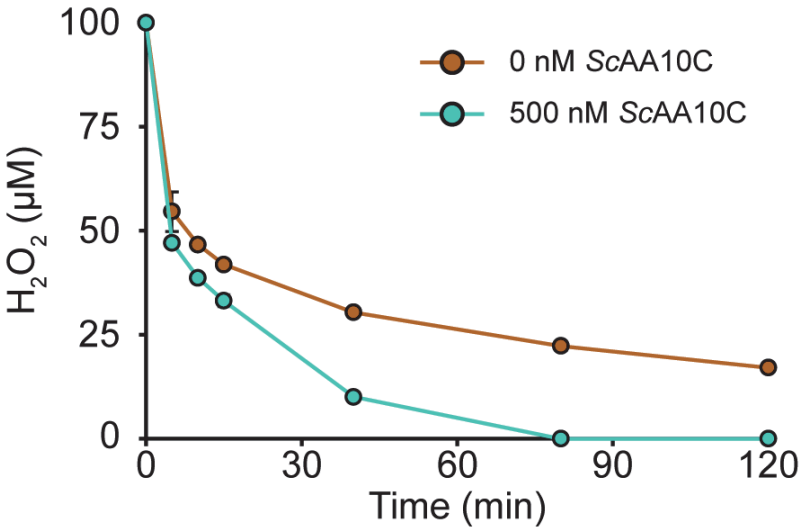

Supplementary Figure 2. Comparison of H_2O_2 consumption in standard dark reaction conditions in the presence or absence of LPMO. The graph shows time courses for consumption of H_2O_2 (added to 100 µM at t = 0) in the presence or absence of *Sc*AA10C (0.5 µM) in reactions with Avicel (10 $g.L^{-1}$) and kraft lignin (0.9 $g.L^{-1}$) in sodium phosphate buffer (50 mM, pH 7.0) at 40°C under magnetic stirring without light-exposure. The data points represent the mean of three independent experiments and error bars show ±s.d.

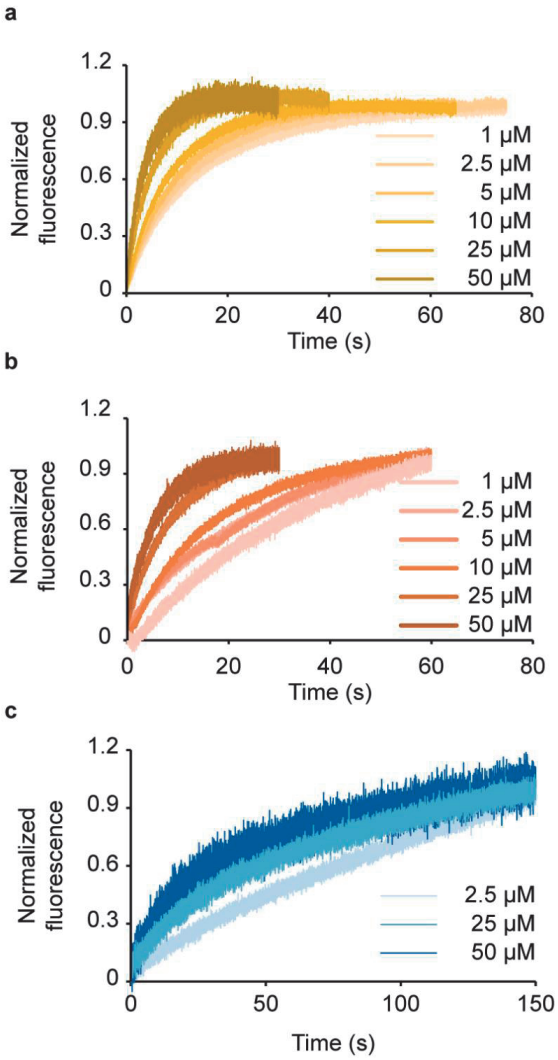

Supplementary Figure 3. Kinetic traces of lignin oxidation by bacterial LPMOs. The figure shows representative replicates for *Sm*AA10A catalyzed oxidation of native (a) and dialyzed (b) kraft lignin, and *Sc*AA10C catalyzed oxidation of dialyzed kraft lignin (c). LPMO-Cu(II) (5 µM, final concentration after mixing) was anaerobically mixed with varying concentrations of kraft lignin and the change in fluorescence following reduction of LPMO-Cu(II) to LPMO-Cu(I) was monitored over time. The fluorescence signal was normalized as $F_N = (F_{max}\text{-}F(t))/(F_{max}\text{-}F_0)$, where F_{max} and F_0 are the fluorescence of the reduced and the oxidized LPMOs, respectively. All reactions were carried out in sodium phosphate buffer (50 mM; pH 7.0) at 25°C. Each experiment was performed as triplicates and a representative replicate is shown.

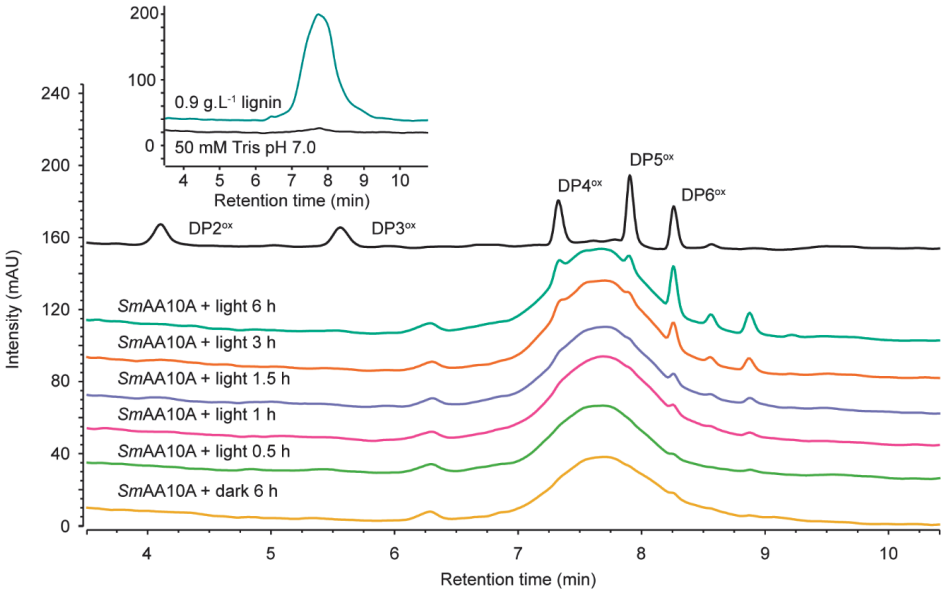

Supplementary Figure 4. Lignin-driven *Sm*AA10A activity on β-chitin. The figure shows chromatographic product profiles obtained for reactions with or without light-exposure containing kraft lignin (0.9 g.L^{-1}), β-chitin (10 g.L^{-1}), and *Sm*AA10A (0.5 µM). All reactions were performed in Tris buffer (50 mM, pH 7.0) at 40°C under magnetic stirring with or without light-exposure (I=10% I_{max}, approx. 16.8 W.cm^{-2}). All reactions were performed as three independent replicates and a representative product profile is shown. Only the final time point for the reaction with *Sm*AA10A in the dark is shown, as LPMO activity in this reaction was negligible. *Sm*AA10A activity on β-chitin was qualitatively assessed by comparing product profiles to product profile of oxidized chito-oligosaccharides with degree of polymerization ranging from 2 to 6 (DP2^{ox} - DP6^{ox}). Product formation over time is clearly visible, despite several product peaks being partially hidden by the broad peak from Kraft lignin eluting between 7 and 9 minutes as shown in the inset.…

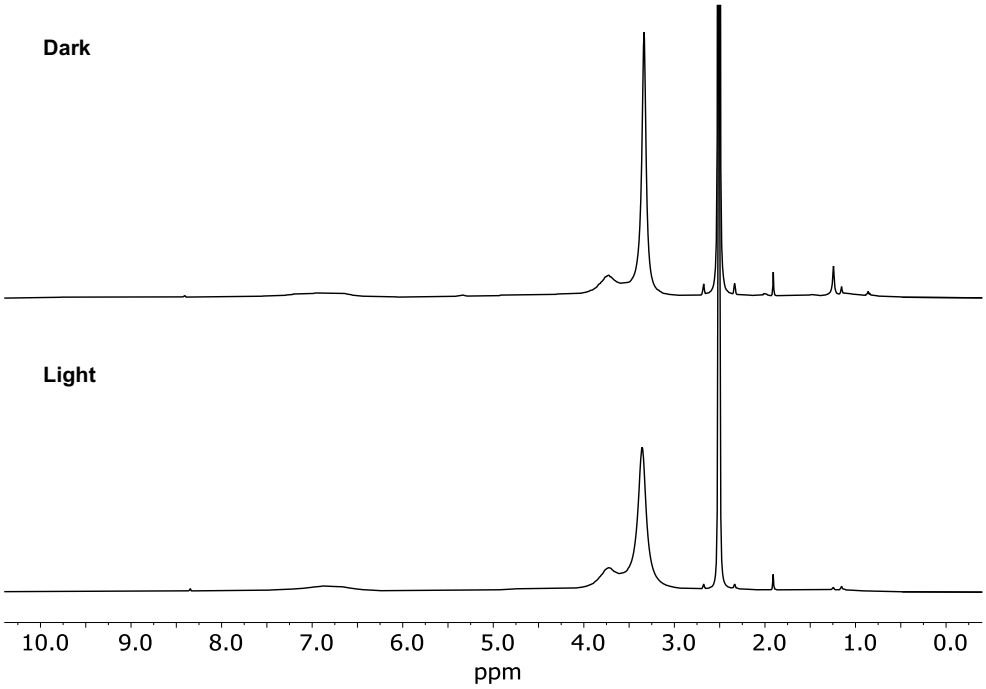

Supplementary Figure 5. Following the effect of light-induced changes on Kraft lignin using 1D proton NMR spectroscopy. The figure shows 1D proton spectra of Kraft lignin treated with light (lower spectrum) and non-treated Kraft lignin (dark, top spectrum). The spectra were recorded in DMSO-d_6 (99.96 atom % D) and normalized using the peak at 3.75 ppm. Following light-exposure, the peaks at 1.23 and 3.35 ppm are reduced compared to the reference reaction in the dark. This figure is prepared from NMR data acquired with a Bruker Avance III 400 MHz spectrometer equipped with a BBFO Plus double resonance probe head at 25 °C. The ^{1}H 1D spectra were acquired using 30-degree pulses, 8 single transients and a recycle delay of 10 s.

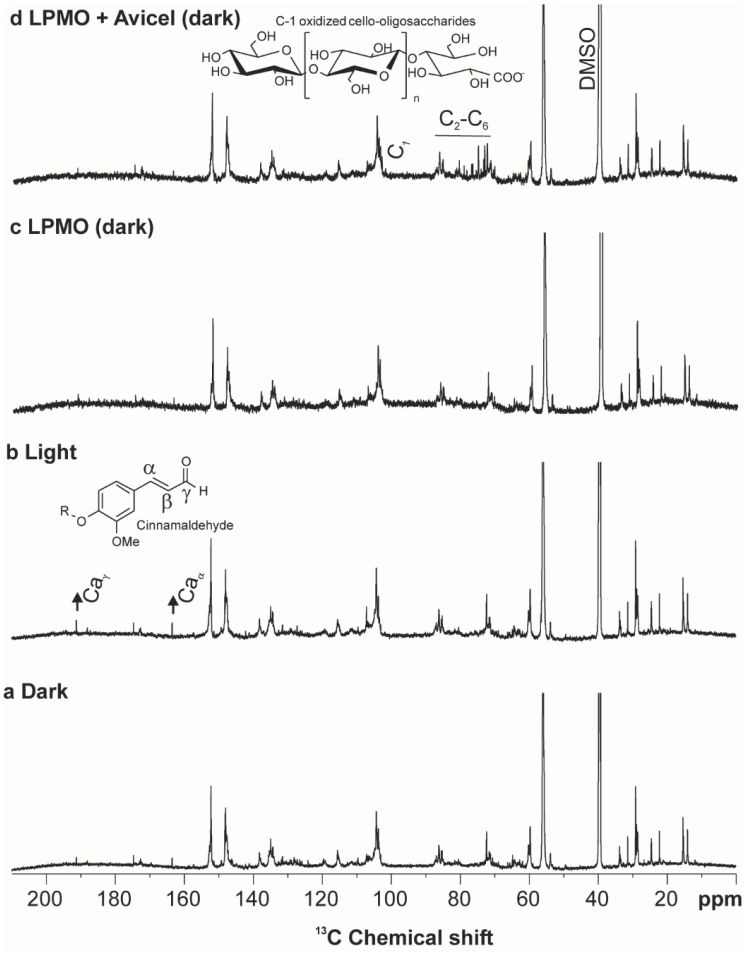

Supplementary Figure 6. Following the effect of light-induced and LPMO-induced changes in organosolv birch lignin using 1D carbon NMR spectroscopy. The panels show spectra obtained for organosolv lignin from birch (10 $g.L^{-1}$) incubated for 24 h in the dark (**a**), with light-exposure (I=10% I_{max}, corresponding to approx. 16.8 $W.cm^{-2}$) (**b**), in the dark with *Sc*AA10C (500 nM) (**c**), and in the dark with *Sc*AA10C (500 nM) and Avicel (10 $g.L^{-1}$) (**d**). All reactions were performed in sodium phosphate buffer (50 mM, pH 6.0) at 40°C with magnetic stirring. The NMR samples were prepared from dissolving 20-40 mg treated lignin in 480 µL DMSO-d_6 (99.96 atom % D) and the carbon spectra were recorded at 25 °C on an 800 MHz instrument. Note that the reactions without LPMO contained approx. 40 mg lignin while the reactions with LPMO contained approx. 20 mg lignin. To account for the differences in lignin concentration the intensity of all spectra was adjusted to be equal for the signal at ~28 ppm. Identification of chemical moieties, indicated in the spectra, is based on partial assignment using ^{13}C-HSQC and previous values reported in the literature. Signals representing the solubilised C-1 oxidized cello-oligosaccharides (C_1 [shoulder], C_2-C_6 where the number refers to the ring carbon of the monosaccharide) (Westereng et al., 2013) are indicated. R indicates further coupling to the lignin polymer (b).

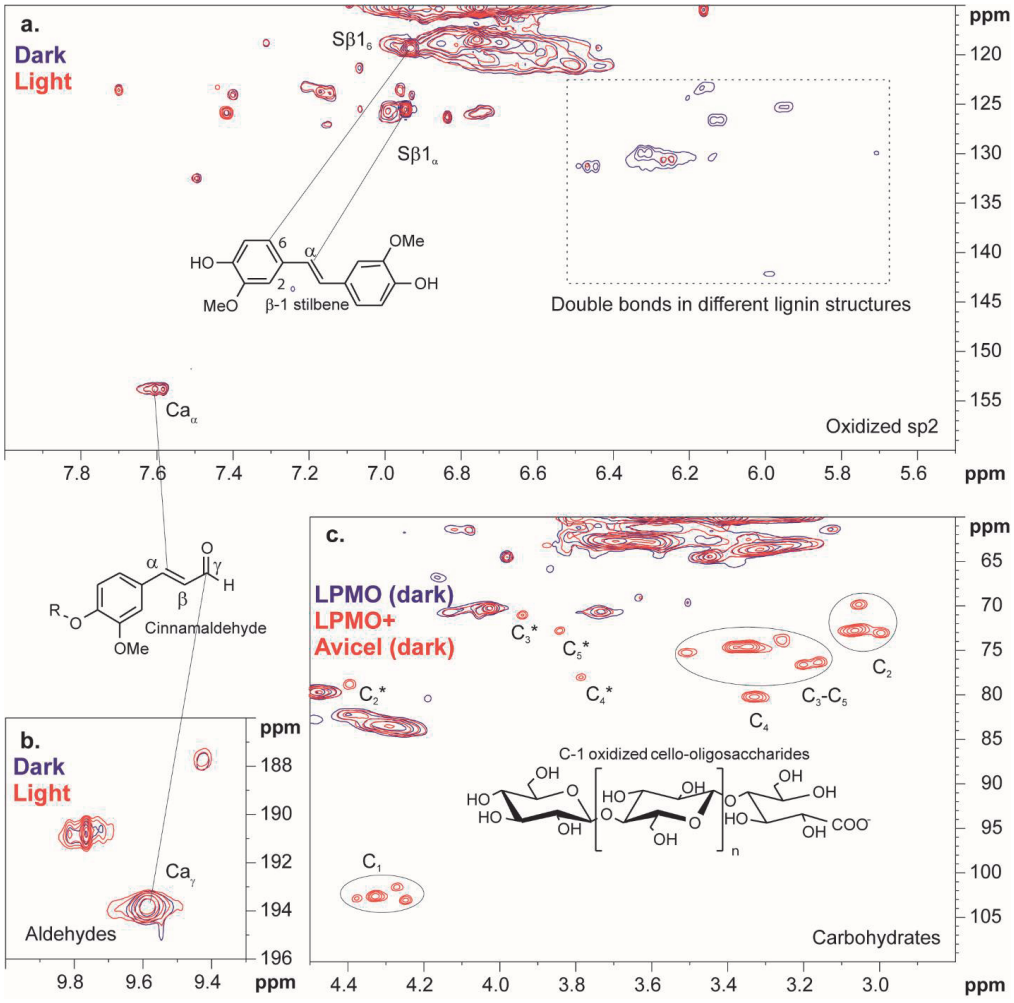

Supplementary Figure 7. **Following the effect of light-induced and LPMO-induced changes in organosolv spruce lignin using 2D HSQC NMR spectroscopy.** The figure shows comparisons between the dark-incubated lignin (purple) and light-exposed lignin (red) for the olefinic region (**a**), aldehyde region (**b**). Panel (**c**) shows the regions with signals from C-1 oxidized cello-oligosaccharides after incubation of lignin with LPMO (*Sc*AA10C, 500 nM) alone (cyan) or LPMO (*Sc*AA10C, 500 nM) and Avicel (10 g.L^{-1}) (red), in the dark. The NMR samples were prepared from dissolving 20-40 mg treated lignin in 480 µL DMSO-d_6 (99.96 atom % D) and the HSQC spectra were recorded at 25 °C on an 800 MHz instrument. Identification of chemical moieties, indicated in the spectra, is based on partial assignment using ^{13}C-HSQC and previous values reported in the literature. Signals from β-1 stilbene (Sβ1$_\alpha$, Sβ1$_2$ and Sβ1$_6$) (Lancefield et al., 2018), cinnamaldehyde (Ca$_\alpha$ and Ca$_\gamma$) (Lancefield et al., 2018; Ralph et al., 2009), and solubilised C-1 oxidized cello-oligosaccharides (C$_1$, C$_2$-C$_6$ where the number refers to the ring carbon for the monosaccharide and *indicates carbons belonging to the oxidized glucose residue (Westereng et al., 2013) are indicated. R indicates further coupling to the lignin polymer.

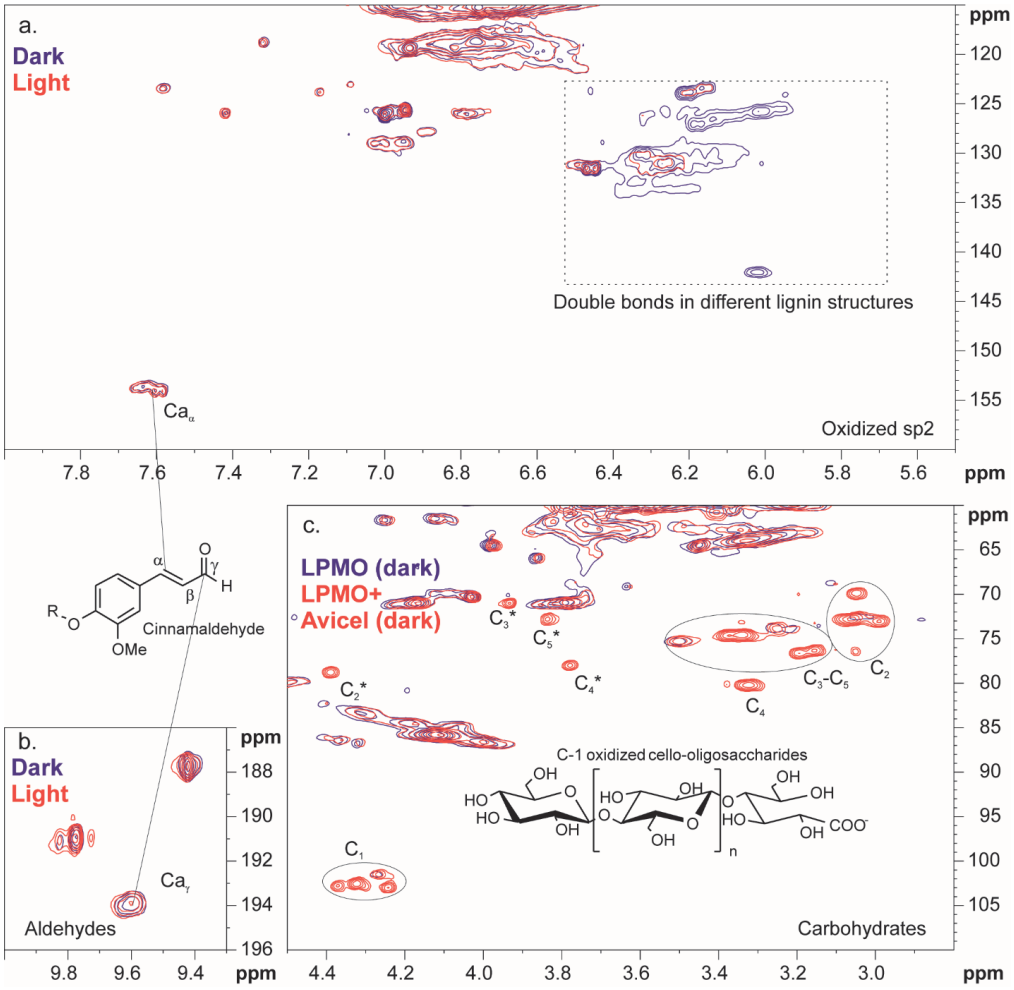

Supplementary Figure 8. **Following the effect of light-induced and LPMO-induced changes on organosolv birch lignin using 2D HSQC NMR spectroscopy.** The figure shows comparisons between the dark-incubated lignin (purple) and light-exposed lignin (red) for the olefinic region (**a**), aldehyde region (**b**). Panel (**c**) shows the regions with signals from C-1 oxidized cello-oligosaccharides after incubation of lignin with LPMO (*Sc*AA10C, 500 nM) alone (cyan) or LPMO (*Sc*AA10C, 500 nM) and Avicel (10 g.L^{-1}) (red), in the dark. The NMR samples were prepared from dissolving 20-40 mg treated lignin in 480 µL DMSO-d_6 (99.96 atom % D) and the HSQC spectra were recorded at 25 °C on an 800 MHz instrument. Identification of chemical moieties, indicated in the spectra, is based on partial assignment using ^{13}C-HSQC and previous values reported in the literature. Signals from cinnamaldehyde (Ca$_\alpha$ and Ca$_\gamma$) (Lancefield et al., 2018; Ralph et al., 2009); and solubilised C-1 oxidized cello-oligosaccharides (C_1, C_2-C_6 where the number refers to the ring carbon for the monosaccharide and *indicates carbons belonging to the oxidized glucose residue (Westereng et al., 2013) are indicated. R indicates further coupling to the lignin polymer..

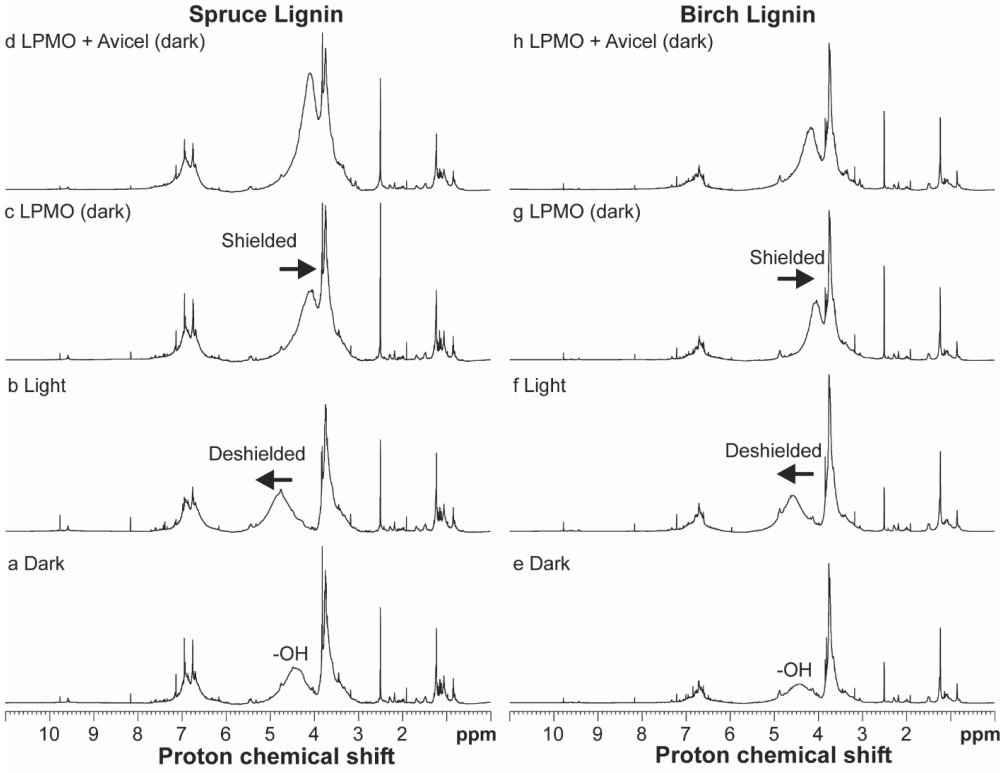

Supplementary Figure 9. Following the effect of light-induced and LPMO-induced changes in organosolv birch and spruce lignin using 1D proton NMR spectroscopy. The panels show spectra obtained for organosolv lignin from spruce (**a-d**) and birch (**e-h**). Lignin (10 $g.L^{-1}$) was either incubated for 24 h in the dark (**a, e**), with light-exposure (I=10% I_{max}, corresponding to approx. 16.8 $W.cm^{-2}$). (**b, f**), in the dark with *Sc*AA10C (500 nM) (**c, g**), or in the dark with *Sc*AA10C (500 nM) and Avicel (10 $g.L^{-1}$) (**d, h**). The broad signal associated with protons of hydroxyl groups is shifted to higher frequency (deshielded) in light incubated reactions, and to a lower frequency (shielded) in reactions containing the LPMO. All reactions were performed in sodium phosphate buffer (50 mM, pH 6.0) at 40°C with magnetic stirring. The NMR samples were prepared from dissolving 20-40 mg treated lignin in 480 µL DMSO-d_6 (99.96 atom % D) and the proton spectra were recorded at 25°C on an 800 MHz instrument. Note that the reactions without LPMO contained approx. 40 mg lignin while the reactions with LPMO contained approx. 20 mg lignin. To account for the differences in lignin concentration the intensity of all spectra was adjusted to be equal for the lowest frequency signal in the spruce or the birch spectrum.

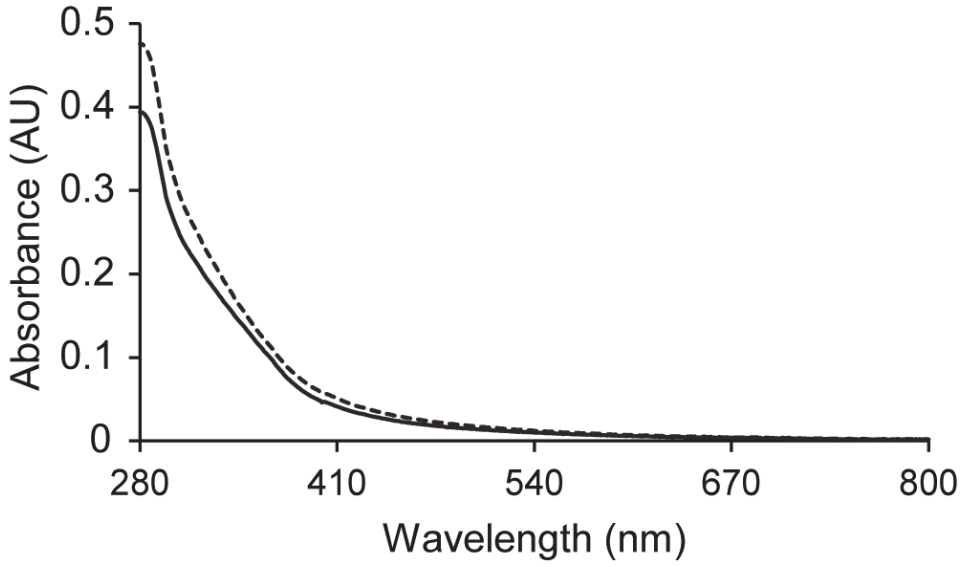

Supplementary Figure 10. UV-Vis absorption spectra of kraft lignin before and after dialysis. The figures show the absorption spectra of 0.1 $g.L^{-1}$ native (solid line) and dialyzed (dashed line) kraft lignin. The spectra were measured in triplicates and the figures show a representative spectrum for each lignin.

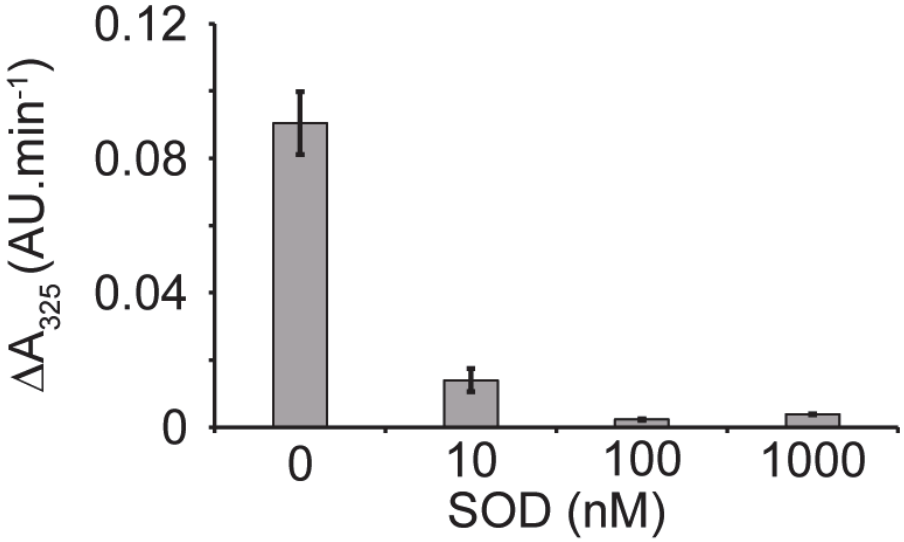

Supplementary Figure 11. Verification of Superoxide Dismutase (SOD) activity. The figure shows the change in absorbance at 325 nm during a 3-min incubation of pyrogallol leading to its autooxidation to purpurogallin, and how increasing amounts of SOD inhibit this reaction. At alkaline pH and aerobic conditions, autooxidation of pyrogallol leads to formation of superoxide radicals that drive formation of purpurogallin, and the latter can be spectrophotometrically measured at 325 nm. Adding SOD removes superoxide and inhibits formation of purpurogallin. The rate was derived using all data points from the 3-min reaction using linear regression. R^2 was > 0.98 for reactions with 0 and 10 nM SOD, while for reactions with 100 and 1000 nM SOD R^2 was > 0.7. Three independent reactions were performed for each SOD concentration and the error bars show ± s.d.

Supplementary references

Lancefield, C. S., Wienk, H. L. J., Boelens, R., Weckhuysen, B. M., & Bruijnincx, P. C. A. (2018). Identification of a diagnostic structural motif reveals a new reaction intermediate and condensation pathway in kraft lignin formation. *Chemical Science*, *9*(30), 6348–6360. https://doi.org/10.1039/C8SC02000K

Ralph, S. A., Ralph, J., & Landucci, L. L. (2009). *NMR Database of Lignin and Cell Wall Model Compounds*.

Westereng, B., Wittrup Agger, J., Horn, S. J., Vaaje-Kolstad, G., Aachmann, F. L., Stenstrøm, Y., & Eijsink, V. G. H. (2013). Efficient separation of oxidized cello-oligosaccharides generated by cellulose degrading lytic polysaccharide monooxygenases. *Journal of Chromatography A*, *1271*(1), 144–152. https://doi.org/http://dx.doi.org/10.1016/j.chroma.2012.11.048

Natural photoredox catalysts promote light-driven lytic polysaccharide monooxygenase reactions and enzymatic turnover of biomass

Kommedal EG, Sæther F, Hahn T, Eijsink VGH

Paper III

Natural photoredox catalysts promote light-driven lytic polysaccharide monooxygenase reactions and enzymatic turnover of biomass

Eirik G. Kommedal[1], Fredrikke Sæther[1], Thomas Hahn[2], Vincent G. H. Eijsink[1*]

[1] Faculty of Chemistry, Biotechnology and Food Science, Norwegian University of Life Sciences (NMBU), 1432 Ås, Norway

[2] Group Bioprocess Engineering, Fraunhofer Institute of Interfacial Engineering and Biotechnology, Nobelstraße 12, 70569 Stuttgart, Germany

*Corresponding author: Vincent G. H. Eijsink

Email: vincent.eijsink@nmbu.no

Keywords

Lytic polysaccharide monooxygenase, photobiocatalysis, photoredox catalysis, catecholamines, chitin, cellulose, biomass conversion

Abstract

Lytic polysaccharide monooxygenases (LPMOs) catalyze oxidative cleavage of crystalline polysaccharides such as cellulose and chitin, and are important for biomass conversion in the biosphere, as well as in biorefineries. The target polysaccharides of LPMOs naturally occur in co-polymeric structures, such as plant cell walls and insect cuticles, that are rich in phenolic compounds, which contribute rigidity and stiffness to these materials. Since these phenolics may be photoactive and since LPMO action depends on reducing equivalents, we hypothesized that LPMOs may enable light-driven biomass conversion. Here, we show that redox compounds naturally present in shed insect exoskeletons enable harvesting of light energy to drive LPMO reactions and, thus, biomass conversion. The primary underlying mechanism is that irradiation of exoskeletons with visible light leads to the generation of H_2O_2, which fuels LPMO

peroxygenase reactions. Experiments with a cellulose model substrate show that the impact of light depends on both light and exoskeleton dosage and that light-driven LPMO activity is inhibited by a competing H_2O_2-consuming enzyme. Degradation experiments with the chitin-rich exoskeletons themselves show that solubilization of chitin by a chitin-active LPMO is promoted by light. The fact that LPMO reactions, and, likely, reactions catalyzed by other biomass-converting redox enzymes, are fueled by light-driven abiotic reactions in Nature provides an enzyme-based explanation for the known impact of visible light on biomass conversion.

Significance Statement

Microbial decomposition of organic litter is faster above ground than below, and this effect has been attributed to sunlight-driven modification of aromatic constituents, leading to increased susceptibility of polysaccharides to enzymatic degradation. We show that such light effects may in fact be due to photobiocatalytic reactions involving polysaccharide-degrading lytic polysaccharide monooxygenases (LPMOs) and redox-active aromatic constituents of the biomass substrates, such as catecholamines in insect exoskeletons and lignin in plant material. Using insect exoskeletons, we show that light promotes abiotic generation of H_2O_2, which fuels LPMO peroxygenase reactions. Thus, we provide an enzymatic explanation for why light promotes biomass conversion and generate insight into the enzymology of LPMOs, which are widely spread in Nature and of considerable industrial importance.

Introduction

Transitioning from non-sustainable fossil feedstocks to sustainable renewable feedstocks for chemicals and energy demands efficient processes for converting renewable resources into chemicals and energy (1). Plant and insect biomass represent vast reservoirs of crystalline polysaccharides, such as cellulose and chitin, respectively, but the complex nature of plant cell walls and insect exoskeletons complicates the extraction and valorization of these carbohydrates. Cellulose-degrading and chitin-degrading microorganisms have solved this challenge by developing advanced enzymatic tools for biomass processing, with major impact on the global carbon cycle.

A key, and relatively recently discovered group of enzymes used for biomass conversion comprises the lytic polysaccharide monooxygenases (LPMOs) (2–4), which are mono-copper enzymes (5, 6) that oxidatively cleave glycosidic bonds in chitin (4) and cellulose (5, 7). LPMOs are widespread in terrestrial eco-systems and are classified in the auxiliary activity (AA) families 9-11 and 13-17 of the Carbohydrate Active enZymes (CAZy) database (8). At the time of discovery, LPMOs were considered to be monooxygenases, but recent work has shown that H_2O_2 is a kinetically relevant co-substrate that allows fast peroxygenase reactions (9–17). LPMOs are ubiquitous enzymes that play an important role in fungal and bacterial biomass conversion by introducing chain breaks in the crystalline surfaces of chitin or cellulose. By doing so, LPMOs enhance the depolymerization activity of glycoside hydrolases in Nature as well as in commercial enzyme cocktails used at industrial scale. Importantly, the discovery of LPMOs has revealed that redox processes are important for polysaccharide conversion in the biosphere, as suggested some 50 years ago (18), raising new insights and questions regarding the interplay between the many components of natural biomass-converting enzyme systems (19).

LPMO catalysis requires two reducing equivalents per catalytic cycle, which, depending on the catalytic mechanism considered, are delivered to the copper site (monooxygenase reaction) or used to convert O_2 to H_2O_2 to enable a peroxygenase reaction (20) (Fig. 1). It is currently being debated whether apparent monooxygenase reactions, which typically entail incubating the LPMO with substrate and a reductant under aerobic conditions, are true monooxygenase reactions or whether these are peroxygenase reactions that are limited by *in situ* generation of H_2O_2. H_2O_2-driven LPMO catalysis is a double-edged sword, as too much H_2O_2 leads to inactivation of the LPMO through non-productive turnover accompanied by oxidative damage to the enzyme (9, 21), while too low access to H_2O_2 leads to low enzyme activity.

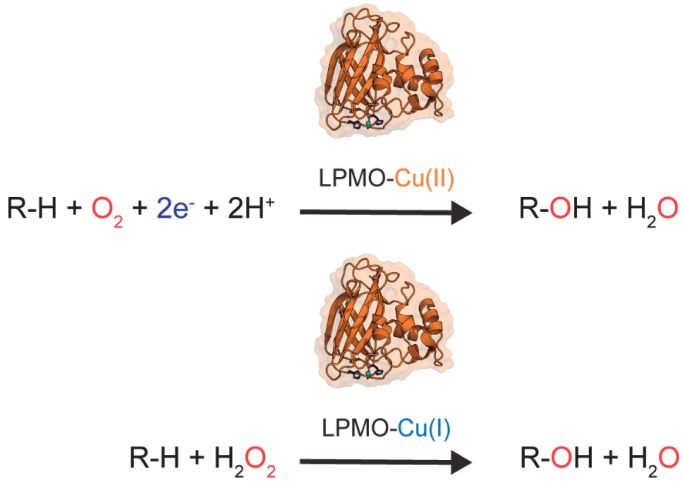

Fig. 1. Possible reaction schemes for LPMOs. In the upper monooxygenase reaction, every catalytic cycle requires channeling of two electrons and two protons to the catalytic center. In the lower peroxygenase reaction, a once reduced ("primed") LPMO can catalyze multiple reactions using H_2O_2 as co-substrate, without any further delivery of protons or electrons (9, 12). Occasionally, LPMOs may become oxidized through off-pathway reactions (14, 21) and re-reduction is then required to regain catalytic competence.

Insect cuticles and plant cell walls, which are major components of organic litter in Nature (22), are complex and rigid co-polymeric structures, which next to chitin and cellulose, respectively, contain light-sensitive aromatic compounds with quinone/hydroquinone redox active moieties. The impact of LPMOs on polysaccharide conversion and the notion that these enzymes act on "redox-active" co-polymeric substrates, raise the issue whether and how light affects LPMO activity and, thus, biomass turnover. Light is an abundant and cheap source of energy that, in the presence of a photoredox catalyst and O_2, can fuel H_2O_2-dependent enzyme reactions (23–25). It has been demonstrated that lignin, a major aromatic component of plant cell walls, can act as photocatalyst for solar-powered H_2O_2-dependent enzyme reactions (26). Photobiocatalytic LPMO reactions were first demonstrated in 2016 for a fungal LPMO acting on amorphous cellulose (PASC) by combining a photosynthetic pigment, chlorophyllin, and a reductant, AscA (27). Later the same year, it was shown that vanadium-doped titanium dioxide (V-TiO_2) allowed light-driven activity of a bacterial LPMO from *Streptomyces coelicolor* (*Sc*AA10C) on crystalline cellulose (Avicel) (28). Both studies discussed the underlying mechanisms for photobiocatalytic LPMO activity but did not consider peroxygenase activity. Later, it was shown that

light-induced formation of H_2O_2 from O_2 was the main driver of these photobiocatalytic LPMO reactions (24).

Shed chitin-rich exoskeletons resulting from insect moulting, collectively referred to as insect (pupal) exuviae, consist of a complex matrix of chitin, proteins, and potentially photosensitive phenolic compounds, in particular catecholamines (29). The latter are incorporated during sclerotization to provide stiffness, hardness, and resistance towards the environment, and are responsible for the dark colour of the exuviae (30). Considering the above, we hypothesized that the catecholamines present in pupal exuviae may act as a photoredox catalyst for *in situ* generation of H_2O_2, which could be used to fuel LPMO-catalyzed turnover of insect biomass in Nature.

To test this hypothesis, we first carried out a detailed study of the degradation of a model cellulose substrate by a well-studied LPMO from the soil actinomycete *Streptomyces coelicolor*, *Sc*AA10C, using light-exposed pupal exuviae for fueling the reaction. We show that exposure to light has a large effect on LPMO activity that correlates with light-fueled generation of H_2O_2. Subsequent studies of the depolymerization of chitin in the pupal exuviae themselves with a chitin-active LPMO (*Sm*AA10A) showed that visible light-exposure has a similar effect on this LPMO and promotes turnover of insect biomass. Thus, our study provides a possible mechanistic framework for the effect of light on biomass turnover in the biosphere.

Results

Proof of concept – fueling LPMO reactions with insect exoskeletons (pupal exuviae) as photocatalyst

To assess the ability of insect biomass to fuel LPMO reactions we used a well-studied C1-oxidizing cellulose-active LPMO from *Streptomyces coelicolor* (*Sc*AA10C, also known as CelS2) and Avicel (i.e., crystalline cellulose). A reaction in the dark with gallic acid, a commonly used reductant in standard LPMO reactions, was included as a reference reaction. The pupal exuviae contain 20% (w/w) chitin and 12.6% (w/w)

phenolic compounds (31). Washing the pupal exuviae removed soluble compounds absorbing in the 240 nm to 800 nm range (Fig. S1) and reduced the total reducing capacity by 72% as measured by the Folin-Ciocalteu assay (32) using gallic acid as a standard (Fig. S2).

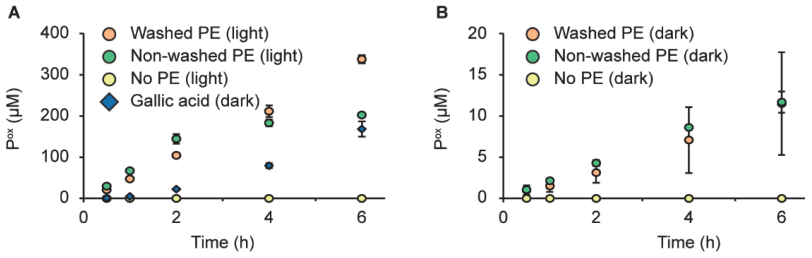

Fig. 2. *Sc*AA10C catalyzed cellulose oxidation fueled by photocatalytic insect exoskeletons. The graphs show time courses for the formation of solubilized oxidized products by *Sc*AA10C (0.5 µM) in reactions with Avicel (10 $g.L^{-1}$) in sodium phosphate buffer (50 mM, pH 6.0) at 40 °C under magnetic stirring with (A) and without (B) irradiation by visible light (note the different scaling of the Y-axes). The reactions contained washed or unwashed pupal exuviae (5 $g.L^{-1}$) or gallic acid (1 mM). Based on determination of total reducing equivalents (Fig. S2), 5 $g.L^{-1}$ corresponds to approx. 0.2 and 0.6 mM gallic acid equivalents for the washed and unwashed material, respectively. Reactions were incubated with magnetic stirring in the dark or exposed to white light (I=10% I_{max}, approx. 16.8 $W.cm^{-2}$). Before product quantification, solubilized oxidized cello-oligosaccharides were converted to a mixture of cellobionic acid and cellotrionic acid by incubation with *Tf*Cel6A at room temperature overnight. The data points represent the mean of three independent experiments and error bars show ± s.d. The high standard deviations in panel B are due to product levels being very low.

Progress curves for Avicel conversion (Fig. 2) showed linear product formation over 6 h for all reactions, except for the reactions lacking pupal exuviae or gallic acid, which did not show any LPMO activity, and the light-exposed reaction with non-washed pupal exuviae, which showed a high initial LPMO rate that started decreasing after approximately 2 h. The reactions with washed or non-washed pupal exuviae in the dark produced identical very low product levels during the 6 h incubation period and apparent reaction rates were more than one order of magnitude lower compared to the reactions exposed to visible light (Fig. 2). Reactions in which the LPMO was replaced by an equal concentration of $CuSO_4$ did not show formation of oxidized products (Fig. S3).

Compared to the reference reaction with 1 mM gallic acid, the reaction with light-exposed washed pupal exuviae was about two times faster and produced two times more product over 6 h, despite the fact that the concentration of gallic acid equivalents in the reaction with exuviae equaled only some 0.2 mM (Fig. S2). The large impact of light is further evidenced by the observation that the reactions with pupal exuviae in the dark were an order of magnitude slower than the reaction with gallic acid, for both the washed (0.2 mM GA equivalents) and the non-washed (0.6 mM GA equivalents) materials (Fig. 2).

While the redox state of the catecholamines that are incorporated into the cuticular matrix is not known (33), it is likely that their hydroquinone/quinone moieties are photoredox active in aqueous solutions, as exemplified by the role of plastoquinone in photosynthetic water splitting in photosystem II (34). As other examples, under aerobic conditions UV light will convert hydroquinone to benzoquinone, hydroxybenzoquinone, and H_2O_2 (35), whereas irradiation using 416 nm at pH 6.0 brings benzoquinone in a reactive triplet excited state leading to the production the semiquinone radicals, $Q^{-\bullet}$ and $QH^{\bullet}$ (36). Regardless of light intensity and wavelength, the primary photochemical process for benzoquinone is reduction (37). Upon light exposure the catecholamines in insect cuticles may undergo reactions similar to those known for other hydroquinones and quinones to generate both the reducing conditions needed for the LPMO to become catalytically active, and the H_2O_2 needed to oxidize the polysaccharide substrate. The results depicted in Fig. 2 show that this indeed is the case. It is worth noting that the reaction with unwashed exuviae in the light shows a progress curve that is typical for LPMO reactions that contain too much H_2O_2 (16, 24, 38): the (too) high availability of the co-substrate leads to a high catalytic rate but also to rapid enzyme inactivation.

To verify whether the low activity in reactions with exuviae in the dark was due to lack of H_2O_2 generation, a control experiment was performed with 5 g/L washed pupal exuviae in which 50 µM H_2O_2 was added after 0, 30, 60 min and the reaction was

sampled at 30, 60 and 90 minutes (before addition of H_2O_2). It is well known from earlier work with *Sc*AA10C that addition of this amount of H_2O_2 gives a fast reaction, provided that the reaction contains sufficient reducing power to bring the LPMO in its catalytically competent reduced state (9, 28). Fig. S4 shows that the dark reaction with exuviae was not boosted by the addition of H_2O_2, suggesting that both reduction of the LPMO and H_2O_2 availability were limiting LPMO activity in the dark, which is not surprising considering that the reduction potential of a catecholamine model compound does not favor reduction of *Sc*AA10C (39).

Characterization of the photobiocatalytic system

Encouraged by the successful proof-of-concept experiments, the influence of the pupal exuviae concentration, light intensity, and substrate concentration on LPMO activity was investigated (Fig. 3). We also monitored H_2O_2 accumulation to unravel possible correlations between LPMO activity and H_2O_2 production.

Increasing the PE concentration from 1.25 to 20 g/L led to a three-fold increase in the apparent rate for the LPMO reaction (Figs. 3A&C), from 0.5 $\mu M.min^{-1}$ at 1.25 g/L to 1.5 $\mu M.min^{-1}$ at 20 g/L (Fig. 3C), as well as a near six-fold increase in the apparent rate of H_2O_2 generation, from 0.12 $\mu M.min^{-1}$ at 1.25 g/L to 0.75 $\mu M.min^{-1}$ at 20 g/L (Figs. 3B&C). Conducting reactions with increasing light intensities showed a clear dose-response effect and resulted in a two order of magnitude increase in the apparent rate of the LPMO reaction, from 0.02 $\mu M.min^{-1}$ in the dark to 2.2 $\mu M.min^{-1}$ for the highest light intensity applied (Figs. 3D&F). H_2O_2 production also increased at higher light intensities (Fig. 3E) and the apparent rate of H_2O_2 formation showed a linear correlation with the light intensity (Fig. 3F). Cellulose particles present in the reaction vessel reduce light transmittance (38) and, indeed, higher Avicel concentrations led to lower LPMO activity (Fig. 3G) and lower H_2O_2 production (Fig. 3H). It is noteworthy that the reaction in absence of Avicel produced most H_2O_2. Taken together, these results show that the combination of PE and light provides a tunable system for driving LPMO reactions and that LPMO activity is correlated to the ability of the system to produce H_2O_2.

The reactions with LPMO generally showed higher product formation than what can be accounted for by H_2O_2 accumulation in identical reactions in the absence of LPMO (Fig. 3). The H_2O_2 concentration measured in the LPMO-free reactions is the net result of formation and decomposition reactions that both will be affected by redox-active components in PE and by light. It has been shown that, in the presence of substrate, reduced LPMOs have high affinity for H_2O_2 (K_m values in the low micromolar range; (15, 16, 21). Thus, it is conceivable that in the reaction with LPMO, H_2O_2 consumption in productive reactions with the enzyme outcompetes abiotic decomposition, which could help explain the product levels. Furthermore, reduction of the LPMO by light-exposed PE may speed up H_2O_2 production in two ways: (1) the resulting modification of the PE may yield compounds that more readily catalyze abiotic H_2O_2 production, (2) the reduced LPMO may catalyze oxidase reactions yielding H_2O_2 (40).

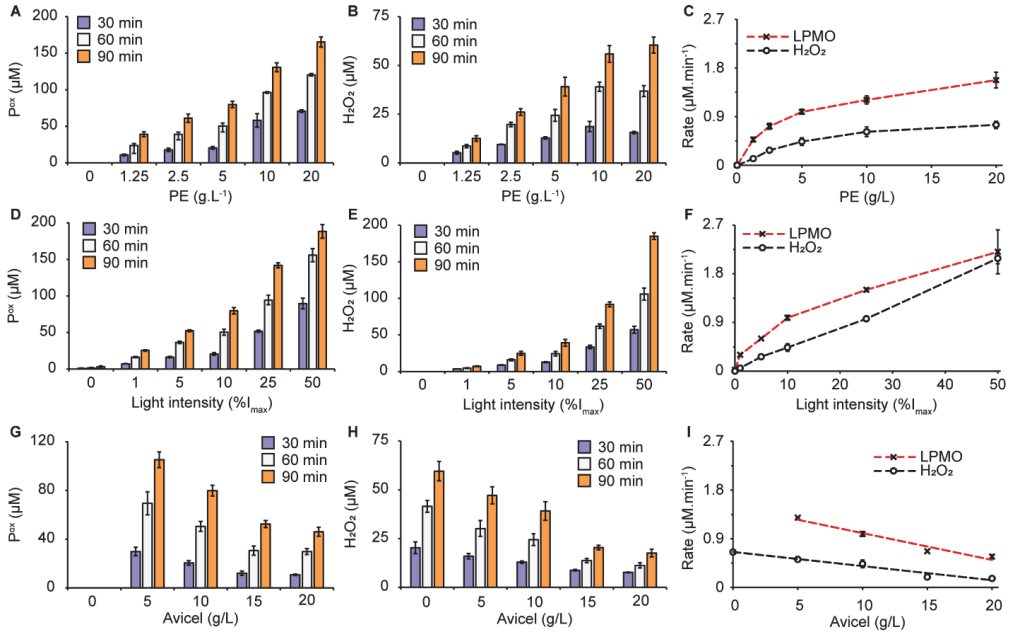

Fig. 3. Influence of PE loading, light intensity, and cellulose concentration on LPMO activity and H_2O_2 production. The graphs show time courses for the formation of solubilized oxidized products in LPMO (*Sc*AA10C, 0.5 uM) reactions with Avicel and exposed to light, at varying PE concentration (10 g.L^{-1} Avicel, I = 10% I_{max}, approx. 16.8 W.cm^{-2}) (**A**), light intensity (5 g.L^{-1} PE, 10 g.L^{-1} Avicel) (**D**), and

Avicel concentration (5 g.L^{-1} PE; I = 10% I_{max}, approx. 16.8 W.cm^{-2}) (**G**). Panels **B, E** and **H** show H_2O_2 accumulation in equivalent reactions lacking the LPMO. The approximate rates obtained for LPMO activity and H_2O_2 accumulation were derived from the three shown time points for all reactions except the LPMO reaction with the highest light intensity (i.e. I = 50% I_{max}), for which only the first two time points were used. All regression analyses displayed an R^2>0.98. The approximate rates for LPMO activity and H_2O_2 accumulation are plotted against the variable parameter in panels **C**, **F**, and **I**. Before product quantification, solubilized cello-oligosaccharides were converted to a mixture of cellobionic acid and cellotrionic acid by overnight treatment with *Tf*Cel6A at room temperature. The data points represent the mean of three independent experiments and error bars show ± s.d. Note that for the dark reaction in panels **D&F**, the final time point was 120 min and not 90 min, and that this is the same reaction as the reaction shown in Fig. 2.

Considering the observations indicating that access to H_2O_2 was limiting the reactions displayed in Fig. 3, and the possible involvement of the LPMO itself in H_2O_2 production, we then assessed whether the amount of LPMO could be limiting the standard reaction with Avicel (10 g.L^{-1}) and PE (5 g.L^{-1}). While the reaction with lowest LPMO concentration (100 nM) showed diminished product formation and cessation of the reaction after about 1 h, product formation in the reactions containing 250 – 2500 nM LPMO was linear over the 3 h incubation period and essentially independent of the LPMO concentration (Figs. 4A&B). Thus, the LPMO concentration does not appear to be a limiting factor in the standard reaction conditions used in this study, further strengthening the idea that light-driven H_2O_2-formation determines LPMO activity.

To further demonstrate that it is the H_2O_2 generated from visible light-irradiated pupal exuviae that drives the LPMO reaction, experiments were conducted with non-washed pupal exuviae and increasing amounts of horseradish peroxidase (HRP). Here, non-washed pupal exuviae were used because the soluble phenolic compounds provide substrates for the peroxidase. Addition of increasing amounts of HRP resulted in increasing inhibition of the LPMO reaction (Fig. 4C). Approximately 11.4 nM HRP was required to achieve 50% inhibition of LPMO activity and plotting the LPMO catalytic rates against the HRP concentration gave a reversed hyperbolic curve showing more than 95% inhibition of LPMO activity with 720 nM HRP (Fig. 4D). These experiments confirm the notion, derived from the above experiments, that H_2O_2 formation by irradiated PE is what drives the LPMO reaction.

Previous light-driven reaction with *Sc*AA10C have been performed using either chlorophyllin or V-TiO_2 as photocatalysts (24). In the case of reactions with chlorophyllin, $O_2^{\bullet-}$ production was demonstrated by showing that superoxide dismutase (SOD), which converts $O_2^{\bullet-}$ to H_2O_2, boosts LPMO activity (24). Later studies have since confirmed $O_2^{\bullet-}$ production by chlorophyllin (41). On the other hand, such a boosting effect of SOD was not observed for LPMO reactions with V-TiO_2, leading to the conclusion that $O_2^{\bullet-}$ is likely not generated in this latter reaction system (24). Addition of SOD to a standard reaction with PE (5 $g.L^{-1}$), Avicel (10 $g.L^{-1}$) and *Sc*AA10C (0.5 μM) did not affect LPMO activity (Fig. 4E). A control reaction with boiled SOD showed identical product levels compared to the reactions with SOD, underpinning that SOD does not affect the reaction (Fig. 4E). Additional experiments with increasing PE concentrations also did not reveal any effect of SOD (Fig. 4F).

The results depicted in Figs. 4E&F indicate that superoxide does not play a role in this photocatalytic system, and that, thus, H_2O_2 is produced directly by reduction of O_2 to H_2O_2 ($O_2 + 2H^+ + 2e^- \rightarrow H_2O_2$) or, perhaps, oxidation of H_2O to H_2O_2 ($2H_2O \rightarrow H_2O_2 + 2H^+ + 2e^-$), as has recently been shown for photoexcited lignin (26). Of note, for the chlorophyllin studies, superoxide was proposed to also act a reductant for the LPMOs. In the photoredox system studied here the LPMO is likely reduced by the photoredox active compounds present in the insect exuviae, primarily upon light-exposure and possibly via formation of a semiquinone radical (36).

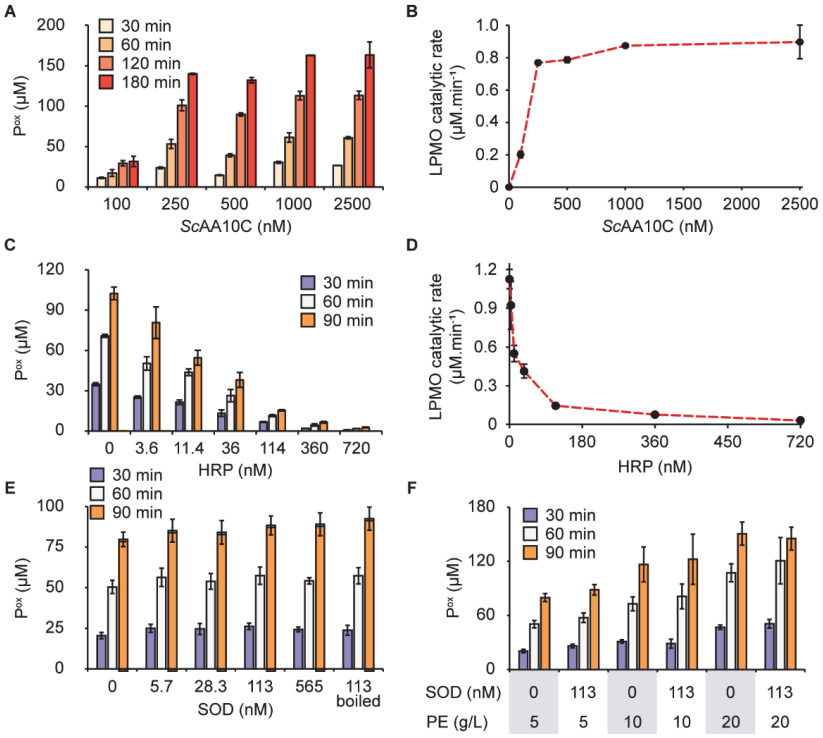

Fig. 4. Probing the role of reactive oxygen species in light-driven LPMO catalysis. The graphs show progress curves for the release of oxidized products from Avicel (10 g.L^{-1}) by *Sc*AA10C in the presence of varying amounts of (A) *Sc*AA10C, (C) horseradish peroxidase (with 0.5 mM LPMO), or (E,F) superoxide dismutase (with 0.5 mM LPMO). All reactions were carried out in sodium phosphate buffer (50 mM, pH 6.0) containing 5 g.L^{-1} PE (unless indicated otherwise), at 40°C under magnetic stirring and exposed to visible light (I=10% I_{max}, approx. 16.8 W.cm^{-2}). Panel F shows data for reactions done with varying PE concentrations. The rates depicted in panels B and D were derived from the reactions in panels A and C using linear regression analysis (all time points, except for the reaction with 100 nM LPMO in panel A for which only the first three time points were used; $R^2 > 0.98$ in all cases). Before product quantification, solubilized cello-oligosaccharides were converted to a mixture of cellobionic acid and cellotrionic acid by treatment with *Tf*Cel6A at room temperature overnight. The reactions were performed as duplicate (A**)** and triplicate reactions (C, E, F) and error bars indicate standard deviations. For the reactions in A, the difference was less than 10% between replicates for all time points except for the last time point with 2500 nM *Sc*AA10C where the difference was 16%. The data points for the reaction without SOD (i.e. 0 nM SOD) in panels E and F are derived from the reaction with PE (5 g.L^{-1}) and Avicel (10 g.L^{-1}) that is displayed in panels A, D, G in Fig. 3.

Light-driven solubilization of α-chitin from Hermetia illucens pupal exuviae

Pupal exuviae from black soldier flies contain approximately 20% chitin (31). Since visible light-exposed pupal exuviae boosted the activity *Sc*AA10C on cellulose, we investigated whether visible light could boost the ability of a chitin-active LPMO from *Serratia marcescens*, *Sm*AA10A (also known as CBP21), to solubilize the chitin present

in the pupal exuviae. For product quantification, soluble oxidized chito-oligomers were converted to a mixture of chitobionic acid and *N*-acetylglucosamine (GlcNAc) by treatment with a chitobiase (42). The light-exposed reaction with *Sm*AA10A led to rapid formation of chitobionic acid (Fig. 5A) with corresponding release of GlcNAc (Fig. 5B) during the first four hours of the reaction and product formation stopped after six hours. The apparent minor increase in product levels between six and 24 h is most likely due to liquid evaporation from the reaction vials. The reaction with *Sm*AA10A in the dark showed much slower, but more linear, formation of chitobionic acid (Fig. 5A) and corresponding release of GlcNAc (Fig. 5B).

Soluble oxidized products released by *Sm*AA10A are expected to contain between 4 and 10 monosaccharides (4). The product concentrations in Fig. 5 show that about five GlcNAc were detected per chitobionic acid, indicating an average product length of seven monosaccharides, well in accordance with previous observations. Assuming a chitin content of 2 g/L the product levels displayed in Fig. 5 indicate that approximately 7% of the chitin had been solubilized after 4 hours in the light-exposed reaction. This fraction, 7%, is compatible with data previously reported for the action of *Sm*AA10A on b-chitin and likely represents the maximum that can be achieved by an LPMO acting in the absence of chitinases.

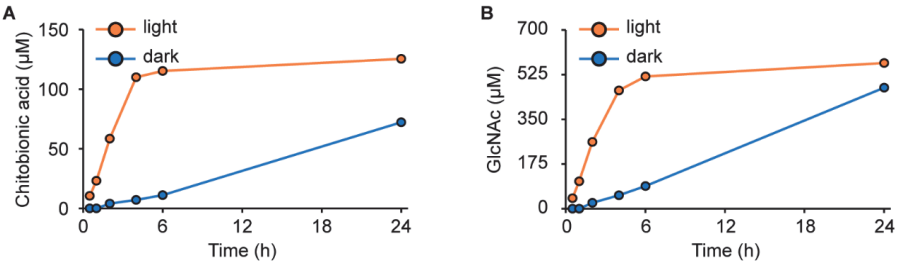

Fig. 5. Depolymerization of α-chitin from *H. illucens* pupal exuviae by *Sm*AA10A. The graphs show time courses for the release of oxidized products from pupal exuviae (10 $g.L^{-1}$; corresponding to a chitin concentration of approx. 2 $g.L^{-1}$ (31) by *Sm*AA10A (0.5 μM) exposed to visible light (orange) or in the dark (blue). All reactions were carried out in sodium phosphate buffer (50 mM, pH 6.0) at 40°C with magnetic stirring and exposed or not to visible light (I = 10% I_{max}, approx 16.8 $W.cm^{-2}$). Before product quantification, solubilized chitooligosaccharides were converted to *N*-acetylglucosamine (GlcNAc) and chitobionic acid by overnight incubation with *Sm*CHB (chitobiase, an *N*-acetylhexosaminidase) at room

temperature (42), and both products are reported, in panels B and A, respectively (see text for more details) The data points represent the mean of two independent experiments. Incubation of pupal exuviae in the absence of enzymes did not yield detectable soluble products. Values obtained for the 24 h samples are overestimated due to liquid evaporation between 6 h and 24 as the reactions are conducted in open glass vials.

Discussion

It has been shown that irradiation of plant litter by sunlight, especially blue-green light, improves the biotic degradation of carbohydrates present in this material. This effect has been ascribed to photodegradation of lignin in the secondary plant cell walls, which would improve the accessibility of cell wall polysaccharides for enzymatic degradation (43–46). Studying chitin degradation, we show here that other mechanisms may be involved and we provide a possible molecular explanation for the observation that light affects biomass turnover in Nature. Chitin is abundantly present in terrestrial eco-systems, being a central structural component of many organisms, including insects, nematodes, and fungi. To our knowledge, nothing is known about the impact of light on chitin solubilization and here we show that such impact can be large. Our findings suggest that light may not only contribute to the direct degradation of rigidifying structural components of plant cell walls and insect cuticles, as shown for lignins (43), but that the presence of these photoredox active components also plays a role in providing electrons and H_2O_2 to oxidative enzymes required for microbial biomass degradation. One interesting question for further research is whether this interplay between light, redox-active structural components, and enzymes such as LPMOs has affected the evolution of the materials and/or the enzyme systems that degrade these.

H_2O_2 is considered a green oxidant for agricultural, environmental, and industrial applications (47). Lignosulfonates and thin lignin films are known to act as homogeneous and heterogeneous photocatalysts, respectively, catalyzing the reduction of O_2 to H_2O_2 when exposed to a violet LED source (λ_{max} = 400 nm), at the cost of lignin photodegradation (47). Similar to lignin, which for a long time was considered as a waste product from the pulp industry (48), pupal exuviae are currently considered a waste stream from insect breeding and farming (31). We show here that this material, with its quinone/hydroquinone redox moieties (33), may be

used for sustainable photocatalytic production of H_2O_2. Photons have been touted as a reagent for the 21st century (49) and using photons to generate H_2O_2 is an appealing green technology.

This study adds to the current debate on whether LPMOs are monooxygenases or peroxygenases, by demonstrating correlations between light-driven LPMO activity and light-driven generation of H_2O_2 in the reaction system. Furthermore, we show that HRP inhibits light-driven LPMO catalysis, again suggesting dependence of the LPMO reaction on H_2O_2. The use of light and a photoredox catalyst may enable fine-tuning of the *in situ* generation of H_2O_2 and, consequently, polysaccharide oxidation by the LPMO. Such control is important since reduced LPMOs are prone to autocatalytic inactivation by surplus H_2O_2 (9, 50). Of note, the use of light to control the LPMO reactions in commercial bioreactors operating with substrates such as lignocellulose at high dry matter concentrations will not be straightforward as light will not penetrate the reaction slurry.

The type of photoredox catalysts used in this study are abundantly present in the natural substrates of LPMOs and other biomass-degrading redox enzymes such as (H_2O_2-dependent) lignin peroxidases. Thus, our findings may have wide implications for biomass conversion in Nature and should trigger further research in the area. Interestingly, these findings may not only relate to "bulk" biomass conversion, but may also be relevant in other important biological processes. For example, it was recently shown that LPMO action promotes plant infection by the potato pathogen *P. infestans* (51); with the current results at hand, one may wonder whether the infection process could be light-sensitive. If one assumes that light-driven H_2O_2 production is a significant contributor to the H_2O_2 pool in biomass degrading ecosystems, our current findings could even affect agronomic practices such as plowing. Plowing biomass into the soil will affect the activity of biomass-degrading peroxidases and peroxygenases not only by reducing access to O_2 but also by reducing access to the light that contributes to the reduction of O_2 to H_2O_2. No matter, the potential wider implications,

the present study provides novel insights into the impact of light on biomass conversion in Nature and the fascinating roles and catalytic abilities of LPMOs.

Materials and Methods

Materials

Unless otherwise stated, chemicals and enzymes were purchased from Sigma-Aldrich. The crystalline cellulose used was Avicel PH-101 (50 µm particles). Pupal exuviae from *Hermetia illucens* were milled using a Retsch® PM100 planetary ball mill with zirconium oxide vessels (500 mL) containing zirconium oxide balls (10 x 10 mm). Milled pupal exuviae (PE) were sieved through a 0.85 mm stainless steel sieve (Retsch) and stored at 4°C. A PE stock suspension of 50 g/L was prepared fresh each day and was washed four times by cycles of centrifugation (2 min, 15 000 g) and resuspending in sodium phosphate buffer (25 mM, pH 6.0) to remove soluble components, unless otherwise specified. The UV-Vis absorption spectrum for the supernatant from each washing step was measured to monitor the removal of soluble components absorbing between 240 and 800 nm (Fig. S1) using a UV-transparent 96-well microtiter plate in a Varioskan Lux plate reader (ThermoFisher Scientific). Stock solutions of AmplexRed (Thermo Fisher Scientific) and gallic acid were prepared in DMSO (10 and 100 mM, respectively), aliquoted and stored at -20°C in the dark. Gallic acid and AmplexRed aliquots were thawed in the dark for 10 min before use and were used only once.

Enzymes

Recombinant *Sc*AA10C (UniProt Q9RJY2) from *Streptomyces coelicolor* was produced and purified as previously described (7). *Sc*AA10C was copper saturated according to Loose et al. (42), carefully desalted using a PD MidiTrap column (G-25, GE Healthcare; (52)), and stored in sodium phosphate (25 mM, pH 6.0). The LPMO from *Serratia marcescens* (*Sm*AA10A, UniProt O83009) was produced and purified as previously described (53), copper-saturated in the same way as *Sc*AA10C, and stored in the same buffer. Mn-dependent superoxide dismutase (Mn-SOD) from *E. coli* (Sigma-Aldrich, S5639) was solubilized in Tris-HCl (10 mM, pH 8.0) and desalted (PD MidiTrap G-25,

GE Healthcare) in the same buffer before use. Horseradish peroxidase (HRP, type II) (Sigma-Aldrich, P8250) was solubilized in Milli-Q water and filtered (Filtropur S, 0.2 µm PES, Sarstedt). All enzymes were stored at 4°C.

Standard photobiocatalytic LPMO reactions

Standard photobiocatalytic reactions were carried out in a cylindrical glass vial (1.1 mL) with a conical bottom (Thermo Scientific) with 500 µL reaction volume unless otherwise specified. The light source (Lightningcure L9588, Hamamatsu) was equipped with a filter with a spectral distribution of 400 – 700 nm (L9588-03, Hamamatsu) and placed approx. 1 cm above the liquid surface. Typical reactions contained *Sc*AA10C (0.5 µM), Avicel (10 $g.L^{-1}$), and PE (5 $g.L^{-1}$) in sodium phosphate buffer (50 mM, pH 6.0). Reactions were incubated in the dark for 15 min at 40 °C under magnetic stirring prior to turning on the light (I=10% I_{max}, equivalent to 16.8 $W.cm^{-2}$) or adding reductant (gallic acid), unless stated otherwise. To stop the LPMO reactions, 60 µL samples were taken from the reaction mixture at regular intervals and filtered using a 96-well filter plate (Millipore) and a vacuum manifold. Filtered samples (35 µL) were stored at -20 °C. Prior to product quantification by HPAEC-PAD analysis, as described below, the filtrate was mixed with 35 µL of a 2 µM solution of purified Cel6A from *Themobifida fusca* (*Tf*Cel6A; (54) prepared in sodium phosphate buffer (50 mM, pH 6.0) and incubated at 40°C overnight to convert solubilized oxidized cello-oligosaccharides to a mixture of C1-oxidized products with a degree of polymerization of 2 and 3 (GlcGlc1A and Glc_2Glc1A). Reactions involving HRP were done with non-washed since non-washed PE contains HRP substrates, alleviating the need for adding the standard Amplex Red substrate. Reactions with SOD were performed using 400 µL reaction volume instead of 500 µL.

Chitin depolymerization experiments

Chitin depolymerization reactions were performed with *Sm*AA10A (0.5 µM) in sodium phosphate buffer (50 mM, pH 6.0) with washed PE (10 $g.L^{-1}$). Reactions were stopped

by filtration to separate soluble from insoluble products using a 96-well filter plate operated with a vacuum manifold (Merck Millipore). Prior to analysis using a Rezex column, 20 µL sample was mixed with 20 µL of a 1 mM solution of purified chitobiase (*Sm*CHB; (42)) and incubated over night at room temperature to convert oxidized chitooligosaccharides to GlcNAc and chitobionic acid, which were analyzed as described below.

Detection and quantification of oxidized and native products

Oxidized cello-oligosaccharides were analyzed by HPAEC-PAD performed with a Dionex ICS5000 system (Dionex, Sunnyvale, CA, USA) equipped with a CarboPac PA200 analytical column (3x250 mm) as previously described (55). Chromatograms were recorded and analyzed using Chromeleon 7.0 software. Quantitative analysis of C1-oxidizing LPMO activity was based on quantification of cellobionic acid (GlcGlc1A) and cellotrionic acid (Glc_2Glc1A), which were obtained after treating reaction filtrates with *Tf*Cel6A, as described above. Standards of GlcGlc1A and Glc_2Glc1A were prepared by treating cellobiose and cellotriose with cellobiose dehydrogenase (56).

Native and oxidized chito-oligosaccharides were analyzed using a Dionex Ultimate 3000 UPLC (Dionex, Sunnyvale, CA, USA), equipped with a Rezex RFQ-Fast acid H+ (8%) 7.8 x 100 mm column (Phenomenex, Torrance, CA) preheated to 85 °C using 5 mM H_2SO_4 as mobile phase at a flow rate of 1 mL/min (57). The solutes were separated isocratically and detected using UV-absorption at 194 nm. Solubilized GlcNAc and chitobionic acid were quantified based on standard curves for GlcNAc and chitobionic acid.

Total reducing capacity

The total reducing capacity of pupal exuviae prior to and after washing was determined according to a published protocol using gallic acid as standard (32). This method is based on electron transfer from phenolic compounds to

phosphomolybdic/phosphotungstic acid complexes in alkaline medium, and can be spectrophotometrically measured. Non-washed and washed pupal exuviae were suspended directly or after the last centrifugation step, respectively, in 95% (v/v) MeOH in concentrations ranging from 1.25 to 20 $g.L^{-1}$ in triplicates. 100 µL of the pupal exuviae suspensions were transferred to 1.5 mL Eppendorf tubes to which 200 µL a 10% (v/v) of Folin-Ciocalteu reagent was added, followed by thorough mixing, addition of 800 µL Na_2CO_3 (0.7 M), thorough mixing, and a 2 h incubation at room temperature. The tubes were spun down for 1 min at 15 000 g to remove any particles and 200 µL of the resulting supernatant was transferred to 96-well microtiter plate also containing identically treated gallic acid samples to provide the standard curve (0-2500 µM). The solutions were shaken for 10 s before recording the absorbance at 765 nm using a Varioskan Lux plate reader (ThermoFisher Scientific).

H_2O_2 accumulation

This method was adapted from previously published protocols (24, 40, 52). Reactions were done in sodium phosphate buffer (50 mM; pH 6.0), with a total volume of 500 µL. Samples (75 µL) were taken after various time intervals and filtered as described for standard photobiocatalytic LPMO reactions, above. To quantify the amount of accumulated H_2O_2, 50 µL of the filtered and, if needed, diluted sample was mixed with 25 µL H_2O and 25 µL of a premix composed of HRP (0.4 µM), AmplexRed (0.4 mM) in sodium phosphate buffer (0.4 M, pH 6.0). The H_2O_2 standard curve (0, 10, 20, 30, 40 µM; final concentrations) was prepared by mixing 25 µL of the same AmplexRed/HRP premix with 50 µL of the supernatant from a PE suspension with the same initial PE concentration as the reactions being measured (or appropriate dilutions thereof) to achieve approximately the same concentration of PE-derived components in the standard curve as in the reactions being measured, and lastly with 25 µL H_2O_2 solution (0, 40, 80, 120, 160 µM) in a 96-well microtiter plate. The reaction mixtures were shaken and incubated for 60 s at 30°C before recording absorbance at 563 nm using a Varioskan Lux plate reader (ThermoFisher Scientific).

Verification of superoxide dismutase (SOD) activity

SOD activity was assessed using a published assay protocol (24, 58). In alkaline conditions, autooxidation of pyrogallol results in formation of a semiquinone and $O_2^{\bullet-}$ and the semiquinones further react to form purpurogallin which absorbs strongly at 325 nm (58). Briefly, a stock solution of pyrogallol (2 mM) was prepared in 10 mM HCl and stock solutions of SOD (0, 56.5, 113, 282.5, 565, 1130, 2825, 5650 nM) were prepared in Tris-HCl (10 mM, pH 8.0). 80 µL Tris-HCl (50 mM final reaction concentration, pH 8.0) was mixed with 10 µL SOD and 10 µL pyrogallol (0.2 mM final concentration) in a 96 well plate. The 96 well plate was shaken at 600 rpm for 5 s prior to recording absorbance at 325 nm every 8 s for 10 min using a Varioskan Lux plate reader (ThermoFisher Scientific), and the inhibitory effect of SOD on purpurogallin formation is shown in Fig. S5.

Acknowledgements

We thank Ole Golten for providing the chitobiase (*Sm*CHB) and Susanne Zibek for helpful discussions.

Author contributions

Conceptualization: E.G.K. and V.G.H.E. Methodology: E.G.K., F.S., T.H., and V.G.H.E. Investigation: E.G.K. and F.S. Visualization: E.G.K.., T.H., V.G.H.E. Supervision: V.G.H.E. Writing (original draft): E.G.K. and V.G.H.E. Writing (review and editing): E.G.K.., F.S., T.H., and V.G.H.E.

Competing interests

The authors declare that they have no competing interests.

Funding

This work was supported by the Norwegian Research Council through grant 262853 (E.G.K., F.S., and V.G.H.E.) and by the German Federal Ministry of Education and Research (ChitoTex, grant number 031A567A; T.H.).

References

1. X. Chen, S. Song, H. Li, G. Gözaydın, N. Yan, Expanding the boundary of biorefinery: organonitrogen chemicals from biomass. *Acc. Chem. Res.* **54**, 1711–1722 (2021).

2. P. V. Harris, *et al.*, Stimulation of lignocellulosic biomass hydrolysis by proteins of glycoside hydrolase family 61: structure and function of a large, enigmatic family. *Biochemistry* **49**, 3305–3316 (2010).

3. G. Vaaje-Kolstad, S. J. Horn, D. M. F. van Aalten, B. Synstad, V. G. H. Eijsink, The non-catalytic chitin-binding protein CBP21 from *Serratia marcescens* is essential for chitin degradation. *J. Biol. Chem.* **280**, 28492–28497 (2005).

4. G. Vaaje-Kolstad, *et al.*, An oxidative enzyme boosting the enzymatic conversion of recalcitrant polysaccharides. *Science* **330**, 219–222 (2010).

5. R. J. Quinlan, *et al.*, Insights into the oxidative degradation of cellulose by a copper metalloenzyme that exploits biomass components. *Proc. Natl. Acad. Sci. U. S. A.* **108**, 15079–15084 (2011).

6. C. M. Phillips, W. T. Beeson, J. H. Cate, M. A. Marletta, Cellobiose dehydrogenase and a copper-dependent polysaccharide monooxygenase potentiate cellulose degradation by *Neurospora crassa*. *ACS Chem. Biol.* **6**, 1399–1406 (2011).

7. Z. Forsberg, *et al.*, Cleavage of cellulose by a CBM33 protein. *Protein Sci.* **20**, 1479–1483 (2011).

8. A. Levasseur, E. Drula, V. Lombard, P. M. Coutinho, B. Henrissat, Expansion of the enzymatic repertoire of the CAZy database to integrate auxiliary redox enzymes. *Biotechnol. Biofuels* **6**, 41 (2013).

9. B. Bissaro, *et al.*, Oxidative cleavage of polysaccharides by monocopper enzymes depends on H_2O_2. *Nat. Chem. Biol.* **13**, 1123–1128 (2017).

10. B. Bissaro, *et al.*, Molecular mechanism of the chitinolytic peroxygenase reaction. *Proc. Natl. Acad. Sci.* **117**, 1504–1513 (2020).

11. J. A. Hangasky, A. T. Iavarone, M. A. Marletta, Reactivity of O_2 versus H_2O_2 with polysaccharide monooxygenases. *Proc. Natl. Acad. Sci.* **115**, 4915–4920 (2018).

12. S. M. Jones, W. J. Transue, K. K. Meier, B. Kelemen, E. I. Solomon, Kinetic analysis of amino acid radicals formed in H_2O_2-driven Cu^I LPMO reoxidation implicates dominant homolytic reactivity. *Proc. Natl. Acad. Sci.* **117**, 11916–11922 (2020).

13. T. M. Hedison, *et al.*, Insights into the H_2O_2-driven catalytic mechanism of fungal lytic polysaccharide monooxygenases. *FEBS J.* **288**, 4115–4128 (2021).

14. S. Kuusk, *et al.*, Kinetic insights into the role of the reductant in H_2O_2-driven degradation of chitin by a bacterial lytic polysaccharide monooxygenase. *J. Biol. Chem.* **294**, 1516–1528 (2019).

15. S. Kuusk, *et al.*, Kinetics of H_2O_2-driven degradation of chitin by a bacterial lytic polysaccharide monooxygenase. *J. Biol. Chem.* **293**, 523–531 (2018).

16. L. Rieder, D. Petrović, P. Väljamäe, V. G. H. Eijsink, M. Sørlie, Kinetic characterization of a putatively chitin-active LPMO reveals a preference for soluble substrates and absence of monooxygenase activity. *ACS Catal.* **11**, 11685–11695 (2021).

17. A. A. Stepnov, *et al.*, The impact of reductants on the catalytic efficiency of a lytic polysaccharide monooxygenase and the special role of dehydroascorbic acid. *FEBS Lett.* **596**, 53–70 (2022).

18. K.-E. Eriksson, B. Pettersson, U. Westermark, Oxidation: an important enzyme reaction in fungal degradation of cellulose. *FEBS Lett.* **49**, 282–285 (1974).

19. B. Bissaro, A. Varnai, Å. K. Røhr, V. G. H. Eijsink, Oxidoreductases and reactive oxygen species in lignocellulose biomass conversion. *Microbiol. Mol. Biol. Rev.* **4** (2018).

20. P. Chylenski, *et al.*, Lytic polysaccharide monooxygenases in enzymatic processing of lignocellulosic biomass. *ACS Catal.* **9**, 4970–4991 (2019).

21. S. Kuusk, P. Väljamäe, Kinetics of H_2O_2-driven catalysis by a lytic polysaccharide monooxygenase from the fungus Trichoderma reesei. *J. Biol. Chem.* **297**, 101256 (2021).

22. L. H. Yang, C. Gratton, Insects as drivers of ecosystem processes. *Curr. Opin. Insect Sci.* **2**, 26–32 (2014).

23. M. M. C. H. van Schie, *et al.*, Cascading g-C_3N_4 and peroxygenases for selective oxyfunctionalization reactions. *ACS Catal.* **9**, 7409–7417 (2019).

24. B. Bissaro, E. Kommedal, Å. K. Røhr, V. G. H. Eijsink, Controlled depolymerization of cellulose by light-driven lytic polysaccharide oxygenases. *Nat. Commun.* **11**, 890 (2020).

25. L. Schmermund, *et al.*, Photo-biocatalysis: biotransformations in the presence of light. *ACS Catal.* **9**, 4115–4144 (2019).

26. J. Kim, F. Hollmann, C. B. Park, Lignin as a multifunctional photocatalyst for

solar-powered biocatalytic oxyfunctionalization of C-H bonds. *ChemRxiv* (2021) https:/doi.org/10.26434/chemrxiv.13650383.v1.

27. D. Cannella, *et al.*, Light-driven oxidation of polysaccharides by photosynthetic pigments and a metalloenzyme. *Nat. Commun.* **7**, 11134 (2016).

28. B. Bissaro, *et al.*, Fueling biomass-degrading oxidative enzymes by light-driven water oxidation. *Green Chem.* **18**, 5357–5366 (2016).

29. K. Y. Zhu, H. Merzendorfer, W. Zhang, J. Zhang, S. Muthukrishnan, Biosynthesis, turnover, and functions of chitin in insects. *Annu. Rev. Entomol.* **61**, 177–196 (2016).

30. S. O. Andersen, Insect cuticular sclerotization: a review. *Insect Biochem. Mol. Biol.* **40**, 166–178 (2010).

31. T. Hahn, *et al.*, Purification of chitin from pupal exuviae of the black soldier fly. *Waste and Biomass Valorization* (2021) https:/doi.org/10.1007/s12649-021-01645-1.

32. E. A. Ainsworth, K. M. Gillespie, Estimation of total phenolic content and other oxidation substrates in plant tissues using Folin–Ciocalteu reagent. *Nat. Protoc.* **2**, 875–877 (2007).

33. S. O. Andersen, "Cuticular Sclerotization and Tanning" in *Insect Molecular Biology and Biochemistry*, L. I. Gilbert, Ed. (Academic Press, 2012), pp. 167–192.

34. G. Renger, T. Renger, Photosystem II: the machinery of photosynthetic water splitting. *Photosynth. Res.* **98**, 53–80 (2008).

35. P. Boule, A. Rossi, J. F. Pilichowski, G. Grabner, Photoreactivity of hydroquinone in aqueous-solution. *New J. Chem.* **16**, 1053–1062 (1992).

36. S. M. Beck, L. E. Brus, Photooxidation of water by *p*-benzoquinone. *J. Am. Chem. Soc.* **104**, 1103–1104 (1982).

37. K. C. Kurien, P. A. Robins, Photolysis of aqueous solutions of *p*-benzoquinone: a spectrophotometric investigation. *J. Chem. Soc. B Phys. Org.*, 855–859 (1970).

38. B. M. Blossom, *et al.*, Photobiocatalysis by a lytic polysaccharide monooxygenase using intermittent illumination. *ACS Sustain. Chem. Eng.* **8**, 9301–9310 (2020).

39. R. Xu, *et al.*, Characterization of products from the reactions of n-acetyldopamine quinone with n-acetylhistidine. *Arch. Biochem. Biophys.* **329**, 56–64 (1996).

40. R. Kittl, D. Kracher, D. Burgstaller, D. Haltrich, R. Ludwig, Production of four *Neurospora crassa* lytic polysaccharide monooxygenases in *Pichia pastoris* monitored by a fluorimetric assay. *Biotechnol. Biofuels* **5**, 79 (2012).

41. Y. Pan, *et al.*, Selective conversion of lignin model veratryl alcohol by photosynthetic pigment via photo-generated reactive oxygen species. *Chem. Eng. J.* **393**, 124772 (2020).

42. J. S. M. Loose, Z. Forsberg, M. W. Fraaije, V. G. H. Eijsink, G. Vaaje-Kolstad, A rapid quantitative activity assay shows that the *Vibrio cholerae* colonization factor GbpA is an active lytic polysaccharide monooxygenase. *FEBS Lett.* **588**, 3435–3440 (2014).

43. A. T. Austin, M. S. Méndez, C. L. Ballaré, Photodegradation alleviates the lignin bottleneck for carbon turnover in terrestrial ecosystems. *Proc. Natl. Acad. Sci.* **113**, 4392–4397 (2016).

44. A. T. Austin, L. Vivanco, Plant litter decomposition in a semi-arid ecosystem controlled by photodegradation. *Nature* **442**, 555–558 (2006).

45. A. T. Austin, C. L. Ballaré, Dual role of lignin in plant litter decomposition in terrestrial ecosystems. *Proc. Natl. Acad. Sci.* **107**, 4618–4622 (2010).

46. P. Berenstecher, L. Vivanco, L. I. Pérez, C. L. Ballaré, A. T. Austin, Sunlight doubles aboveground carbon loss in a seasonally dry woodland in Patagonia. *Curr. Biol.* **30**, 3243-3251.e3 (2020).

47. E. Miglbauer, M. Gryszel, E. D. Głowacki, Photochemical evolution of hydrogen peroxide on lignins. *Green Chem.* **22**, 673–677 (2020).

48. A. J. Ragauskas, *et al.*, Lignin valorization: Improving lignin processing in the biorefinery. *Science* **344**, 709-719 (2014).

49. H. E. Bonfield, *et al.*, Photons as a 21st century reagent. *Nat. Commun.* **11**, 804 (2020).

50. A. Kadić, A. Várnai, V. G. H. Eijsink, S. J. Horn, G. Lidén, In situ measurements of oxidation–reduction potential and hydrogen peroxide concentration as tools for revealing LPMO inactivation during enzymatic saccharification of cellulose. *Biotechnol. Biofuels* **14**, 46 (2021).

51. F. Sabbadin, *et al.*, Secreted pectin monooxygenases drive plant infection by pathogenic oomycetes. *Science* **373**, 774–779 (2021).

52. A. A. Stepnov, *et al.*, Unraveling the roles of the reductant and free copper ions in LPMO kinetics. *Biotechnol. Biofuels* **14**, 28 (2021).

53. G. Vaaje-Kolstad, D. R. Houston, A. H. K. Riemen, V. G. H. Eijsink, D. M. F. van Aalten, Crystal structure and binding properties of the *Serratia marcescens* chitin-binding protein CBP21. *J. Biol. Chem.* **280**, 11313–11319 (2005).

54. R. E. Calza, D. C. Irwin, D. B. Wilson, Purification and characterization of two β-1,4-endoglucanases from *Thermomonospora fusca*. *Biochemistry* **24**, 7797–7804 (1985).

55. B. Westereng, *et al.*, Efficient separation of oxidized cello-oligosaccharides generated by cellulose degrading lytic polysaccharide monooxygenases. *J. Chromatogr. A* **1271**, 144–152 (2013).

56. M. Zámocký, *et al.*, Cloning, sequence analysis and heterologous expression in *Pichia pastoris* of a gene encoding a thermostable cellobiose dehydrogenase from *Myriococcum thermophilum*. *Protein Expr. Purif.* **59**, 258–265 (2008).

57. S. Mekasha, *et al.*, A trimodular bacterial enzyme combining hydrolytic activity with oxidative glycosidic bond cleavage efficiently degrades chitin. *J. Biol. Chem.* **295**, 9134–9146 (2020).

58. X. Li, Improved pyrogallol autoxidation method: a reliable and cheap superoxide-scavenging assay suitable for all antioxidants. *J. Agric. Food Chem.* **60**, 6418–6424 (2012).

Supplementary Information for

Natural photoredox catalysts promote light-driven lytic polysaccharide monooxygenase reactions and enzymatic turnover of biomass

Eirik G. Kommedal[1], Fredrikke Sæther[1], Thomas Hahn[2], Vincent G. H. Eijsink[1*]

[1] Faculty of Chemistry, Biotechnology and Food Science, Norwegian University of Life Sciences (NMBU), 1432 Ås, Norway

[2] Group Bioprocess Engineering, Fraunhofer Institute of Interfacial Engineering and Biotechnology, Nobelstraße 12, 70569 Stuttgart, Germany

[*] Corresponding author; Vincent Eijsink

Email: vincent.eijsink@nmbu.no

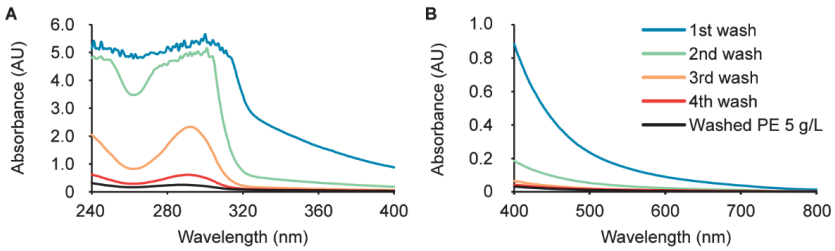

Fig. S1. UV-Vis spectra of pupal exuviae supernatants after washing. The panels show the absorption spectra from 240 – 400 nm (A) and 400 – 800 nm (B) for supernatants obtained after each washing step and the supernatant of the final pupal exuviae suspension used in LPMO reactions (referred to as "PE" in the main manuscript). The pupal exuviae were washed with sodium phosphate buffer (25 mM; pH 6.0) using 50 $g.L^{-1}$ suspensions, and the supernatants after each step were diluted 10-fold in sodium phosphate buffer (25 mM; pH 6.0) prior to measuring the absorption spectra, as the standard pupal exuviae concentration applied in the LPMO reactions was 5 $g.L^{-1}$. The spectra were measured in triplicate and the figures show a representative spectrum for each fraction.

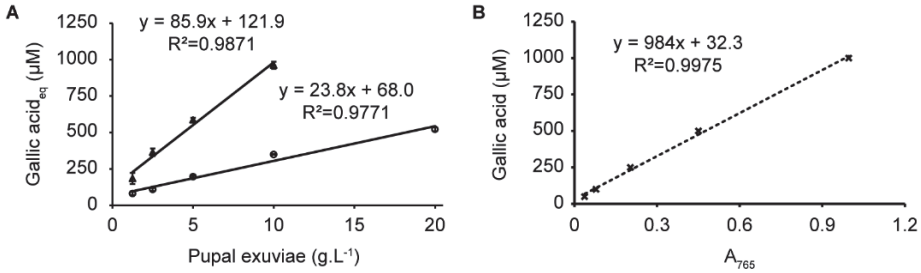

Fig. S2. Total reducing capacity of pupal exuviae. The graphs show the total reducing capacity in suspensions of washed (circles) and non-washed (triangles) PE expressed as gallic acid equivalents (A) and the standard curve with gallic acid (B). The signal for 20 g.L^{-1} non-washed PE fell outside the standard curve.

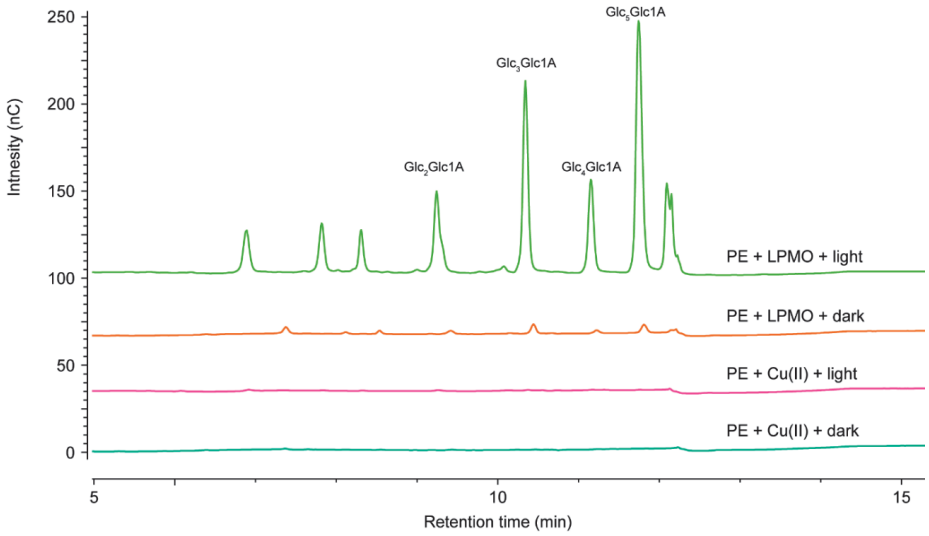

Fig. S3. Control reactions to probe for copper-catalyzed Fenton chemistry. The picture shows chromatographic product profiles obtained for reactions with or without light-exposure containing pupal exuviae (PE; 5 $g.L^{-1}$), Avicel (10 $g.L^{-1}$), and $Cu(II)SO_4$ (0.5 µM) or *Sc*AA10C (LPMO; 0.5 µM). All reactions were carried out in sodium phosphate buffer (50 mM, pH 6.0) at 40°C with magnetic stirring. Three independent replicates were performed for the reactions with $Cu(II)SO_4$ and a representative product profile is shown. Characteristic soluble oxidized cello-oligosaccharides are labeled in the upper chromatogram.

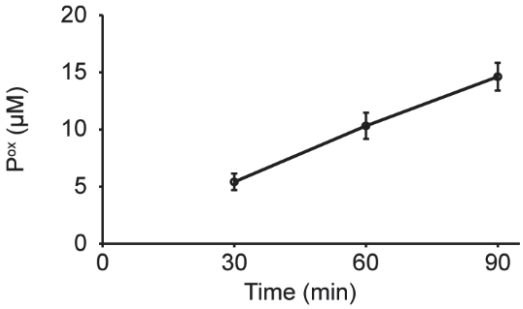

Fig. S4. Control reaction to probe for reduction of the LPMO by pupal exuviae in the dark. The graph shows a time course for the formation of solubilized oxidized products (P_{ox}) by *Sc*AA10C in a reaction in the dark with washed pupal exuviae (5 $g.L^{-1}$), Avicel (10 $g.L^{-1}$), and repetitive additions of H_2O_2 (to 50 µM final concentration at each addition) at 0, 30, 60 min, after sampling. The reactions were carried out in sodium phosphate buffer (50 mM, pH 6.0) at 40°C under magnetic stirring. Before product quantification, solubilized oxidized cello-oligosaccharides were converted to a mixture of cellobionic acid and cellotrionic acid by incubation with *Tf*Cel6A at room temperature overnight. The data points represent the mean of three independent experiments and error bars show ± s.d.

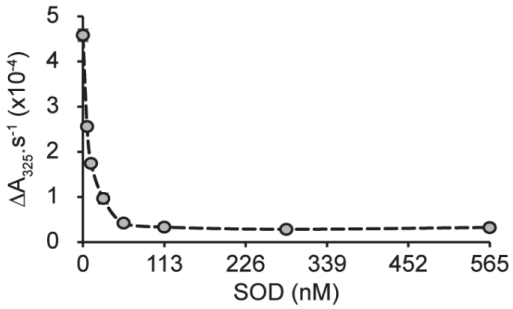

Fig. S5. Verification of Superoxide Dismutase (SOD) activity. The figure shows the change in absorbance at 325 nm during a 10-min time course monitoring of the formation of pupurogallin. Pyrogallol oxidation at alkaline pH (pH 8.0) in aerobic conditions leads to the formation of superoxide radicals and formation of purpurogallin, where the latter can be monitored spectrophotmetrically at 325 nm. Addition of SOD inhibits the formation of purpurogallin by removing superoxide radicals (1). The stock solution of pyrogallol (2 mM) was prepared in 10 mM HCl to prevent autooxidation. The reaction without SOD shows the maximum rate for pyrogallol oxidation and contained pyrogallol (200 µM) in Tris-HCl (50 mM; pH 8.0). Addition of increasing amounts of SOD, prepared in Tris-HCl (10 mM; pH 8.0), shows a dose-dependent decrease in purpurogallin formation. All reactions were performed at room temperature in a 96 well plate using a Varioskan Lux plate reader (ThermoFisher Scientific). Reactions were performed in triplicates; errors bars indicating standard deviations, which were small, are hidden by the bullets.

SI References

1. X. Li, Improved pyrogallol autoxidation method: a reliable and cheap superoxide-scavenging assay suitable for all antioxidants. *J. Agric. Food Chem.* **60**, 6418–6424 (2012).

ISBN: 978-82-575-1911-7
ISSN: 1894-6402

Norwegian University
of Life Sciences

Postboks 5003
NO-1432 Ås, Norway
+47 67 23 00 00
www.nmbu.no

114076 / ANDVORDGRAFISK.NO